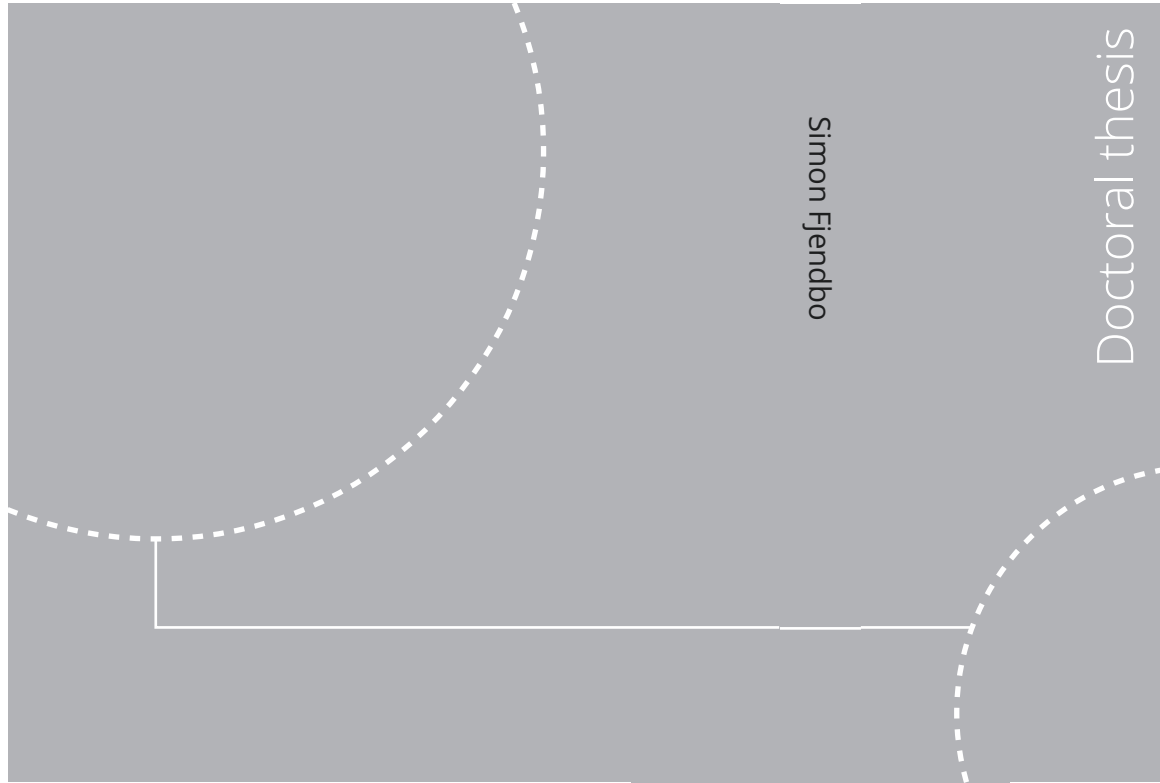


ISBN 978-82-326-6071-1 (printed ver.)
ISBN 978-82-326-6659-1 (electronic ver.)
ISSN 1503-8181 (printed ver.)
ISSN 2703-8084 (electronic ver.)



Doctoral theses at NTNU, 2022:173

Simon Fjendbo

Application of marine field data for prediction of chloride ingress in concrete

Doctoral theses at NTNU, 2022:173

NTNU
Norwegian University of
Science and Technology
Thesis for the degree of
Philosophiae Doctor
Faculty of Engineering
Department of Structural Engineering

Simon Fjendbo

Application of marine field data for prediction of chloride ingress in concrete

Thesis for the degree of Philosophiae Doctor

Trondheim, June 2022

Norwegian University of Science and Technology
Faculty of Engineering
Department of Structural Engineering



Norwegian University of
Science and Technology

NTNU

Norwegian University of Science and Technology

Thesis for the degree of Philosophiae Doctor

Faculty of Engineering
Department of Structural Engineering

© Simon Fjendbo

ISBN 978-82-326-6071-1 (printed ver.)
ISBN 978-82-326-6659-1 (electronic ver.)
ISSN 1503-8181 (printed ver.)
ISSN 2703-8084 (electronic ver.)

Doctoral theses at NTNU, 2022:173



Printed by Skipnes Kommunikasjon AS

Preface

The doctoral thesis was submitted to the Norwegian University of Science and Technology (NTNU) in Trondheim for the degree Philosophiae Doctor (PhD). The main supervisor was Professor Mette Rica Geiker (NTNU) and the co-supervisors were Professor Klaartje De Weerd (NTNU) and Product Manager Henrik Erndahl Sørensen (Danish Technological Institute).

The thesis is the product of an industrial PhD project funded by the Danish Technological Institute through the contract “E5 Field exposure and monitoring to extend the service life of infrastructure” (translation from Danish) granted by the Danish Ministry of Higher Education and Science. The project started in October 2018, where the candidate got employed at the Danish Technological Institute and ended in October 2021.

The research was carried out partly at the Department of Structural Engineering, Faculty of Engineering Science and Technology, NTNU, Trondheim, Norway and partly at the Danish Technological Institute, Taastrup, Denmark. During the period of this PhD project, field data was obtained from the Fehmarn Belt Exposure Site after ten years of exposure. This data supplements already available data from a half, two and five years of exposure. The vast majority of the experimental work was conducted at the Danish Technological Institute.

The thesis consists of the following parts:

Part I: Extended summary

Part II: Appended papers

Part III: Appendices

Simon Fjendbo

May 2022

Acknowledgements

The Danish Technological Institute (DTI) is acknowledged for financing this PhD through the contract “E5 Field exposure and monitoring to extend the service life of infrastructure” (translation from Danish) granted by the Danish Ministry of Higher Education and Science. Femern A/S is acknowledged for sharing field data from the Fehmarn Belt Exposure Site and for allowing me to extract additional samples not included in the original program.

I would like to thank my main supervisor Mette Rica Geiker not only for pushing me and commenting on drafts around the clock, but also for several dinner invitations and ensuring a good atmosphere at meetings. Further my thanks go to my co-supervisors Henrik Erndahl Sørensen for helping me to settle in at the Danish Technological Institute and aid me with his Excel macro skills and Klaartje De Weerd for her skilled feedback. Ulla Hjorth Jakobsen is acknowledged for valuable discussions and support regarding optical microscopy.

The laboratory staff of the Danish Technological Institute is acknowledged for carrying out all experimental work used in the thesis, which was acquired prior to the initiation of the PhD project, and for aiding and instructing me in carrying out the experimental work during the PhD project. In particular Mikael Dissing for preparing thin sections, Sten Røtting Nielsen, Peter Matthias Dissing and Henrik Bertelsen for core drilling, sawing and performing mechanical tests, Sten Røtting Nielsen, Mette Gressmann and Finn Lykke Østergård for aiding in analyzing chloride and calcium content and finally Thomas Lennart Svensson for coordinating the staff and for discussions on possibilities for further testing.

Further acknowledgements go to Kurt Kielsgaard from the Technical University of Denmark for assistance with pressure saturation for the determination of macro porosity, and to Tone H. Nilsen and Pamela Zuschlag from NTNU for assistance with the thermogravimetric analysis. I would also like to thank my nice and supportive colleagues both in the concrete group at NTNU and at DTI. Especially Petter Hemstad for useful discussions on chloride binding while exercising in the gym.

My final thanks go to my ever supportive and understanding family.

Abstract

A fixed link is about to be built across the Fehmarn Belt between Denmark and Germany. The main structure of the link is a submerged reinforced concrete tunnel with a design service life of 120 years considering corrosion initiation as limit state. With the aim of supporting the design and operation of the reinforced concrete structures for the fixed link, Femern A/S in 2010 established the Fehmarn Belt Exposure Site in Rødbyhavn, Denmark, where 15 concretes differing in binder composition are exposed.

Chloride-induced corrosion of embedded reinforcement steel is an important deterioration mechanism in marine exposed reinforced concrete structures. Concrete acts as a protective layer for the steel, both physically by impairing chloride ingress and chemically by passivating the steel due to the high pH of concrete. However, when a sufficiently high content of chlorides has penetrated through the concrete and reached the embedded steel reinforcement, steel corrosion is initiated. The focus of this study was to test and further develop the basis for application of chloride ingress models for service life design and reassessment of marine exposed reinforced concrete structures.

The topic was approached by conducting an evaluation of which chloride data to use and how to use them for chloride ingress predictions by analyzing a) microstructural changes in the concretes and their impact and b) the assumptions made if correcting for paste fraction. By comparing chloride profiles combined with petrographic analysis of tidal and submerged concrete after ten years of marine exposure, supplemented with moisture and portlandite profiles of the submerged exposed concrete and earlier data on microstructure and chloride ingress, the relationship between chloride profiles and microstructural changes was investigated. Because of stochastic variation in the paste fraction and systematic variations due to geometrical restraints at cast surfaces, data for total chloride content are occasionally calibrated using parallelly measured calcium content as a measure of the actual paste fraction assuming non-calcareous aggregates and no calcium leaching. The assumption of no calcium leaching was investigated by comparing calcium profiles measured after a half, two, five and ten years from the same concrete panels exposed at the Fehmarn Belt Exposure Site and by analyzing the impact of calibration on chloride profiles.

The earlier made square root observation of a linear relationship between the penetration depth of 0.05% chloride by wt. of concrete versus square root of time was generalized. The applicability and limitations were assessed, and the scope of validity widened with the aim of proposing it as a method (the square root method). Field data from marine submerged, tidal, splash, atmospheric and from inland deicing salt exposure at various Northern European locations was analyzed for a range of reference chloride contents. The square root method was compared to selected engineering models by evaluating the ability to predict data achieved after ten years of submerged exposure at the Fehmarn Belt Exposure Site based on data achieved up to five years of exposure. The tested models were (i) the *fib* Model Code, which include a time-dependent apparent diffusion coefficient (D_a); (ii) the HETEK model,

which include both time-dependent D_a and surface chloride content (C_s) and (iii) the ClinConc model, which include time-dependent D_a and indirectly time-dependent C_s (through time dependent chloride binding).

The results showed a microstructurally changed zone extending up to ten millimeters from the exposed surface was a general feature for all concretes exposed for ten years at the Fehmarn Belt Exposure Site. When comparing to previous results from the same panels, it was noted that the depth of the microstructurally changed zone progressed inwards over time. A correlation was observed between chloride profiles and microstructural changes. The depth of the maximum chloride content ($x_{C_{max}}$) was found to almost coincide with the depth of the microscopically changed zone (x_{MCZ}). A steady increase was observed in $x_{C_{max}}$ from 0.6-2.5 mm after six months to 4.5-10 mm after ten years and in x_{MCZ} from 1-2.5 mm after six months to 4-10 mm after ten years depending on binder type with least progression for a concrete containing 67% ground granulated blast-furnace slag. Calcium calibration of chloride profiles is sometimes used to account for the higher paste fraction in the surface near region due to the wall effect and for stochastic variations in the paste content in concrete in general. However, calcium leaching can introduce errors to the calibrated chloride contents in the leached part of the profile. It was found that the calcium content in the surface near region (up to 10 mm) decreased systematically over the period of 10 years. This results in the calcium content no longer being a suitable measure of the paste fraction up to this depth. As a result of the decreasing calcium content to a depth typically extending beyond that of the maximum chloride content (“chloride peak”), it was found that the calibrated maximum chloride content in several cases was higher than the uncalibrated. Based on the findings, it is recommended to exclude datapoints from the microstructurally changed zone, i.e., the outermost datapoints including the maximum chloride content, when using field data for testing of chloride ingress prediction models, unless reactive transport models are used.

Analyses of chloride profiles with 237 combinations of concrete, exposure and reference contents showed that chloride ingress of a reference content followed a linear relationship with an average R^2 of 0.96, when the penetration depth of the reference content was plotted against the square root of exposure time. This square root observation appeared valid for the studied Portland cement based concretes with fly ash, silica fume and ground granulated blast furnace slag exposed in submerged and tidal exposure zones, when applying reference contents of 0.1-1.8 % chloride by wt. of binder, and in atmospheric zone when applying reference contents of 0.1-0.5 % chloride by wt. of binder. It was found that the parameters describing the straight line depended on the chosen reference content. Faster ingress was seen for low compared to high contents. Further the slope of the straight line (ingress parameter) depended on the exposure with faster ingress for tidal than for submerged exposure. It was concluded that the square root method appears to be a promising method for reassessment of chloride ingress, among others because it does not rely on data affected by the microstructurally changed zone or calcium leaching. When comparing the square root method to other ingress models for reassessment, the square root method predicted with the lowest residual standard error (best), but currently it is only applicable for reassessment and not yet for design.

Table of Contents

PREFACE	III
ACKNOWLEDGEMENTS	V
ABSTRACT	VII
TABLE OF CONTENTS	IX
LIST OF APPENDED PAPERS	X
LIST OF SYMBOLS	XI
LIST OF ABBREVIATIONS	XI

Part I – Extended summary

1. INTRODUCTION	- 1 -
1.1 OBJECTIVES	- 2 -
1.2 SCOPE AND LIMITATIONS.....	- 2 -
1.3 OVERVIEW OF THESIS	- 3 -
2. THEORETICAL BACKGROUND	- 4 -
2.1 CHLORIDE INGRESS AND BINDING.....	- 4 -
2.2 CHLORIDE INGRESS PREDICTION MODELS	- 5 -
3. APPROACH	- 6 -
3.1 ESTABLISHMENT AND EVALUATION OF FIELD DATA.....	- 6 -
3.2 THE SQUARE ROOT METHOD	- 8 -
3.3 COMPARISON OF MODELS FOR CHLORIDE INGRESS PREDICTION	- 12 -
4. MAIN FINDINGS	- 15 -
4.1 ESTABLISHMENT AND EVALUATION OF FIELD DATA.....	- 15 -
4.2 THE SQUARE ROOT METHOD	- 18 -
4.3 COMPARISON OF MODELS FOR CHLORIDE INGRESS PREDICTION	- 20 -
5. CONCLUSION	- 22 -
6. PERSPECTIVES AND FUTURE RESEARCH OPPORTUNITIES	- 24 -
6.1 FIELD DATA; COLLECTION AND APPLICATION.....	- 24 -
6.2 REASSESSMENT	- 24 -
6.3 DESIGN	- 24 -
6.4 FUTURE RESEARCH.....	- 25 -
7. REFERENCES	- 25 -

Part II – Appended papers

See separate list

Part III – Appendices

- Appendix A Details on the Fehmarn Belt Exposure Site
- Appendix B Details on exposed concretes and constituent materials
- Appendix C Additional experimental work
- Appendix D Investigation of carbonation of selected concretes in urban environment
- Appendix E Overview of chloride ingress models

List of appended papers

The thesis includes the following appended papers, which are referred to by their roman numbers:

- I. The square root method for chloride ingress prediction – Applicability and limitations**
Materials and structures, volume 54 issue 2 article 61 (2021).
<https://doi.org/10.1617/s11527-021-01643-8>
Simon Fjendbo; Henrik E. Sørensen; Klaartje De Weerd; Mette R. Geiker
- II. Correlating the development of chloride profiles and microstructural changes in marine concrete up to ten years**
Cement and Concrete Composites (2022)
<https://doi.org/10.1016/j.cemconcomp.2022.104590>
Simon Fjendbo; Henrik E. Sørensen; Klaartje De Weerd; Ulla Hjorth Jakobsen; Mette R. Geiker
- III. Testing of chloride ingress models versus 10 years field data from the Fehmarn Belt marine exposure site**
DRAFT
Simon Fjendbo; Henrik E. Sørensen; Mette R. Geiker
- IV. When and how should chloride profiles be calibrated for paste fraction?**
Nordic Concrete Research (2022)
Simon Fjendbo; Henrik E. Sørensen; Klaartje De Weerd; Mette R. Geiker

Declaration of authorship

Simon Fjendbo contributed significantly to conducting a scheduled experimental program on concrete panels from the Fehmarn Belt Exposure Site after 10 years of exposure. In addition, Simon Fjendbo planned and conducted experiments on additional cores for determining degree of capillary saturation, relative humidity, total porosity and moisture profiles.

Simon Fjendbo evaluated the results and wrote the major part of the appended papers. The co-authors contributed in discussing and evaluating the results and by assisting in writing the papers. For Paper II language support was provided by the LANGUAGE SUPPORT CENTRE Denmark (Lawrence White).

List of symbols

See separate list of symbols for PIII immediately before appended paper III.

Symbol	Unit	Explanation
a_{Cr}	$\text{mm}/\sqrt{\text{year}}$	Slope of straight line fitted to x_{Cr} plotted vs \sqrt{t} (the subscript "Cr" may be replaced by C_r expressed in wt.% of concrete, e.g. $a_{0.75}$)
b_{Cr}	mm	Intercept of straight line fitted to x_{Cr} plotted vs \sqrt{t} (the subscript "Cr" may be replaced by C_r expressed in wt.% of concrete, e.g. $b_{0.75}$)
C_i	wt.% of binder or wt.% of concrete	Initial chloride content
C_{\max}	wt.% of binder or wt.% of concrete	Maximum chloride content
C_r	wt.% of binder or wt.% of concrete	Reference chloride content
C_s	wt.% of binder or wt.% of concrete	Surface chloride content
D_a	m^2/s	Apparent diffusion coefficient
t_{ini}	years	Time period of initiation
t_x	-	Exposure time x (e.g. t_1 for the earliest exposure time)
$x_{C_{\max}}$	mm	Ingress depth of C_{\max}
x_{Cr}	mm	Ingress depth corresponding to C_r (the subscript "Cr" may be replaced by C_r expressed in wt.% of concrete, e.g. $x_{0.75}$)
x_{MCZ}	mm	Depth of microstructurally changed zone

List of abbreviations

Symbol	Unit	Explanation
AFm	-	Family of hydrated calcium aluminates, where OH ⁻ may be substituted by SO ₄ ²⁻ or CO ₃ ²⁻ and some Fe(III) may substitute for aluminium
CH	-	Portlandite
C-S-H	-	Calcium silicate hydrate
CT	wt.%	Chloride threshold
DCS	%	Degree of capillary saturation
DTI	-	Danish Technological Institute
FA	-	Fly ash
GGBS	-	Ground granulated blast furnace slag
M-S-H	-	Magnesium silicate hydrate
MCZ	-	Microstructurally changed zone
PC	-	Portland cement
PF		Pore protection factor
RCMT		Rapid chloride migration test
RH		Relative humidity
RMSE	-	Root Mean Square Error
SEM-EDX	-	Scanning Electron Microscopy with Energy Dispersive X-Ray analysis
SF	-	Silica fume
SSE	-	Sum of squared errors

Part I – Extended summary

1. Introduction

A fixed link is about to be built across the Fehmarn Belt between Denmark and Germany. The main structure of the link is a submerged tunnel with a design service life of 120 years considering corrosion initiation as limit state [1].

Chloride-induced corrosion of embedded reinforcement steel is one of the most common deterioration mechanisms in marine exposed reinforced concrete structures [2]. Concrete acts as a protective layer for the steel, both physically by impairing chloride ingress and chemically by passivating the steel due to the high pH of concrete. However, when a sufficiently high content of chlorides has penetrated through the concrete and reached the embedded steel reinforcement, steel corrosion is initiated.

The corrosion process is often divided into an initiation phase and a propagation phase according to Tuutti [3]. The propagation phase can be further divided into multiple states, which is illustrated by the limit states suggested in the *fib* Model Code for Service Life Design [4]:

- Initiation phase; limit state
 - Depassivation of steel (assumed initiation of reinforcement corrosion)
- Propagation phase, limit states
 - Cracking due to reinforcement corrosion (not always)
 - Spalling of concrete cover due to reinforcement corrosion (not always)
 - Collapse due to loss of cross section of the reinforcement.

However, chloride induced corrosion will either not visually manifest itself or do so very late by crack formation or spalling [5].

In a performance based approach for service life design, the owner sets requirements to design service life, limit state and accepted probability of failure [4, 6]. In the design phase, many owners use depassivation of reinforcement as the limit state, see e.g. [7].

Considering depassivation of reinforcement corrosion as the limit state, the service life is modelled as the time until reaching a chloride content at the embedded steel reinforcement causing depassivation, the so-called chloride threshold value – also called critical chloride content. In this respect two main factors are of interest:

- Rate of chloride ingress (further described in Section 2.1 & 2.2)
- Chloride threshold value

This PhD study focused on the rate of chloride ingress.

1.1 Objectives

The overall goal of the PhD project was to test and further develop the basis for application of chloride ingress models for service life design and reassessment of marine exposed reinforced concrete structures.

To reach the overall goal, the following objectives were defined:

1. Establishment and evaluation of field data
 - Establish and evaluate ten years data from the Fehmarn Belt Exposure Site with the purpose of providing data and suggesting which chloride data is suitable for chloride ingress prediction.
2. The square root method
 - Test the applicability and limitations of the square root observation [8] for chloride ingress prediction.
3. Comparison of models for chloride ingress prediction
 - Compare the applicability (design and reassessment) of the square root method with selected established models for chloride ingress prediction.

1.2 Scope and limitations

The thesis focusses mainly on chloride ingress prediction in marine exposed concrete. The main focus for chloride ingress prediction was on well-defined exposure conditions where diffusion was the governing ingress mechanism, i.e. submerged conditions. In addition, the square root method was tested on the exposure conditions: marine tidal, marine atmospheric and Inland deicing. The study made use of field data both from the literature (Träslövsläge, Sweden [9], Østmarkneset, Norway [10], Dornoch, Scotland [11] and RV40 field exposure site, Sweden [12-14]) and from an ongoing study of marine field exposed concrete at the Fehmarn Belt Exposure Site, which is located at the Danish connection point of the Fehmarn Fixed Link, Rødbyhavn, Denmark (chloride content 6.6 g/L). At the Fehmarn Belt Exposure Site 15 well hydrated concrete panels with varying binder compositions and eq. w/c of approximately 0.40 are exposed. Further details on compositions and exposure can be found in (Appendix A and Appendix B). Data obtained after a half, two and five years of exposure were partly earlier published [15, 16], partly available in-house. Data after ten years were obtained during this study, partly as part of the PhD study [17, 18], partly as consultancy work for Fehmarn Belt A/S. In addition, data are used from duplicates exposed in urban environment at the Danish Technological Institute, Taastrup, Denmark.

The square root method [8, 19], was compared with the following selected established models: (i) the *fib* Model Code [4], which include a time-dependent D_a ; (ii) the HETEK model [20], which include both time-dependent apparent diffusion coefficient (D_a) and surface content (C_s), and (iii) the ClinConc model (engineering expression) [21], which include time-dependent D_a and indirectly time-dependent C_s (through time dependent chloride binding). Chloride ingress predictions were performed using mean values corresponding to a 50% probability.

1.3 Overview of thesis

The thesis consists of three parts:

- Part I: Extended summary
- Part II: Appended papers
 - The square root method for chloride ingress prediction – Applicability and limitations
 - Correlating the development of chloride profiles and microstructural changes in marine concrete up to ten years
 - Testing of chloride ingress models versus 10 years field data from the Fehmarn Belt marine exposure site
 - When and how should chloride profiles be calibrated for paste fraction?
- Part III: Appendices
 - Appendix A: Information on the Fehmarn Belt Exposure Site
 - Appendix B: The exposed concretes at the Fehmarn Belt Exposure Site
 - Appendix C: Additional experimental work on the samples from the Fehmarn Belt Exposure Site
 - Appendix D: Results obtained on samples from the Fehmarn Belt Exposure Site
 - Appendix E: Overview of chloride ingress models.

The appended papers and appendices are linked to the objectives as shown in Table 1.

Table 1: Overview of link between objectives and appended papers and appendices

Objective	Paper				Appendix				
	I	II	III	IV	A	B	C	D	E
1. Evaluation of field data		x		x	x	x	x	x	
2. The square root method	x		x		x	x			
3. Chloride ingress prediction	x	x	x	x	x	x			x

2. Theoretical background

2.1 Chloride ingress and binding

The mechanisms of chloride ingress in concrete are complicated. Diffusion, convection and migration as well as physical- and chemical binding are acting mechanisms.

Diffusion is transport of ions due to a gradient in chemical potential – or simplified – movement of ions from a zone with high concentration to a zone with lower concentration due to the random movement of ions. Sea water and solutions of typical deicing salts contain chloride ions, whereas concrete is produced with the aim of minimizing the initial chloride content (C_i). This scenario causes chloride to diffuse from sea water or water contaminated with deicing salts into concrete.

At initial exposure to chloride ions, concrete is due to self-desiccation and possible initial drying normally not fully saturated, that is why initial chloride ingress, also in marine submerged exposure, might be enhanced by capillary suction (convection) of sea water or water contaminated with deicing salts.

Chloride in concrete can be found either free in the pore solution, physically bound (adsorbed) to calcium silicate hydrate (C-S-H) or chemically bound in chloride containing AFm e.g. Friedel's or Kuzel's salt [22]. Only free chloride is able to penetrate concrete by diffusion or convection and depassivate the steel to initiate corrosion [23].

Multiple ions in sea water - such as magnesium, sulfate and carbonate ions – combined with leaching of e.g. calcium, potassium and hydroxyl ions influence chloride ingress by altering the microstructural properties, the binding capacity of the paste and even cause surface scaling [24-28]. Magnesium can precipitate as brucite as it encounters the high pH of the concrete [29] or form the non-cementing magnesium silicate hydrate (M-S-H) [30, 31]. M-S-H replaces C-S-H, which leads to a reduction in the chloride binding [24, 31]. Sulfate reduce chloride binding as sulfates compete with chloride for incorporation in C-S-H and calcium aluminate phases [32]. Bound chlorides can be liberated by leaching or carbonation, which cause them to be redistributed or washed out. This feature can result in a low chloride content near the surface and/or a sub-surface chloride peak.

The pH of the pore solution has an impact on chloride binding. This is linked to the stability of chloride containing phases such as AFm and potentially also C-S-H. E.g. found an increase in total chloride binding for a Portland cement (PC) paste when the pH was decreased from 13 to 12. Lowering the pH below 12 reduced chloride binding partly due to dissolution of AFm and most likely a reduction in the adsorption of chlorides by C-S-H until it approached zero at pH 9 [33, 34].

2.2 Chloride ingress prediction models

Several chloride ingress prediction models exist, which aim to estimate chloride ingress in concrete structures based on e.g. concrete composition, execution procedure (curing) and exposure conditions [4, 6, 35-37]. Depending on the model and the input parameters used, widely different estimates are obtained [37]. Thus, there is a need to increase the validity and reliability of chloride ingress prediction models.

Chloride ingress prediction models range from taking only total chloride into consideration [4, 6, 38], over free chloride and hydroxyl [21] to finally include practically all ions present in the system [36, 39].

Many empirical chloride ingress prediction models are based on the error function solution to Fick's 2nd law of diffusion considering the total chloride content as the driving force [4, 6, 38, 40]. Motivations for this include that the governing ingress mechanism is considered to be diffusion and although only free chloride ions are able to penetrate concrete by diffusion and initiate corrosion, methods for determining free chloride are questionable [41]. When the error function solution to Fick's 2nd law of diffusion is fitted to experimental data, the apparent diffusion coefficient, D_a , is known to decrease over time and the surface content, C_s , is known to increase [37]. Hence, an ageing factor is often applied to transform D_a to a time dependent variable [4, 6]. Additionally, in some cases C_s is treated as time dependent [20, 21]. In recognition of that an ageing factor applied to D_a at the entire lifespan can lead to optimistic service life estimations, Life-365 only applies an ageing factor for the first 25 years [42].

Reactive transport models exist, which combine physical transport modeling (e.g. Nernst-Planck and Poisson) with chemical equilibrium modeling (e.g. GEMS and PHREEQC). Examples include Stadium [36], DuCOM [39] etc. [43, 44]. As an example physical aspects of Stadium consist in that it in addition to diffusion of ions and moisture, takes the effects of dissolution/precipitation reactions into account. The diffusion of multiple ions present in the system is modeled by solving sets of extended Nernst-Planck and Poisson equations. Capillary suction is calculated by a diffusion equation. The effects of dissolution/precipitation reactions are modeled through a chemical equilibrium code, which is uncoupled from the transport phenomena. First all equations are written at the microstructural level, where after they are averaged over a Representative Elementary Volume (REV) in order to describe the transport process at a macroscopic level [36, 45]. However, the disclosed information and user-friendliness of the reactive transport models vary.

An overview of selected chloride ingress prediction models is given in Appendix E.

3. Approach

Section 1.1 list the set of objectives put forth to answer the goal of the PhD study and in Table 1 in Section 1.3 their link to the associated papers and appendices is given.

The following subsections give a summary of the approach applied to obtain the stated objectives.

3.1 Establishment and evaluation of field data

This section describes the work related to Objective 1: *Establish and evaluate ten years data from the Fehmarn Belt Exposure Site with the purpose of providing data and suggesting which chloride data is suitable for chloride ingress prediction*. Further details are given in Paper II and Paper IV.

Table 2 contains an overview of experimental work conducted after ten years of exposure, related to the scope of this thesis (See Appendix A for conditions at exposure site). Data was obtained and experimental work conducted on panels from both tidal and submerged exposure at the Fehmarn Belt Exposure Site. The main focus was on the well-defined exposure condition submerged, where diffusion is the governing ingress mechanism. Above water additional parameters influence chloride ingress such as height above mean sea level, windspeed and direction, precipitation etc. [46]. The concretes exposed at Fehmarn Belt Exposure Site were divided in two groups. In this study focus was on six well hydrated concrete panels with eqv. w/c of 0.40 covering different powder compositions (Group I, see Table 3 and Appendix B). At the time of initiating the PhD project, data up to five years of exposure was available from the Fehmarn Belt Exposure Site. An overview of testing performed on the listed concretes including testing done after a half, two and five years can be found in Appendix C. All of the experimental work done at exposure times prior to ten years was conducted by technicians at the Danish Technological Institute (DTI). In addition to the concrete panels exposed at Fehmarn Belt Exposure Site, duplicates were exposed in urban environment outside of DTI, Taastrup, Denmark.

Table 2: Overview of experimental work. Conducted experimental work where the candidate has contributed significantly is marked with bold **X**. The concretes exposed at the Fehmarn Belt Exposure Site were divided in two groups. In this study focus was on six well hydrated concrete panels with eqv. w/c of 0.40 covering different powder compositions (Group I, see Table 3 and Appendix B).

Exposure site	Fehmarn Belt Exposure Site				
	Exposure type	Tidal		Submerged	
Concretes (see Table 3 ^a)		Group I	Group II	Group I	Group II
Property	Level ^b [mm]				
Chloride & calcium profiles	-1175, 25	X (W & E)	X (W & E)	X (W & E)	X (W & E)
Elemental profiles	-125			(SG only)	
Microstructure	-1025, -125	x	x	X	
Moisture profiles (macro-, capillary- and gel porosity and degree of capillary saturation)	-1025			X	
Relative humidity	-1025			X	
Portlandite (CH) profiles	-1175			X	
Compressive strength	-875, -725, -575			x	x

a) Concrete compositions and details on constituent materials are given in Table 3 and in further detail in Appendix B.

b) Cores are taken at the given depth (mm) below mean tide level (negative values refer to below mean tide level).

Table 3: Mixture proportions of concrete exposed at the Fehmarn Belt Exposure Site [kg/m³] [15]. Further details are found in Appendix B.

Concrete ID in thesis	PC	15FA	25FA	25FA_SCC	4SF	12FA4SF	12FA4SF_noAEA	12FA4SF_high_wc	12FA4SF_low_wc	12FA4SF_SCC	SG	SG_noAEA	SG_SCC	SG_rapid
Original concrete ID	A	B	C	D	E	F	G	H	I	J	K	L	M	N
Group I	x	x	x		x	x					x			
Group II				x			x	x	x	x		x	x	x
Powder composition [wt.%]	CEM I 42.5N -SR5	100	85	75	75	96	84	84	84	84				
	CEM I 52.5N													30
	CEM III ^a)										100	100	100	
	FA ^b)		15	25	25		12	12	12	12				
	SF ^c)					4	4	4	4	4				
	GGBS ^d)													70
w/(c+2SF+0.5FA+GGBS)	0.40	0.40	0.40	0.40	0.40	0.40	0.40	0.45	0.35	0.40	0.40	0.40	0.40	0.40

a) GGBS content: 67% by wt.

b) FA = Fly ash

c) SF = Silica fume (dry matter)

d) GGBS = Ground Granulated Blast-furnace Slag

To improve the understanding of processes occurring in the outer part of marine exposed concrete and thereby enable a suggestion of which data to utilize for empirical chloride ingress prediction models, additional data was established after ten years (see Table 2).

Prior to the scheduled field investigation, core drilling and laboratory investigations, the need for additional input data for testing of chloride ingress prediction models was assessed. It was identified that the water accessible porosity after six months was required as input for ClinConc. This was not determined earlier. Thus, to provide an estimate, a cylinder was drilled in the submerged part of Group I concretes (PC, 15FA, 25FA, 4SF, 12FA4SF and SG) next to the cylinder for chloride profiling. This cylinder was used to determine the suction porosity in the bulk after drying at 50 °C according to a modified PF-method. This was taken as the best estimate of the water accessible porosity after six months. Additionally, relative humidity and moisture profiles were determined on this cylinder to improve the understanding of the influence of moisture on chloride ingress.

Determination of both chloride profiles and microstructure (elemental zonation) in tidal and submerged exposure allowed a comparison between the two exposure zones for identical concretes.

Portlandite profiles were obtained to enable a comparison between leaching, chloride ingress, moisture and microstructural changes. The decrease in the portlandite profiles towards the exposed surface gives an indication of the extent of leaching. Note that the decrease in portlandite could not be explained by carbonation, as the depth of carbonation was 1-3 mm, whereas the depth of leaching was 10-15 mm. Comparable depths of carbonation were found in tidal and submerged exposure.

Calcium calibration of chloride profiles is used to account for the higher paste fraction in the surface near region due to the wall effect and for stochastic variations in the paste content in concrete in general [51, 52]. Following calcium calibration, the chloride content can be expressed per wt.% of binder. The impact of potential correction of chloride profiles for variation in paste content using calcium profiles was investigated using parallel chloride and calcium profiles on cores from six concrete panels differing in binder compositions determined after a half, two, five and ten years of submerged and tidal exposure.

To evaluate to which extent carbonation should be a concern, carbonation depths were measured at duplicates of PC, 25FA, 12FA4SF and SG after eight years of urban exposure. Measurements were conducted both with thymolphthalein indicator and by optical microscopy. Further details on the conducted experiments can be found in Appendix D.

3.2 The square root method

This section describes the work related to Objective 2: *Test the applicability and limitations of the square root observation [8] for chloride ingress prediction*. Further details are mainly given in Paper I and Paper III.

To test the applicability and limitations of the square root observation [8, 16] for chloride ingress prediction, the following steps were taken:

Various researchers were contacted to obtain field exposure data from in-situ exposed concretes from marine field exposure sites including exposure sites at Fehmarn, Denmark [16]; Träslövsläge, Sweden [9]; Østmarksneset, Norway [10] and Dornoch, Scotland [11]. Analyzed marine exposure conditions include submerged, tidal, splash and atmospheric. Additionally data from concretes exposed in deicing environment at the inland field exposure site RV40, Sweden were analyzed [14]. The locations are shown in Figure 1. Data was achieved from 53 marine exposed concretes and 33 concretes from the inland field exposure site RV40. For each concrete composition and exposure condition data from three to eight exposure times, ranging from six months and up to 31 years, were reported.

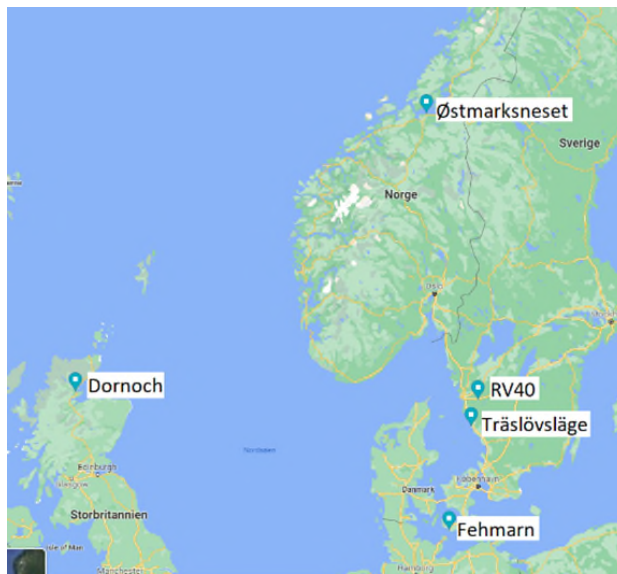


Figure 1: Locations of field exposure sites from which data was achieved.

The square root dependency of a reference chloride content, C_r , proposed for chloride ingress prediction by Poulsen and Sørensen [8], was used to analyze the data:

$$x_{Cr}(t) = a_{Cr} \times \sqrt{t} + b_{Cr} \quad (\text{Eq. 1})$$

where t is the exposure time, $x_{Cr}(t)$ is the depth of C_r at t , and a_{Cr} and b_{Cr} are constants.

By applying the steps described in Figure 2, it was ensured that only data suggested suitable for chloride ingress prediction following Objective 1 was used.

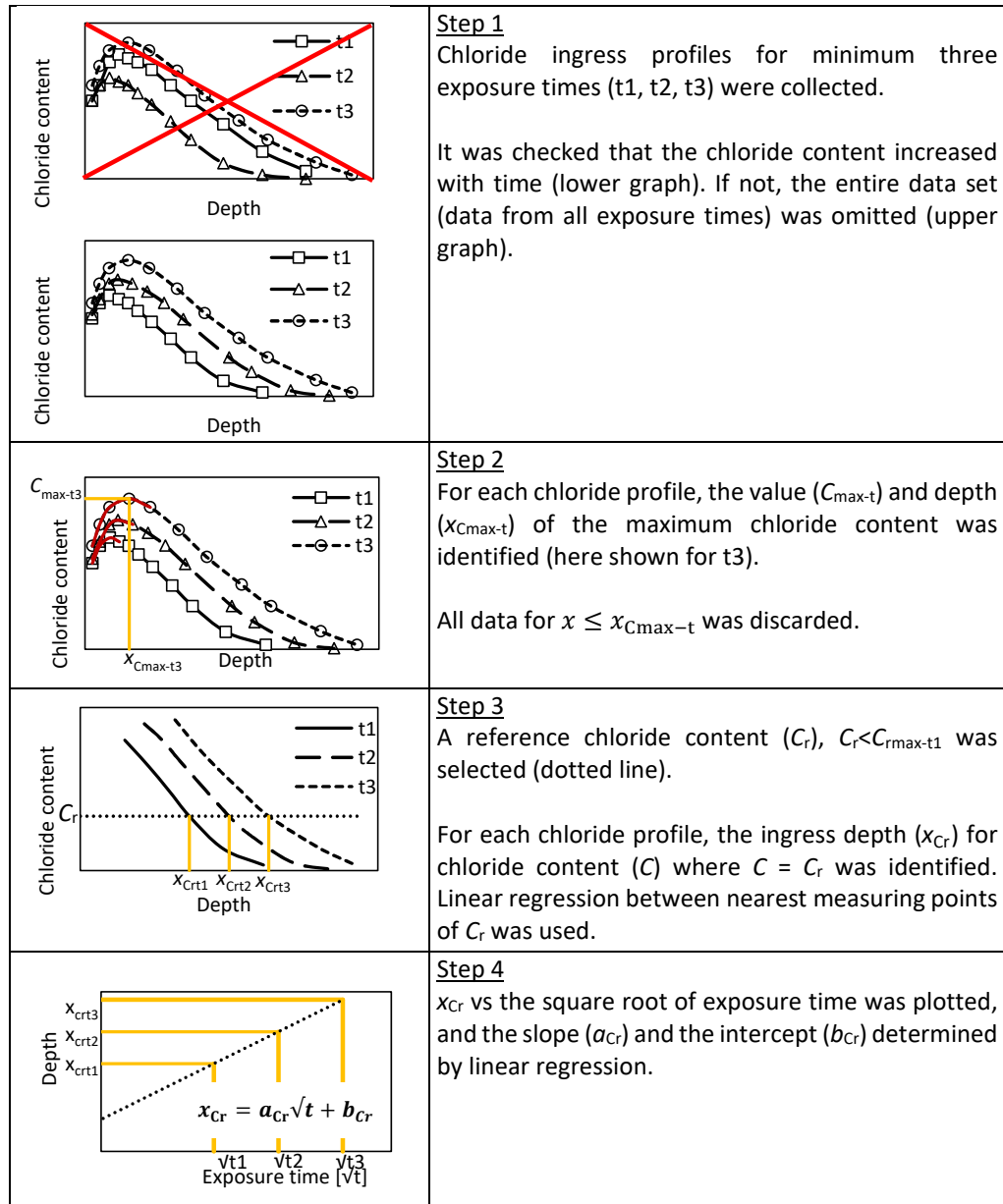


Figure 2: Application of the square root method for determination of the chloride ingress constants a_{C_r} and b_{C_r} (Eq. 1) [19].

Data from 34 concretes adding up to 59 combinations of exposure sites, exposure conditions and concrete compositions qualified through step 1 (Figure 2). For each combination five C_r values were applied, which resulted in 237 sets of a_{C_r} , b_{C_r} and R^2 values.

At the start of exposure ($t=0$), a given concrete contains only the initial chloride concentration, C_i . According to the square root dependency $x_{Cr} = b_{Cr}$ at $t = 0$, so (Eq. 1) is not valid at $t = 0$ and at early exposure times. To test whether the data point corresponding to the earliest t_1 available in this study (203-370 days exposure) was valid, the ingress depth of the reference chloride content C_r of 0.75% chloride by wt. of binder at t_1 was predicted by the square root method using data from t_2 and t_3 and compared to the ingress depth found by linear interpolation on the measured chloride profiles for t_1 . The criterium for a valid t_1 was that no systematic overestimation of x_{Cr} was observed when predicted by the square root method in comparison to the ingress depth found by linear interpolation on the measured chloride profiles.

The applicability of the method to predict further chloride ingress was tested on data sets comprising minimum four sampling times by a prediction where all data sets but the oldest were used and then comparing the predicted result with the measured result for the oldest sampling time.

The influence of exposure environment was investigated by comparing identical concrete compositions exposed in different environments. The influence of binder was investigated by comparing all concretes in submerged exposure at a C_r of 0.25- and 0.75% chloride by wt. of binder. An investigation on the dependency of a_{Cr} , b_{Cr} and R^2 on C_r was undertaken to determine the span of valid C_r and to discover possible trends.

For comparison with established prediction models, the number of data points for the square root method was first transformed to a continuous function, where a_{Cr} and b_{Cr} are functions of C_r . Based on trends in how a_{Cr} and b_{Cr} vary with C_r , a_{Cr} and b_{Cr} can for a given exposure time be described as functions of C_r . In this way individual predicted ingress depths (x_{Cr} 's) can be transformed to a continuous function describing the ingress depth as a function of chloride content for the chosen exposure time by both interpolation and extrapolation (square root function):

$$\text{Square root } f(C_r) = a_{Cr}(C_r) \times \sqrt{t} + b_{Cr}(C_r) \quad (\text{Eq. 2})$$

Advantages of the square root function compared to the square root method include that the chloride content at a given depth can easily be found and that the ingress depth of reference chloride contents $C_r > C_{\max-t_1}$ can be found for $t > t_1$. For C_r values in the interval $C_r + 0.03 < C_r < C_{\max-t_1}$ with a step size of 0.1, the dependency of a_{Cr} on C_r was described by an exponential function and the dependency of b_{Cr} on C_r was described by a linear function. An example of both the interpolation and the extrapolation is shown in Figure 3 for PC submerged. From the expressions of $a_{Cr}(C_r)$ and $b_{Cr}(C_r)$ based on data up to t_3 , extrapolations matching experimental data for t_4 were achieved for $C_r > C_{\max-t_1}$. The method is described in further detail in Paper III. The applicable interval of valid C_r should be further investigated, but as a first approximation, the upper bound of C_r could, based on findings in [17], be the chloride content calculated at the depth of the zone with microstructural changes and the lower bound could be the initial chloride content $C_i + 0.03\%$ by wt. of binder.

Figure 3 also shows the difference between predictions performed by the square root method and the square root function for PC after 10 years of exposure (t_4) based on data up to 5 years of exposure (t_3). The square root function is defined for x values in the interval between the depth of microstructural changes and that where the concentration drops to $C_r + 0.03$. Further details on the square root function can be found in Paper III.

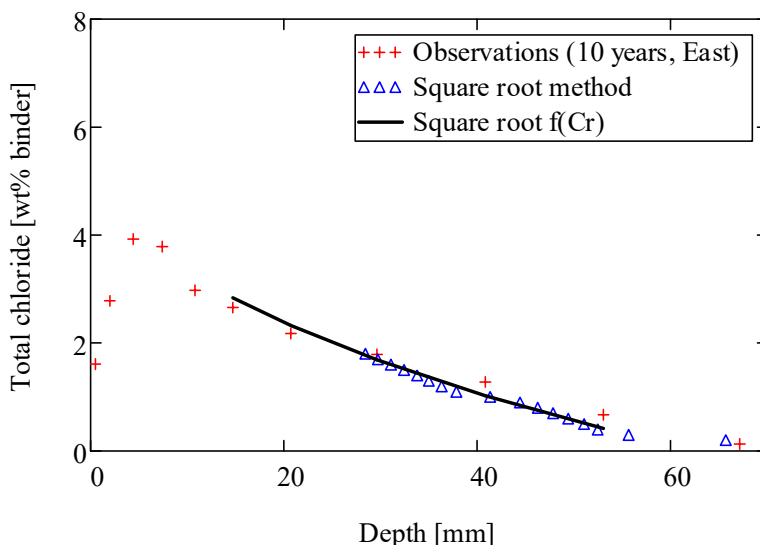


Figure 3: The resulting square root $f(C_r) = x_{Cr(C_r)} = \sqrt{t} \times 17.4 \times e^{-0.39Cr} - 4Cr + 7.95$ for predicting chloride ingress after 10 years in PC based on exposure data up to 5 years (black line) along with ingress depths found by the square root method for predicting chloride ingress after 10 years in PC based on exposure data up to 5 years (blue triangles) and 10 years exposure data for PC east facing panel side after 10 years of submerged exposure (red +).

If the chloride threshold value would be known and within the span of C_r values described in [19], no function of C_r would have to be derived and the ingress of the chloride threshold value (C_r) over time could be found directly by the square root method.

3.3 Comparison of models for chloride ingress prediction

This section describes the work related to Objective 3: *Compare the applicability (design and reassessment) of the square root method with selected established models for chloride ingress prediction.* Further details are found in Paper III.

The applicability in design and reassessment of the square root method [19], which describes a linear relationship when the penetration depth of a reference content is plotted against the square root of the exposure time, was compared with the following selected established models: (i) the *fib* Model Code [4], which include a time-dependent D_a ; (ii) the HETEK model [20], which include both time-dependent D_a and C_s , and (iii) the ClinConc model (engineering expression) [21], which include time-dependent D_a and indirectly time-dependent C_s (through time dependent chloride binding).

The ability of selected chloride ingress prediction models to fit exposure data achieved after ten years of exposure at the Fehmarn Belt Exposure Site was tested based on both design parameters and field exposure data achieved up to five years of exposure.

An overview of the chloride ingress predictions performed for ten years exposure can be found in

Table 4.

Table 4: Overview of input data and performed predictions for ten years exposure (further details in Paper III).

Scenario	Model	Input data				Prediction	
		Lab data (pretesting)		Field data			
				½y	2y		5y
1 Design	<i>fib</i>	D28					
		Chloride binding isotherms					
	ClinConc	D6m					
		Porosity Chloride binding isotherms Thermogravimetric analysis				10y	
HETEK	-						
2 Reassessment	<i>fib</i>	D28		x	x	x	
		C _s 5 years					
	ClinConc	D6m					
		Porosity Chloride binding isotherms Thermogravimetric analysis		x	x	x	10y
		HETEK	-		x	x	x
Square root f(C _r)	-		x	x	x		

Chloride data was obtained from the concrete panels PC, 12FA4SF and SG described in Table B1 in Appendix B. One chloride profile is available for each concrete panel from six months and two years of exposure (west-facing surface), whereas two chloride profiles are available at five and ten years of exposure (both west- and east-facing surface). In the reassessment scenario (2), each chloride profile was used equally, which provides a larger weight on the later exposure times. As mentioned in [17], the chloride profiles from the PC panel measured after two and ten years for the west-facing surface are outliers and therefore not included in this study.

It was chosen to omit the peak chloride content and all measured contents closer to the surface as only after the peak content, the chloride content can be assumed to decrease with increasing depth. It was also chosen to omit data corresponding to total chloride contents below C_r+0.03% by wt. of binder.

Graphs are expressed with chloride content in wt.% of binder calibrated for variation in paste fraction using the calcium content as an indicator for paste fraction assuming no calcareous aggregate and no calcium leaching (at depths from which chloride data is utilized).

The calibration of parameters for reassessment was conducted by minimizing the sum of squared errors (SSE) to field exposure data achieved up to five years of exposure by non-linear Levenberg-Marquardt regression analysis.

For regression equations, which are non-linear in their parameters, R^2 cannot be used to describe the goodness of a fit [47]. Therefore, for both design and reassessment scenarios instead the Root Mean Square Error (RMSE) was used for evaluating the goodness of the fits [48]. The RMSE takes the number of observations into account by a division in the number of data points:

$$RMSE = \sqrt{\frac{SSE}{n}} \quad (\text{eq:3})$$

Where n is the number of observations (utilized data points)

The “measured” data points are here defined as the average between the results measured at the west- and east-facing panel sides after 10 years.

To increase the number of data points for the square root method at which residuals could be found, it was first transformed to a continuous function, where a_{Cr} and b_{Cr} are functions of C_r as described in Section 3.2 and in further detail in Paper III.

4. Main findings

The following subsections give a summary of the main findings for the stated objectives.

4.1 Establishment and evaluation of field data

This section describes the main findings related to Objective 1: *Establish and evaluate ten years data from the Fehmarn Belt Exposure Site with the purpose of providing data and suggesting which chloride data is suitable for chloride ingress prediction*. Further details are given in Paper II and Paper IV.

Chloride profiles after ten years of exposure varied depending on the binder type, but they were for the same binder to a large extent comparable in the submerged and tidal zones. A peaking behavior was observed, and the depth of the maximum chloride content ($x_{C_{max}}$) progressed inwards over time in both tidal and submerged exposure. The maximum chloride content (C_{max}) was in general about 10% higher for tidal exposure compared to submerged exposure. It is noted that for reasons discussed later in this section the chloride profiles, which the discussions in this section are based on, are given in wt.% of concrete and not as wt.% of binder.

A microstructurally changed zone (MCZ) was a general observed feature for all the investigated concretes. After ten years of exposure, the zone extended inwards to a depth of up to ten mm from the exposed surface. The feature was independent of the binder type and observed both for tidal and submerged exposure. Starting from the exposed surface the following was observed: minor surface scaling, a black leached and microcracked zone, a zone with bicarbonate precipitation, and a zone with a diffuse, opaline shine. In earlier studies conducted after two and five years it was established that the black leached zone was rich in magnesium and the opaline zone was rich in sulfur [24, 27]. When comparing to previous results from the same panels [24, 27], it was noted that the depth of the microstructurally changed zone progressed inwards over time.

An example of a comparison of the depth of the microstructurally changed zone (x_{MCZ}) with DCS, portlandite and chloride profiles for concrete 12FA4SF after ten years of submerged exposure is shown in Figure 4. A correlation was observed between chloride profiles and microstructural changes. The depth of the maximum chloride content ($x_{C_{max}}$) was found to almost coincide with the depth of the microscopically changed zone (x_{MCZ}). This is in agreement with literature stating that chloride binding in paste is reduced due to preferred binding of sulfates with aluminates in AFt and adsorption of sulfates on C-S-H [32, 49]. As a result, the maximum chloride content in the paste was observed at the deeper end of the sulfur-rich zone i.e. at the end of the sulfur rich microstructurally changed zone. Moisture ingress into the initially self-desiccated concrete caused the degree of capillary saturation (DCS) to increase towards the exposed surface from a bulk level of about 90% at a depth of 30-40 mm of the submerged concrete. This lower DCS in the bulk compared to the outer surface will limit further chloride ingress by diffusion – e.g. at a DCS of 85-89% as found in this study, the effective diffusion coefficient was found by Olsson et al. [50] to reduce to 45-75% compared to saturated conditions. Due to leaching in the outer zone, all Portlandite profiles decreased from a bulk level towards the exposed surface. For the FA containing concretes,

moisture ingress and Portlandite depletion progressed to a depth far beyond that of the microscopically changed zone.

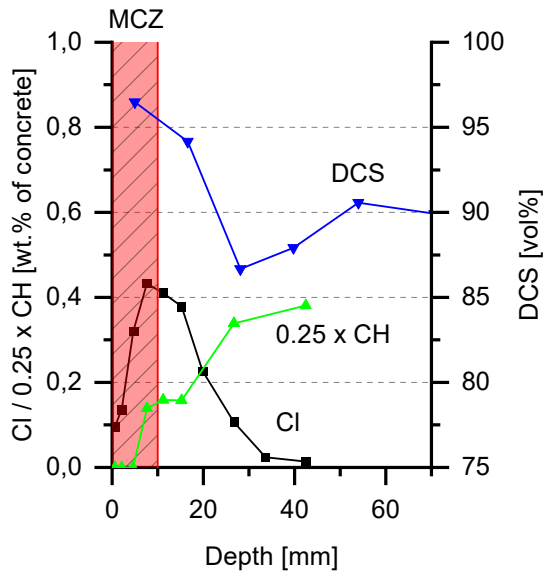


Figure 4: Depth of observed microstructurally changed zone (MCZ) compared to corresponding chloride (Cl), degrees of capillary saturation (DCS) and portlandite (CH) profiles for 12FA4SF after ten years of submerged exposure. In order to fit the results in one graph portlandite has been scaled to one fourth. The chloride and portlandite profiles are given in wt.% of concrete, whereas the DCS is in vol%. All data are from the west facing surface.

A binder dependent increase was observed in $x_{C_{max}}$ from 0.6-2.5 mm after six months to 4.5-10 mm after ten years and in x_{MCZ} from 1-2.5 mm after six months to 4-10 mm after ten years; least progression was observed for slag containing concrete. Examples illustrating the relation between $x_{C_{max}}$ and x_{MCZ} and their evolution over time are shown for 12FA4SF and SG in Figure 5.

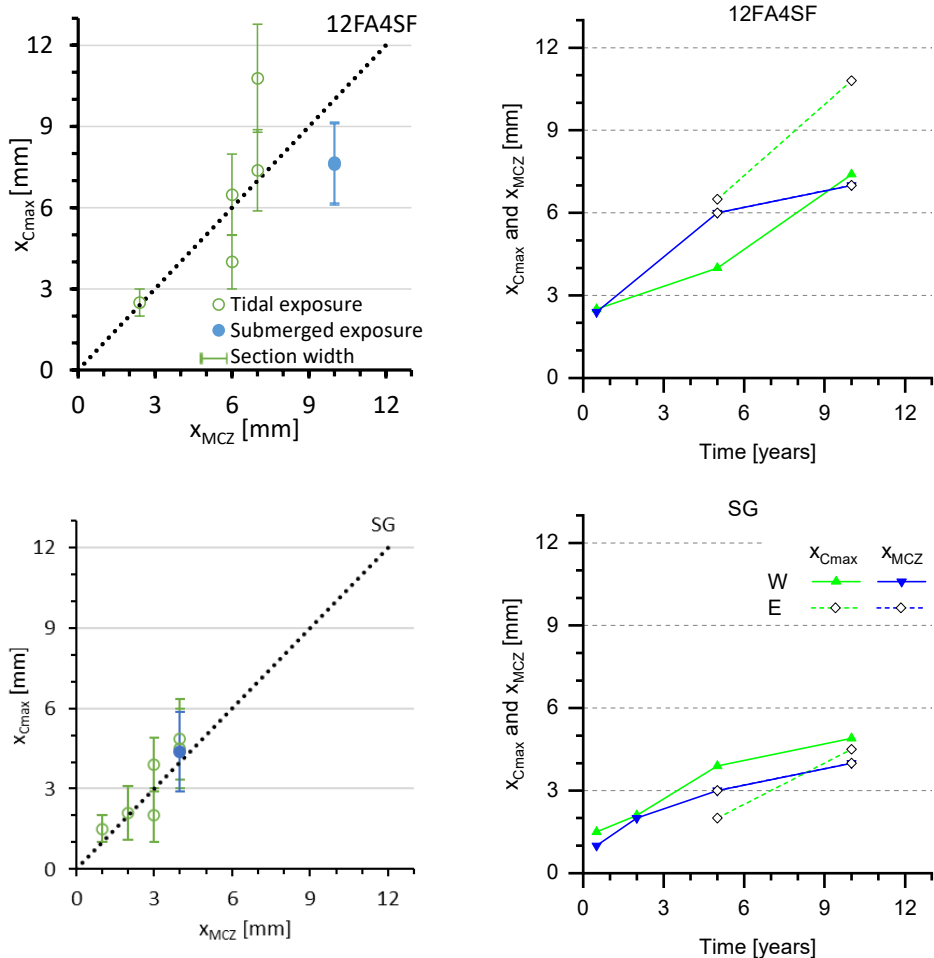


Figure 5: Left side: Comparison of depth of microstructurally changed zone (x_{MCZ}) with depth of maximum chloride content (x_{Cmax}). x_{Cmax} from both the west and east-facing surfaces of the panels are included to give an impression of the uncertainties. Data for the tidal zone covers a half, two, five and ten years while only ten years data are available for the submerged concrete. Unfilled circles = tidal exposure. Filled circles = submerged exposure. The line $x = y$ is included as a guidance for the eye. Right side: Development of x_{Cmax} and x_{MCZ} over time. The figure is based on chloride profiles given in wt.% of concrete. For simplicity only data from tidal zone is shown. Note that x_{MCZ} for west and east facing surface of the panels overlap for the examples 12FA4SF and SG.

In Papers II and IV, the chloride content is not calibrated to parallel calcium measurements because after five to ten years of exposure, the calcium content in the surface near region (up to ten mm) was observed to decrease systematically (see Paper IV). For PC, 15FA, 4SF and 12FA4SF a drop in calcium content due to leaching extending from the surface and beyond x_{Cmax} caused C_{max} to artificially increase with time. A consequence of calibrating to calcium content was that the calibrated chloride content in the surface near region increased more over time than the uncalibrated – an effect which intensified with proximity to the concrete surface. In some cases, the depth dependent impact of calibration on C_{max} affected x_{Cmax} .

Although the calcium content varied in depth and time in the surface near zone due to both the wall-effect [51, 52] and leaching, calibration for the paste fraction based on the calcium content may account for unsystematic variations in paste fraction between samples at depths unaffected by calcium leaching.

Based on the experimental investigations, it is recommended that data from the microstructurally changed zone are excluded when using data from the Fehmarn Belt Exposure Site - and other field data - for testing of chloride ingress prediction models unless reactive transport models are used. When data from the microstructurally changed zone are excluded, it can be an advantage to perform calibration for paste fraction based on calcium content (assuming non-calcareous aggregates are used in the concrete). However, the repeatability of the calcium determination should be checked.

The carbonation depths after eight years of urban exposure were measured at ten different locations on samples of PC, 25FA, 12FA4SF and SG by both thymolphthalein indicator (80 mm wide sample) and optical microscopy (40 mm wide samples) (see Appendix D). Although the measured mean was similar for the two methods, a larger range was found for optical microscopy. Carbonation depths after 120 years based on an assumption of the carbonation depth being linear with square root time were predicted to less than 2 mm for PC and 12FA4SF, whereas SG reached 4.0 mm (mean), 7.9 mm (max) and 25FA reached 9.1 mm (mean), 25.1 mm (max). Based on these predicted carbonation depths, carbonation is not expected to be a cause of reinforcement corrosion of the Fehmarn Belt link in a 120 years' time frame.

4.2 The square root method

This section describes the main findings related to Objective 2: *Test the applicability and limitations of the square root observation [8] for chloride ingress prediction*. Further details are given in Paper I.

After applying the square root method for a total of 237 times (49 profiles – not all on five C_r values) on the collected field exposure data, a linear relationship was found, with an average R^2 of 0.96, when plotting the penetration depth of the reference chloride content (C_r) against the square root of the exposure time [19].

The square root method appeared valid for marine exposed concrete in submerged, tidal, splash and atmospheric zone. Too little data passing Step 1 of the square root method was available for assessing the applicability for concrete exposed to de-icing salts, as most of the data from de-icing exposure did not unambiguously show an increase in chloride content with time.

The square root method appeared valid for the investigated PC, SF, FA, FA+SF and GGBS containing concretes. For the investigated concretes and conditions, a_{cr} was found to be constant after 200 days of exposure, which was the earliest t_1 available in this study. The square root method was found to be valid for the whole range of tested reference chloride contents (C_r): 0.125–1.80% chloride by wt. of binder for submerged, tidal and low splash; 0.1–0.5% chloride by wt. of binder for high splash and atmospheric exposure. A decreasing trend of a_{cr} with increasing C_r was observed for submerged and tidal exposure. It was most

pronounced for PC, SF and GGBS containing concretes. A clear decreasing trend of b_{cr} with increasing C_r was observed for FA, SF and SF+FA containing concretes in submerged and tidal exposure.

For the limited number of concretes from Träslövsläge for which minimum five data points of up to 20 years was available (approximately one, two, five, ten and 20 years), the deviation between the predicted and measured ingress depth was found to be similar for the measured ingress depths up to ten years to which the prediction was fitted (9% deviation) as to the measured ingress depth at 20 years, which was not used for fitting the straight line (12% deviation). Figure 6 gives an illustration of the ability of the square root method to predict future chloride ingress. The data from Träslövsläge is shown in the top left. A similar approach was applied for concretes from the Fehmarn Belt Exposure Site, where data up to five years was used to predict ingress after ten years (see Figure 6). For all graphs shown in Figure 6 it is seen that the hollow symbols which represent the measured chloride ingress depths after 10 or 20 years are rather close to the predicted ingress lines which are based on the earlier observations shown as filled symbols. This demonstrates that the square root method can be used to predict future chloride ingress.

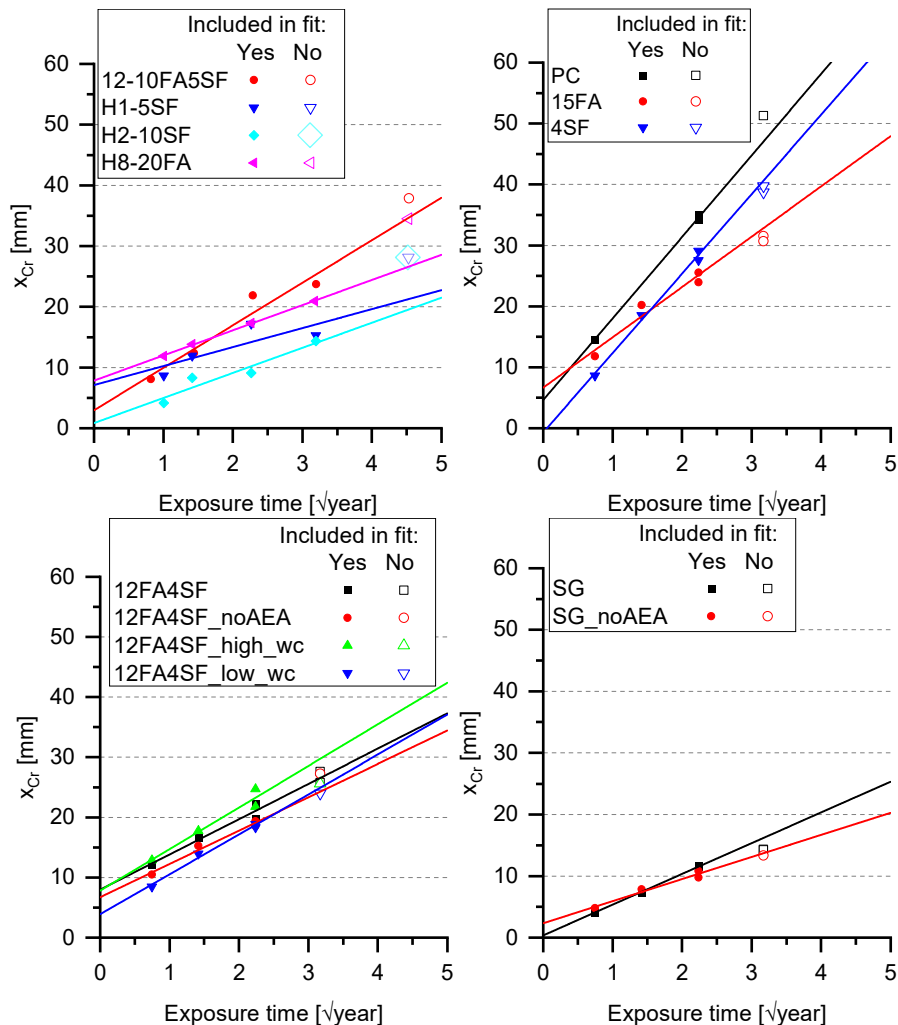


Figure 6: Top left: Predicted versus measured chloride ingress ($C_r = 0.75\%$ chloride by wt. of binder) at 20 years for four submerged concretes exposed at Träslövsläge Field Exposure Site. Prediction was made from data up to ten years exposure (shown with filled markers). The symbol size of the data point for T-H2-10SF_sub, which was not included in the fit is doubled to distinguish it from that of T-H1-5SF_sub. The wt.% of supplementary cementitious material is given by the name – e.g. 20FA means 20 wt.% of the binder is FA. Top right: Predicted versus measured chloride ingress ($C_r = 0.75\%$ chloride by wt. of binder) for PC, 15FA and 4SF after ten years of submerged exposure at Fehmarn Field Exposure Site. Predictions were made from data up to five years exposure (shown with filled markers). Bottom row: as top right but for variants of 12FA4SF and SG.

4.3 Comparison of models for chloride ingress prediction

This section describes the main findings related to Objective 3: *Compare the applicability (design and reassessment) of the square root method with selected established models for chloride ingress prediction.* Further details are found in Paper III.

At the current stage, the square root method is not applicable for design. The square root method is therefore only included for reassessment.

For evaluation of goodness of fit, the Root Mean Square Errors (RMSE) between predicted and measured datapoints in the interval $C_i + 0.03 < C_r < C_{\max-t4}$ were determined for PC, 12FA4SF and SG. To allow this, the square root method was expressed as a continuous function of C_r (see Section 3.2 and Paper III). The RMSE determined when applying the HETEK and ClinConc models and the fib Model Code, for design are shown in the left graph in Figure 7; and RMSE determined for the HETEK and ClinConc models, the fib Model Code, and the square root $f(C_r)$ when used for reassessment are shown in the right graph in Figure 7. As expected, the goodness of fits (RMSE) was generally better (lower) when the models were calibrated to field data (Reassessment) compared to when design values were used (Design) – spanning from 0.09-0.66 when calibrated (reassessment) vs. 0.28-1.37 when design values were used (see Figure 7).

For reassessment the square root $f(C_r)$ predicted with the lowest RMSE for 12FA4SF, whereas a prediction on par with ClinConc and fib model code was achieved for PC and SG (RMSE ranging from 0.09-0.42 for the square root $f(C_r)$ vs 0.22-0.66 for the remaining models).

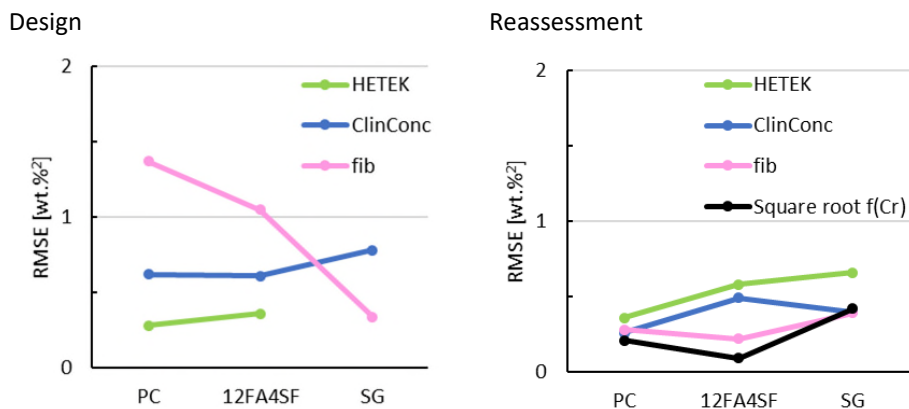


Figure 7: Evaluation of ability to fit exposure data achieved after 10 years of submerged exposure. The RMSE determined when applying the HETEK and ClinConc models and the fib Model Code, for design are shown in the left; RMSE determined for the HETEK and ClinConc models, the fib Model Code, and the square root $f(C_r)$ when used for reassessment are shown in the right.

5. Conclusion

Below the objectives and their main conclusions are given.

1. Establishment and evaluation of field data

- Objective 1: Establish and evaluate ten years data from the Fehmarn Belt Exposure Site with the purpose of providing data and suggesting which chloride data is suitable for chloride ingress prediction.
 - 1) Chloride profiles after ten years of exposure in the submerged and the tidal zones were to a large extent comparable. A maximum chloride content below the concrete surface was observed in both tidal and submerged exposure. The maximum chloride content was in general about 10% higher for tidal exposure compared to submerged exposure.
 - 2) For all the investigated concretes, a microstructurally changed zone (MCZ) was a generally observed feature, its depth (x_{MCZ}) which was found to almost coincide with the depth of the maximum chloride content ($x_{C_{max}}$). A steady increase was observed in $x_{C_{max}}$ from 0.6-2.5 mm after six months to 4.5-10 mm after ten years and in x_{MCZ} from 1-2.5 mm after six months to 4-10 mm after ten years depending on binder type with least progression for the slag containing concrete.
 - 3) The calcium content in the surface near region (up to ten mm) was observed to decrease systematically over time. For PC, 15FA, 4SF and 12FA4SF a drop in calcium content due to leaching extending from the surface and beyond $x_{C_{max}}$ caused C_{max} to artificially increase with time.
 - 4) Based on the above it is recommended that data from the microstructurally changed zone (MCZ) are excluded when using data from the Fehmarn Belt Exposure Site - and other field data - for verification of chloride ingress prediction models unless reactive transport models are used. When data from the microstructurally changed zone are excluded, it can be an advantage to perform calibration for paste fraction based on calcium content (assuming non-calcareous aggregates are used in the concrete). Though the repeatability of the calcium determination should be checked.

2. The square root method

- Objective 2: Test the applicability and limitations of the square root observation [8] for chloride ingress prediction.
 - 1) It was concluded that the square root method showed promising capabilities for predicting further chloride ingress based on data from depths beyond the microstructurally changed zone.
 - 2) Chloride ingress in marine submerged, tidal, splash and atmospheric exposure showed that the ingress depth of a fixed reference chloride content is a linear function of the square root of time.

- 3) In general, a decreasing ingress rate with increasing reference chloride content was observed for submerged and tidal exposure (not investigated for splash and atmospheric). The trend was clear for plain Portland cement concrete, silica fume and slag containing concretes, but for fly ash containing concretes the ingress rate appeared independent of the reference content.
- 4) The ingress rate for a given reference content for each combination of the investigated concretes and conditions, was constant in the investigated timespan (approximately 200 days of exposure and up to 21 years).
- 5) A method description was developed for using the square root observation and a function was developed, which allows x_{Cr} to be described as a continuous function of C_r (interpolation) and to describe x_{Cr} for $C_r > C_{max-t1}$ for $t > t1$ (extrapolation).

3. Comparison of models for chloride ingress prediction

- Objective 3: Compare the applicability (design and reassessment) of the square root method with selected established models for chloride ingress prediction.
 - 1) The square root method is only applicable for reassessment – not yet in the design stage.
 - 2) The goodness of fits measured as Root Mean Square Error (RMSE) was generally better (lower) when the models were calibrated to field data compared to when design values were used – in the range 0.09-0.66 when calibrated vs. 0.28-1.37 when design values were used.
 - 3) In a reassessment scenario, where parameters optimized on observations achieved within 5 years of exposure at the Fehmarn Belt Exposure Site are used to predict chloride ingress after 10 years of exposure, the square root $f(C_r)$ predicts with the lowest RMSE for 12FA4SF, whereas a prediction on par with ClinConc and *fib* model code is achieved for PC and SG (RMSE ranging from 0.09-0.42 for the square root $f(C_r)$ vs 0.22-0.66 for the remaining models).

6. Perspectives and future research opportunities

6.1 Field data; collection and application

Frequently, measured chloride profiles are described in greater detail near the surface to describe the part of the chloride profiles where large variations are observed. However, as found in Paper II, the data near the surface is subject to microstructural changes and therefore not recommended to be used for chloride ingress prediction models unless reactive transport models are used. Further, as shown in Paper IV, calcium is leached out at depths exceeding the depth of the maximum chloride content, which renders the calcium content in this zone a poor indicator of the paste fraction after exposure and thereby not an appropriate measure to correct for the higher paste fraction near the surface due to geometrical constraints (the “wall-effect”).

The purpose of service life modeling is to predict when a critically high concentration of chlorides has penetrated through the concrete and reached the embedded steel reinforcement. Rebars are located deeper than the position of the maximum chloride content which implies that microstructural changes and leaching are limited deeper into the concrete, and chloride data can be calibrated for the paste fraction based on the calcium content. Further, the chloride threshold values are typically much lower than the maximum chloride contents observed in this study [53]. Thus, it might be advantageous using data from the non-microstructurally changed zone only.

6.2 Reassessment

As described in Paper I and III, the square root method shows promising capabilities for predicting future chloride ingress for reassessment purposes based on chloride profiles from three different time steps. The square root method is an example of a method capable of predicting chloride ingress using data, which:

- is from the non-microstructurally changed zone only.
- is unaffected by the “wall-effect”.
- can be calibrated for the paste fraction based on calcium content as described in Paper IV.

6.3 Design

Although the square root method is promising for predicting continued chloride ingress, further work must be done to improve the usefulness in the design phase. It was found that a_{Cr} and b_{Cr} in the square root method depend on multiple factors including concrete composition (binder type and w/b), exposure, and chosen C_r . Further research could investigate how a_{Cr} and b_{Cr} depend on these factors and additional factors for which sufficient data were not available. Artificial intelligence could be trained on datasets with known results such as the 237 results published as electronic “Supplementary Material 2” for Paper I [19] and used for interpolation. Analysis on additional field data could extend the current limitations for interpolation to include e.g. field data from warmer climates. For the investigated concretes and conditions, a_{Cr} was found to be constant after 200 days of exposure, which was the earliest t_1 available in this study. It is not excluded that earlier data could be applicable – this should be investigated as earlier data could potentially significantly increase the span of data points on the square root time axis and facilitate the use in pretesting.

6.4 Future research

Chloride ingress predictions were performed only by using mean values corresponding to a 50% risk of failure. Probabilistic predictions could be performed to provide a probability distribution of the estimated service life.

7. References

- [1] U. Jönsson, The development of the Concrete requirements for the Fehmarnbelt Fixed Link, Femern A/S, 2015.
- [2] L. Bertolini, B. Elsener, P. Pedferri, E. Redaelli, R. Polder, Corrosion of steel in concrete, Wiley Online Library, 2013.
- [3] K. Tuutti, Corrosion of steel in concrete, Swedish Cement and Concrete Research Institute, Stockholm, 1982.
- [4] *fib*, Model code for service life design - bulletin 34, fédération internationale du béton (*fib*), Lausanne, Switzerland, 2006.
- [5] M.R. Geiker, M.A.N. Hendriks, B. Elsener, Durability-based design: the European perspective, Sustainable and Resilient Infrastructure 2021 1-16.
<https://doi.org/10.1080/23789689.2021.1951079>.
- [6] S. Englund, General guidelines for durability design and redesign: DuraCrete, probabilistic performance based durability design of concrete structures [Gouda]: [CUR], 2000.
- [7] M.R. Geiker, C. Edvardsen, Service life design of reinforced concrete structures, developments in the Danish approach, Proceedings of the 3rd International Conference on Service Life Design for Infrastructure. Keynote Speech, 2014.
- [8] S.L. Poulsen, H.E. Sørensen, Chloride ingress in old Danish bridges, Proceedings 2nd International Congress on Durability of Concrete (ICDC), New Delhi, India, 2014.
- [9] D. Boubitsas, L. Tang, P. Utgenannt, Chloride Ingress in Concrete Exposed to Marine Environment-Field data up to 20 years' exposure, CBI Report to SBUF Project 12684 2014.
- [10] O. Skjolsvold, H. Justnes, T. Hammer, P. Fidjestol, Long-term chloride intrusion in field-exposed concrete with and without silica fume, Ninth CANMET/ACI International Conference on Fly Ash, Silica Fume, Slag, and Natural Pozzolans in Concrete, 2007, pp. 199-210.
- [11] J. Kim, W.J. McCarter, B. Suryanto, S. Nanukuttan, P.M. Basheer, T.M. Chrisp, Chloride ingress into marine exposed concrete: A comparison of empirical-and physically-based models, Cement and Concrete Composites 72 2016 133-145. <https://doi.org/10.1016/j.cemconcomp.2016.06.002>.
- [12] A. Lindvall, Chloride Ingress in a Swedish Road Environment: Five Years Exposure for Three Concrete Compositions, 1st ed., Chalmers University of Technology, Göteborg, 2002.
- [13] L. Tang, P. Utgenannt, Chloride Ingress and Reinforcement Corrosion in Concrete under De-Icing Highway Environment-A study after 10 years' field exposure, SP Technical Research Institute of Sweden, Borås, 2007.
- [14] L. Tang, D. Boubitsas, P. Utgenannt, Z. Abbas, Chloride Ingress and Reinforcement Corrosion-After 20 years' field exposure in a highway environment, RISE Research Institutes of Sweden, 2018.
- [15] Fehmarnbelt Exposure Site, 2015. <http://www.concreteexpertcentre.dk/30663>. (Accessed 15th of March 2021).
- [16] S.L. Poulsen, H.E. Sørensen, U. Jönsson, Chloride ingress in concrete blocks at the Rødbyhavn marine exposure site – Status after 5 years, 4th International Conference on Service Life Design for Infrastructures (SLD4), Delft, Netherlands, 2018, pp. 192-203.
- [17] S. Fjendbo, H.E. Sørensen, K.d. Weerd, M.R. Geiker, Correlating the development of chloride profiles and microstructural changes in marine concrete up to ten years, Manuscript submitted for publication 2021.
- [18] S. Fjendbo, H.E. Sørensen, K.d. Weerd, M.R. Geiker, When and How Should Chloride Profiles be Calibrated for Paste Fraction?, Manuscript submitted for publication 2021.
- [19] S. Fjendbo, H.E. Sørensen, K. De Weerd, M.R. Geiker, The square root method for chloride ingress prediction—Applicability and limitations, Materials and Structures 54 2021 61.
<https://doi.org/10.1617/s11527-021-01643-8>.
- [20] L. Mejlbro, The complete solution of Fick's second law of diffusion with time-dependent diffusion coefficient and surface concentration, in: P. Sandberg (Ed.), Durability of concrete in saline environment, Cementa AB, Lund, Sweden, 1996, pp. 127-158.

- [21] L. Tang, Engineering expression of the ClinConc model for prediction of free and total chloride ingress in submerged marine concrete, *Cement and Concrete Research* 38(8-9) 2008 1092-1097. <https://doi.org/10.1016/j.cemconres.2008.03.008>.
- [22] F.P. Glasser, J. Marchand, E. Samson, Durability of concrete – Degradation phenomena involving detrimental chemical reactions, *Cement and Concrete Research* 38(2) 2008 226-246. <https://doi.org/10.1016/j.cemconres.2007.09.015>.
- [23] L. Tang, Chloride transport in concrete-measurement and prediction, Chalmers University of Technology, Gothenburg, Sweden, 1996.
- [24] U.H. Jakobsen, K. De Weerd, M.R. Geiker, Elemental zonation in marine concrete, *Cement and Concrete Research* 85 2016 12-27. <https://doi.org/10.1016/j.cemconres.2016.02.006>.
- [25] J. Marchand, E. Samson, D. Burke, P. Tourney, N. Thaulow, S. Sahu, Predicting the Microstructural degradation of concrete in marine environment, *Special Publication* 212 2003 1127-1154.
- [26] A. Chabreli, E. Gallucci, K. Scrivener, U. Müller, Durability of field concretes made of Portland and silica fume cements under sea water exposure for 25 years, *Nordic Exposure Sites – Input to revision of EN206-1, Hirtshals, Denmark, 2008*, pp. 275-294.
- [27] U.H. Jakobsen, Microstructural surface deterioration of concrete exposed to seawater; results after 2 years of exposure, *14th Euroseminar on Microscopy Applied to Building Materials, Helsingør, Denmark, 2013*.
- [28] P.K. Mehta, P.J. Monteiro, *Concrete: microstructure, properties, and materials*, McGraw-Hill Education, 2014.
- [29] N.R. Buenfeld, J.B. Newman, The development and stability of surface layers on concrete exposed to sea-water, *Cement and Concrete Research* 16(5) 1986 721-732. [https://doi.org/10.1016/0008-8846\(86\)90046-3](https://doi.org/10.1016/0008-8846(86)90046-3).
- [30] K. De Weerd, H. Justnes, M.R. Geiker, Changes in the phase assemblage of concrete exposed to sea water, *Cement and Concrete Composites* 47 2014 53-63. <https://doi.org/10.1016/j.cemconcomp.2013.09.015>.
- [31] K. De Weerd, H. Justnes, The effect of sea water on the phase assemblage of hydrated cement paste, *Cement and Concrete Composites* 55 2015 215-222. <https://doi.org/10.1016/j.cemconcomp.2014.09.006>.
- [32] K. De Weerd, D. Orsáková, M.R. Geiker, The impact of sulphate and magnesium on chloride binding in Portland cement paste, *Cement and Concrete Research* 65 2014 30-40. <https://doi.org/10.1016/j.cemconres.2014.07.007>.
- [33] K. De Weerd, Chloride binding in concrete – recent investigations and recognised knowledge gaps: RILEM Robert L’Hermite Medal Paper 2021, *Materials and Structures* in press.
- [34] P. Hemstad, A. Machner, K. De Weerd, The effect of artificial leaching with HCl on chloride binding in ordinary Portland cement paste, *Cement and Concrete Research* 130 2020 105976. <https://doi.org/10.1016/j.cemconres.2020.105976>.
- [35] L. Nilsson, P. Sandberg, E. Poulsen, L. Tang, A. Andersen, J.J.D.R.D.R. Frederiksen, HETEK, a system for estimation of chloride ingress into concrete, *Theoretical background*, 83 ed., Danish Road Directorate Denmark, 1997.
- [36] J. Marchand, Modeling the behavior of unsaturated cement systems exposed to aggressive chemical environments, *Materials and Structures* 34(4) 2001 195-200. <https://doi.org/10.1007/BF02480588>.
- [37] L. Tang, L.-O. Nilsson, P.A.M. Basheer, *Resistance of concrete to chloride ingress: Testing and modelling*, 1st ed., Spon Press, London, 2012.
- [38] M. Collepardi, A. Marcialis, R. Turriziani, The kinetics of chloride ions penetration in concrete, *Il cemento* 67 1970 157-164.
- [39] Y. ELAKNESWARAN, T. ISHIDA, Development Of A Physical And Geochemical Model For Long-Term Performance Of Cementitious Materials, *Society for Social Management Systems Internet Journal* 2012.

- [40] A.J.M. Siemes, C. Edvardsen, T.N.O. Bouw, Duracrete: Service life design for concrete structures, in: M.A. Lacasse, D.J. Vanier (Eds.) NRC Research Press, Ottawa, Canada, 1999.
- [41] U. Angst, B. Elsener, C.K. Larsen, Ø. Vennesland, Critical chloride content in reinforced concrete—A review, *Cement and concrete research* 39(12) 2009 1122-1138. <https://doi.org/10.1016/j.cemconres.2009.08.006>.
- [42] Life-365™ Consortium III, Life-365™ v2. 23 User's Manual, 2018. <http://life-365.org/>. (Accessed 10-10 2021).
- [43] V.Q. Tran, A. Soive, V. Baroghel-Bouny, Modelisation of chloride reactive transport in concrete including thermodynamic equilibrium, kinetic control and surface complexation, *Cement and Concrete Research* 110 2018 70-85. <https://doi.org/10.1016/j.cemconres.2018.05.007>.
- [44] A. Michel, V. Marcos-Meson, W. Kunther, M.R. Geiker, Microstructural changes and mass transport in cement-based materials: A modeling approach, *Cement and Concrete Research* 139 2021 106285. <https://doi.org/10.1016/j.cemconres.2020.106285>.
- [45] J. Marchand, E. Samson, Y. Maltais, R. Lee, S. Sahu, Predicting the performance of concrete structures exposed to chemically aggressive environment—Field validation, *Materials and Structures* 35(10) 2002 623-631. <https://doi.org/10.1007/BF02480355>.
- [46] O. Skjølsvold, Gimsøystraumen Bru: spesialinspeksjon 1992-kloridprofiler. Vudering av kloridbelastning og-diffusjonskoeffisient, 1st ed., Statens Vegvesen, Oslo, 2001.
- [47] A.-N. Spiess, N. Neumeyer, An evaluation of R 2 as an inadequate measure for nonlinear models in pharmacological and biochemical research: a Monte Carlo approach, *BMC pharmacology* 10(1) 2010 1-11. <https://doi.org/10.1186/1471-2210-10-6>.
- [48] G. Smith, *Essential statistics, regression, and econometrics*, 2nd ed., Academic press, London, UK, 2015.
- [49] P.K. Mehta, *Concrete in the marine environment*, 1st ed., CRC Press, London, 2019.
- [50] N. Olsson, B. Lothenbach, V. Baroghel-Bouny, L.-O. Nilsson, Unsaturated ion diffusion in cementitious materials—The effect of slag and silica fume, *Cement and Concrete Research* 108 2018 31-37. <https://doi.org/10.1016/j.cemconres.2018.03.007>.
- [51] R. Zou, A. Yu, The packing of spheres in a cylindrical container: the thickness effect, *Chemical engineering science* 50(9) 1995 1504-1507. [https://doi.org/10.1016/0009-2509\(94\)00483-8](https://doi.org/10.1016/0009-2509(94)00483-8).
- [52] F. De Larrard, *Concrete mixture proportioning: a scientific approach*, 1st ed., CRC Press, London, 1999.
- [53] Y. Cao, C. Gehlen, U. Angst, L. Wang, Z. Wang, Y. Yao, Critical chloride content in reinforced concrete—An updated review considering Chinese experience, *Cement and Concrete Research* 117 2019 58-68. <https://doi.org/10.1016/j.cemconres.2018.11.020>.
- [54] Google, [Map showing location of Fehmarn Belt Exposure Site]. <https://goo.gl/maps/hbGYJgbSeqPDC9JL9>. (Accessed June 8 2020).
- [55] A.D. Herholdt, C.F.P. Justesen, P. Nepper-Christensen, A. Nielsen, *Beton-Bogen, Cementfabrikkernes tekniske oplysningskontor, Aalborg Portland, Aalborg, Denmark*, 1985.
- [56] DS-EN 197-1:2011, *Cement - Part 1: Composition, specifications and conformity criteria for common cements*, Danish standard.
- [57] DS/EN 196-2:2013, *Method of testing cement - Part 2: Chemical analysis of cement*, Danish Standard.
- [58] E. Poulsen, L. Mejlbro, *Diffusion of chloride in concrete: theory and application*, 1st ed., Taylor & Francis, London, 2006.

Part II – Appended papers

Paper I

The square root method for chloride ingress prediction – Applicability and limitations

Materials and structures, volume 54 issue 2 article 61 (2021)

Simon Fjendbo; Henrik E. Sørensen; Klaartje De Weerd; Mette R. Geiker



The square root method for chloride ingress prediction— Applicability and limitations

Simon Fjendbo · Henrik E. Sørensen · Klaartje De Weerd · Mette R. Geiker

Received: 2 October 2020 / Accepted: 31 January 2021 / Published online: 4 March 2021
© The Author(s) 2021

Abstract A recent observation showed a square root time dependency of the ingress depth of a fixed (reference) chloride concentration of 0.05% chloride by mass of concrete for submerged exposure in Kattegat and the Baltic Sea. The purpose of this paper is to assess the applicability and limitations of the observation, widen the scope of validity and propose it as a method. Field data from submerged, tidal, splash, atmospheric and inland deicing salt exposure at various geographical locations was analyzed at a range of reference concentrations. In total 237 combinations of concrete, exposure, and reference concentration were analyzed. Our results showed that chloride ingress of a reference concentration followed a linear relationship with an average R^2 of 0.96, when the penetration depth of the reference concentration was plotted against the square root of the exposure time. The square root observation appeared valid for the studied Portland cement based concretes with fly

ash, silica fume and ground granulated blast furnace slag exposed in submerged and tidal exposure zones, when applying reference concentrations of 0.1–1.8% chloride by mass of binder, and reference concentrations of 0.1–0.5% chloride by mass of binder in atmospheric exposure zone. It was found that the parameters describing the straight line depended on the chosen reference concentration and concrete composition, and that the slope of the straight line (ingress parameter) in addition depended on the exposure. It was concluded that the square root method appears to be a promising method for predicting further chloride ingress into concrete.

Keywords Concrete · Chloride ingress · Diffusion · Field exposure · Service life prediction

1 Introduction

It is of increasing importance to predict the long-term chloride ingress in concrete as ever longer design service life requirements are prescribed. Roughly, two types of models for chloride ingress prediction exists: empirical and physical. Empirical models are widely used by engineers in practical applications, which is probably due to their simplicity relative to physical models. Physical models seek to model chloride ingress by e.g. including free chloride as driving

Supplementary Information The online version contains supplementary material available at <https://doi.org/10.1617/s11527-021-01643-8>.

S. Fjendbo (✉) · H. E. Sørensen
Danish Technological Institute, Taastrup, Denmark
e-mail: simon.fjendbo@ntnu.no

S. Fjendbo · K. De Weerd · M. R. Geiker
Department of Structural Engineering, Norwegian
University of Science and Technology (NTNU),
Trondheim, Norway



force, chloride binding, additional transport processes besides diffusion, multi-ionic characteristics, moisture and dissolution/precipitation reactions [1–3].

Empirical chloride ingress models generally require fewer input parameters. Commonly chloride ingress is modeled by the error function solution to Fick's 2nd law of diffusion for a semi-infinite medium. The total chloride content is often considered as the driving force, although only free chloride is available for diffusion [4–7]. To account for the observed decrease of the diffusion coefficient over time, often ingress prediction models include an ageing function [1, 4–11]. A drawback of the ageing function is that it causes the chloride ingress to stop at infinite age (the diffusion coefficient goes towards zero). To avoid this issue, the service life model Life 365 keeps the apparent chloride diffusion coefficient (D_a) constant after 25 years exposure [12]. The surface concentration (C_s) is constant in many models, although it has been observed to increase over time. The HETEK model takes this into account by a time dependent surface concentration [8] based on work by Mejlbro [11]. Finally, the maximum concentration is often observed at a certain depth; either due to convection (as accounted for in e.g. [4]) or due to elemental zonation and leaching [13, 14], which is currently only accounted for by omitting the outer measuring point(s) when fitting data [4].

Another empirical approach to predict chloride ingress could be to follow the ingress of a chloride concentration of interest (e.g. the critical chloride content) rather than the entire chloride profile. Poulsen and Sørensen [15] observed a linear relationship between a reference concentration of 0.05% chloride by mass of concrete and the square root of time and termed this the “square root observation”. Poulsen et al. [16] showed an excellent correlation with experimental data of up to 20 years for submerged exposure in Träslövsläge Field Exposure Site in Kattegat and up to five years for submerged exposure at Fehmarn Belt Exposure Site.

According to Poulsen et al. [16] the ingress depth of a reference concentration of 0.05% chloride by mass of concrete ($x_{0.05}$) can for their data be described by Eq. (1).

$$x_{0.05}(t) = a_{0.05} \times \sqrt{t} + b_{0.05} \quad (1)$$

where $a_{0.05}$ is the slope of a straight line, when $x_{0.05}$ is plotted against the square root of exposure time, and $b_{0.05}$ is the intercept. Poulsen et al. [16] interpreted $a_{0.05}$ as an indicator for the long-term chloride penetration rate of the reference concentration ($C_r = 0.05\%$ chloride by mass of concrete), while $b_{0.05}$ is interpreted as an indicator for the ingress relatively faster than $a_{0.05}$ occurring at early age. Hereafter the slope of the straight line for a C_r is mentioned as a_{C_r} (ingress parameter), the intercept as b_{C_r} (early ingress depth), and the ingress depth as x_{C_r} .

In the square root observation, the ingress parameter is constant with square root of exposure time and the challenge of the chloride ingress approaching zero exponentially for long term exposure is thereby overcome. However, the analysis by Poulsen et al. [16] only applied the square root method on data from submerged exposure at Fehmarn Belt and Träslövsläge Exposure Sites and only for a reference concentration of 0.05% chloride by mass of concrete.

Covering other types of exposure (wetting and drying), Thomas and Matthews [17] plotted the depth of penetration of 0.4% chloride by mass of binder versus the square root of exposure time for concrete with water-to-cement ratio (by mass) (w/c) 0.37–0.57 and 0–50% fly ash (FA) substitution for tidal exposure. They found that the ingress depth of 0.4% chloride by mass of binder was 18–21 mm already after 28 days, but only increased to 28–31 mm after ten years for concrete with 30% FA substitution [17]. Thomas and Matthews [17] plotted the ingress depth of 0.4% chloride by mass of binder versus the square root of time, but did not mention a linear relationship, although the graph indicated it.

Baroghel-Bouny et al. [18] found a linear relationship with a R^2 of > 0.95 between the average free chloride penetration depth measured by 0.1 N AgNO₃ spray test (assumed equal to 0.15% chloride by mass of binder) and the square root of the number of wetting–drying cycles after 10 years at marine tidal field exposure.

Based on the observations by Thomas and Matthews [17], Baroghel-Bouny et al. [18], Poulsen and Sørensen [15] and Poulsen et al. [16] it is likely that the observation of an ingress depth versus square root of time dependency can be generalized. The square root observation is based on a very simple linear relationship between the ingress depth of a single reference



concentration and the square root of exposure time. This linear relationship is consistent with the error function solution to Fick's 2nd law of diffusion for a semi-infinite medium with constant D_a and C_s [5]. However, the square root observation adds an intercept value to account for early ingress.

This paper formulates the square root observation as a method and analyzes the applicability to describe chloride ingress by including field data from submerged, tidal, atmospheric and inland deicing salt exposure at various geographical locations. Five different reference concentrations were analyzed for each exposure condition and geographical location. By applying the square root method on additional exposure conditions, it can be tested under which conditions the square root method is applicable.

2 Data

This paper analyzes data from a number of studies of in-situ exposed concretes from marine field exposure sites including exposure sites at Fehmarn, Denmark [16]; Träslövsläge, Sweden [19]; Østmarksneset, Norway [20] and Dornoch, Scotland [21]. Analyzed marine exposure conditions include submerged, tidal, splash and atmospheric. Further analyzed are data from concretes exposed in deicing environment at the inland field exposure site RV40, Sweden [22]. For each concrete composition and exposure condition data from three to eight exposure times, ranging from six months and up to maximum 31 years, were reported.

An overview of exposure conditions, curing and sampling is given in Table 1. An overview of mixture proportions of the analyzed concretes is given in Table 2. All cement notations are according to EN 197-1 [23]. The nomenclature (IDs) used in this study reflects the exposure site and the original ID used in the reference paper. When results obtained from the concretes are displayed in figures, the label additionally includes the content of supplementary cementitious materials (SCMs) and information on the exposure type, e.g. F-G12FA4SF_sub stands for Fehmarn Belt Exposure Site, concrete G, which include 12% fly ash (FA) and 4% silica fume (SF) and is exposed at submerged exposure. Binder types are described in groups comprising plain Portland cement (PC) and blends with FA, SF, ground

granulated blast furnace slag (GGBS) and combinations of fly ash and silica fume (FA + SF).

3 The square root method for chloride ingress prediction

The square root dependency of a constant (reference) chloride concentration, C_r , proposed for chloride ingress prediction by Poulsen and Sørensen, was used to analyze the data [15, 32]:

$$x_{C_r}(t) = a_{C_r} \times \sqrt{t} + b_{C_r} \quad (2)$$

where t is the exposure time, $x_{C_r}(t)$ is the depth of C_r at t , and a_{C_r} and b_{C_r} are constants.

The method was applied using the steps described in Fig. 1.

3.1 Selection of input data for the square root method

In this study, only data sets with minimum three exposure times were used, and for which the chloride fronts penetrating from opposing sides of the specimens did not overlap. The entire data set (data from all exposure times) was omitted when lower chloride ingress was measured at a given exposure time relative to an earlier exposure time. This was the case for the combinations of concrete and exposure listed in Table 3.

A minimum exposure time of 200 days was applied in this study and the applicability of the data from the first exposure time was checked (see Sect. 5.1). The minimum exposure time was selected based on studies by Tang [33]. Investigating a range of binders (PC, SF) and w/b (0.32–0.70) Tang [27] found six months as sufficient time for laboratory samples to obtain an insignificant change of properties [e.g. water assessable porosity and diffusivity determined by the rapid chloride migration test (RCMT)] for prediction of free and total chloride ingress in submerged marine concrete using the so-called engineering expression of the ClinConc model [1].

3.2 Selection of input parameters for the square root method

Based on the range of observed $C_{\max-t}$ values (see Online Resource 1), two sets of C_r values were chosen.



Table 1 Overview of exposure conditions, curing and sampling at included exposure sites

Exposure	Marine				Deicing RV40
	Fehmarn	Träslövs läge	Østmarks neset	Dornoch	
Exposure site					
Main reference(s)	[16]	[19]	[20]	[21]	[22, 24, 25]
Number of concrete types	14	11	3 (6 ^a)	1	1
Exposure					
Marine					
Submerged	×	×		× ^{b)}	
Tidal	×		×	×	
Splash				×	
Atmospheric		×		×	
Inland					
Deicing					×
Avg. temperature (atmosphere) (°C)	10 ^c	8 ^d	5 ^e	9 ^f	6 ^f
Avg. temperature (seawater) (°C)	9 ^g	11 ^h	8 ^e	9 ⁱ	NA
Chloride content (seawater) (g/l)	7 ^g	14 ^h	17 ^e	20 ⁱ	NA
Age at exposure					
(days)	–	9–19	28 ^e	35 ⁱ	37 ^j
(maturity days)	40–49	–	28 ^e	–	–
Thickness of specimens (mm)	200	100	500	1593	300
Sampling (years)	0.5, 2, 5	0.7, 1, 2, 5, 10, 20	1.5, 14, 21.5, 31	1.3, 2.3, 2.8, 3.3, 4.2, 5.5, 6.3, 21	1–2, 5, 10, 20
Diameter of extracted cores (mm)	100	100	100	30	100
Method for chloride analysis	k	k	^l (1.5 years) ^m (14 years +)	n	k
Method for paste correction	o	o	p	q	o

^aPairwise identical

^bConcrete exposed below mid tide level claimed to be permanently saturated, although not permanently submerged[21]

^c[26]

^d[27]

^e[20]

^f[28]

^g[29]

^h[19]

ⁱ[30]

^j[22, 31]

^kProfile grinding followed by potentiometric titration principally in accordance with AASHTO T260/NT BUILD 208

^lSawing of discs. Crushed and boiled in distilled water followed by potential measurements

^mProfile grinding followed by nitric acid treatment and spectrophotometric analyses with iron thiocyanate as color indicator in accordance with SINTEFs procedure KS70 109

ⁿBS1881 part 124 and BS 6337 part 4

^oChloride content corrected for potential variations in paste content as function of profile depth by using measured calcium profiles

^pCalculated based on concrete composition

^qUnknown



Table 2 Mixture proportions of concretes used in this study

Field exposure site	Fehmarn													
Concrete ID in this study	F-A	F-B	F-C	F-D	F-E	F-F	F-G	F-H	F-I	F-J	F-K	F-L	F-M	F-N
<i>Mixture proportions of concrete exposed at Fehmarn Belt Exposure Site (kg/m³) [16]</i>														
Original concrete ID	A	B	C	D	E	F	G	H	I	J	K	L	M	N
Powder composition (wt%)														
CEM I	100	85	75	75	96	84	84	84	84	84				
FA ^a		15	25	25		12	12	12	12	12				
SF ^b					4	4	4	4	4	4				
CEM III											100	100	100	100
CEM I-SR5 42.5 N ^c	365	322	300	336	340	300	310	276	330	350				
CEM I 52.5 N ^c														108
CEM III/B 42.5 N ^{c,d}											360	375	410	
FA		57	100	112		43	44	39	47	50				
SF (added as slurry)					14	14	15	13	16	17				
GGBS ^e														252
Water	146	140	140	157	147	140	145	145	135	163	144	150	164	144
Sand	695	671	642	678	695	677	731	700	671	687	689	702	686	689
Coarse aggregates	1172	1182	1179	1053	1172	1192	1182	1182	1182	1067	1161	1185	1065	1162
w/(c + 2SF + 0.5 FA)	0.40	0.40	0.40	0.40	0.40	0.40	0.40	0.45	0.35	0.40	0.40	0.40	0.40	0.40
w/b ^f	0.40	0.37	0.35	0.35	0.42	0.39	0.39	0.44	0.34	0.39	0.40	0.40	0.40	0.40
Field exposure site	Träslövsläge													
Concrete ID in this study	T-1	T-OE	T-2	T-3	T-10	T-12	T-H1	T-H2	T-H4	T-H5	T-H8			
<i>Mixture proportions of concrete exposed at Träslövsläge Field Exposure Site (kg/m³) [19]</i>														
Original concrete ID	1–35	OE	2–40	3–35	10–40	12–35	H1	H2	H4	H5	H8			
Powder composition (wt%)														
CEM I	100	100	100	95	78.5	85	95	90	95	95	80			
FA					17	10					20			
SF				5	4.5	5	5	10	5	5				
CEM I-SR5 42.5 N					330									
CEM I-SR3 42.5 N	450	430		428		383	475	450	399	523	493			
CEM I 42.5 R			420											
FA					71	45					123			
SF (added as slurry)							25	50	21	28				
SF (added as powder)				23	19	23								
Water	158	163	168	158	148	146	150	150	168	138	159			
Sand	839	813	871	801	770	781	836	820	840	806	680			
Coarse aggregates	839	840	804	868	905	917	942	963	840	946	865			
w/(c + 2SF + 0.5 FA)	0.35	0.38	0.40	0.33	0.37	0.33	0.29	0.27	0.38	0.24	0.29			
w/b	0.35	0.38	0.40	0.35	0.35	0.33	0.30	0.30	0.40	0.25	0.26			
Field exposure site	Østmarkneset							Dornoch		RV40				
Concrete ID in this study	Ø-EF	Ø-EF	Ø-GH	Ø-GH	Ø-IJ	Ø-IJ	Dor		RV206					
<i>Mixture proportions of concrete exposed at Østmarkneset [20], Dornoch [21] and RV40 field exposure sites (kg/m³) [22, 24, 25]</i>														
Original concrete ID	E	F	G	H	I	J					206			



Table 2 continued

Field exposure site Concrete ID in this study	Østmarkneset						Dornoch	RV40
	Ø-EF	Ø-EF	Ø-GH	Ø-GH	Ø-IJ	Ø-IJ	Dor	RV206
Powder composition (wt%)								
CEM I	80	80	90	90	80	80	100	95
SF	20	20	10	10	20	20		5
CEM I 52.5 R	234	234	457	457	394	394		
CEM I 42.5 N							460	
CEM I-SR3 42.5 N								399
SF (as slurry)	47	47	46	46	79	79		21
Water	194	194	204	204	218	218	184	168
Sand	847	847	752	752	749	749	700	860
Coarse aggregates	1032	1032	919	919	905	905	1050	860
w/(c + 2SF + 0.5 FA)	0.59	0.59	0.37	0.37	0.40	0.40	0.40	0.38
w/b	0.69	0.69	0.41	0.41	0.46	0.46	0.40	0.40

^aFA = Fly ash^bSF = Silica fume (dry matter)^cAccording to EN 197-1^dGGBS content: 67 wt%^eGGBS = Ground granulated blast furnace slag^fWater-to-binder ratio (by mass)

One set for submerged and tidal exposure and another set for splash, atmospheric, and deicing exposure, see Table 4. When choosing the maximum C_r value a compromise was made between (1) ensuring that all C_r values could be applied for all concretes (maximum $C_r \leq$ minimum $C_{\max-t1}$) and (2) including the widest possible span of C_r values. The compromise was made slightly below the 20th percentile of the $C_{\max-t1}$ values, thus ensuring that all C_r values were tested for at least 80% of the concretes. The remaining up to 20% of the concretes (see Table 4) were still tested at lower C_r values present in those concretes. Additionally, four reference concentrations were chosen as the pentiles. All chloride profiles are given in Online Resource 1 with the utilized C_r values marked as horizontal lines.

4 Results

Before applying the square root method on all the data (Sect. 2), it was checked, whether the assumption made in the methods section (Sect. 3), that a_{C_r} is constant, when using data after minimum 200 days exposure ($t1$), is correct.

4.1 Applicability of the chosen $t1$

Initially, it was verified whether the $t1$ applied in this study i.e. 203–370 days, is sufficient to have reached insignificant changes of properties as mentioned in Sect. 3.1. The result of this verification is seen in Fig. 2, where the ingress depth of $C_r = 0.75\%$ chloride by mass of binder ($x_{0.75}$) at $t1$ predicted by the square root method using data from $t2$ and $t3$ is compared to the ingress depth found by linear interpolation on the measured chloride profiles for $t1$. Data from submerged exposure for Fehmarn Belt and Träslövsläge Field Exposure Sites (Fig. 2a) as well as data from tidal exposure from Fehmarn Belt Exposure Site (Fig. 2b) was used for this comparison.

The data points are closely distributed around the line $x = y$ with a single outlier on either side, which indicate, that the chloride profiles from $t1$, can be used in the square root method without any systematic change of a_{C_r} and b_{C_r} . The remaining data series show similar behavior. This implies that for the investigated concretes and exposures, the quality of the datapoint ($x_{C_r-t1}, t1$) is as good as the remaining data points.



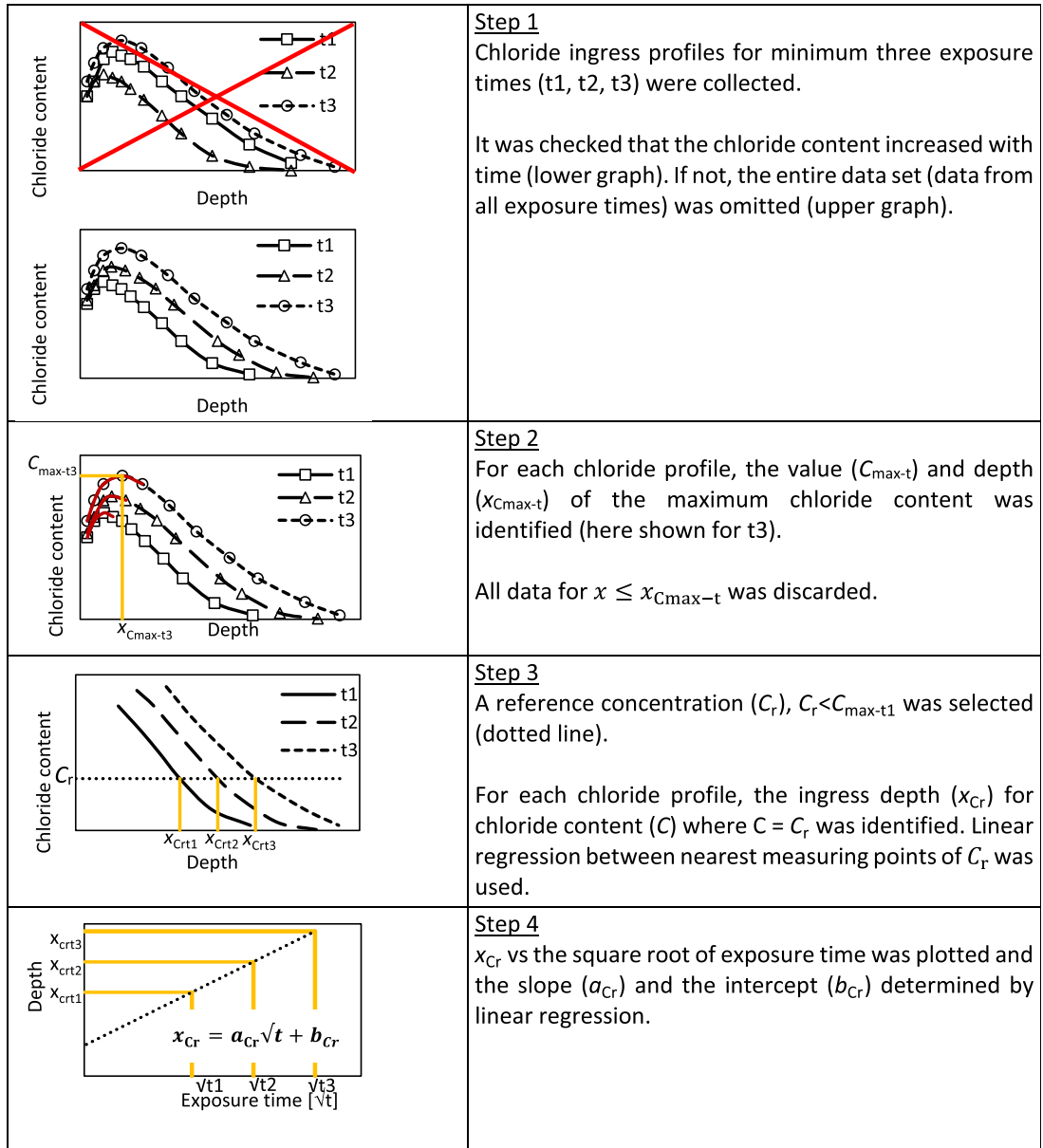


Fig. 1 Application of the square root method for determination of the chloride ingress constants a_{Cr} and b_{Cr} (Eq. 3)

4.2 Application of the square root method

Data from 59 combinations of exposure site, exposure condition and concrete were treated by the method described in Fig. 1 for five different C_r values. The

resulting a_{Cr} , b_{Cr} and R^2 values (237 sets in total) are tabulated in Online Resource 2.

Figure 3 illustrates the results of the application of the square root method at five different C_r values on



Table 3 Excluded combinations of concrete and exposure conditions due to measured lower chloride ingress at a given exposure time relative to an earlier exposure time

Exposure	Fehmarn (see Table 2)	Träslövsläge (see Table 2)
Submerged	F-A, F-C	T-1, T-3
Tidal	F-F	–
Atmospheric	–	T-OE, T-H2, T-H3, T-H5, T-H8

Table 4 Range, average and 20th percentile of observed $C_{\max-t1}$ and chosen range of C_r for all analyzed concretes and exposure types

Exposure	$C_{\max-t1}$ (% by mass of binder)			Sets of selected C_r (%by mass of binder)	Concretes, where max C_r was not present at t1 (see Online Resource 1)
	Range	Average	20th percentile		
Submerged	0.68–3.62	2.01	1.38	0.25, 0.50, 0.75, 1.00 and 1.25	F-M, F-N, T-H5
Tidal	0.44–3.70	2.07	1.37		F-M
Splash	0.76–0.78	0.77	^a	0.10, 0.20, 0.30, 0.40 and 0.50	
Atmospheric	0.65–0.93	0.83	0.73		
Deicing	0.80	0.80	^a		

^aToo little data to perform statistical analysis

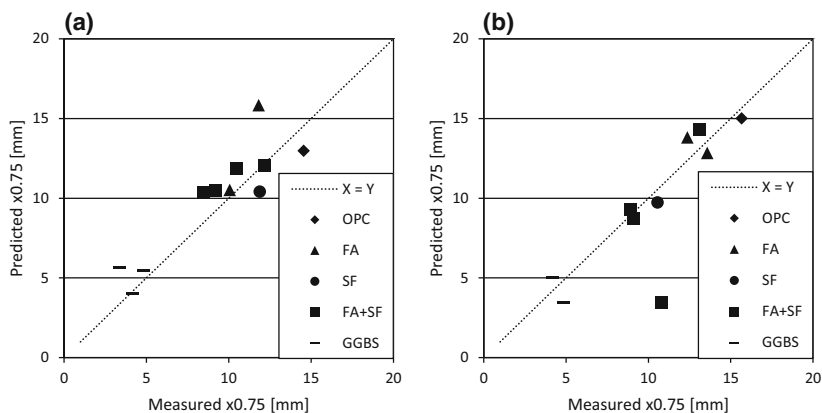


Fig. 2 The ingress depth of a concentration of 0.75% chloride by mass of binder ($x_{0.75}$) at $t1$ predicted by the square root method using data from $t2$ and $t3$ compared to the ingress depth found by linear interpolation on measured data for $t1$. $t1$ varied

concrete T-H8 submerged exposed at Träslövsläge Field Exposure Site.

between 203 and 217 days. **a** Data from submerged exposure for Fehmarn and Träslövsläge was used. **b** Data from tidal exposure from Fehmarn was used. A dotted straight line corresponding to $x = y$ is drawn as guidance

5 Discussion

This section includes discussions on the impact of the choice of C_r on a_{C_r} , b_{C_r} , R^2 and x_{C_r} . Further the impact of exposure condition and binder is treated and hypotheses for the observed linearity of x_{C_r} versus



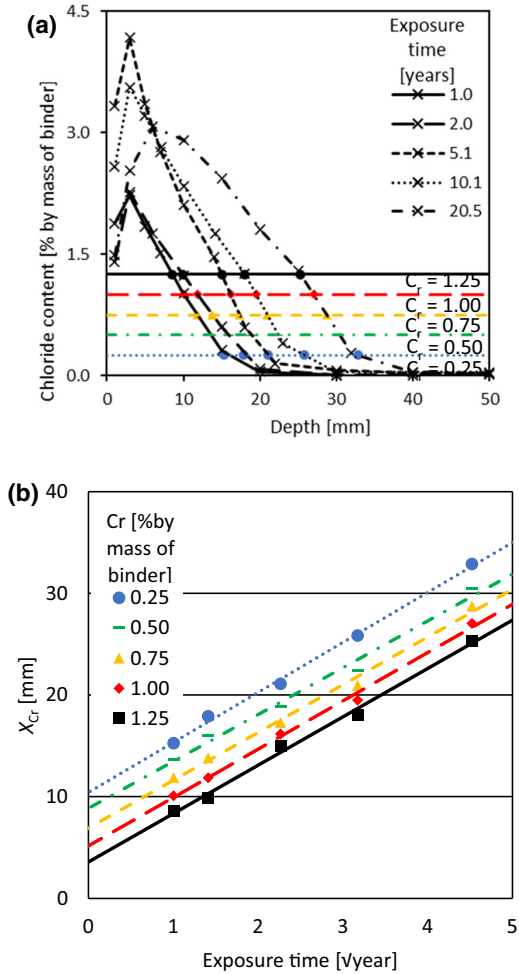


Fig. 3 Application of the square root method at five different C_r values (in % chloride by mass of binder) on concrete T-H8 submerged exposure at Träslövsläge Field Exposure Site. **a** Example of application of step 3 of the square root method (see Fig. 1). Concrete T-H8 exposed submerged at Träslövsläge Field Exposure Site (see Table 3). Interpolated ingress depths of $C_r = 0.25, 0.50, 0.75, 1.00$ and 1.25% chloride by mass of binder are marked with symbols. **b** Example of application of step 4 of the square root method (Eq. 3; see Fig. 1). Concrete T-H8 submerged exposed at Träslövsläge Field Exposure Site (see Table 3). x_{Cr} = penetration depth of C_r

\sqrt{t} are proposed. Finally, the ability of the square root method to predict further ingress is evaluated and suggestions are given on how to use the method.

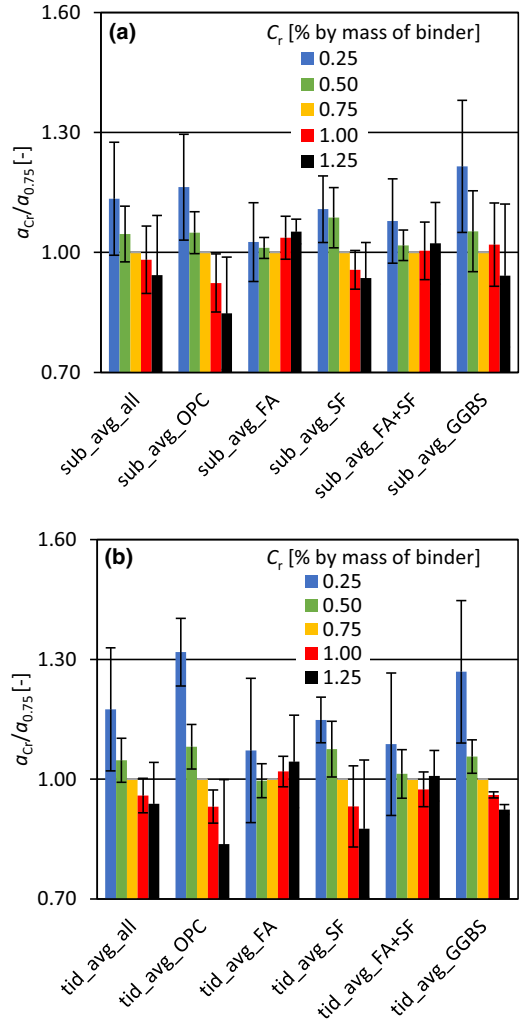


Fig. 4 Influence of chosen C_r on average a_{Cr} value for concretes based on different binders in **a** submerged and **b** tidal exposure. Note that a_{Cr} is normalized to $a_{0.75}$. Error bars show ± 1 standard deviation

5.1 Impact of reference concentration, C_r

As mentioned in Sect. 3, to apply the square root method a reference concentration, C_r , must be chosen. In this section, the influence of the chosen C_r is discussed. The datasets for submerged and tidal exposure are used, as they represent the widest variety of concretes and identical C_r values, see Online Resource 2.



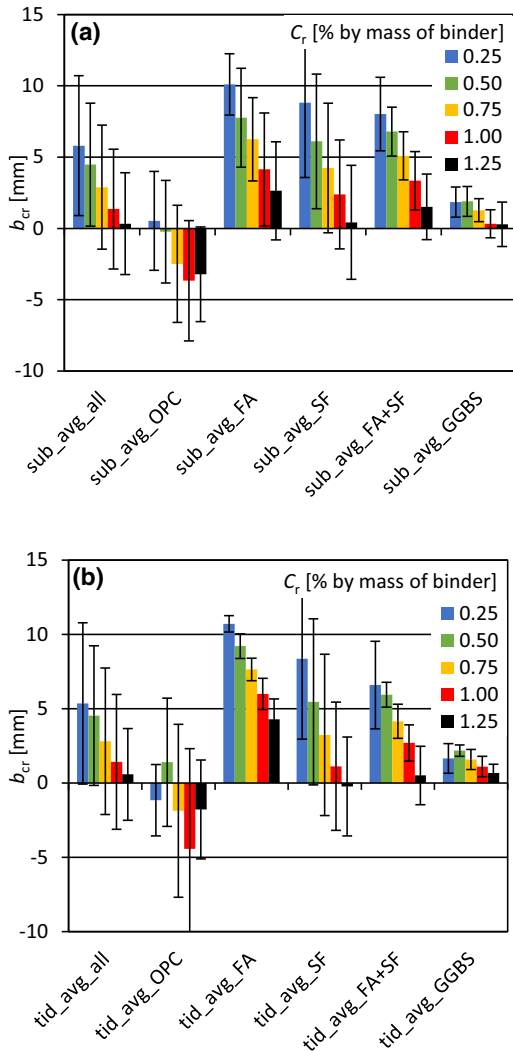


Fig. 5 Influence of chosen C_r on average b_{C_r} value for concretes based on different binders in **a** submerged and **b** tidal exposure. Error bars show ± 1 standard deviation. Note that the values of b_{C_r} are not normalized as some $b_{0.75}$ are near zero and the corresponding concretes thus affect the average too much

The influence of C_r on a_{C_r} , b_{C_r} and R^2 is separated by binder type and exposure to highlight potential differences. The influence of binder is further treated in Sect. 5.4.

5.1.1 Impact of C_r on a_{C_r}

Figure 4 shows the calculated ingress parameter, a_{C_r} , as a function of the reference chloride concentration, C_r , for submerged conditions (Fig. 4a) and tidal conditions (Fig. 4b). For each combination of concrete and exposure, a_{C_r} is normalized to $a_{0.75}$. Thereafter the results are grouped and averaged per binder type (PC, FA, SF, FA + SF, GGBS); see Online Resource 3 for an example of how data is normalized and averaged. From Fig. 4 it is seen, that there is in general a slightly decreasing trend of $a_{C_r}/a_{0.75}$ with increasing C_r . This trend is most pronounced for PC, SF and GGBS containing concretes, whereas $a_{C_r}/a_{0.75}$ for concretes with FA (FA and FA + SF) is almost independent of the C_r . The varying dependency between binders of $a_{C_r}/a_{0.75}$ on C_r implies that $a_{C_r}/a_{0.75}$ could be higher for a concrete based on binder i than binder ii at one C_r , while the opposite is the case at another C_r (See Online Resource 4).

Figure 4 shows decreasing $a_{C_r}/a_{0.75}$ with increasing C_r . This means, that the calculated ingress parameter is lower for higher C_r . Physically this observed trend coincide with a reduction in the driving force for diffusion, as the concentration gradient decreases with increasing C_r (all other things being equal).

When comparing the results from submerged exposure (Fig. 4a) with the ones from tidal exposure (Fig. 4b), there is a trend that $a_{0.25}/a_{0.75}$ is higher for tidal exposure than for submerged exposure irrespective of the binder type.

5.1.2 Impact of C_r on b_{C_r}

The impact of the selected C_r on b_{C_r} is illustrated in Fig. 5. It is seen that b_{C_r} depends on both C_r and the binder composition. A clear decreasing trend of b_{C_r} with increasing C_r is seen for FA, SF and SF + FA containing concretes independent of exposure condition (submerged and tidal). The analyzed PC and GGBS containing concretes have b_{C_r} values near 0 irrespective of C_r in the range 0.25–1.25. This implies that a_{C_r} governs the chloride ingress for the analyzed PC and GGBS concretes.

Figure 5 shows a decreasing b_{C_r} with increasing C_r . This might be explained by two competing sets of mechanisms:

- (i) Capillary suction and high diffusivity at early age

Poulsen et al. [16] interpreted b_{Cr} as partly due to initial capillary suction due to self-desiccation or partial drying and partly due to limited degree of hydration resulting in a concrete, which is initially more permeable than in a more mature state. Thus, it is expected that chloride ingress proceeds faster initially, than what can be described by a_{Cr} alone. This leads to a positive contribution to b_{Cr} .

- (ii) Gradual phase changes and increasing C_{max} .

Selecting a high C_r which is only present in the concrete after e.g. 4 years, the intercept at the x -axis of the straight line constituting x_{Cr} versus the square root of time (step 4, Fig. 1) would be 2 ($\sqrt{4}$). As the ingress parameter a_{Cr} is positive, this implies that b_{Cr} is negative. An increasing C_{max} could e.g. be caused by phase changes as ions from the sea water such as chloride are bound in the system and others leached [13, 34]. The higher the chosen C_r , the longer time it will take for the reference concentration to be present in the concrete and the larger the negative contribution on b_{Cr} will be.

The set of mechanisms (1) is relatively independent of C_r and therefore relatively more pronounced at low C_r , whereas the set of mechanisms (2) is concentration dependent and more pronounced at high C_r . As b_{Cr} is the sum of positive and negative contributions, the result is a decreasing b_{Cr} with increasing C_r .

5.1.3 Discussion on limits of reference concentration

For service life modeling the reference concentration of interest is typically the critical chloride content causing corrosion initiation. However, the critical chloride content can vary considerably [35, 36]. It is therefore important to know the range of reference concentrations with which the square root method can be applied.

Choosing a C_r value higher than the maximum chloride content at the earliest recorded exposure times naturally rules out the use of these chloride profiles for the square root method. Additionally, for a fixed exposure time, it forces the use of a point closer to the concrete surface, which could potentially lead to disturbances caused by leaching and elemental zonation [13, 34].

The lower limit of the C_r value must be related to the method of obtaining the chloride profile, as well as the detection limit and accuracy. The lowest C_r value

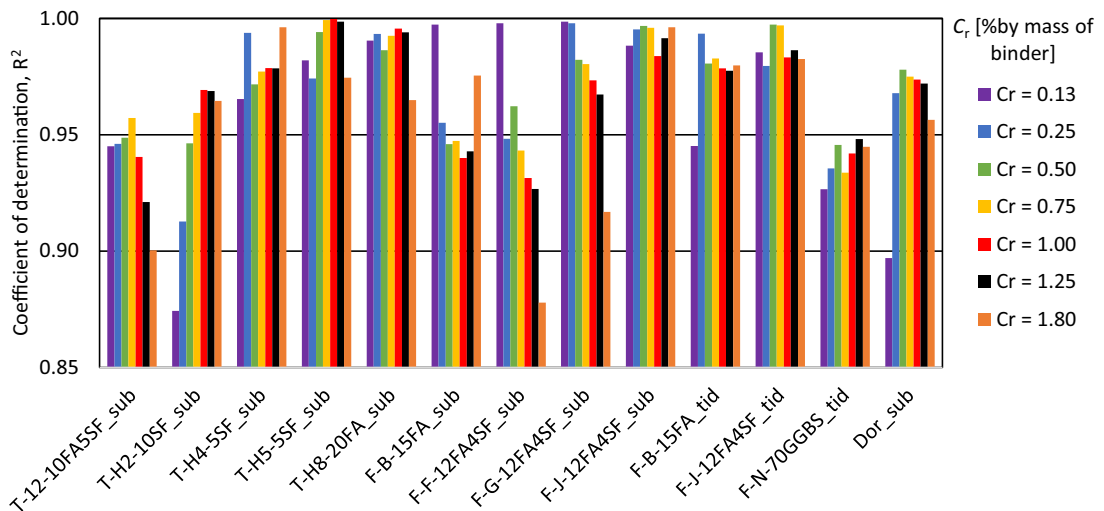


Fig. 6 R^2 value of linear regression on x_{Cr} versus square root of time for five concretes from submerged exposure at Träslövsläge Field Exposure Site, when using C_r values of 0.125 and

1.8% chloride by mass of binder in comparison to the five C_r values used throughout this study for submerged and tidal exposure

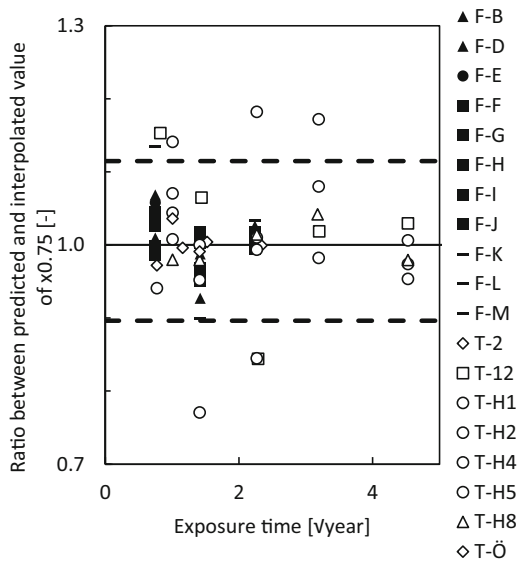


Fig. 7 Ratio between $x_{0.75}$ predicted by Eq. (1) ($x_{C_r}(t) = a_{C_r} \cdot x \sqrt{t} + b_{C_r}$) and measured by linear interpolation between the nearest data points directly below and above the reference concentration (0.75% chloride by mass of concrete). white fill = Fehmarn, black fill = Träslövsläge, diamond = PC, triangle = FA, circle = SF, square = FA + SF, line = GGBS. The dashed lines show a 90% confidence interval

must be distinguishable from the initial chloride content (C_i). Further, to enable interpolation, the profile grinding must be conducted deep enough to detect a concentration lower than the lowest C_r value.

To test the chloride concentration range in which the method is applicable; the square root method was applied on concretes exposed in submerged and tidal zones for C_r values of 0.125 and 1.8% chloride by mass of binder. (Note that for some of the combinations, the highest concentration was not reached at the shortest analyzed exposure time.) From Fig. 6 it can be seen that R^2 for both C_r values was comparable to R^2 for the C_r values generally used in this paper (see Table 4), except when using $C_r = 1.8\%$ chloride by mass of binder for T-12, F-F and F-G and $C_r = 0.125\%$ chloride by mass of binder for T-H2 and Dor_sub, where a decreasing tendency of R^2 is observed. It can be concluded that the square root method is valid for the investigated concretes in submerged and tidal exposure for the whole range of tested C_r values, i.e. 0.125–1.80% chloride by mass of binder. Similarly, the method was found applicable for concretes in the

atmospheric zone using C_r values in the range 0.1–0.5% chloride by mass of binder (data not shown here).

5.1.4 Selection of C_r for remaining discussion

When investigating the influence of exposure conditions and binders in further detail, it was chosen to proceed with a C_r of 0.75% chloride by mass of binder for tidal and submerged exposure. For atmospheric and deicing exposure, it was chosen to proceed with a C_r of 0.3% chloride by mass of binder. These reference concentrations were chosen from a perspective of benefitting from using as much of the raw data as possible, i.e. avoiding the challenge of using a C_r which is yet not obtained at t1 or which is not measured due to lack of grinding depth. In theory, if the chloride threshold value is known and within the limits of reference concentrations discussed in Sect. 5.1.3, it could be chosen as C_r .

5.2 Accuracy of interpolation

Figure 7 shows the ratio between the ingress depth of $C_r = 0.75\%$ chloride by mass of binder calculated by the square root method by using data from all available exposure times, and the ingress depth found by linear interpolation between the nearest data points directly below and above the C_r in the measured chloride profiles ($x_{0.75}(\text{predicted})/x_{0.75}(\text{measured})$).

For the analyzed concretes, $x_{0.75}(\text{predicted})/x_{0.75}(\text{measured})$ varied by $\pm 11\%$ (90% confidence interval). The largest variation is observed for concretes containing SF, whereas the least variation is observed for concretes with PC or FA. Considering the usual variation in service life estimates, a prediction error of 11% (90% confidence interval) appears acceptable [21, 37, 38].

5.3 Impact of exposure condition

Considering a_{C_r} describes the ingress of chloride ions over the square root of time, a given concrete should have a higher a_{C_r} value, the higher the environmental load it is exposed to. The environmental load can be described by chloride, moisture and temperature load. When tidal, submerged and atmospheric exposure are compared, a_{C_r} is expected to be lowest for atmospheric exposure due to the relatively low chloride and



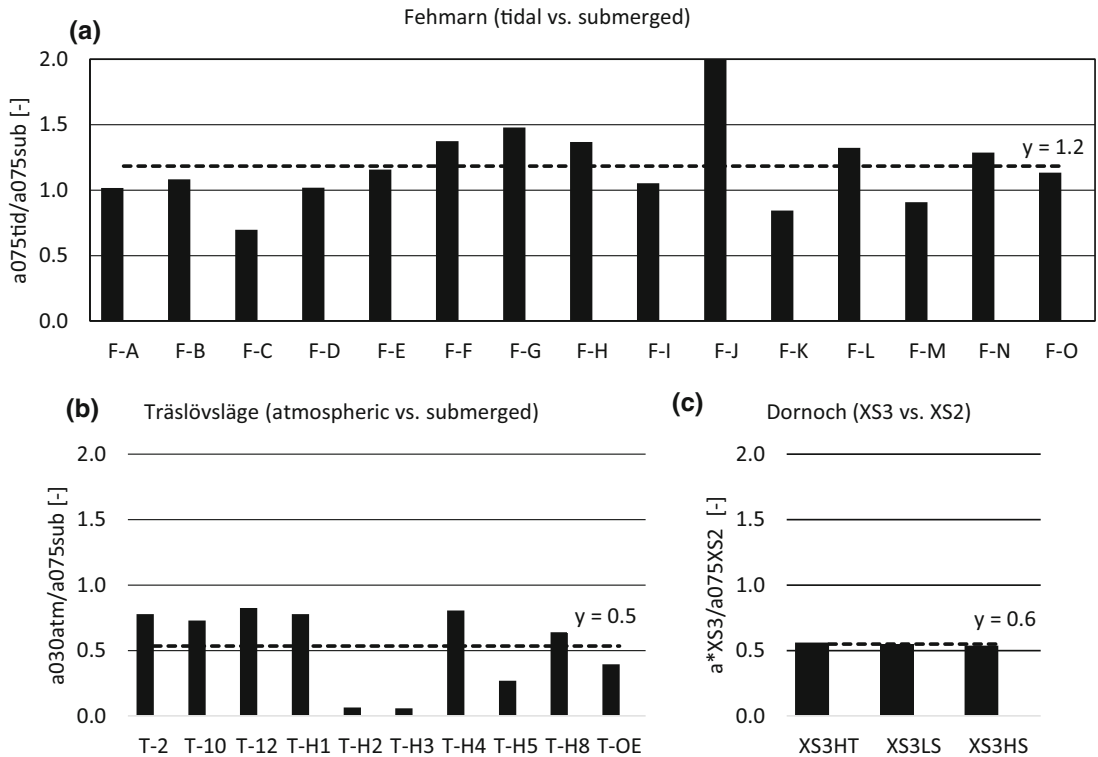


Fig. 8 **a** Ratio between $a_{0.75}$ for concretes in tidal vs. submerged exposure at Fehmarn Belt Exposure Site. The dashed line indicates the average ratio. **b** Ratio between $a_{0.30}$ for concretes in atmospheric versus $a_{0.75}$ for concretes in submerged exposure at Träslövsläge Field Exposure Site. The

dashed line indicates the average ratio. **c** Ratio between a_{Cr} for the concrete Dor exposed at XS3HT (high tide, $C_r = 0.75$), XS3LS (low splash, $C_r = 0.75$) and XS3HS (high splash, $C_r = 0.30$) versus XS2 (below mid tide, $C_r = 0.75$) at Dornoch Field Exposure Site. The dashed line indicates the average ratio

moisture load present there. The relative ingress rate in the tidal and submerged exposure is expected to be depth dependent; in the tidal zone convection will cause rapid ingress and accumulation of chlorides in the surface near region giving rise to a high chloride gradient, whereas an expected higher moisture state of submerged concrete will facilitate a higher diffusion coefficient [39].

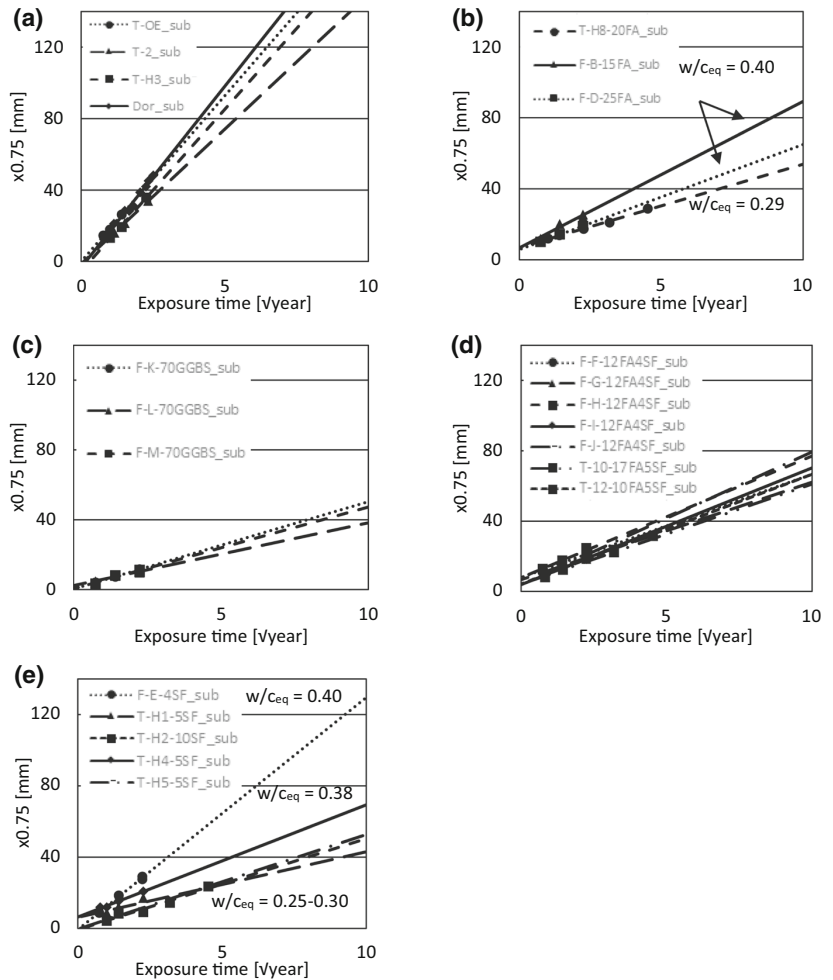
As shown in Table 1, in this study data has been analyzed from three exposure sites, where elements of the same concrete composition are exposed under different exposure conditions. A comparison between a_{Cr} at $C_r = 0.75$ (submerged, tidal, low splash) and $C_r = 0.3$ (atmospheric, high splash) for identical concretes in different exposure conditions is shown in Fig. 8a–c.

For Dornoch Field Exposure Site no data is available for submerged exposure. However, one

concrete composition is exposed in almost saturated below mid tide level and thus used as reference [21].

Figure 8a–c indicates that for the compared exposure conditions, a_{Cr} depends not only on the material, but also on the exposure. Large variations are observed between concrete compositions. However, for the investigated combination of concretes, exposure conditions and C_r , a_{Cr} typically descended in the order: tidal > submerged > atmospheric, high tidal and splash. The mentioned order of descension did not change by varying C_r within the investigated span (not reported here). Note that lower C_r values were used for atmospheric and high splash exposure than for submerged. However, due to the increasing trend of a_{Cr} with decreasing C_r (Fig. 4), the ratio is expected to be lower, if a_{Cr} for atmospheric and splash exposure was compared to a_{Cr} for submerged exposure at the same C_r . Thus, this effect would increase the influence

Fig. 9 Experimental data (markers) and graphical result of the square root method (lines) for concretes in submerged exposure. **a** PC, **b** FA, **c** GGBS, **d** FA + SF, **e** SF. $C_r = 0.75$. Although concretes with similar binders are compared for submerged exposure and identical C_r , some differences are seen between the concretes due to differences in w/c_{eq} , exposure temperature, salinity etc



of environment as compared to what is shown in Fig. 8a–c.

The square root method was applied on data for deicing exposure from the highway RV40 field exposure site in Sweden [22, 24, 25]. However, only a single concrete complied to the criteria set up in Sect. 3.1. The other concrete compositions failed on the criterium of having an increasing chloride concentration with time. This could partly be due to seasonal changes as de-icing salts are spread during the cold seasons and the chloride profiles were measured at different times of the year (January, May, June, July and September). Further the de-icing procedure changed, while the data collection was ongoing. When only summer sampling (May–July)

from vertical surfaces is utilized for concrete 206, R^2 values of 0.98–1.0 are obtained—see Online Resource 2. However, as data from only a single concrete in de-icing exposure complied to the criteria set up in Sect. 3.1 and the data due to seasonal variations is expected less reliable, de-icing is not treated further.

5.4 Influence of binder

Based on the findings in Sects. 5.1 and 5.3, the analysis on the influence of binders is conducted for a fixed C_r of 0.75 and submerged exposure conditions. Submerged exposure is chosen as the widest variety of binder compositions is available for this exposure condition. Figure 9 shows the experimental and



Table 5 a_{Cr} , b_{Cr} and R^2 values for concretes in submerged exposure. Binder groups are divided by thick borders (FA = Fly ash, GGBS = Ground granulated blast furnace slag, SF = Silica fume). $C_r = 0.75$

Binder	Concrete	a_{Cr} (mm/ $\sqrt{\text{year}}$)	b_{Cr} (mm)	R^2 (–)	Predicted ingress after 100 years (mm)	Binder	Concrete	a_{Cr} (mm/ $\sqrt{\text{year}}$)	b_{Cr} (mm)	R^2 (–)	Predicted ingress after 100 years (mm)
PC	T-OE	18.6	0	0.99	186	FA	T-H8	4.7	7	0.99	54
	T-2	15.1	– 1	1.00	150		F-B	8.3	7	0.95	90
	T-H3	18.1	– 6	1.00	175		F-D	5.9	6	1.00	65
	Dor	20.3	– 3	0.97	200	GGBS	F-K	5.0	0	1.00	50
FA + SF	F-F	5.9	8	0.94	67		F-L	3.6	2	0.96	38
	F-G	5.6	7	0.98	63	F-M	4.7	0	0.94	47	
	F-H	6.9	8	0.95	77	SF	F-E	13.0	– 1	0.99	129
	F-I	6.6	4	0.99	70		T-H1	3.7	6	0.87	43
	F-J	7.6	4	1.00	80		T-H2	5.1	– 1	0.96	50
	T-10	5.7	4	1.00	61		T-H4	6.3	6	0.98	69
	T-12	6.2	4	0.96	66		T-H5	5.3	0	1.00	53

modelled chloride ingress data for concretes with different binder types (PC, FA, GGBFS, FA + SF and SF). Table 5 presents the corresponding parameters of the square root fits.

Note that the choice of C_r has an impact on the predicted chloride ingress as described in Sect. 4.2 i.e. if a lower C_r was chosen, the predicted chloride ingress in a PC concrete would be even higher relative to a FA containing concrete. An example of the influence of C_r on the ingress depth is given in Online Resource 4, where the graphical result of the square root method applied on concretes exposed at submerged exposure for $C_r = 0.75$ (as shown at Fig. 9) is compared to the graphical result for $C_r = 0.25$.

As expected, some differences are seen between the concretes in Fig. 9. Although concretes with similar binders are compared for submerged exposure and identical C_r , differences exist in w/c, exposure temperature, salinity etc. (see Table 1). a_{Cr} is e.g. expected to increase with increasing w/c.

From Fig. 9, Table 5, Online Resource 2 and Online Resource 3 it is seen that the regression coefficients are very high. Further it is noted that similarities exist between similar compositions. e.g. a_{Cr} of the analyzed PC concretes are all in the range 15–20 mm/ $\sqrt{\text{year}}$, which is higher than for any other concretes. Contrary, b_{Cr} is low for the PC concretes. A low b_{Cr} combined with a high a_{Cr} is interpreted as the PC concretes quickly obtain their maximal potential chloride

resistance in the given environment they are exposed to, but that this maximal potential chloride resistance is relatively poor (assuming similar moisture level).

The values of a_{Cr} obtained for FA, FA + SF and GGBS concretes are low compared to the PC concretes and they are all in the same range (4–8 mm/ $\sqrt{\text{year}}$). The long-term chloride resistance is high for both FA, FA + SF and GGBS, but due to an additional high early resistance, reflected in the low b_{Cr} , the GGBS concretes have the lowest extrapolated ingress depths after 100 years as shown in Fig. 9c.

5.5 Hypotheses for linearity of x_{Cr} versus \sqrt{t}

The ingress of ions (1) in concrete might be explained by the Nernst–Planck equation (Eq. 1). The left hand term of the equation describes the change of concentration over time. The three right hand terms describe diffusion, migration and convection respectively [40]:

$$\frac{\partial c_i}{\partial t} = \nabla (D_i \nabla c_i + z_i u_{m,i} F c_i \nabla V - c_i v) \quad (1)$$

where c_i = ionic concentration, D_i = ionic diffusion coefficient, z_i = electrical charge, $u_{m,i}$ = the ionic mobility, F = Faradays constant, V = electrostatic potential, v = velocity of the solvent.

Assuming one-dimensional diffusion in a non-reactive and homogeneous media, the diffusion

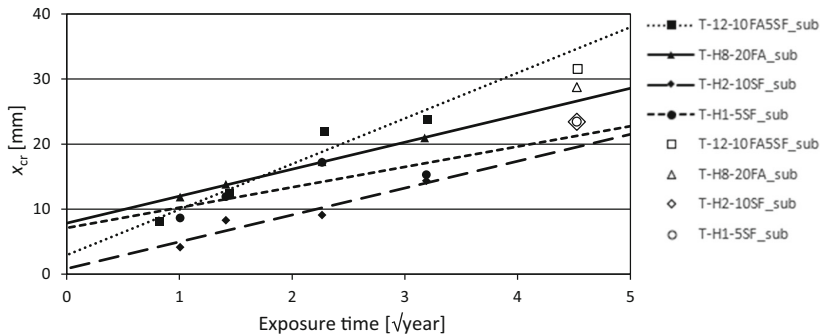


Fig. 10 Predicted versus measured chloride ingress ($C_r = 0.75$) at 20 years for four submerged concretes exposed at Träslövsläge Field Exposure Site. Prediction was made from

data up to 10 years exposure (shown with filled markers). The diameter of the measured data point for T-H2-10SF_sub is doubled to distinguish it from that of T-H1-5SF_sub

coefficient is constant, and the diffusion is square root of time dependent.

At initial exposure to chloride ions, concrete is in general neither fully saturated nor fully hydrated. Therefore, initial ingress might be enhanced by capillary suction (convection) and a higher initial diffusion due to an initial higher and more interconnected porosity. The latter is especially expected for concretes containing slowly reacting SCMs as e.g. fly ash.

Over time it is expected that convection ceases or becomes insignificant compared to diffusion. However, other factors such as elemental zonation [13], leaching [41], moisture [42] and temperature [43] are also known to influence the ingress, binding and resulting chloride profiles. Predicting the ingress depth of a total fixed (reference) chloride concentration, the concentration dependency of chloride binding (illustrated with a non-linear binding isotherm), can be neglected. In addition, the potential impact of leaching and elemental zonation on chloride binding is reduced. Finally, focusing on deeper ingress depths, limited impact of moisture changes on the transport coefficient is expected.

In summary, when the dominant chloride ingress mechanism is diffusion and the diffusion coefficient and chloride binding capacity are constant, linearity is expected of x_{Cr} versus \sqrt{t} , as the square root of the diffusion coefficient is length/ \sqrt{t} .

5.6 Ability to predict further ingress

To test the ability of the square root method to predict further ingress, the dataset from Träslövsläge Exposure Site comprising data from five exposure times up to 20 years was used. The square root method was applied to the first four data points (up to 10 years or $3.3 \sqrt{\text{year}}$) and the predicted ingress after 20 years was compared to the measured ingress. The deviation between the predicted and measured ingress depth was similar for the measured ingress depths of t_1 – t_4 to which the prediction was fitted (9% deviation) as to the measured ingress depth at t_5 , which was not used for fitting the straight line (12% deviation)—see Fig. 10 and Online Resource 5. It can therefore be concluded that the square root method is able to predict chloride ingress with an acceptable accuracy over 20 years.

5.7 Suggestions of how to use the square root method

The square root method is suggested to be used for (1) estimating remaining service life of existing structures. Depending on the availability of data, it might also be used for service life design of new structures.

When used for estimating the remaining service life of existing structures, the following information is required:

- Chloride threshold value. The reference chloride concentrations, C_r , should reflect the expected range of chloride threshold values for corrosion initiation.
- Cover depth.



- Chloride profiles to establish a straight line by the square root method considering the following aspects:
- Chloride profiles must be measured with a sufficient period in time between them to allow the difference in chloride content to exceed the measurement uncertainties.
- The exposure time of the first data point must be sufficiently long, so potential initial effects of e.g. capillary suction and prolonged hydration have ceased. The present investigation indicates the applicability of data from the earliest recorded exposure times (200 days for concrete initially cured for 43–49 maturity days and 217–370 days for concrete initially cured for 12–19 maturity days).
- Although two exposure times are sufficient to establish a straight line by the square root method, it is suggested to determine three profiles at minimum three exposure times. If any of the points deviate from the long-term trend (e.g. with R^2 less than 0.95), additional data points should be obtained.

When estimating the ingress depth for a long design service life (e.g. 100 years) by the square root method, the impact of a_{C_r} heavily exceeds that of b_{C_r} (see Table 5). Based on the findings in Sects. 5.1–5.4 multiple parameters including binder composition and exposure conditions do have an influence on the parameters a_{C_r} and b_{C_r} . There exists a potential of improving design values for new structures by increasing the number of investigated datasets and parameters to include e.g.:

- The influence of binder compositions.
- The influence of production and execution.
- The influence of exposure time and conditions.
- The influence of maintenance.

6 Conclusion

Based on analysis by the square root method of 34 concretes containing various amounts of PC, FA, SF and GGBS field exposed in up to five environments, it is concluded that:

- The ingress depth (x_{C_r}) of a fixed (reference) chloride concentration (C_r) in the investigated

concretes followed a square root of time dependency: $x_{C_r}(t) = a_{C_r}x\sqrt{t} + b_{C_r}$, where a_{C_r} and b_{C_r} are constants.

- The square root method appeared valid for marine exposed concrete in submerged, tidal, splash and atmospheric zone. Too little data was available for assessing the applicability for concrete in de-icing exposure.
- The square root method was found to be valid for the whole range of tested C_r values (0.125–1.80% chloride by mass of binder for submerged, tidal and low splash; 0.1–0.5% chloride by mass of binder for high splash and atmospheric exposure).
- The square root method appeared valid for the investigated PC, SF, FA, FA + SF and GGBS containing concrete.
- For the analyzed concretes, $x_{0.75}(\text{predicted})/x_{0.75}(\text{measured})$ varied by $\pm 11\%$ (90% confidence interval).
- For the investigated concretes and conditions, a_{C_r} was found to be constant after 200 days of exposure.
- A decreasing trend of a_{C_r} with increasing C_r was observed for submerged and tidal exposure. It was most pronounced for PC, SF and GGBS containing concretes.
- A clear decreasing trend of b_{C_r} with increasing C_r was observed for FA, SF and SF + FA containing concretes in submerged and tidal exposure.
- Based on a dataset from 1 to 10 years of exposure we were able to predict the chloride ingress after 20 years with a deviation of 12%.

In summary, the square root method seems to offer a reliable possibility to predict chloride ingress.

Acknowledgements The authors would like to thank Femern A/S, S. V. Nanukuttan and O. Skjølsvold for sharing field data from the field exposure sites Fehmarn Belt, Dornoch Bridge and Østmarkneset, respectively. This work was supported by the Danish Ministry of Higher Education and Science through the contract “E5 Field exposure and monitoring to extend the service life of infrastructure (translation from Danish)” granted to the Danish Technological Institute (DTI).

Authors’ contributions SF, MRG and HES contributed to the study conception and design. Data collection was performed by HES and SF. Data analysis was performed by SF. All authors contributed to discussing and evaluating the results. The first draft of the manuscript was written by SF and all authors commented on drafts of the manuscript. All authors read and approved the final manuscript.



Funding Open access funding provided by NTNU Norwegian University of Science and Technology (incl St. Olavs Hospital - Trondheim University Hospital).. This work was supported by the Danish Ministry of Higher Education and Science through the contract “E5 Field exposure and monitoring to extend the service life of infrastructure (translation from Danish)” granted to the Danish Technological Institute (DTI).

Code availability Not applicable.

Compliance with ethical standards

Conflict of interest Not applicable.

Availability of data and material The paper uses already published data to which references are given. Original tabulated chloride ingress data has been received from the authors to ensure accuracy. All chloride ingress data is shown graphically in the Online Resources. Data on concrete compositions and exposure conditions is given in the manuscript.

Open Access This article is licensed under a Creative Commons Attribution 4.0 International License, which permits use, sharing, adaptation, distribution and reproduction in any medium or format, as long as you give appropriate credit to the original author(s) and the source, provide a link to the Creative Commons licence, and indicate if changes were made. The images or other third party material in this article are included in the article's Creative Commons licence, unless indicated otherwise in a credit line to the material. If material is not included in the article's Creative Commons licence and your intended use is not permitted by statutory regulation or exceeds the permitted use, you will need to obtain permission directly from the copyright holder. To view a copy of this licence, visit <http://creativecommons.org/licenses/by/4.0/>.

References

- Tang L (2008) Engineering expression of the ClinConc model for prediction of free and total chloride ingress in submerged marine concrete. *Cem Concr Res* 38(8–9):1092–1097
- Marchand J (2001) Modeling the behavior of unsaturated cement systems exposed to aggressive chemical environments. *Mater Struct* 34(4):195–200
- Marchand J, Samson E, Maltais Y, Lee R, Sahu S (2002) Predicting the performance of concrete structures exposed to chemically aggressive environment—field validation. *Mater Struct* 35(10):623–631
- fib (2006) Model code for service life design, vol fib bulletin 34. CEB-FIB
- Collepardi M, Marcialis A, Turriziani R (1970) The kinetics of chloride ions penetration in concrete. II *Cemento* 67:157–164
- Engelund SE, Mohr L (2000) General guidelines for durability design and redesign, vol 15c. The European Union DuraCrete, New York
- Siemes A, Edvardsen C (1999) Duracrete: service life design for concrete structures. NRC Research Press, Ottawa
- Nilsson L, Sandberg P, Poulsen E, Tang L, Andersen A, Frederiksen JJDRDR (1997) Report no. 83: HETEK, a system for estimation of chloride ingress into concrete, theoretical background. vol 83. Danish Road Directorate
- Poulsen E, Mejlbro L (2006) Diffusion of chloride in concrete: theory and application. Taylor & Francis, London
- Frederiksen JM, Mejlbro L, Nilsson L-O (2008) Report TVBM-3146: fick's 2nd law-complete solutions for chloride ingress into concrete. Lund Institute of Technology, Sweden
- Mejlbro L (1996) The complete solution of Fick's second law of diffusion with time-dependent diffusion coefficient and surface concentration. *Durability of concrete in saline environment* 127–158
- Ehlen MA, III L-C (2018) Life-365™ v2. 23 User's manual. Accessed 25 Feb, 2019
- Jakobsen UH, De Weerd K, Geiker MR (2016) Elemental zonation in marine concrete. *Cement Concr Res* 85:12–27
- De Weerd K, Orsakova D, Muller AC, Larsen CK, Pedersen B, Geiker MR (2016) Towards the understanding of chloride profiles in marine exposed concrete, impact of leaching and moisture content. *Constr Build Mater* 120:418–431. <https://doi.org/10.1016/j.conbuildmat.2016.05.069>
- Poulsen SL, Sørensen HE (2014) Chloride ingress in old Danish bridges. In: *Proceedings 2nd international congress on durability of concrete (ICDC)*, New Delhi, India
- Poulsen SL, Sørensen HE, Jönsson U (2018) Chloride ingress in concrete blocks at the Rødbyhavn marine exposure site—status after 5 years. In: *Paper presented at the 4th international conference on service life design for infrastructures (SLD4)*, Delft, The Netherlands
- Thomas M, Matthews J (2004) Performance of pfa concrete in a marine environment—10-year results. *Cement Concr Compos* 26(1):5–20
- Baroghel-Bouny V, Dierkens M, Wang X, Soive A, Saillio M, Thiery M, Thauvin B (2013) Ageing and durability of concrete in lab and in field conditions: investigation of chloride penetration. *J Sustain Cement Based Mater* 2(2):67–110
- Boubitsas D, Tang L, Utgenannt P (2014) Chloride ingress in concrete exposed to marine environment-field data up to 20 years' exposure. CBI report to SBUF Project 12684
- Skjolsvold O, Justnes H, Hammer T, Fidjestol P (2007) Long-term chloride intrusion in field-exposed concrete with and without silica fume. In: *Paper presented at the Ninth CANMET/ACI international conference on Fly Ash, Silica Fume, Slag, and Natural Pozzolans in Concrete*
- Kim J, McCarter WJ, Suryanto B, Nanukuttan S, Basheer PM, Chrisp TM (2016) Chloride ingress into marine exposed concrete: a comparison of empirical-and physically-based models. *Cement Concr Compos* 72:133–145
- Tang L, Boubitsas D, Utgenannt P, Abbas Z (2018) Chloride ingress and reinforcement corrosion-after 20 years' field exposure in a highway environment. RISE Research Institutes of Sweden
- EN B (2011) 197-1: 2011. Cement, composition, specifications and conformity criteria for common cements. British Standard Institution (BSI), London

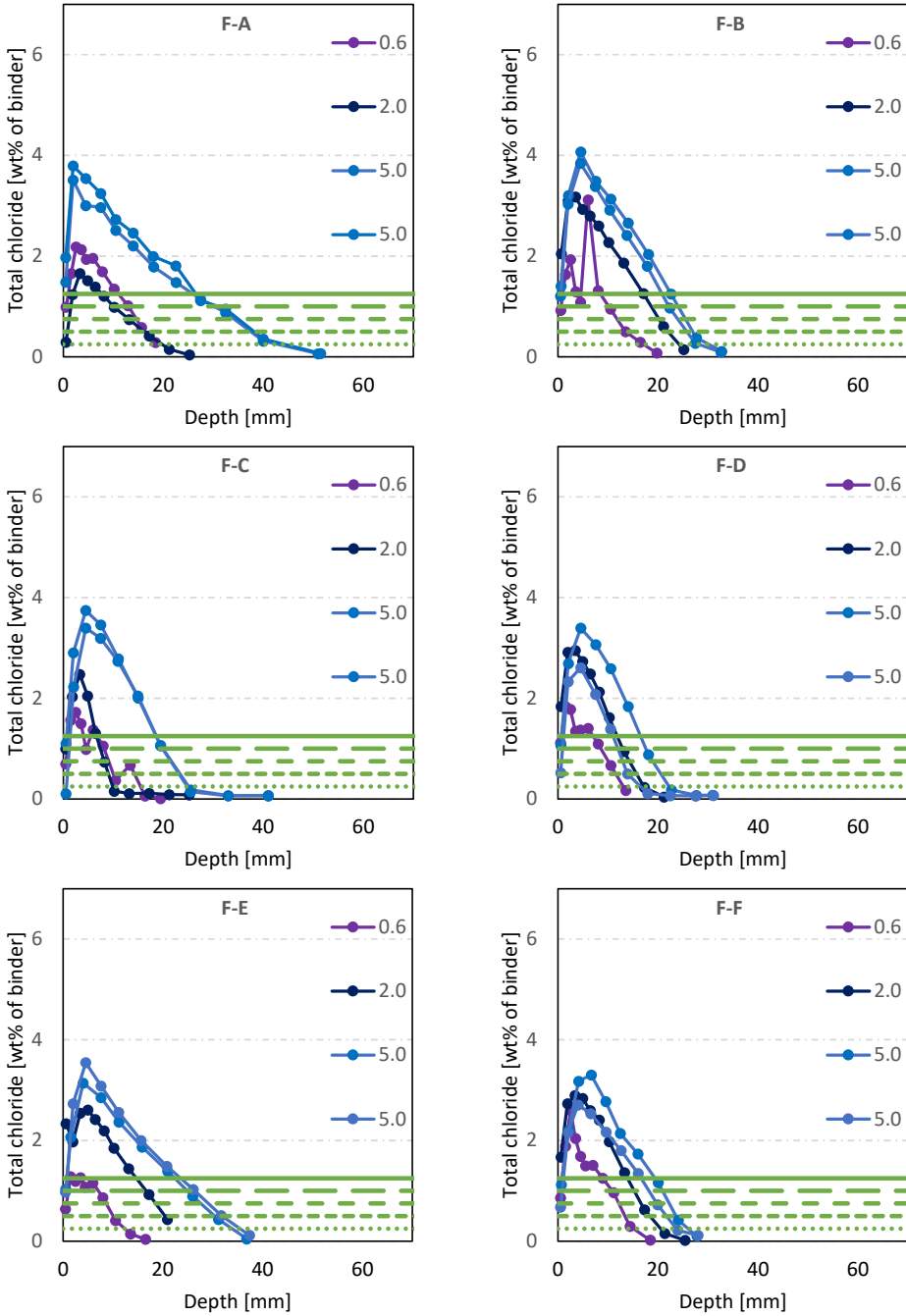


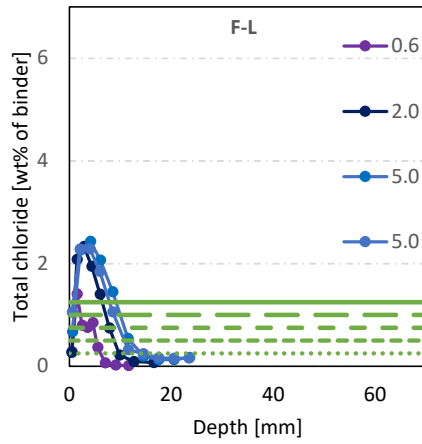
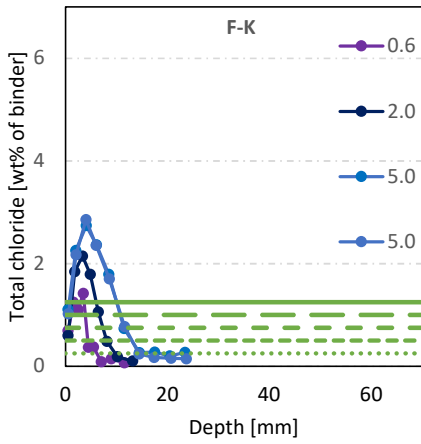
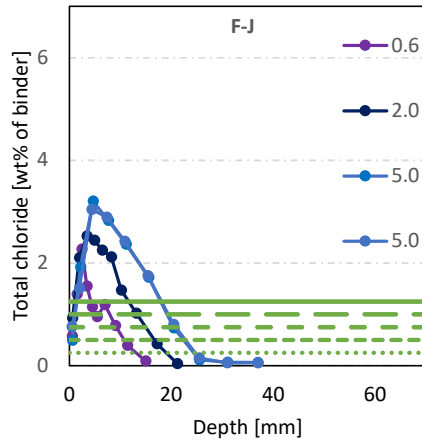
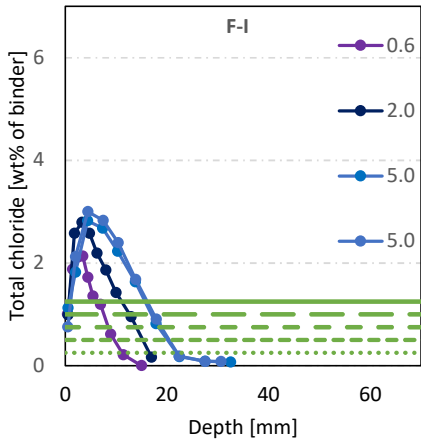
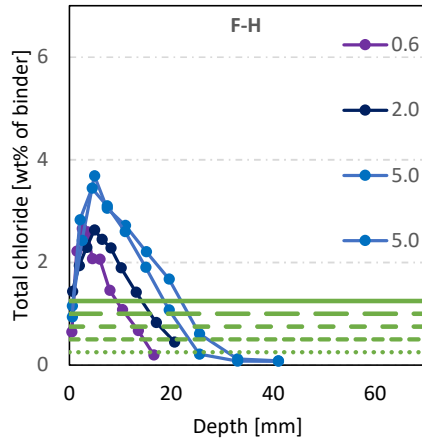
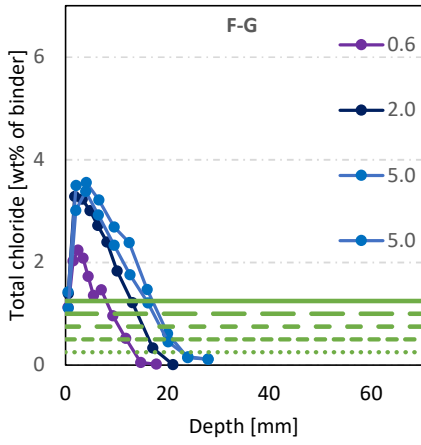
24. Lindvall A (2002) Chloride ingress in a swedish road environment: five years exposure for three concrete compositions. Chalmers tekniska högsk
25. Tang L, Utgenannt P (2007) Chloride Ingress and Reinforcement Corrosion in Concrete under De-Icing Highway Environment-A study after 10 years' field exposure, vol SP Report 2007:76. SP Technical Research Institute of Sweden,
26. DMI (2020) Danish meteorological institute. <https://www.dmi.dk/vejarkiv/>. Accessed 03 Jan, 2020
27. timeanddate.com (2020) Climate & Weather Averages in Träslövsläge, Sweden. <https://www.timeanddate.com/weather/@3326117/climate>. Accessed 17th of Jan 2020
28. CLIMATE-DATA.ORG (2020) DORNOCH CLIMATE. <https://en.climate-data.org/europe/united-kingdom/scotland/dornoch-29436/>. Accessed 17th of Jan 2020
29. Andersen I (1994) Salt-og temperaturforhold i de indre danske farvande (Salt and temperature conditions in the inner Danish waters). Danish Meteorological Institute, Copenhagen, Technical Report (94-4)
30. Kim J, McCarter W, Suryanto B, Nanukuttan S, Basheer P, Chrisp TJC, C (2016) Chloride ingress into marine exposed concrete: A comparison of empirical-and physically-based models. *Cem Concr Compos* 72:133–145
31. CLIMATE-DATA.ORG (2020) BORÅS CLIMATE. <https://en.climate-data.org/europe/sweden/vaestra-goetalands-laen/boras-6325/>. Accessed 17th of Jan 2020
32. Poulsen SL (2018) Chloride ingress in concrete blocks at the Rødbyhavn marine exposure site—status after 5 years. In: 4th International conference on service life design for infrastructures (SLD4). Delft, The Netherlands
33. Tang L (1996) Electrically accelerated methods for determining chloride diffusivity in concrete—current development. *Mag Concr Res* 48(176):173–179
34. De Weerd K, Orsáková D, Müller AC, Larsen CK, Pedersen B, Geiker MR (2016) Towards the understanding of chloride profiles in marine exposed concrete, impact of leaching and moisture content. *Constr Build Mater* 120:418–431
35. Angst UM, Geiker MR, Alonso MC, Polder R, Isgor OB, Elsener B, Wong H, Michel A, Hornbostel K, Gehlen C (2019) The effect of the steel–concrete interface on chloride-induced corrosion initiation in concrete: a critical review by RILEM TC 262-SCI. *Mater Struct* 52(4):88
36. Angst U, Elsener B, Larsen CK, Vennesland Ø (2009) Critical chloride content in reinforced concrete—a review. *Cem Concr Res* 39(12):1122–1138. <https://doi.org/10.1016/j.cemconres.2009.08.006>
37. Justnes H, Geiker M (2012) A critical view on service life predictions based on chloride induced corrosion. *Proc MicroDurability*
38. Reddy ARA, Agarwal A, Pillai RG (2013) Service life prediction models for concrete structures—a comparative study. In: Rehabilitation and restoration of structures and advances in building sciences. Chennai, India
39. Olsson N, Wahid FA, Nilsson L-O, Thiel C, Wong HS, Baroghel-Bouny V (2018) Wick action in mature mortars with binary cements containing slag or silica fume—The relation between chloride and moisture transport properties under non-saturated conditions. *Cem Concr Res* 111:94–103
40. Michel A (2013) Reinforcement corrosion: numerical simulation and service life prediction. Technical University of Denmark, Lyngby
41. Hemstad P, Machner A, De Weerd K (2020) The effect of artificial leaching with HCl on chloride binding in ordinary Portland cement paste. *Cem Concr Res* 130:105976
42. Olsson N, Lothenbach B, Baroghel-Bouny V, Nilsson L-O (2018) Unsaturated ion diffusion in cementitious materials—the effect of slag and silica fume. *Cem Concr Res* 108:31–37
43. Flint M, Michel A, Billington S, Geiker MR (2014) Influence of temporal resolution and processing of exposure data on modeling of chloride ingress and reinforcement corrosion in concrete. *Mater Struct* 47(4):729–748

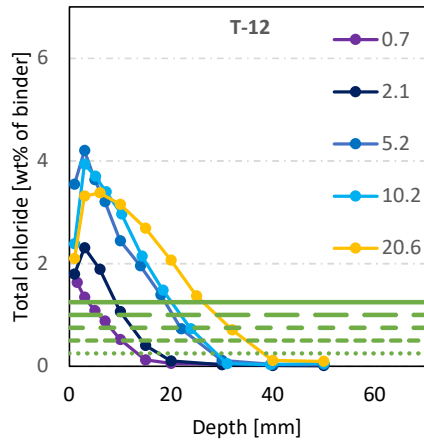
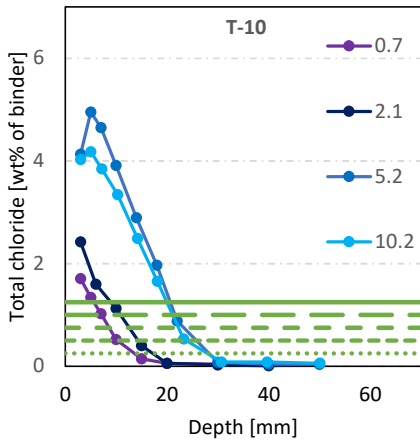
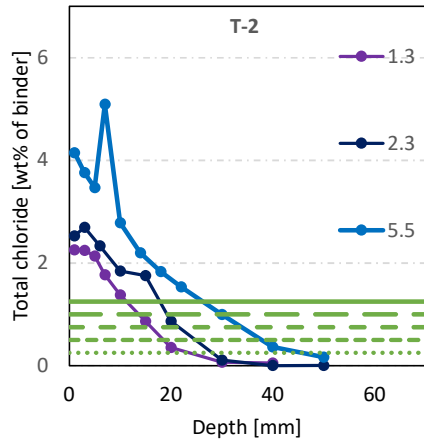
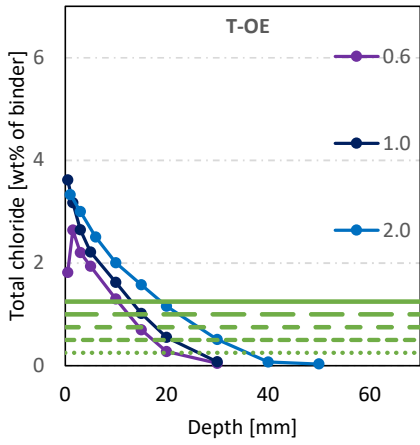
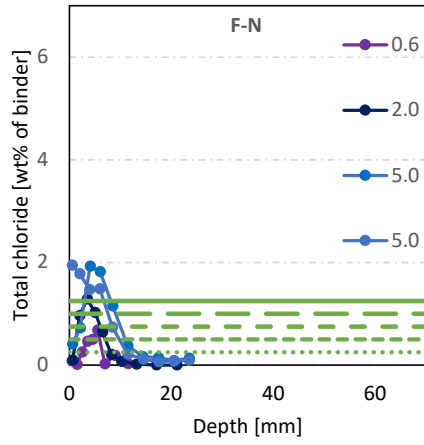
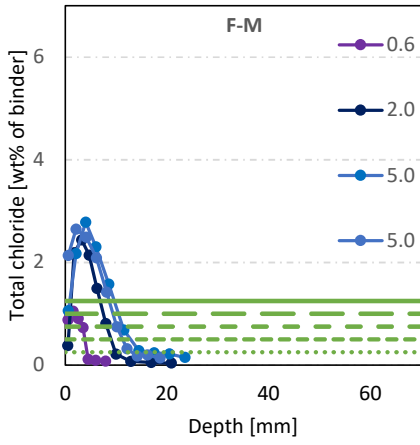
Publisher's Note Springer Nature remains neutral with regard to jurisdictional claims in published maps and institutional affiliations.

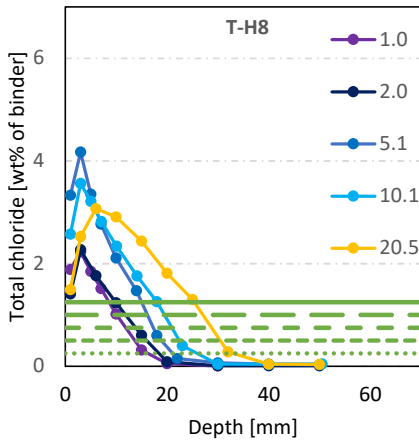
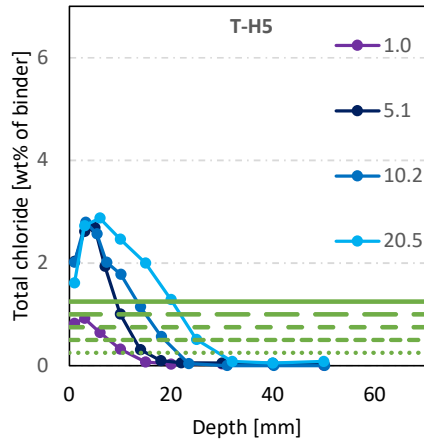
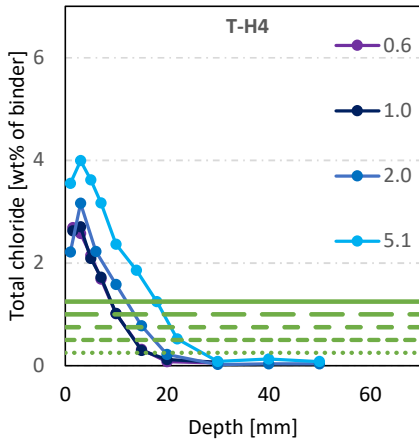
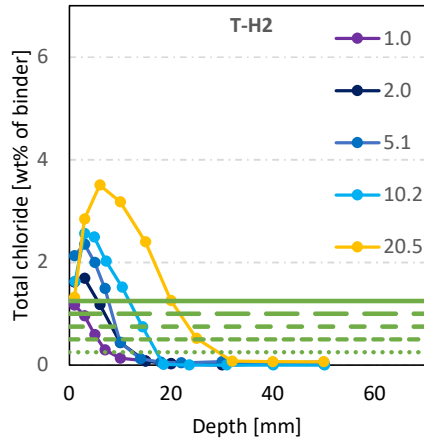
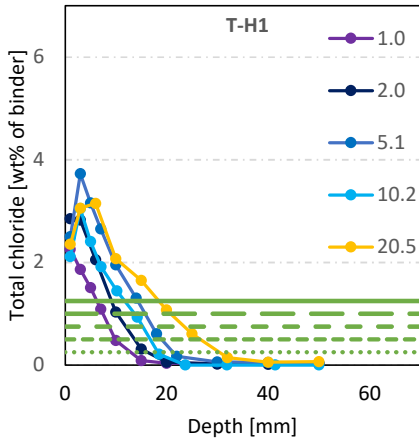


Chloride profiles – Submerged exposure

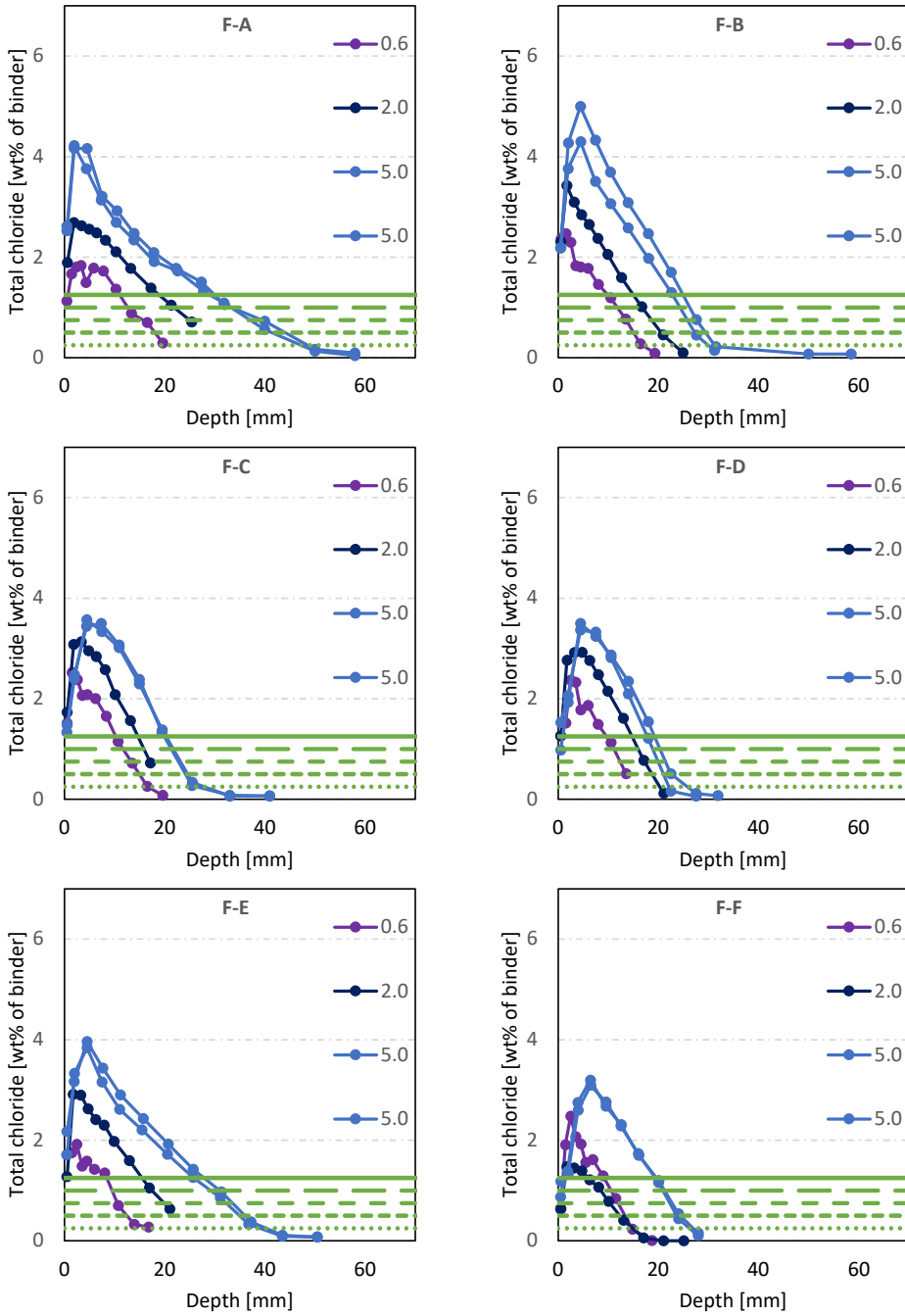


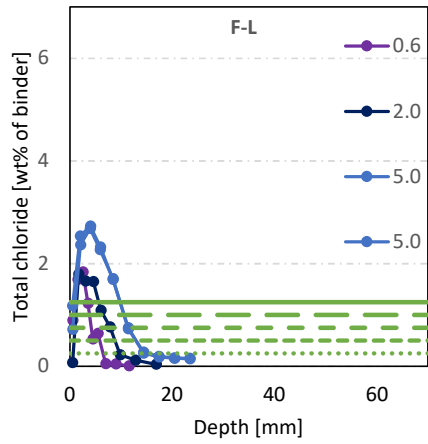
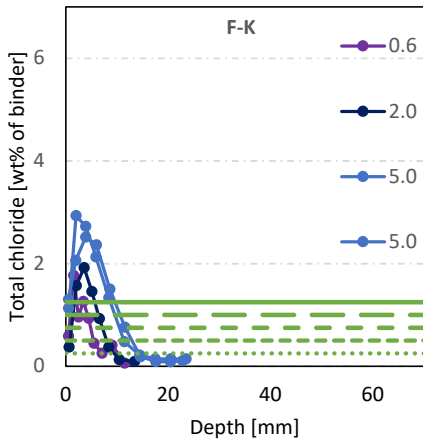
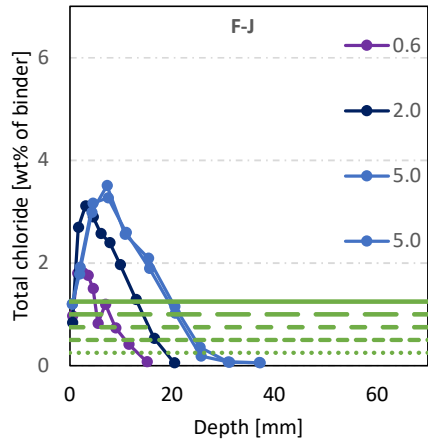
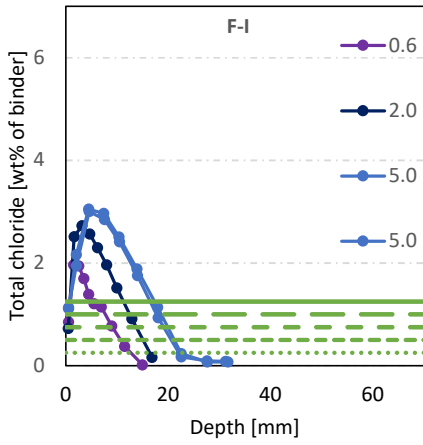
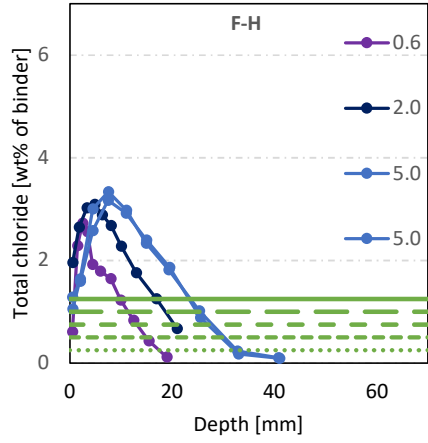
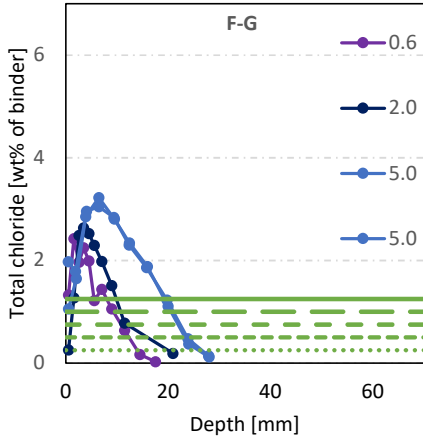


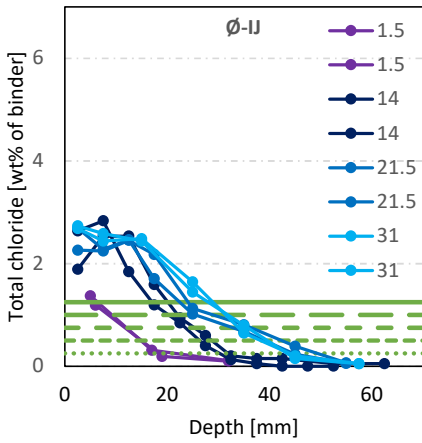
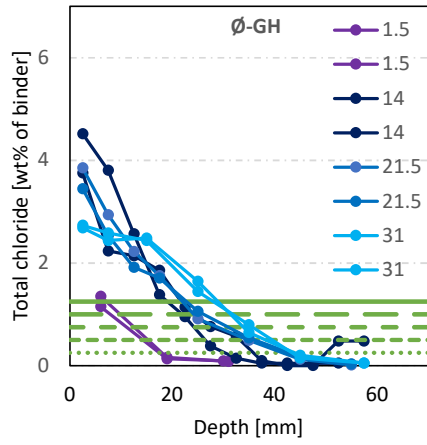
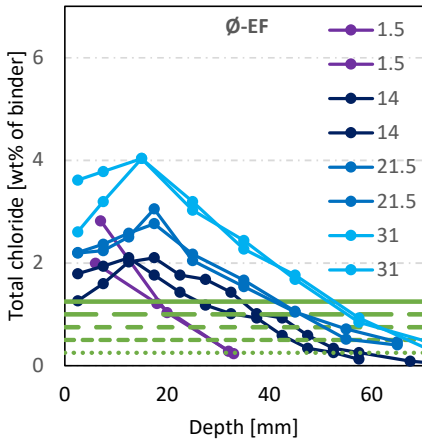
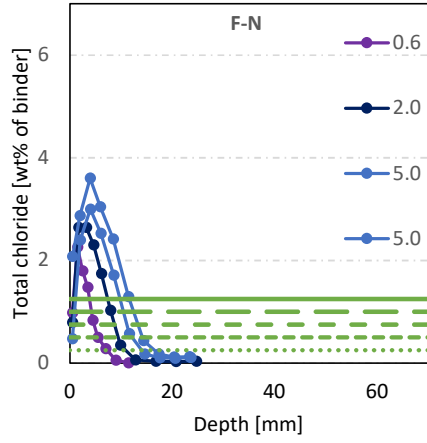
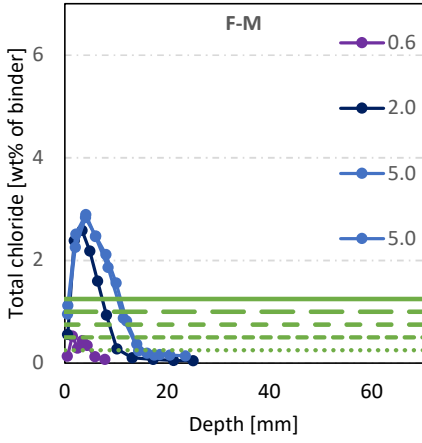




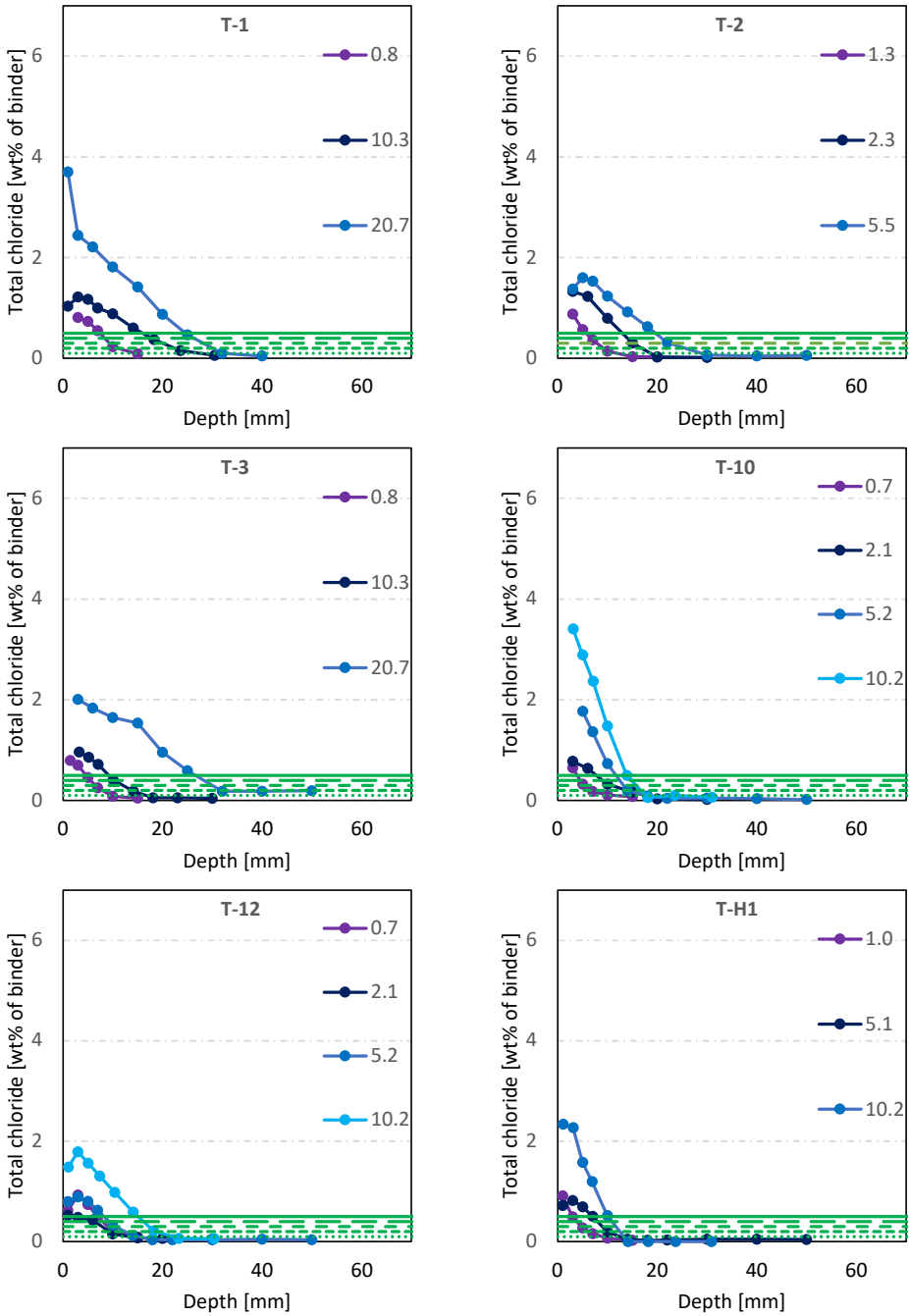
Chloride profiles – Tidal exposure

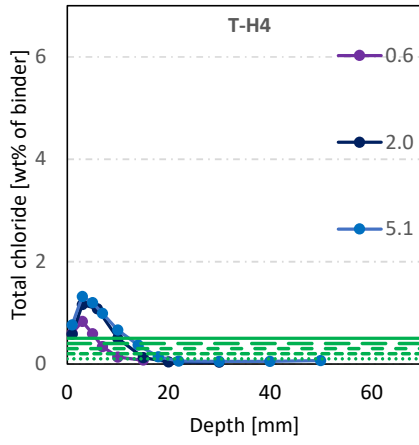




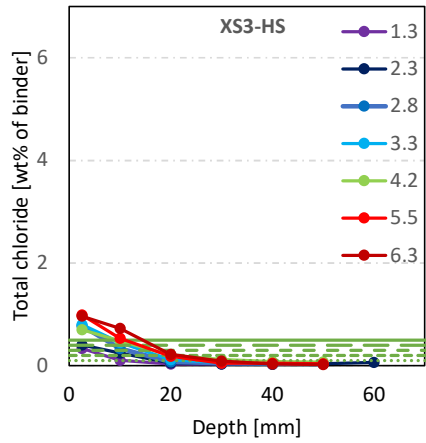
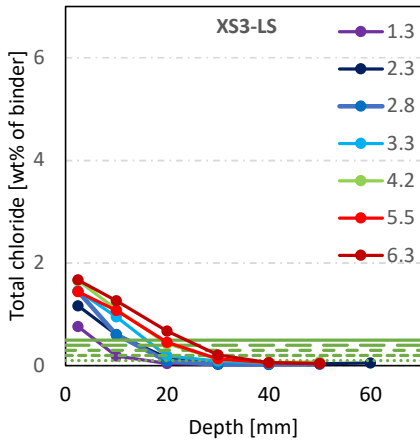
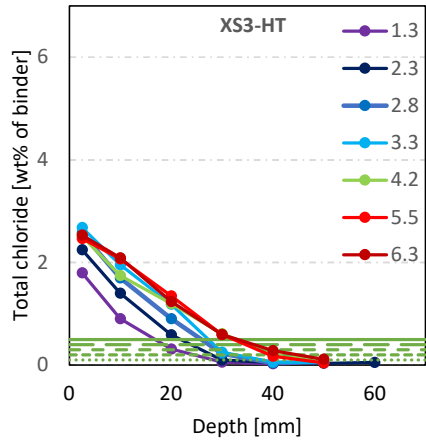
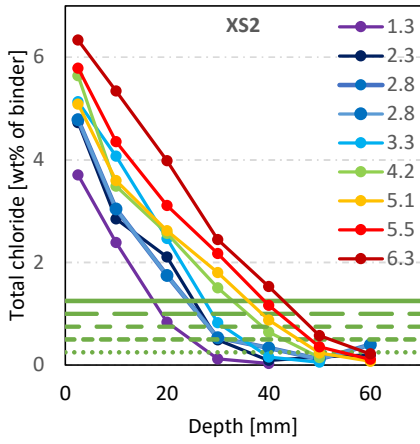


Chloride profiles – Atmospheric exposure





Chloride profiles – Dornoch



Square root method results for Fehmarn (Submerged exposure)

Field exposure site		Fehmarn														
Concrete ID		F-A	F-B	F-C	F-D	F-E	F-F	F-G	F-H	F-I	F-J	F-K	F-L	F-M	F-N	
Powder composition [wt%]	CEM I	100	85	75	75	96	84	84	84	84	84					
	FA ¹⁾		15	25	25		12	12	12	12	12					
	SF ²⁾					4	4	4	4	4	4					
	CEM III ³⁾											100	100	100	100	
Exposure	C_r															
Submerged	a_{Cr}	0.25	na	7.8	na	6.1	15.0	6.4	6.3	na	7.1	7.6	5.5	4.7	5.9	3.7
		0.50	na	8.2	na	6.0	14.0	6.1	5.6	7.1	7.0	7.8	5.8	3.9	5.3	3.1
		0.75	na	8.3	na	5.9	13.0	5.9	5.6	6.9	6.6	7.6	5.0	3.6	4.7	na
		1.00	na	8.3	na	6.0	12.3	5.8	5.6	7.2	6.3	9.1	4.7	4.6	5.1	na
		1.25	na	8.5	na	6.3	12.6	6.0	5.5	7.4	6.3	9.0	4.4	4.3	na	na
	b_{Cr}	0.25	na	12	na	8	1	11	9	na	6	8	2	3	0	3
		0.50	na	8	na	7	0	9	8	10	5	5	0	3	1	3
		0.75	na	7	na	6	-1	8	7	8	4	4	0	2	0	na
		1.00	na	5	na	4	-2	7	5	6	3	-1	0	-1	-1	na
		1.25	na	3	na	2	-5	5	4	4	2	-2	0	-1	na	na
	R^2	0.25	na	0.95	na	1.00	1.00	0.95	1.00	na	1.00	1.00	1.00	0.97	0.94	0.92
		0.50	na	0.95	na	1.00	0.99	0.96	0.98	0.92	0.99	1.00	1.00	0.96	0.94	0.92
		0.75	na	0.95	na	1.00	0.99	0.94	0.98	0.95	0.99	1.00	1.00	0.96	0.94	na
		1.00	na	0.94	na	1.00	0.99	0.93	0.97	0.94	0.99	0.98	1.00	0.92	0.92	na
		1.25	na	0.94	na	1.00	0.98	0.93	0.97	0.94	1.00	0.99	0.99	0.91	na	na

1) FA = Fly ash; 2) SF = Silica fume; 3) CEM III = Blast furnace slag cement or blast furnace slag combination according to BS 8500.

Square root method results for Fehmarn and Østmarkneset (Tidal exposure)

Field exposure site		Fehmarn														Østmarkneset			
Concrete ID		F-A	F-B	F-C	F-D	F-E	F-F	F-G	F-H	F-I	F-J	F-K	F-L	F-M	F-N	Ø-EF	Ø-GH	Ø-IJ	
Powder composition [wt%]	CEM I	100	85	75	75	96	84	84	84	84	84					80	90	80	
	FA ¹⁾		15	25	25		12	12	12	12	12								
	SF ²⁾					4	4	4	4	4	4					20	10	20	
	CEM III ³⁾											100	100	100	100				
Exposure	C_r																		
Tidal	a_{Cr}	0.25	na	9.2	na	6.7	16.2	na	8.2	na	7.0	8.9	na	5.3	6.4	5.3	na	7.8	6.2
		0.50	na	9.0	na	6.1	15.4	na	7.7	na	6.9	8.9	4.6	4.8	na	5.1	9.2	6.8	6.1
		0.75	15.3	8.9	6.5	6.0	15.1	na	8.2	9.4	7.0	9.1	4.2	4.8	na	4.9	8.3	6.2	5.7
		1.00	13.8	9.2	6.6	6.1	14.0	na	8.3	9.0	7.0	10.3	4.0	4.6	na	4.8	7.9	5.7	5.3
		1.25	12.4	9.5	6.6	6.4	12.5	na	9.6	9.0	7.7	9.6	3.9	4.4	na	4.5	7.6	5.3	5.1
	b_{Cr}	0.25	na	10	na	11	3	na	8	na	8	6	na	2	0	3	na	7	12
		0.50	na	8	na	9	1	na	6	na	5	4	2	2	na	2	16	6	7
		0.75	4	7	8	8	-1	na	3	6	4	2	2	1	na	1	14	3	5
		1.00	2	5	7	7	-1	na	2	5	3	-2	1	0	na	1	10	2	2
		1.25	2	2	5	5	-1	na	-2	4	0	-2	0	0	na	1	6	0	0
	R^2	0.25	na	0.99	na	1.00	1.00	na	1.00	na	0.99	0.98	na	1.00	0.99	0.94	na	0.97	0.85
		0.50	na	0.98	na	0.98	1.00	na	0.98	na	1.00	1.00	0.96	1.00	na	0.95	0.96	0.96	0.90
		0.75	0.99	0.98	0.99	0.99	1.00	na	0.90	0.99	1.00	1.00	0.97	1.00	na	0.93	0.98	0.96	0.94
		1.00	1.00	0.98	1.00	0.99	0.99	na	0.91	0.99	0.99	0.98	0.97	1.00	na	0.94	0.96	0.96	0.98
		1.25	1.00	0.98	1.00	0.99	0.99	na	0.98	0.99	0.99	0.99	0.98	0.99	na	0.95	0.92	0.95	0.98

1) FA = Fly ash; 2) SF = Silica fume; 3) CEM III = Blast furnace slag cement or blast furnace slag combination according to BS 8500.

Square root method results for Träslövsläge

Field exposure site		Träslövsläge											
Concrete ID		T-1	T-OE	T-2	T-3	T-10	T-12	T-H1	T-H2	T-H4	T-H5	T-H8	
Powder composition [wt%]	CEM I	100	100	100	95	78.5	85	95	90	95	95	80	
	FA ¹⁾					17	10					20	
	SF ²⁾				5	4.5	5	5	10	5	5		
Exposure	C_r												
Submerged	a_{Cr}	0.25	na	23.3	19.3	na	6.1	6.5	4.3	5.5	8.0	5.5	4.9
		0.50	na	20.4	16.3	na	5.6	6.5	4.1	5.3	6.2	5.0	4.6
		0.75	na	18.6	15.0	na	5.7	6.2	3.7	5.1	6.3	5.3	4.7
		1.00	na	15.7	13.7	na	5.9	6.1	3.5	5.1	6.6	4.0	4.8
		1.25	na	13.3	12.3	na	6.1	5.9	3.0	4.7	6.4	3.9	4.8
	b_{Cr}	0.25	na	3	0	na	9	9	9	2	9	4	10
		0.50	na	1	0	na	6	6	7	0	8	2	9
		0.75	na	0	-1	na	4	4	6	-1	6	0	7
		1.00	na	0	-2	na	2	2	5	-2	4	3	5
		1.25	na	0	-2	na	0	1	5	-2	3	2	4
	R ²	0.25	na	1.00	0.99	na	1.00	0.95	0.83	0.91	0.99	0.99	1.00
		0.50	na	0.99	1.00	na	1.00	0.95	0.86	0.95	0.97	0.99	0.99
		0.75	na	0.99	1.00	na	1.00	0.96	0.87	0.96	0.98	1.00	0.99
		1.00	na	0.99	1.00	na	1.00	0.94	0.86	0.97	0.98	0.94	1.00
		1.25	na	1.00	0.98	na	1.00	0.92	0.81	0.97	0.98	0.96	0.99
Atmospheric	a_{Cr}	0.1	4.9	na	14.0	na	2.2	5.0	2.1	na	4.7	na	na
		0.2	5.2	na	13.4	6.1	3.6	5.4	2.9	na	5.2	na	na
		0.3	5.1	na	11.8	6.0	4.2	5.4	3.2	na	5.0	na	na
		0.4	4.8	na	11.4	5.7	4.2	5.6	3.3	na	4.6	na	na
		0.5	4.6	na	11.2	5.5	4.2	7.3	3.3	na	4.3	na	na
	b_{Cr}	0.1	11	na	-4	na	12	5	7	na	9	na	na
		0.2	6	na	-5	0	6	1	3	na	6	na	na
		0.3	5	na	-5	-1	3	-1	2	na	4	na	na
		0.4	4	na	-5	-2	2	-2	1	na	4	na	na
		0.5	3	na	-6	-2	1	-8	0	na	3	na	na
	R ²	0.1	0.99	na	0.99	na	0.55	0.90	0.93	na	0.99	na	na
		0.2	1.00	na	0.97	0.82	0.76	0.97	1.00	na	0.95	na	na
		0.3	0.99	na	0.96	0.81	0.92	0.95	1.00	na	0.93	na	na
		0.4	0.98	na	0.95	0.78	0.95	0.95	1.00	na	0.92	na	na
		0.5	0.97	na	0.94	0.79	0.96	1.00	1.00	na	0.93	na	na

1) FA = Fly ash; 2) SF = Silica fume

Square root method results for Dornoch

Field exposure site			Dornoch												
Concrete ID	Dor					Dor									
Powder composition [wt%]	CEM I		100		CEM I			100		CEM I			100		
Exposure	C_r		Exposure			C_r		Exposure			C_r		Exposure		
Below mid-tidal zone (XS2)	a_{Cr}	0.25	21.3	High-tidal zone (XS3)	a_{Cr}	0.25	14.5	Low-splash zone (XS3)	a_{Cr}	0.25	13.6	High-splash zone (XS3)	a_{Cr}	0.1	14.1
		0.50	21.0			0.50	12.3			0.50	12.0			0.2	10.2
		0.75	20.3			0.75	11.4			0.75	11.1			0.3	10.9
		1.00	19.4			1.00	10.9			1.00	8.7			0.4	11.2
		1.25	18.3			1.25	9.8			1.25	5.5			0.5	7.4
	b_{Cr}	0.25	4		b_{Cr}	0.25	6		b_{Cr}	0.25	-6		b_{Cr}	0.1	-4
		0.50	-1			0.50	4			0.50	-7			0.2	-3
		0.75	-3			0.75	2			0.75	-9			0.3	-8
		1.00	-4			1.00	-1			1.00	-8			0.4	-11
		1.25	-4			1.25	-2			1.25	-5			0.5	-5
	R^2	0.25	0.94		R^2	0.25	0.93		R^2	0.25	0.95		R^2	0.1	0.71
		0.50	0.98			0.50	0.91			0.50	0.95			0.2	0.89
		0.75	0.97			0.75	0.87			0.75	0.95			0.3	0.91
		1.00	0.97			1.00	0.85			1.00	0.9			0.4	0.82
		1.25	0.97			1.25	0.83			1.25	0.7			0.5	0.88

Square root method results for Deicing

Field exposure site				
Concrete ID	RV206		RV206 Summe	
Powder composition [wt%]	CEM I		95	
	SF ¹⁾		5	
Exposure	C_r			
Deicing	a_{Cr}	0.1	7.2	7.8
		0.2	7.1	7.6
		0.3	7.0	7.2
		0.4	6.3	6.7
		0.5	5.5	6.2
	b_{Cr}	0.1	13	12
		0.2	9	8
		0.3	6	6
		0.4	4	4
		0.5	3	3
	R^2	0.1	0.97	1.0
		0.2	0.97	1.0
		0.3	0.97	0.99
		0.4	0.93	0.99
		0.5	0.83	0.98

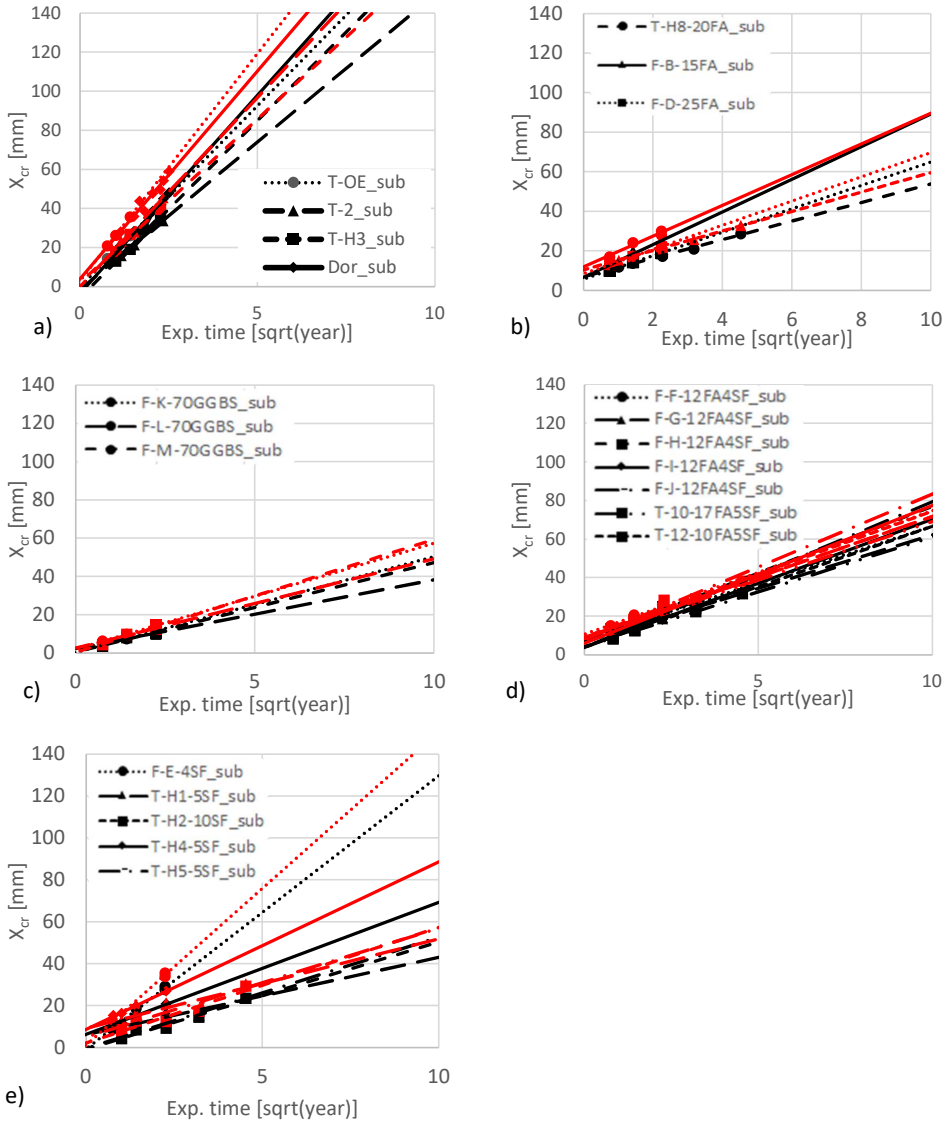
1) SF = Silica fume

Example of averaging normalized a_{cr}

Concrete		F-A	T-2	T-Ö	Dor	
Submerged	a_{cr}	0.25	19.6	19.3	23.4	21.3
		0.50	15.8	16.3	20.4	21.0
		0.75	15.0	15.1	18.6	20.3
		1.00	13.4	13.7	15.8	19.4
		1.25	11.8	12.3	13.3	18.3

Concrete		F-A	T-2	T-Ö	Dor	Avg	
Submerged	Normalized a_{cr}	0.25	1.30	1.28	1.25	1.05	1.16
		0.50	1.06	1.08	1.10	1.03	1.05
		0.75	1.00	1.00	1.00	1.00	1.00
		1.00	0.89	0.91	0.85	0.96	0.92
		1.25	0.78	0.81	0.72	0.90	0.85

Graphical application of the square root method at C_r 0.25 and 0.75



Graphical result of the square root method applied on concretes exposed at submerged exposure. a) PC, b) FA, c) GGBS, d) FA+SF, e) SF. Black = $C_r = 0.75$. Red = $C_r = 0.25$. Note, that the extrapolated ingress depth after 100 years of $C_r = 0.25$ is higher for T-H4-5SF_sub than for F-J-12FA4SF_sub, whereas the opposite is the case for $C_r = 0.75$.

Deviation between predicted and measured ingress depth after 20 years of exposure

Absolute errors of predicted versus measured chloride ingress of $C_r = 0.75$ for four submerged concretes exposed at Träslövsläge Field Exposure Site after t1, t2, t3, t4 and t5. Prediction made based on data up to ten years.

	t1	t2	t3	t4	Average (t1-t4)	t5
T-12-10FA5SF_sub	7%	5%	15%	6%	9%	9%
T-H1-5SF_sub	16%	4%	21%	11%	13%	10%
T-H2-10SF_sub	17%	24%	11%	2%	14%	20%
T-H8-20FA_sub	1%	1%	0%	0%	1%	8%
Average	10%	8%	12%	5%	9%	12%

Paper II

**Correlating the development of chloride profiles and microstructural changes
in marine concrete up to ten years**

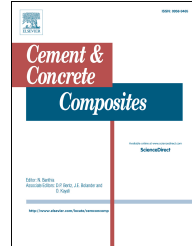
Submitted to Cement and Concrete Composites (2021)

Simon Fjendbo; Henrik E. Sørensen; Klaartje De Weerd; Ulla Hjorth Jakobsen; Mette R. Geiker

Journal Pre-proof

Correlating the development of chloride profiles and microstructural changes in marine concrete up to ten years

Simon Fjendbo, Henrik E. Sørensen, Klaartje De Weerd, Ulla H. Jakobsen, Mette R. Geiker



PII: S0958-9465(22)00184-6

DOI: <https://doi.org/10.1016/j.cemconcomp.2022.104590>

Reference: CECO 104590

To appear in: *Cement and Concrete Composites*

Received Date: 22 December 2021

Revised Date: 4 April 2022

Accepted Date: 9 May 2022

Please cite this article as: S. Fjendbo, H.E. Sørensen, K. De Weerd, U.H. Jakobsen, M.R. Geiker, Correlating the development of chloride profiles and microstructural changes in marine concrete up to ten years, *Cement and Concrete Composites* (2022), doi: <https://doi.org/10.1016/j.cemconcomp.2022.104590>.

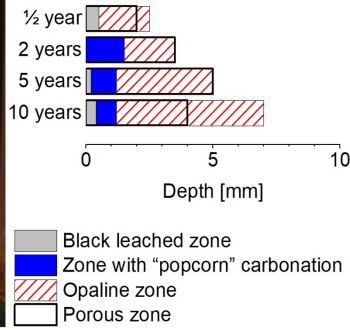
This is a PDF file of an article that has undergone enhancements after acceptance, such as the addition of a cover page and metadata, and formatting for readability, but it is not yet the definitive version of record. This version will undergo additional copyediting, typesetting and review before it is published in its final form, but we are providing this version to give early visibility of the article. Please note that, during the production process, errors may be discovered which could affect the content, and all legal disclaimers that apply to the journal pertain.

© 2022 Published by Elsevier Ltd.

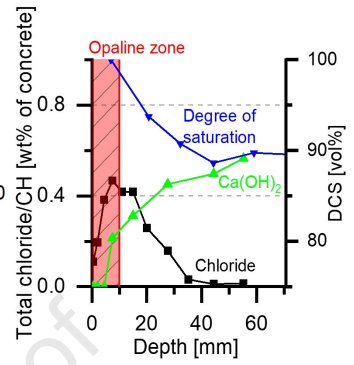
Femern Belt Marine Exposure Site, Denmark



Microstructural zonation



Multiple changes after 10 years submerged



Journal Pre-proof

Highlights

- A peaking behavior was observed in both tidal and submerged marine exposure.
- Leaching explains the chloride peaking behavior in submerged exposure.
- The chloride peak shifts towards higher concentrations and depths over time.
- Gradual development of microstructural zonation in marine exposed concrete.
- The chloride peak almost coincides with the depth of the so-called opaline zone.

Journal Pre-proof

Correlating the development of chloride profiles and microstructural changes in marine concrete up to ten years

Simon Fjendbo^{a,b,*}, Henrik E. Sørensen^a, Klaartje De Weerd^b, Ulla H. Jakobsen^a, Mette R. Geiker^b

^a Danish Technological Institute, Taastrup, Denmark

^b Norwegian University of Science and Technology (NTNU), Department of Structural Engineering, Trondheim, Norway

* Corresponding author: Tel.: +45 72201115; E-mail address: sifj@teknologisk.dk

Abstract

After ten years of marine exposure, chloride and calcium profiles and petrographic data were obtained from the tidal and submerged zones of six concrete panels differing in binder composition. Moisture and portlandite profiles were also determined on the submerged concrete. The data enables us to improve our understanding of the impact of sea water exposure and can also be used for service life modeling.

The depth of the maximum chloride content and the depth of the microstructurally changed zone were comparable. Both depths progressed over time and reached a depth of as much as 10 mm after ten years of exposure.

When using these and other field data for testing of chloride ingress prediction models, we recommend excluding datapoints from the microstructurally changed zone, i.e., the outermost datapoints including the maximum chloride content, unless reactive transport models are used.

Keywords: Concrete, Chloride ingress, Field exposure, Elemental zonation, Microstructure

1 Introduction

Chloride ingress profiles are often used for the design and residual service life assessment of reinforced concrete structures susceptible to reinforcement corrosion. In 2010, Femern A/S established a field exposure station in Rødbyhavn, Denmark, as part of the preparatory work for the upcoming Fehmarn Belt fixed link between Denmark and Germany. The purpose was to support the design and operation of the reinforced concrete structures for the fixed link. Chloride profiles taken from concrete subject to tidal and submerged exposure for five years at the Fehmarn Belt Exposure Site [1] and petrographic analysis of concrete subject to five years' tidal exposure [2] have already been reported. Recently, chloride ingress data from

several exposure sites, including the Fehmarn Belt Exposure Site, have been compiled and analyzed using a square root of exposure time vs. chloride ingress depth approach [3].

Multiple factors influence chloride ingress in concrete [4-21]. In partly saturated concrete, chloride can enter both by capillary suction and by diffusion. The rate of diffusion depends on the concentration difference and the diffusion coefficient, which increases with increasing moisture content [5-9]. Nielsen and Geiker [6] proposed an approach based on Powers' model for deriving the dependency of the chloride diffusion coefficient on the degree of saturation of the capillary porosity. Olsson et al. [7] concluded that there is a clear relationship between the calculated diffusion coefficient and the moisture content for individual binders based on experiments that showed an exponential increase in the relative diffusion coefficient with an increasing degree of saturation. Concrete in the marine splash and tidal zone will suffer chloride ingress by capillary suction of sea water in the convection zone and chloride ingress by diffusion at greater depths. During drying, chlorides will accumulate at the evaporation front, which could lead to an expectation that at early ages the rate of chloride ingress would be faster in concrete exposed to wetting and drying due to a higher surface concentration, whereas at later ages the concrete with highest moisture content might suffer deeper ingress due to a higher diffusion coefficient. Geiker [22] gives examples of chloride ingress in marine concrete, and Jensen et al. [23] have calculated the apparent chloride diffusion coefficient and surface concentration using the error function solution to Fick's second law and omitting surface near data points where reduced chloride content was measured based on the chloride profiles from submerged exposure and level 0.35, 0.5, 0.7–0.9 and 1.5 m above mean water level. In general, they found that a) the highest diffusion coefficients and medium surface concentrations were in the submerged zone, and b) the highest surface concentrations and medium diffusion coefficients were in the lower part of the splash zone.

Multiple ions in sea water, such as magnesium, sulfate and carbonate ions, combined with the leaching of calcium, potassium and hydroxyl ions can influence chloride ingress by altering the microstructural properties and the binding capacity of the paste, and they can change the porosity in the outer surface and even cause surface scaling [10-14]. For marine-exposed concretes, elemental zonation has been observed as a general feature, consisting of a magnesium-enriched zone near the surface, followed by a sulfur-enriched zone, and finally a chloride-enriched zone [10, 15]. This explains why the chloride concentration is not highest at the surface, both in cases with convection zones and also in submerged exposure [10].

Depending on the difference in composition and concentrations of ions in sea water and in the concrete pore solution, some ions ingress while others are leached out. Typically the ions mentioned in the previous paragraph ingress, while the portlandite leach out and calcium-silicon ratio of the C-S-H gel decreased with increased exposure time [16]. De Weerd et al. [19] showed that, for long-term marine-exposed concrete, the depth of portlandite leaching might be comparable to the depth of chloride ingress. A well-known consequence of leaching is an increase in porosity and a potential decrease in mechanical

strength [17]. However, what seems less recognized is that leaching also affects the chloride binding capacity, initially causing an increase, but later a decrease.

Chloride in concrete can be found free in the pore solution, physically bound (adsorbed) in calcium silicate hydrate (C-S-H), or chemically bound in chloride-containing AFms like Friedel's or Kuzel's salt [17]. Hemstad et al. [18] found that the pH of the pore solution influences the chloride binding capacity in Portland cement pastes. Lowering the pH from 13 to 12 increased chloride binding, which was associated with increased chloride binding in the AFm phases and potentially also the C-S-H. However, lowering the pH below 12 reduced chloride binding, partly due to the dissolution of AFms and most likely a reduction in the adsorption of chlorides by C-S-H [18, 24]. The intermediate step with increased chloride binding explains the observed gradually inwards-moving maximum chloride content [18]. Machner et al. [25] recently demonstrated that leaching has a profound impact on the chloride ingress profiles and briefly discussed implications for both performance testing and service life prediction.

Sulfate is expected to reduce chloride binding because sulfates compete with chlorides for incorporation in C-S-H and calcium aluminate phases [20]. Sulfate ions in concrete can react to form gypsum, ettringite and thaumasite. Typically, gypsum is formed near the surface [2], and ettringite and thaumasite are found slightly deeper in [17]. The formation of ettringite and thaumasite typically leads to a significant volume increase which could result in cracking [26], but when they form in the large voids in the sulfur-rich zone of marine-exposed concrete, cracking is limited or absent [10, 27].

Magnesium originating from sea water can precipitate as brucite when it encounters the high pH of the concrete [28] or as the non-cementing magnesium silicate hydrate (M-S-H) [21, 29]. M-S-H replaces C-S-H, which leads to a reduction in the chloride binding [10, 21]. It has also been reported to result in a weak, cracked and porous zone [10], which might be absent in field samples due to abrasion [13, 17].

The precipitation of a surface layer of brucite and/or calcite on the concrete and the formation of ettringite in the near-surface region due to the presence of magnesium, carbonate or sulphate ions from the sea water [30] have not been observed to limit chloride ingress in concrete [10, 31].

For design and reassessment purposes, the error function solution to Fick's 2nd law of diffusion is often used for chloride ingress prediction [32-36]. Among other things, this use is based on the assumptions that concrete is a homogeneous material and that no reactions occur between solids and the diffusing species [37]. These assumptions are questionable not only due to variations in the initial material, but also due to the multitude of reactions occurring over time in the surface of concrete exposed to sea water, as discussed above [10, 12, 13, 16-21, 26-29, 31, 38, 39]. There are various views on how to overcome this challenge [36, 40].

For design purposes, *fib* [36] proposes a so-called transfer function Δx , which is to be added to the calculated ingress depth for splash and tidal exposures to account for rapid chloride ingress (by convection) down to a given depth, but not for submerged exposure [36].

Similarly, Toutlemonde et al. [41] propose a so-called convection depth (Δx) for splash and tidal but not submerged exposures in a draft of a background document for the revision of EN1992, in which they also propose the use of a slightly greater convection depth for a design service life of 100 years than for 50 years (10 vs. 8 mm). For the assessment of chloride profiles where neither the maximum chloride content (C_{\max}) nor its position ($x_{C_{\max}}$) are time-dependent, Andrade et al. [40] propose that the external layer showing an increase in chloride content with depth should be neglected when fitting a chloride profile with a maximum beyond the concrete surface. They propose that the fitting should be performed on a rescaled profile where the origin is moved to $x_{C_{\max}}$ [40]. When later predicting chloride ingress, $x_{C_{\max}}$ is to be added to the predicted chloride ingress depth [40]. This approach corresponds to the assumption of the non-Fickian behavior observed in the outer surface is caused by rapid ingress by convection applied in the *fib* Model Code for Service Life Design. Andrade et al. [40] further note that in cases where the value and position of the maximum chloride content progress, the controlling mechanisms have not yet been identified. In these cases, they recommend not making a prediction without emphasizing its limitations [40]. This paper investigates the relationship between chloride profiles and the development of a microstructurally changed zone. The investigation covers chloride profiles combined with petrographic analysis of tidal and submerged concrete after ten years of marine exposure, supplemented with moisture and portlandite profiles of the submerged exposed concrete and earlier data on microstructure and chloride ingress.

The main findings are a gradually progressing microstructurally changed zone correlating with the observed peaking behavior of chloride profiles in submerged marine exposed concrete. After 10 years exposure, the comparable depth of the maximum chloride content and the depth of the microstructurally changed zone had a non-negligible depth of 10 mm.

Based on the experimental data, we recommend that only data unaffected by the microstructural changes should be applied for service life predictions unless reactive transport models are used.

2 Experimental

2.1 Materials

We investigated cores from six out of 15 unreinforced concrete panels subjected to marine exposure for ten years at the Fehmarn Belt Exposure Site, Rødbyhavn, Denmark.

2.1.1 Concrete panels, composition, and production

Table 1 gives an overview of the mixture proportions of the six different concretes analyzed, along with the IDs used in this paper. All cement notations are according to EN 197-1 [42]. Table 2 gives information on the chemical composition of binders as measured by X-ray fluorescence according to EN 196-2 [43].

Table 1: Concrete compositions[kg/m³][1].

ID used in this paper		PC	15FA	25FA	4SF	12FA4SF	SG
Original concrete ID [44]		A	B	C	E	F	K
Powder composition [% by wt.]	CEM I	100	85	75	96	84	
	FA ¹⁾		15	25		12	
	SF ²⁾				4	4	
	CEM III						100
CEM I 42.5 N-SR5 ³⁾		360	319	298	340	297	
CEM III/B 42.5 N ^{3,4)}							359
FA ¹⁾			56	99		42	
SF ²⁾					14	14	
Water		146	140	140	147	140	144
Superplasticizer 1 ⁵⁾			2.3	2.2			
Superplasticizer 2 ⁶⁾		2.7			2.6	2.9	2.4
Air entraining agent		1.7	1.7	2.2	0.6	1.5	0.8
Sand (0–2 mm)		686	655	630	693	670	687
Coarse aggregates (4–22 mm)		1155	1182	1170	1167	1192	1157
w/b ⁷⁾		0.40	0.37	0.35	0.42	0.40	0.40
w/(c + 2SF + 0.5 FA)		0.40	0.40	0.40	0.40	0.40	0.40
Density [kg/m ³]		2346	2345	2329	2349	2346	2320
Air [% by vol.]		5.8	5.4	5.5	4.8	5.2	4.4

1) FA = Fly ash

2) SF = Silica fume (dry matter), (added as slurry)

3) According to EN 197-1

4) SG = Ground Granulated Blast-furnace Slag (GGBS) content: 67% by wt.

5) BASF Glenium SKY 532 S (Polycarboxylate ether)

6) BASF Glenium SKY 540 (Polycarboxylate ether)

7) w = Water. b = CEM (I or III) + SF + FA

Table 2: Chemical composition and physical properties of binders. The chemical composition was measured by X-ray fluorescence according to EN 196-2.

“-” means that the amount has not been measured.

Property		CEM I	FA	SF	CEM III
		[% by wt.]	[% by wt.]	[% by wt.]	[% by wt.]
Oxide	Al ₂ O ₃	2.91	20.5	-	9.44
	SiO ₂	24.8	60.3	95.4	30.5
	CaO	65.6	1.56	0.32	47.8
	CO ₂	0.15	-	-	0.75
	Cl ⁻	0.00	0.01	0.04	0.08
	Fe ₂ O ₃	2.34	7.39	-	0.74
	MgO	0.75	-	-	4.88
	SO ₃	2.24	0.46	0.23	2.54
	Na ₂ O _{eq}	0.40	2.76	0.72	0.78
	Na ₂ O	-	-	0.19 ¹⁾	0.33 ¹⁾
	K ₂ O	-	-	0.80 ¹⁾	0.48 ¹⁾
Loss on ignition		0.65	3.17	1.34	1.05
Blaine surface [m ² /kg]		366	-	23740	487
Density [kg/m ³]		3190	2348	-	2961
Fineness (wt% passing 0.045 mm sieve)		-	84	-	-

1) Value declared by producer in a technical data sheet.

Following the experience of two-sided ingress in some 0.1 m thick concrete panels exposed at Träslövsläge Field Exposure Site, it was decided to produce the panels for the Fehmarn Belt Exposure Site with a thickness of 0.2 m to considerably delay the time when two-sided ingress would occur. The concrete for the panels was produced in 0.230 m³ batches and mixed in the Danish Technological Institute's Haarup counterflow mixer with a capacity of 0.250 m³. Two batches were required for each concrete panel, and they were therefore transferred to and homogenized in a 0.540 m³ pan mixer. After homogenization, the concrete panels were cast by filling from the top of the formwork (plywood, dimensions 2.0 m height, 1.0 m width, 0.2 m thickness) at a maximum drop height of 2.2 m. The concrete was cast in five layers, each of which was compacted using a small poker vibrator. Due to the wall effect (restricted aggregate packing in the outermost zone), there was a higher paste content in the outer section than in the bulk. Calcium profiles measured after six months give a rough impression of the magnitude of the wall effect, see Appendix A.

Maturity gain was monitored using embedded temperature sensors. Demolding was performed at a maturity of at least 24 hours. After demolding, the panels were wrapped in plastic and stored indoors (approx. 20 °C) for at least 14 maturity days. The concretes were produced over a period of two months but exposed to the marine environment at the same time. To obtain similar maturity (approximately 45 days) at exposure, some panels were moved to a lower temperature (minimum 5 °C) for part of the curing period.

2.1.2 Exposure

Knowledge of the exposure environment is important because the condition of a concrete after a given exposure time is a result of the environment to which it has been exposed. The six concrete panels were exposed to sea water at the exposure site at a maturity of 43–49 days [44]. Figure 1 shows the variation in temperature and salinity of the sea water and the water level over one year. Table 3 shows annual averages, including air temperature, using sensors installed by the Danish Hydraulic Institute. The panels were exposed partly submerged with 0.7 m of the 2.0 m high panels located above mean water level. Note that the recorded chloride content (7 g/l) is considerably less than the chloride content of the Atlantic Ocean (19 g/l), but the ratio between ions is similar [10, 45].

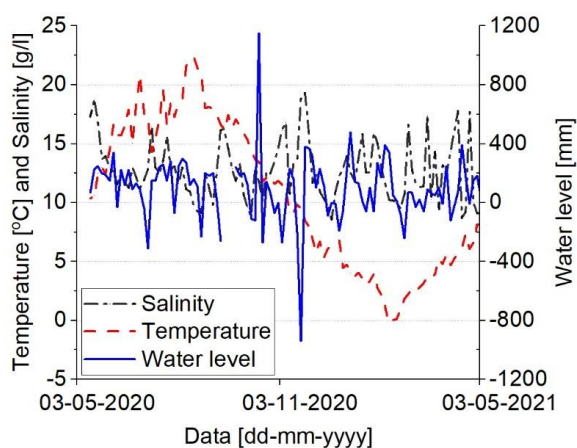


Figure 1: Exposure conditions: water temperature, salinity, and water level (one year).

Table 3: Exposure conditions (average of one year using data from Figure 1).

Average temperature (atmosphere) [°C]	11.2 (monthly min.: 2.1, monthly max.: 18.2)
Average temperature (sea water) [°C]	10.5 (min.: -0.3, max.: 22.4)
Average salinity (sea water) [g/l]	12.7 (min.: 8.6, max.: 19.3)
Average chloride content (sea water) [g/l]	7.0 ^{a)} (min.: 4.7, max.: 10.6)

a) Assuming a distribution of ions in the sea water as in the Baltic Sea [46].

2.1.3 Sample extraction

After ten years of exposure, the concrete panels were extracted from the sea water and brought to the laboratory at the Danish Technological Institute, and seven Ø100 mm cores were drilled from each concrete panel.

The positions of the cores investigated in this study and the notations used are shown in Figure 2. Appendix B shows the entire sampling plan made during the design of the elements (more than ten years ago). Table 4 gives an overview of the cores investigated in this study: their position, exposure, orientation, investigated properties, and methods applied. The cores were drilled through the panels. The orientation west (W) and east (E) refers to the orientation faced by the analyzed surfaces. The panels are attached perpendicular to the quay. The short side of the panels nearest to the quay is facing north. The prevailing wind is coming from west, but the panels are mounted with a short distance of 20 cm to each other, and no significant differences are expected based on orientation. The subdivision of the cores is described in more detail in the following method descriptions. The numbering of the cores in Figure 2 and Table 4 does not include 6 or 7, because no core was extracted at these core positions (In Appendix B these are marked as “Extra” as cores can be drilled here at later exposure times).

Table 4: Overview of cores: position (distance from bottom of element), exposure zone, orientation, property measured, and methods applied.

Core # (vertical position)	Position, mm from bottom	Exposure zone	Orientation (E = east; W = west)	Property measured	Comment
9	1325	Tidal	W, E	Chloride and calcium profiles	See Section 2.2.5
8	1175	Tidal	W, E	Microstructure and air void structure	See Section 2.2.3 Three thin sections per core (two surfaces and one center)
			W	Elemental analysis	See Section 2.2.4 One polished section from SG
5	725	Submerged		Compressive strength	See Section 2.2.2
4	575	Submerged			
3	425	Submerged			
2	275	Submerged	W	Degree of capillary saturation, RH, total porosity, moisture profile	See Section 2.2.7

			W	Microstructure and air void structure	See Section 2.2.3. One thin section per core (west-facing surface)
1	125	Submerged	W, E	Chloride and calcium profiles	See Section 2.2.5
			W	Portlandite profiles	See Section 2.2.6

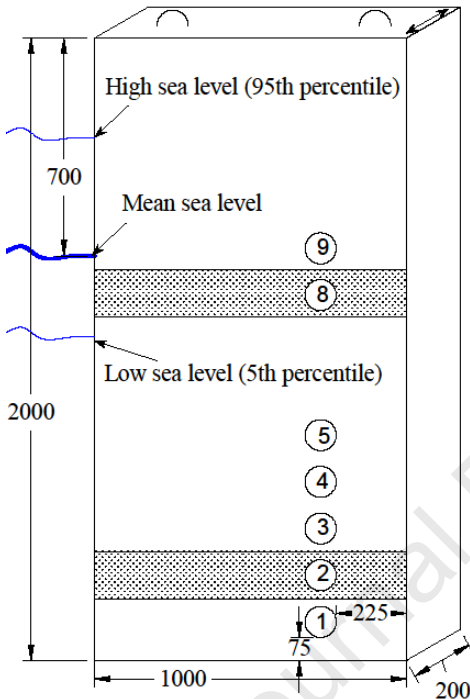


Figure 2: Location of cores extracted after ten years of exposure. The pattern covering positions #2 and #8 indicates that they were not cleaned prior to coring. Vertical distances from core center to bottom of the panel are shown in Table 4. All measures are in mm. “low” and “high” sea level are the 5th and 95th percentiles of the water level.

Before coring, organic growth was scraped off to allow space for the drilling equipment and limit bad odor during processing, except for the horizontal bands where cores #2 and #8 are positioned (see Figure 2); they were not cleaned prior to core drilling because a fully intact surface was desired for petrographic analysis.

Right after coring, each core was cleaned by dipping it in a bucket of tap water and wiping the surface dry with a moist cloth and wrapped in plastic. All cores were stored sealed in plastic bags at 5 °C, except for cores #2 and #8 which were immediately processed for moisture and porosity determination and/or impregnated with epoxy in preparation for petrography as described in Sections 2.1.4, 2.2.3 and 2.2.7.

The abbreviations used to refer to the cores (or samples) are based on the concrete composition and, in the case of chloride ingress and petrography results only, the exposure condition (Tidal or Submerged) and the direction of the exposed surface (East or West). E.g.,

12FA4SF-S-W stands for a concrete, which contains 12% fly ash and 4% silica fume, submerged exposure and west-facing surface, also referred to simply as 12FA4SF.

2.1.4 Subdivision of cores

The #1 and #9 cores were cut off at a depth corresponding to the estimated ingress depth +15 mm to ensure that they retained material sufficiently deep to obtain the background chloride level. The chloride ingress depth after ten years of exposure was estimated by the square root method based on chloride ingress data after half a year, two, or five years of exposure [3]. The cores were further treated as described in Section 2.2.5.

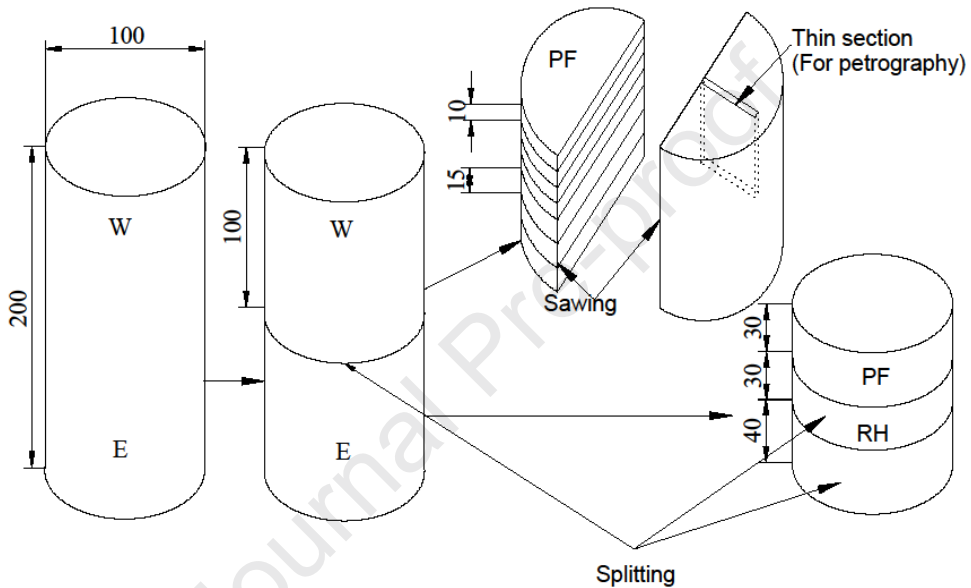


Figure 3: Subdivision of #2 cores. Position of samples for determination of relative humidity (RH) as well as degree of capillary saturation (DCS) and porosity (marked “PF”, see method description in 2.2.7). All measures are in mm. W: west-facing, E: east-facing.

The #2 cores were subdivided as shown in Figure 3. To limit moisture redistribution and drying, the pieces were subdivided immediately after core drilling. Several scales were drawn on the cores to keep track of the actual splitting depths. The cores were first split into two approximately equal-sized half-cores. One half (east-facing) was further split into slices and used for determining (i) the degree of capillary saturation (DCS) and porosity using a modified version of the so-called “pore protection factor method” (PF), and (ii) the relative humidity (RH) of the “bulk”, whereas the other half (west-facing) was used for measuring DCS and porosity profiles in sawn discs. The (east-facing) half cores used for “bulk” DCS, porosity and RH were split so the sample for DCS and porosity determination was positioned closest to the split surface and the sample for RH next to it, as shown in Figure 3. The slices labeled PF and RH were further processed as described in Section 2.2.7. The other (west-facing) half core used for moisture profiles and petrography was sawn using a water-cooled mechanical saw. First, the coarse surface originating from splitting was sawn off. Then the

half-cores were divided axially in half, and one of these half cylinders was subdivided inwards from the exposed surface into seven slices, where the four outermost slices were 10 mm thick, the next two were 15 mm thick, and the last slice was approximately 10 mm. Immediately after being sawn, the slices were dipped in water, wiped surface-dry with a moist cloth and weighed. Then the sample heights were measured, and their actual position in the panel calculated assuming equal loss due to sawing between each slice. From the second half cylinder of the west-facing part, a thin section was prepared for petrography (see Figure 3).

The #3, #4 and #5 cores were ground clean on the surface using a grinding cup to achieve a specimen flatness conforming with DS/EN 12390-1:2000 [47] and used for testing of compressive strength (dimensions approx. $\varnothing 100 \times 196$ mm).

Three thin sections were prepared from the #8 cores using the technique described by Jakobsen et al. [48]. One at a similar position at the west-facing surface as shown in Figure 3 and an additionally one at the east-facing surface, and one in the center of the cores.

2.2 Methods

2.2.1 Visual inspection

The concrete panels were visually inspected after being lifted out of the water and again after scraping off organic matter from parts of the panels. The panels were examined for organic growth, scaling, cracks, and mechanical damage originating from handling.

2.2.2 Determination of mechanical properties

Compressive strength was measured on #3, #4 and #5 cores in accordance with DS/EN 12390-3 [49]. Density was measured in accordance with DS/EN 12390-7:2012 [50].

2.2.3 Petrography

The petrographic examination was performed on fluorescent-impregnated thin sections from the #2 and #8 cores using a Leica DM2500P optical polarizing microscope equipped with a fluorescent facility. Each section was vacuum impregnated with an epoxy resin containing a fluorescent dye. Next, the impregnated section was mounted on a glass plate, and ground to a thickness of 20 μm . Finally, the section was covered by a cover glass. The thin section was then examined in a polarizing optical microscope using transmitted light, crossed polarized light, and blue transmitted light through a BG12 excitation filter with a K530 yellow blocking filter (fluorescent mode).

The vacuum impregnation of the section with epoxy fills all voids and cavities with fluorescent epoxy. When fluorescent light is transmitted through the thin section in the microscope, the fluorescent epoxy emits yellow light that makes voids, cavities, and cracks easy to identify. The fluorescent epoxy also impregnates the capillary pores in the hardened cement paste, which makes a dense cement paste with low capillary porosity appear a darker green than a more porous cement paste with a high capillary porosity.

The water-to-cement ratio (w/c) of the concrete was estimated with an accuracy of ± 0.02 by comparing with known w/c references [48].

The thin sections were analyzed for scaling, carbonation, leaching, micro-cracks, capillary porosity, and re-precipitation of solids. Cracks were divided into three types, depending on the crack width: 1) Coarse cracks: > 100 μm ; 2) Fine cracks: 10–100 μm ; 3) Microcracks: < 10 μm .

2.2.4 Elemental analysis

As identification of some phases by petrography in the very dense slag containing concrete (SG) after 10 years exposure proved difficult due to a highly dense texture, a polished section was prepared for SEM from #2 core of SG. The polished section was placed next to the thin section and examined in a FEI Quanta 400 ESEM equipped with a Thermo SNN EDS analysis unit operated in high vacuum mode at an accelerating voltage of 20 keV. The samples were analyzed for the elements: Na, Mg, Al, Si, S, P, Cl, K, Ca, Mn, Ti and Fe. Results were obtained by performing line traverses from the surface to a depth of 85–105 μm in selected paste areas measuring 10x10 μm . The analysis step size was 20 μm in the outer 100 μm , followed by steps of 100 μm up to 1 mm depth, then 0.25–0.5 mm up to 4 mm depth, 1 mm up to 10 mm depth, 2 mm up to 20 mm depth, and then finally 10 mm for the rest of the depth. Cement grains and aggregate were selectively avoided in the area selection.

2.2.5 Determination of chloride and calcium content

The #1 and #9 cores (see Figure 2) were divided into 10–12 sections spanning over the estimated ingress depth with lowest depth increments near the surface. Sections up to 4 mm depth were profile-ground, whereas sections of 6–15 mm were cut using a water-cooled precision diamond saw and subsequently crushed.

Approx. 5 g of the concrete powder of each section was weighed after drying at 105 °C overnight. The dried powder was dissolved in 50 ml 75 °C warm (1:10) HNO_3 and left to digest overnight. The samples were filtrated the following day. After the initial filtration, the filter was washed twice with 1% HNO_3 and the container with the filtrate was filled up to 100 ml by adding demineralized water. The filtrate was used for both chloride and parallel calcium analyses to ensure comparable results.

For chloride analysis, 50 ml of filtrate was added to 50 ml demineralized water.

For calcium analysis 5 ml of filtrate was added to 90 ml demineralized water, 5 ml Triethylamine, 5 ml 5.0 M NaOH, and 0.15 g calcein indicator.

The chloride and calcium contents were measured using potentiometric titration with a TitroLine 7000 titrator from SI Analytics. The chemicals used for titration were 0.1 M AgNO_3 for chloride and 0.1 M EDTA disodium salt for calcium analysis.

The chloride profiles presented in the paper are total chloride content and not calibrated for calcium content.

For completeness calcium calibrated chloride profiles are shown in Appendix C. The equation used to calibrate for paste fraction is given in Eq. 1.

$$Cl_{calibrated} = \frac{wt\%Cl_{measured}}{wt\%CaO_{measured} \times \frac{40}{56}} \times wt\%Ca_{Theoretical} \quad (1)$$

where $Ca_{Theoretical}$ is calculated based on the binder content of the concrete (Table 1) and the calcium content of the binders as measured by X-ray Fluorescence (Table 2). The molar weight of calcium is 40 g/mol, and 56 g/mol is the molar weight of calcium oxide. The calibration for the calcium content was originally done to correct for potential variations in the paste fraction, e.g., due to the wall effect. However, as discussed in a separate paper [51], leaching reduces the calcium content in the concrete, which is therefore not a stable measure for the paste fraction.

2.2.6 Determination of portlandite

To quantify the degree of leaching in the samples, portlandite (CH) profiles were obtained using a Mettler Toledo TGA/DSC 3+. Approximately 300 mg of the profile-ground powder from each section from #1 cores were loaded in 600 μ l corundum crucibles. The samples were heated from 60 to 850 $^{\circ}$ C at a rate of 10 $^{\circ}$ C/min while using N_2 as purge gas at a flow of 50 mL/min. The mass loss of the samples was monitored as a function of temperature.

The mass loss due to CH decomposition was quantified by using the tangential method in the range 400–500 $^{\circ}$ C [52, 53]. The limits of the temperature interval are determined based on the derivative of the mass loss curve. The CH content by wt.% of concrete was normalized to the dry sample weight at 850 $^{\circ}$ C in accordance with Eq. 2.

$$CH = \frac{w_{400} - w_{500}}{w_{850}} \times \frac{74}{18} \quad (2)$$

where w_{400} , w_{500} and w_{800} are the sample weights at approx. 400, 500 and 850 $^{\circ}$ C respectively, 74 g/mol is the molar weight of $Ca(OH)_2$, and 18 g/mol is the molar weight of H_2O .

2.2.7 Determination of moisture content and porosity

The moisture content was characterized as relative humidity (RH) and degree of capillary saturation (DCS). Porosity was determined as suction porosity relative to either drying at 50 $^{\circ}$ C or 105 $^{\circ}$ C, and macro porosity.

After subdivision as described in Section 2.1.4, the saw-cut concrete slices from the west-facing half #2 cores (labeled PF in Figure 3) were immediately cleaned by dipping in a bucket of water, dried with a moist cloth, and weighed (w_{start}). The split slice from the east-facing half #2 cores were used directly. The timeframe from core drilling to measuring w_{start} was approximately ten minutes. Each slice was subsequently partly submerged in a water bath for one day to avoid trapping of air, and thereafter fully submerged until it reached a constant mass (<0.02% weight change/day). The capillary-saturated slices were weighed in air (w_{sata}) and under water (w_{satw}) to determine their volume ($V = w_{sata} - w_{satw}$).

RH was determined on the slice labeled RH in Figure 3. Initially, the edges were chiseled off to obtain a sample unaffected by drilling and potential immediate moisture loss. The sample was then crushed in a jaw crusher, and the finest parts most susceptible to moisture loss

were quickly discarded through a 2 mm sieve, while the larger pieces measuring 2–4 mm were placed in a glass test tube and sealed with a rubber plug. Duct tape was used to secure the rubber plug. The filled test tubes were placed in a temperature-controlled room (22 ± 2 °C). The RH was measured with a Novasina HygroDat 100 system (sensor precision $\pm 0.5\%$ RH in the range 11–95% at 25 °C) and recorded daily starting from three days after placement in the analyzer.

A modified version [19] of the PF method originally proposed by Sellevold and Farstad [54] was used for porosity, DCS, and moisture content measurements. The method was applied both on concrete slices (labeled PF in Figure 3) obtained by sawing (dry sample weight 63–120 g) and splitting (dry sample weight 413–569 g) – in both cases by using a scale with 0.01 g accuracy.

The capillary-saturated slices were dried at 50 °C for six weeks with weekly measurements until a constant mass ($<0.02\%$ weight change/day) was reached to obtain their dry weight after drying at 50 °C (w_{dry50}), and then dried at 105 °C for 17 days with a measurement after 16 days to conclude a constant mass ($<0.02\%$ weight change/day) was reached to obtain their dry weight (w_{dry105}).

The dry slices were again partly submerged in a water bath for one day to avoid trapping of air and thereafter fully submerged for four months, until a constant mass ($<0.02\%$ weight change/day) was reached, and then weighed in air (w_{sata-2}) and under water (w_{satw-2}) for control. Finally, the re-saturated slices were placed in a water-filled pressure tank exerting 5–15 MPa for two days and weighed within two minutes of releasing the pressure to prevent loss of water (w_{pres}).

The weights determined were used to calculate the following properties:

$$V = w_{sata} - w_{satw} \quad (3)$$

$$\text{Suction porosity at 50 °C ("capillary porosity")} = (w_{sata} - w_{dry50})/V \quad (4)$$

$$\begin{aligned} \text{Suction porosity at 105 °C ("capillary and gel porosity")} \\ = (w_{sata} - w_{dry105})/V \end{aligned} \quad (5)$$

$$\text{Macro porosity} = (w_{pres} - w_{sata})/V \quad (6)$$

$$\text{Degree of capillary saturation} = (w_{start} - w_{dry105})/(w_{sata} - w_{dry105}) \quad (7)$$

3 Results

3.1 Visual appearance and exposure

All concrete surfaces exhibited some organic growth. Figure 4 shows a typical example of organic growth on a concrete panel right after pulling it out of the water. The part below

mean tide level (red line, 1.3 m from the bottom) is covered with barnacles and mussels, the upper approx. 0.35 m is dry, and in between is a gradual transition from heavy to light organic growth.

All cores were taken in accordance with the coring plan (Figure 2) from visually intact areas (without macroscopic cracks, scaling or mechanical damage). From Figure 1 and Figure 2, it can be deduced that the #8 cores from the tidal zone for petrography were submerged the vast majority of the time, while the #9 cores from the tidal zone for chloride analysis were submerged approximately half of the time with assumed frequent wetting from waves. Figure 4 shows heavy organic growth with barnacles and mussels, not only on the submerged part of the panel, but also where the #9 cores for chloride analysis were taken.

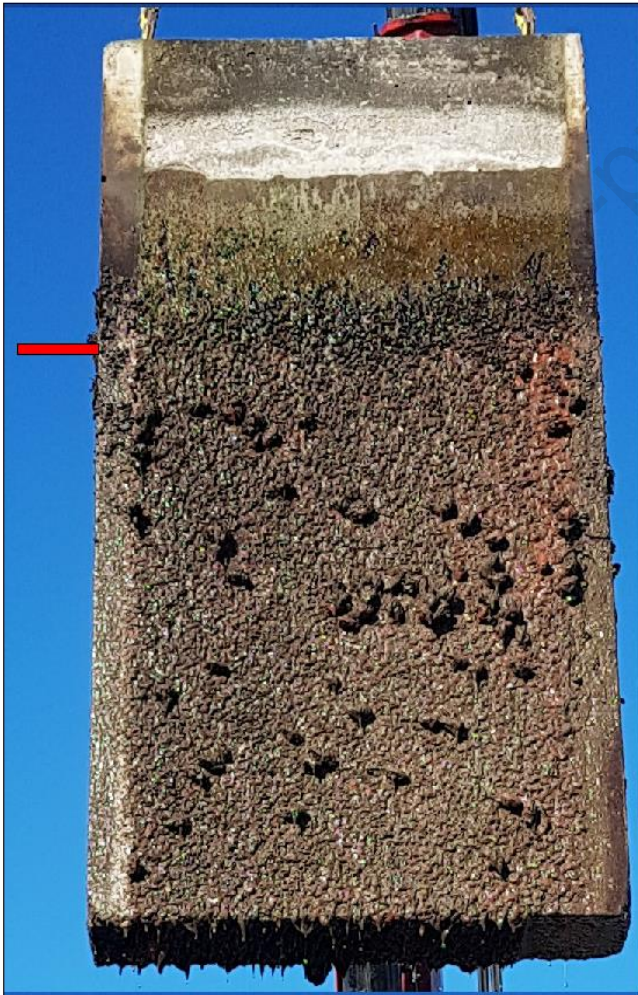


Figure 4: Visual appearance of an entire concrete panel right after lifting out of the water. The part below mean sea level (red line, 1.3 m from the bottom) is covered with barnacles and mussels, the upper approx. 0.35 m is dry, and in between is a gradual transition from heavy to light organic growth.

3.2 Mechanical properties

Table 5 shows the compressive strength of cores extracted after ten years of exposure. The failure mode of all cores was normal, meaning compression failure at approx. the middle of the height of the core.

Table 5: Compressive strength [MPa] of cores extracted after ten years of exposure.

Concrete ID	PC	15FA	25FA	4SF	12FA4SF	SG
#3 cores	64.8	76.4	76.2	76.5	73.9	67.0
#4 cores	65.4	76.6	74.2	79.1	78.2	67.2
#5 cores	64.3	79.0	73.6	75.6	73.1	65.4
Average	64.9	77.3	74.7	77.1	75.1	66.5
Standard deviation	+/- 0.6	+/- 1.2	+/- 1.1	+/- 1.5	+/- 2.2	+/- 0.8

3.3 Microstructure

The petrographic analysis using optical polarizing microscopy showed that all the concretes exhibited a microstructurally changed zone in the outer approximately 10 mm of the panel after ten years of exposure. This zone comprised minor surface scaling, a leached and micro-cracked zone, a zone with bicarbonate precipitation, and a zone with a diffuse, opaline shine. The various microstructural features are explained in the following paragraphs, examples are shown in Figure 5 and further details are found in Jakobsen et al. [10]. Table 6 and Figure 6 summarize the depths to which the features were found.

All concretes exhibited uneven surfaces with exposed sand grains indicating minor surface scaling typically less than 0.5 mm in depth (Appendix D). Occasionally, the slightly scaled surfaces were covered by a thin calcite crust (CaCO_3), but without any sign of intermixing with brucite ($\text{Mg}(\text{OH})_2$). The reason no brucite was observed might be that organic growth (as depicted in Figure 4) has hampered the formation of a brucite layer for both exposure conditions [28].

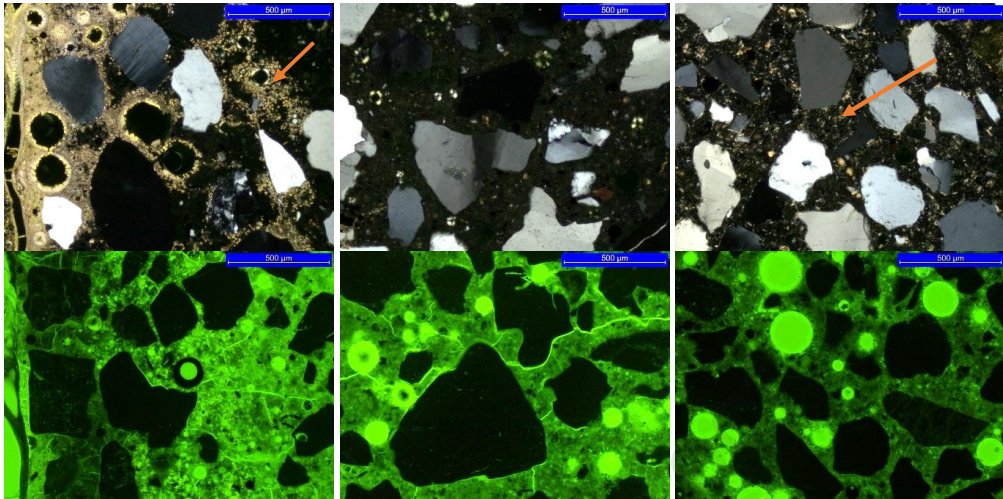
From the surface to a maximum depth of 1 mm (Table 6), the paste appears completely black when viewed in cross-polarized light due to the depletion of calcium, not only from C-S-H but also from portlandite ($\text{Ca}(\text{OH})_2$). This leached zone (Figure 5, top left) contains brittle micro-cracks, many of which after ten years appear to have self-healed with calcium carbonate. Earlier SEM-EDX studies of the concrete showed that calcium in the former Ca-containing phases had been replaced by magnesium originating from sea water forming M-S-H. This is the main phase of the black zone.

Below and/or intermixed with the black leached zone, there is a zone containing a popcorn-like calcite formation to a maximum depth of 2 mm. The phrase “popcorn carbonation” describes the morphology. Popcorn carbonation is commonly observed when concrete is submerged in water rich in dissolved bicarbonate, resulting in a very distinct split of the paste into a decalcified C-S-H phase and a popcorn-like calcite phase (Figure 5, top left). Typically, such a process results in a weakening of the paste [55, 56].

The zone stretching deepest and about 10 mm into the concrete was optically observed to deviate from the bulk. In this zone, the paste appears somewhat micro-cracked and with a diffuse and opaline shine (Figure 5 center). Earlier studies, including SEM-EDX analysis on the same concretes, have shown that this zone is enriched in both sulfur and chloride [10, 13]. The special appearance of this so-called “opaline” zone is recognized in cross-polarized light in the optical polarizing microscope. The shine is due to infilling of the capillary pores, e.g., by secondary precipitation products such as ettringite. When the light in the polarizing microscope passes through such a “blocked” paste, it spreads in all directions making it difficult to identify individual phases in the paste such as portlandite.

In this study, the opaline zone was optically confirmed in all the concretes except the concrete containing slag (SG), as the highly dense texture of the slag concrete after 10 years exposure blurred the identification. In earlier studies using SEM-EDX, Jakobsen et al. [10] found that the depth of the opaline zone coincided with a sulfur enrichment of the paste, so in this study we also used SEM-EDX analysis to get a measurement for the depth of the opaline zone in the slag concrete (SG).

All the concretes showed higher porosity within the outer 10 mm of the concrete (Table 6). Using the fluorescent-light mode, the increased porosity observed in the surface region corresponds to an apparent w/c ratio of 0.70 or more (based on its green tone). The increased paste porosity stretched over the black leached and popcorn-carbonated zones as well as a part of the opaline zone (Table 6). Note the difference in green tone going from left to right in the bottom row in Figure 5.



Surface zone (Typical <1 mm depth): intermixed leached paste and popcorn carbonation (marked with arrow), high porosity.

Opaline zone (Typical of 2–10 mm depth): no visible CH, with increased porosity and micro-cracking.

Bulk (Typical of >10 mm depth): visible CH (marked with arrow) and apparent w/c of 0.40.

Figure 5: An example (concrete 15FA) of the microstructural change appearing in the surface region after ten years of submerged exposure to sea water (core #2; exposed surface is to the left). Images were taken in cross-polarized (top row) and fluorescent-light mode (bottom row) and measure 1.5 mm in width. The scale bar = 500 µm. The microstructurally changed zone includes: (left column) a slightly scaled surface zone with intermixed leached and popcorn-carbonated paste and high porosity; (center column) an opaline zone with a blurred appearance and no visible portlandite (CH), but often with ettringite and/or thaumasite in air voids; and (right column) bulk concrete with visible CH and an apparent w/c ratio of 0.40.

Table 6 gives the surface condition, maximum depth of zonation, micro-cracks (width < 10µm), and precipitation products for the tidal and submerged concrete in the investigated samples as the average depths to which they extend, and Figure 6 shows the zonation in graphic form. All future references to depths of zonation in this paper refer to these depths. We observed that in all investigated panels the porous zone was deeper in the submerged exposed part than in the tidal exposed part. The opaline zone was generally similar for tidal and submerged exposure, except for concretes 15FA and 12FA4SF where the opaline zone was slightly deeper for submerged exposure. The depth of the opaline zone in SG was significantly less than for the remaining concretes in both tidal and submerged exposure.

Table 6: Depths of various microstructurally changed zones, precipitated phases, and micro-cracks observed in the optical polarizing microscope after ten years of exposure (west-facing surface). Note that the depth of the zones was measured from the current surface and differs from the depth from the initial surface due to scaling.

Concrete ID		Depth of zonation [mm]											
		PC		15FA		25FA		4SF		12FA4SF		SG	
Submerged (S) or tidal (T)		T	S	T	S	T	S	T	S	T	S	T	S
Microstructurally changed zone	Black leached zone [mm]	1.2	0.3	0.4	0.3	0.2	0.8	0.2	0.3	0.6	0.4	0.4	0.4
	Zone with popcorn carbonation [mm]	2.0	1.2	1.2	1.6	1.0	1.2	1.2	1.2	2.0	1.2	2.0	3.0
	Opaline zone [mm]	10	10	7	10	10	10	8	8	7	10	- ^d	- ^d
	Porous zone [mm]	5	10	4	10	3	10	4	8	5	10	3	4
Excess ettringite in voids [mm]		8	10	10	6	6	11	6	9	10	6.5	13	10
Thaumasite in voids [mm]		4	4 ^a	2	3	3	4 ^b	3	3 ^c	3	3	-	-
Depth with increased # of micro-cracks [mm]		10	10	8	10	6	9	15	8	20	10	12	5
Self-healing micro-cracks in outer max 2 mm		x	x	x	x	x	x	x	x	x	x	x	x

^a Significant until 1.2 mm

^b Where surface is scaled. Only around 0.5 where surface is intact.

^c Very systematic starting directly below the “popcorn-carbonated” zone down to about 1.5 mm below it, but locally found down to 4 mm, coinciding with the maximum depth of “popcorn” carbonation.

^d Not seen for GGBS-based concrete.

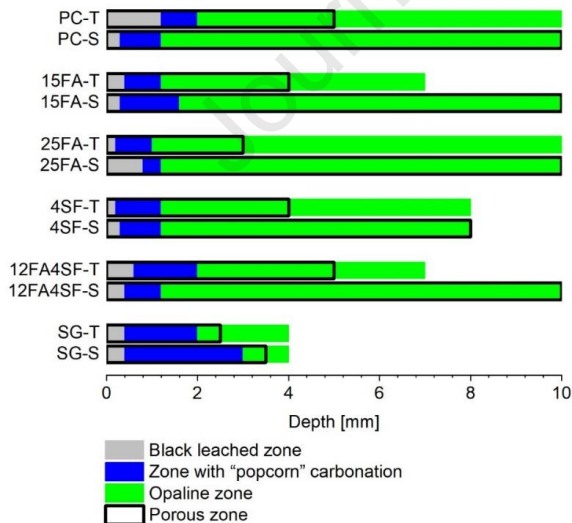


Figure 6: Graphical representation of the extent of zonation observed by petrography on thin sections from the ten-year marine-exposed concretes. Note that the figure is simplified (in reality, the depth varies across the thin sections as seen in Figure 5 for 4SF-T-W). Popcorn carbonation may be intermixed with the black leached zone. The opaline zone in SG was estimated from SEM-EDX data.

3.4 Chloride content

Figure 7 shows all the analyzed chloride profiles for ten years of exposure organized by concrete. The same chloride profiles, but organized by exposure type, are shown in Appendix E. Appendix C shows the chloride profiles corrected for paste content using Eq. 1 in Section 2.2.5 and given as % by wt. of binder.

Journal Pre-proof

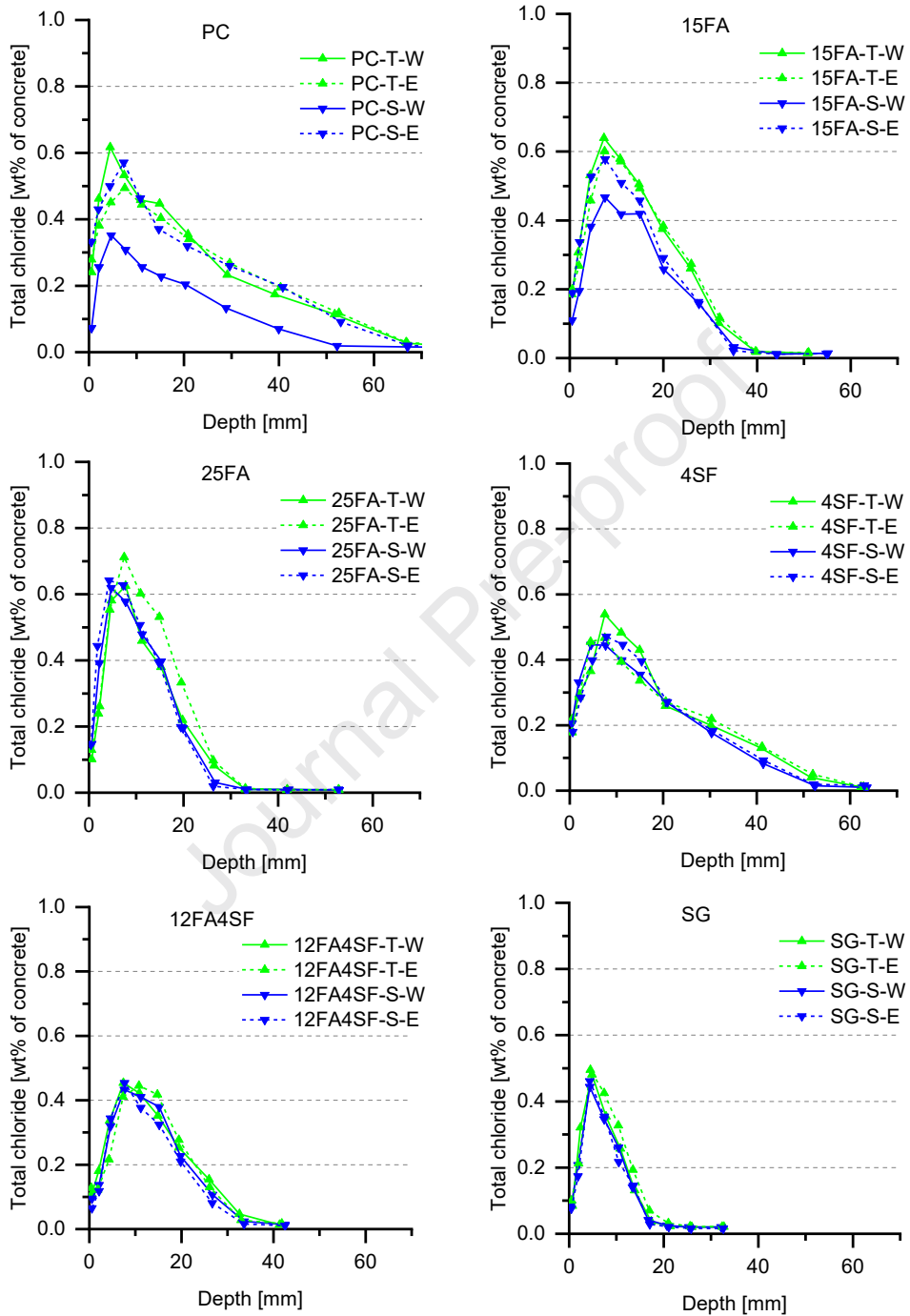


Figure 7: Chloride profiles after 10 years of tidal (T) and submerged (S) exposure measured from the west and east-facing surfaces.

Out of all the chloride profiles determined after ten years of exposure, there seems to be one outlier, namely the PC-S-W, which shows considerably less chloride ingress than the other cores taken from the PC concrete (see Figure 7, top left). The core from the neighboring position of the PC-S-W, which was extracted after two years, was also an outlier. This indicates a potential nonrepresentative concrete composition in this lower corner of the panel.

If using the penetration depth of 0.1% chloride by wt. of concrete as a measure for the chloride ingress resistance, the six concretes can after 10 years of exposure be ranked as follows for increasing chloride ingress resistance (independent of submerged or tidal exposure): PC < 4SF < 15FA < 12FA4SF < 25 FA < SG. It is noted that the shape of the chloride profiles for PC and 4SF is much flatter than for the remaining concretes.

3.5 Portlandite content

The portlandite content (CH) determined by TGA is shown in Figure 8 as a function of depth from the exposed surface of all the analyzed concretes.

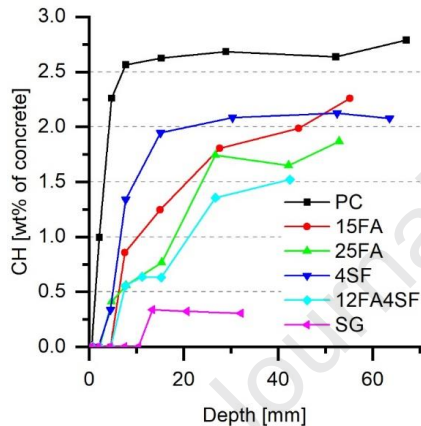


Figure 8: Amount of portlandite (CH) as determined by TGA plotted against depth from the exposed surface for all the investigated concretes.

Four of the six investigated concretes show a near constant CH content in the deeper sections investigated. This CH content can be considered as the bulk CH content in the concrete. The highest bulk CH content is, as expected, observed for PC concrete. For the other concretes, the bulk CH content is lower due to the dilution of the Portland cement (which provides the CH) by the supplementary cementitious materials (SCMs) and due to the pozzolanic reaction of the SCMs (which consumes CH).

All CH profiles decrease towards the exposed surface, which can be mainly attributed to CH leaching in the outer zone [57]. However, enhanced reaction of the SCMs in this zone might also contribute to the decrease in the CH content. Nevertheless, calcium can still increase towards the surface due to the formation of a calcite crust and due to the wall effect during casting, which causes an increase in paste fraction towards the surface.

3.6 Moisture content and porosity

Table 7 gives the relative humidity of pieces taken from the center of a layer 40–70 mm from the east-facing surface of #2 cores. RH values in the range 86–91% were obtained, which are similar to those obtained by De Weerd et al. [57], who reported RH values ranging between 88% and 92% at a depth of 70 mm in concrete submerged for 16 years. The values reported in Table 7 are single measurements. A similar setup was used by De Weerd et al. [57], from which a standard deviation of approximately 1% RH was obtained on three replicates for a series of four concretes. Taking into account a similar standard deviation, there is no great difference between the concretes investigated in this study. There is, however, an indication that the PC concrete has a slightly higher RH than the SCM-containing concretes.

Table 7: Relative humidity [%] of a concrete piece taken from the center of a slice 40–70 mm from the east-facing surface of the #2 core from each of the six concretes and the temperature at which it was measured.

Concrete ID	PC	15FA	25FA	4SF	12FA4SF	SG
Relative humidity [%]	91	87	86	87	90	87
Temperature [°C]	22.3	22.3	22.3	22.2	22.2	22.3

Figure 9 shows the degree of capillary saturation (DCS) and porosity measured on the sawn slices and the split “bulk” samples from #2 cores. The depth of the data points shown in Figure 9 represents the center of the slices used. The thickness of the slices varied between 8 and 15 mm as explained in Section 2.1.4. Thinner slices would have provided a more detailed graph, but the errors would increase due to the greater influence of water from sawing and the reduction in the sample size. The data points plotted at depth 115 mm correspond to 85 mm depth from the east-facing surface and relate to the measurements performed on the split “bulk” samples.

Figure 9a and -b show the measured suction porosity as a function of depth from the west-facing surface relative to dry weight at 50 °C and 105 °C, respectively. The suction porosities are fairly similar for all six concretes. From a depth of approx. 15 to 130 mm, there are only minor variations, and they all seem to lie between 5 and 10% by vol. when expressed relative to the dry mass at 50 °C, and between 10 and 13% by vol. when expressed relative to the dry mass at 105 °C. All concretes showed an increase in the suction porosity of the outermost slice (approx. 8–13 mm) at the exposed surface, which can be expected due to the “wall-effect”. As the exposed surface is a cast surface, the outermost zone cannot host large aggregate particles and consequently there was a higher paste content in these sections compared to the bulk. This higher paste content will give rise to a higher suction porosity. In addition, leaching might have led to an increase in the suction porosity due to the loss of material. From optical microscopy (see Figure 6), the depth with higher porosity than the bulk, the porous zone, was measured to be approx. 10 mm for the submerged cores, which agrees well with the observed higher suction porosity in the outer 8–13 mm. The measured suction porosities agree well with De Weerd et al. [19], who found suction

porosities about 1% higher for concretes with slightly higher w/b ratios (0.42–0.44 vs. 0.4) and similar suction porosities for a concrete with w/b 0.4.

Figure 9c shows the macro porosity of the concretes as a function of depth from the west-facing surface. The macro porosity seems to decrease in the outermost section. This could be due to either instability of air voids in the outermost section and/or filling of the air voids with reaction products, such as calcite, ettringite or thaumasite. The lower measured macro porosity in the outermost layer (ranging from 8 to 13 mm) agrees well with observations in the microscope, which showed that excess ettringite was present in the air voids in the outer 6–13 mm (see Table 6). The measured macro porosity agrees well with the target air content of 3.5–5.5%, and that the air content was slightly above target for PC (5.8%), which shows the highest macro porosity in Figure 9c. In comparison, De Weerd et al. [19] found a macro porosity of approximately 1.8% independent of depth for concretes with a fresh air content of 3–3.6%.

Figure 9d shows the DCS of the concretes as a function of depth from the west-facing surface. The reason the outermost point is above 100% for some concretes is assumed to be insufficient cleaning of organic matter prior to making the measurement. The consequence, according to the method described in 2.2.7, is a " w_{start} " that is too high, which causes the measured DCS to be too high in the outermost point. The measured porosities shown in Figure 9a–c are expected to be unaffected. The DCS decreases from nearly saturated conditions at the surface to around 90% at a depth of approx. 30 mm and deeper in. The low bulk DCS shown in Figure 9 and the RH values in Table 7 indicate self-desiccation, while the increase in DCS as the surface is approached indicates moisture uptake from the environment.

If we compare the results obtained on the sawn slices at a depth of for example 50 to 90 mm with the split bulk sample (depth 115 mm), they are in good agreement, indicating relatively little impact of water added from the water-cooled saw or from size-related uncertainties. The exception is the slag-containing concrete (SG), where DCS of the split bulk sample is around 5% less than for all the sawn samples of SG. We have no explanation for this single lower value, except that it might be a measurement error.

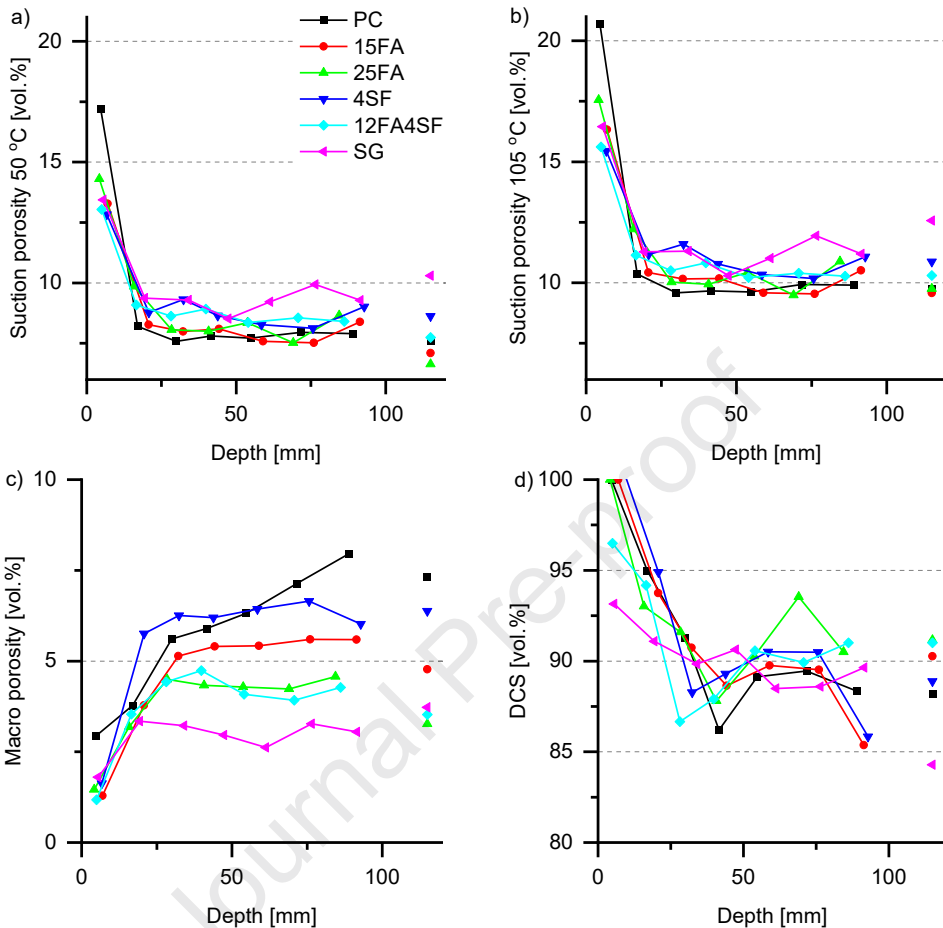


Figure 9: Porosity and DCS of the sawn samples plotted at their average depth as well as split “bulk” samples taken at an average depth of 115 mm from the west-facing surface (85 mm from the east-facing surface): a) Suction porosity obtained by drying at 50 °C (capillary porosity); b) Suction porosity obtained by drying at 105 °C (gel and capillary porosity); c) Macro porosity; and d) DCS. Note that the outermost point is assumed to be too high due to insufficient cleaning of organic matter prior to measurement.

4 Discussion

4.1 Material changes over time

4.1.1 Development of compressive strength

As binders hydrate, the porosity of concrete decreases and it becomes denser and gains strength [58]. As a check on the development of hydration at a macroscopic level, we determined the change in compressive strength over time. By comparing the measured compressive strength with previous results (Figure 10, tabulated in Appendix F), we can see that the development of compressive strength stopped after five years. For most of our

concretes, there was even a slight drop in the compressive strength over the following five years, but the reason for this slight drop is unknown.

There is not much in the literature on the long-term development (more than five years) in compressive strength. Generally, a slight increase in compressive strength is reported after five years [59-63], but a few papers show a decrease after five years of exposure for some concretes: OPC, SF and FA concretes with w/c 0.45–0.8 in hot and arid conditions in Kuwait [62], and SF concrete in field exposure, but not in laboratory-stored samples [61]. In a study of 50-year-old concretes exposed outdoors in northern USA, Washa and Wendt [59] found that the compressive strength of concretes made with coarsely ground cement with high C_2S content continued to increase over the 50-year period, whereas concrete made with finely ground cement and low C_2S content reached a maximum after 10–25 years. So, the above-mentioned literature suggests that a retrogression after five years in field-exposed concrete is uncommon, but not excluded.

For the concretes examined in this study, the outer 3 mm of each #3, #4 and #5 core end was ground off using a grinding cup to achieve a specimen flatness conforming with EN 12390-1 [47] prior to measuring the compressive strength. This means that the black leached zone with severe cracking as determined by optical polarizing microscopy in Section 3.3 was ground off, but not the entire depth with micro-cracks and chemical degradation, which reached deeper (see Table 6). The present data does not allow for further evaluation of the observed slight decrease in compressive strength after 10 years of exposure.

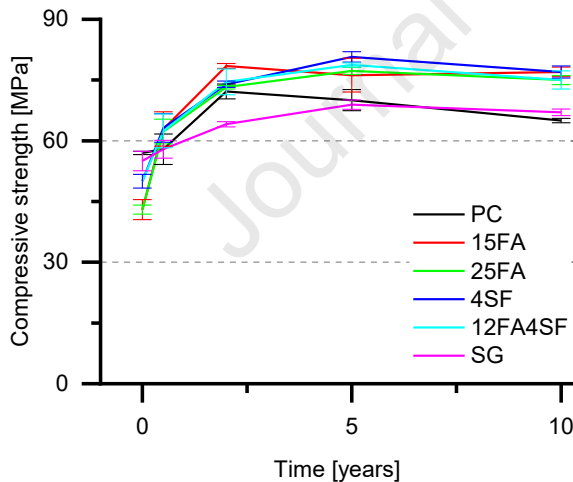


Figure 10: Development in compressive strength with exposure time for all six concretes. Error bars show \pm std. dev.

4.1.2 Development of zonation

For concrete exposed in the tidal zone, petrographic investigations, similar to those presented here for ten years exposed concrete, were carried out after half a year, two, and five years [44]. Figure 11 shows a comparison of the observed development of zonation. Similar results were obtained from the west and east-facing sides of the panels, so only results from the west-facing surface of the panels are shown. We should note that, due to a

lack of quantification of surface scaling (see Section 3.3 and Appendix D), a small offset of the depth has not been included in the figure.

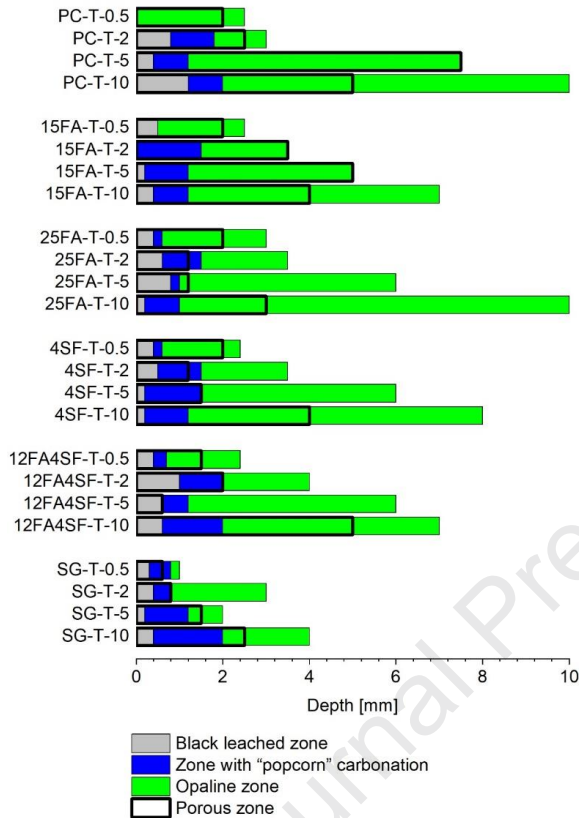


Figure 11: Presence of zones (measured from the surface level at the time of coring) as observed after half a year, two, five, and ten years marine tidal exposure (west-facing panel sides). The opaline zone in SG was estimated from SEM-EDX data.

There is no clear trend between exposure time and the depth for either the black leached zone or the popcorn-carbonated zone, which would be expected due to the ingress of magnesium and bicarbonate. This could be explained by the amount of surface scaling, which could be at significant levels when compared to the limited depths of these zones. A progressing surface scaling would effectively alter the starting point from which the depth is measured. The scaling after ten years of exposure is estimated to be around 0.5 mm, which is significant compared to the observed depth of both the black leached zone (0.2–1.2 mm) and the popcorn-carbonated zone (1–2 mm).

If we look at the depth of the opaline zone, which is much greater than the estimated scaling, there is a clear trend of increasing depth (and width) of the zone with increasing exposure time (Figure 11).

Figure 11 shows a trend of increasing depth of the porous zone with increasing exposure time. The depth of the porous zone is greater after ten years than after six months of exposure for all six concretes (50–300% increase in depth depending on the concrete).

4.1.3 Development of chloride profiles

For comparison, chloride profiles from up to ten years of tidal and submerged exposure are plotted in Figure 12 and Figure 13, respectively.

Journal Pre-proof

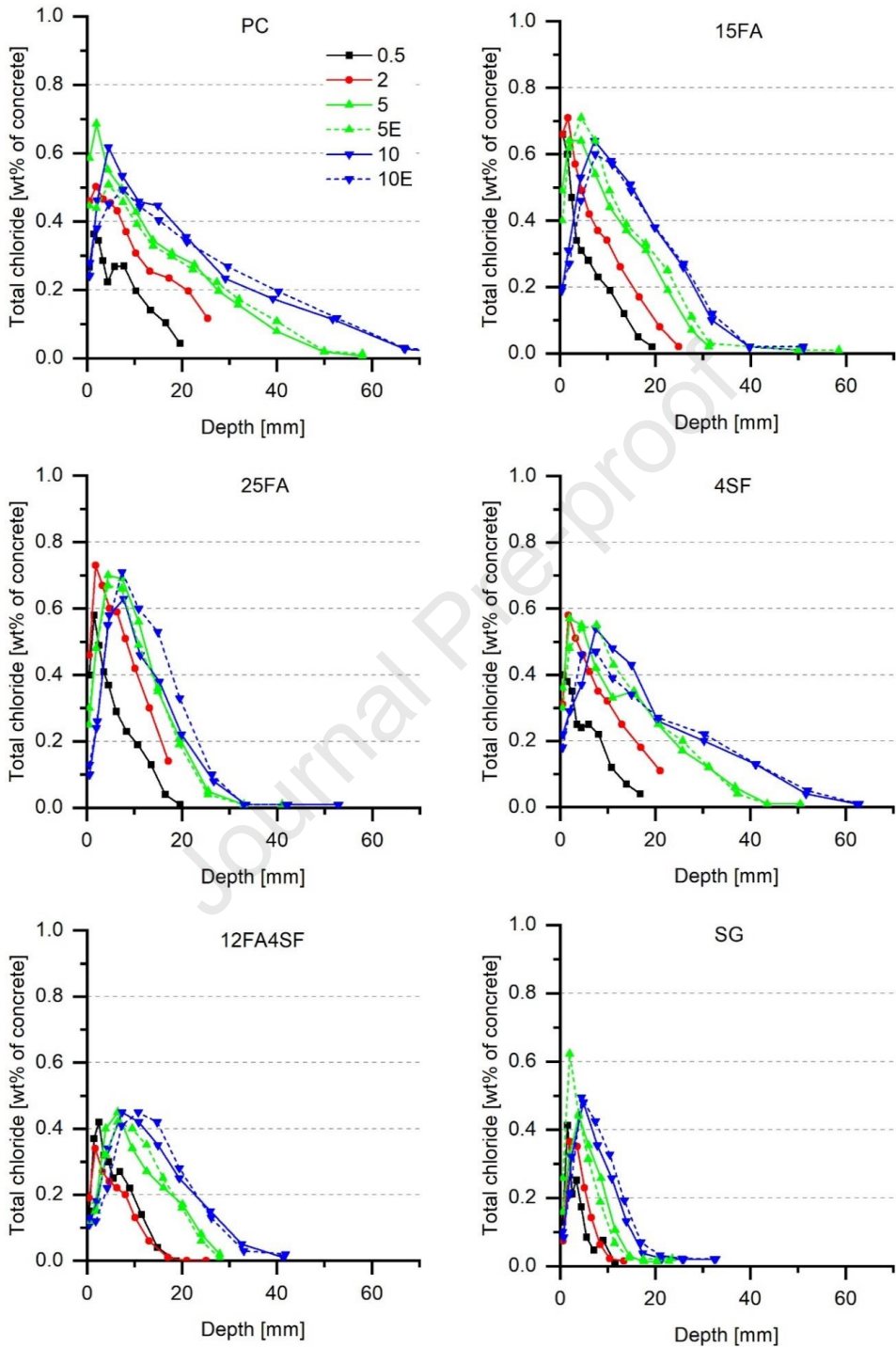


Figure 12: Chloride profiles after half a year, two, five, and ten years in tidal exposure. All profiles are from the west-facing side of the panels, unless marked (E, dashed line) for the east-facing side.

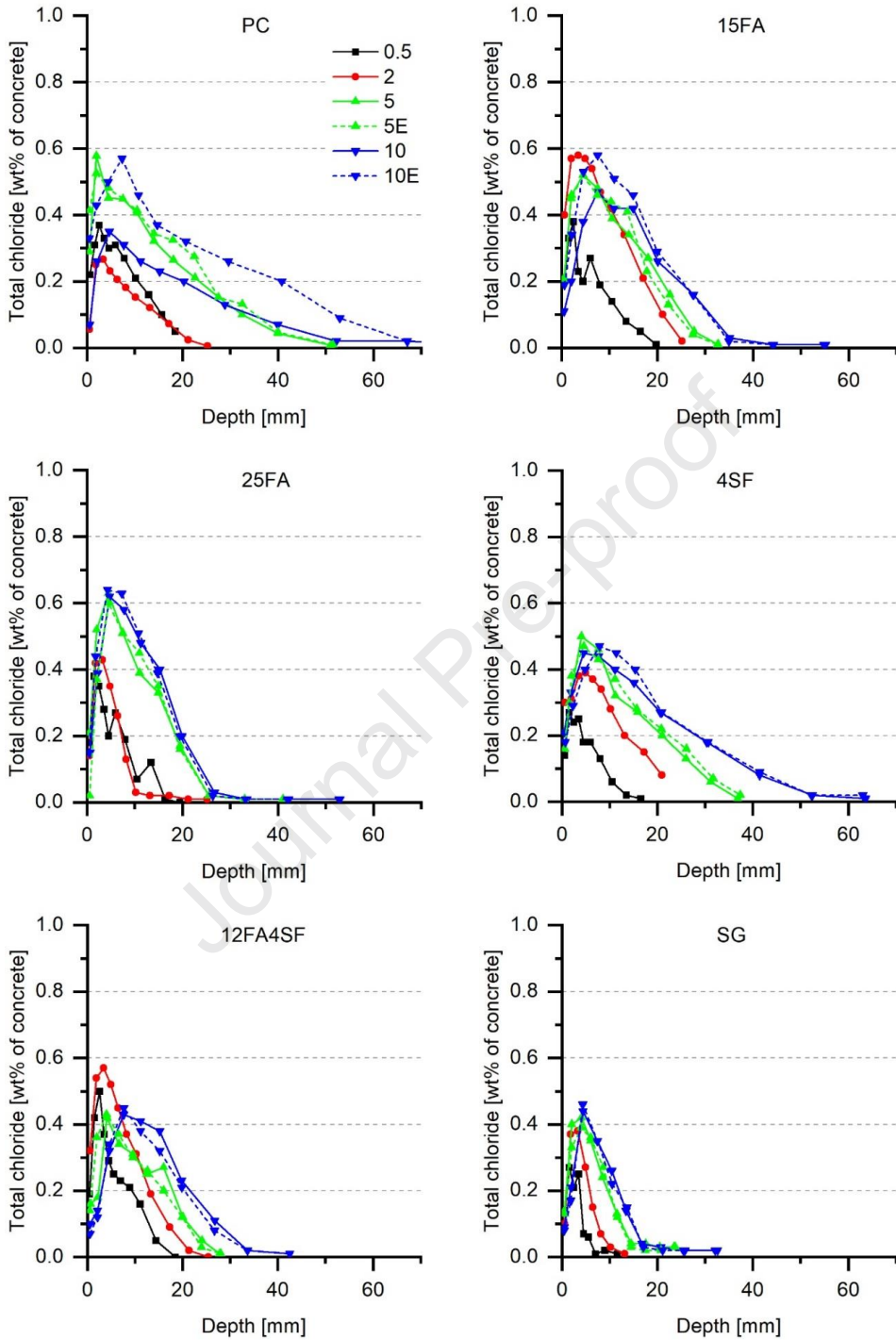


Figure 13: Chloride profiles after half a year, two, five, and ten years in submerged exposure. All profiles are from the west-facing side of the panels, unless marked (E, dashed line) for the east-facing side.

With the exception of the outlier PC-S-W, all the chloride profiles measured after ten years show higher maximum chloride content (C_{\max}) and deeper chloride penetration than for previous exposure times. Furthermore, when using the penetration depth of 0.1% chloride by wt. of concrete as a measure for the chloride ingress resistance, the ranking in chloride ingress resistance suggested for the blocks after five years by Poulsen et al. [1] is maintained after ten years of exposure (PC < 4SF < 15FA < 12FA4SF < 25 FA < SG). The increased resistance towards chloride ingress as a result of mineral additions and in particular GGBS is confirmed in numerous previous studies [64-66].

The progress of C_{\max} and the position of the maximum chloride content ($x_{C_{\max}}$) obtained from the chloride profiles for tidal exposure shown in Figure 12 are tabulated in Table 8. We should note that the tabulated $x_{C_{\max}}$ is the middle of the section in which it is present. The thickness of the sections varied with the depth from surface, the exposure time, and the binder (approx. 1 mm for the outermost section, 2 mm for the second, 3 mm for the following two, and 4 mm for the fifth section – the deepest section containing any C_{\max} in this study). In contrast to the actual maximum chloride content and its position in a sample, the measured C_{\max} and $x_{C_{\max}}$ depends on the thickness of the respective section. For the measured C_{\max} , the chloride content is averaged over the section, thus a thicker section might result in a lower C_{\max} . This could for example be the reason why the measured C_{\max} is higher for 15FA, 25FA and SF after two years than after ten years: the values after two years were averaged over a sample spanning 1 mm, compared to the values after ten years which were the average of a 3 mm depth increment.

Table 8: C_{\max} [% by wt. of concrete] and the sampling interval that contains $x_{C_{\max}}$ [mm] of chloride profiles obtained for tidal exposure for all measured exposure times and panel surfaces.

Exposure time [years] and orientation (W/E)	PC		15FA		25FA		4SF		12FA4SF		SG	
	C_{\max} [%wt.]	$x_{C_{\max}}$ [mm]	C_{\max} [%wt.]	$x_{C_{\max}}$ [mm]	C_{\max} [%wt.]	$x_{C_{\max}}$ [mm]	C_{\max} [%wt.]	$x_{C_{\max}}$ [mm]	C_{\max} [%wt.]	$x_{C_{\max}}$ [mm]	C_{\max} [%wt.]	$x_{C_{\max}}$ [mm]
0.6 W	0.36	1.4	0.66	0.6	0.58	1.6	0.38	1.5	0.42	2.5	0.41	1.5
2 W	0.50	1.9	0.71	1.7	0.73	1.8	0.58	1.7			0.37	2.1
5 W	0.69	1.9	0.64	4.5	0.70	4.5	0.57	2.0	0.43	4.0	0.44	3.9
5 E	0.51	4.5	0.71	4.5	0.67	4.4	0.55	7.7	0.42	6.5	0.62	2.0
10 W	0.62	4.5	0.64	7.3	0.63	7.7	0.54	7.5	0.45	7.4	0.48	4.9
10 E	0.49	7.6	0.60	7.4	0.71	7.4	0.47	7.5	0.45	11	0.50	4.5

Table 8 shows that the position of the highest chloride content, $x_{C_{\max}}$, gradually moves towards greater depths with time. The shift of $x_{C_{\max}}$ towards greater depths is related to phase changes. This topic is further discussed in 4.3. After ten years of exposure, $x_{C_{\max}}$ is reached at a depth of 4–11 mm from the surface, depending on binder type. The lowest penetration depth is seen for SG.

Based on the C_{\max} values given in Table 8, initially C_{\max} increases, but already after two years, it appears stable. There was a slight decrease in the C_{\max} values for some concretes after ten years compared to the C_{\max} values after two years, e.g., for 15FA and 25FA. This is due to the

difference in section thickness where the C_{\max} occurs, as mentioned earlier. After two years the C_{\max} value is averaged over a 1 mm interval, whereas the C_{\max} value after ten years is the average of a 3 mm depth increment.

Table 8 also shows that C_{\max} as a general trend is higher for the concretes containing fly ash as the only SCM than for the remaining concretes. This agrees with Taylor's statements Taylor [30] that *"With Portland cements, the Cl⁻/OH⁻ ratios decreased with potential C₃A content; cements containing 30% FA or 65% GGBS gave lower ratios than any of the Portland cements. The OH⁻ concentrations were lower for the composite cements, and the low Cl⁻/OH⁻ were presumable due to greater uptake of Cl⁻ in the hydration products"* and *"replacement of cement by silica fume may be expected both to lower the OH⁻ concentration and to decrease the content of AFm phase able to take up Cl⁻"*.

The combination of a relatively high C_{\max} for fly ash concretes and a good chloride ingress resistance resulted in steep chloride profiles for 15FA and 25FA. In contrast, for 4SF a lower binding capacity and a poorer chloride ingress resistance resulted in a flatter chloride profile. This tendency was observed to become more pronounced with time.

4.2 Tidal vs. submerged

In the panels we investigated no major differences were observed in the microstructural changes and chloride profiles between concrete exposed to tidal and submerged conditions for ten years. The extent of zonation, micro-cracks, and precipitated products in voids were comparable, but the surface was typically less scaled for submerged exposure (see Table 6 and Figure 6), which is for instance in agreement with Mehta [15], and the chloride profiles showed only slightly higher peaks for tidal exposure, where also slightly deeper ingress was observed (Figure 7).

One explanation for the similar observations could be that the actual exposure conditions were to a large extent similar. Figure 1 and Figure 2 indicate that the #9 cores for chloride analysis from the tidal zone were submerged approximately half of the time, with assumed frequent wetting from waves. Moreover, Figure 4 shows heavy organic growth with barnacles and mussels not only on the submerged part of the blocks, but also in the tidal zone where the #9 cores for chloride analysis were taken. Both frequent wetting and organic growth prevent drying and accumulation of chloride at the evaporation front, which could explain why the maximum chloride content is only slightly higher for the chloride profiles obtained from tidal exposure than for those from the submerged exposure.

4.3 Correlation of chloride profiles with microstructural and moisture changes for submerged exposure

Figure 14 shows a comparison of the depth of the microstructurally changed zone (x_{MCZ}), and the chloride, DCS and CH profiles for all six concretes after ten years of submerged exposure. The influence of moisture, microstructural changes as observed in optical polarizing microscope, and measured CH profiles on chloride ingress is discussed in the subsections 4.3.1, 4.3.2 and 4.3.3 respectively.

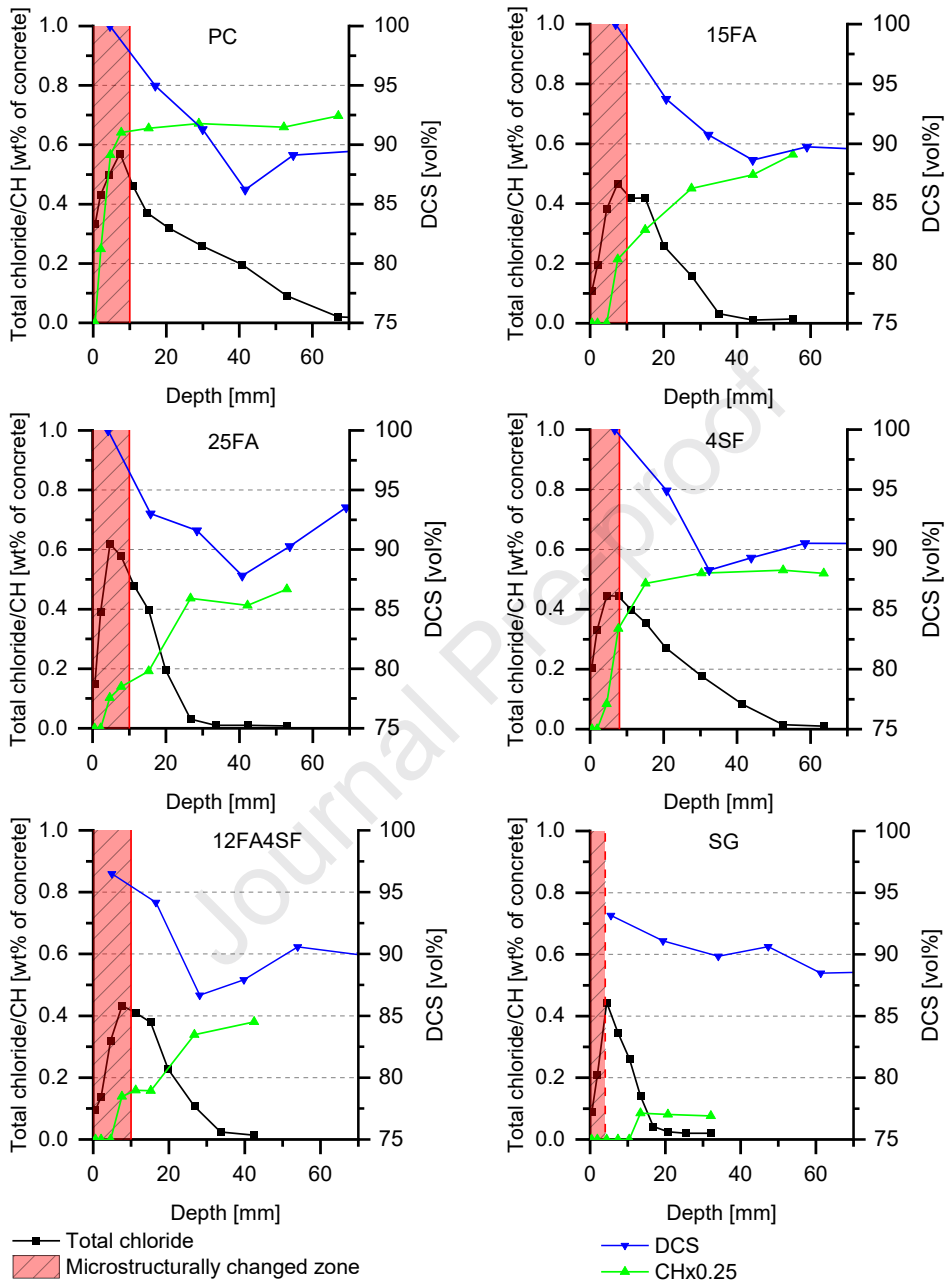


Figure 14: Depth of observed microstructurally changed zone compared to corresponding chloride, DCS and portlandite (CH) profiles after ten years of submerged exposure. To fit the results in one graph, CH has been scaled to one fourth. The chloride profile and CH are given as % by wt. of concrete, whereas the DCS is in % by vol. The titles correspond to the concrete compositions. Note that for PC the chloride profile shown is from the east-facing surface. The microstructurally changed zone in SG was estimated from SEM-EDX data (dashed red line).

4.3.1 Effect of moisture content on chloride ingress

The chlorides present as free chlorides in the suction porosity only represent a fraction of the total chloride content. If we consider a suction porosity of 10% by volume or 100 L/m³ concrete, which is a fair assumption when we look at Figure 9, and fill this hypothetically with sea water (7 g Cl/L, see Table 3), this would create a chloride content of 0.7 kg/m³ concrete. If we divide this by the density of the concrete, 2383 kg/m³ (PC concrete in Table 1), we obtain a chloride content of 0.03% by wt. of concrete, which is similar to the background level. This suggests that a major part of the chlorides we measure are not free but bound [24].

Nevertheless, porosity and the DCS play a major role when it comes to the ingress of chlorides. This is illustrated in Figure 14, where the chloride profiles are compared to the change in DCS measured with depth. The chloride concentration decreases to the background level shortly after the DCS reaches the bulk level. This is explained by a reduced diffusion rate of chlorides when the DCS decreases, as found by Nielsen and Geiker [6] and Olsson et al. [7]. At a DCS of 85–89% as found in this study, the effective diffusion coefficient was found by Olsson et al. [7] to decrease to approximately 45–75% compared to saturated conditions.

4.3.2 Relationship between microstructural changes and chloride profiles

In Figure 14, the depth of the maximum chloride content ($x_{C_{max}}$) for all concretes coincides with the inner part of the microstructurally changed zone. This observation is in line with previous observations on concretes exposed to sea water [19, 27], including those analyzed in this paper but at earlier exposure times [10]. Jakobsen et al. [10] and De Weerd et al. [19] found that C_{max} followed immediately after the sulfur-enriched zone. They explained that the low chloride content in the outermost black leached zone might be due to a low chloride binding capacity of M-S-H [10, 57] and the decomposition of chloride-containing AFms in the low pH of this zone. In the sulfur-rich microstructurally changed zone, the chloride binding in the paste decreases due to the preferred binding of sulfates with aluminates in AFts and the adsorption of sulfates in C-S-H [20, 27]. As a result, the maximum chloride content in the paste is observed at the deeper end of the sulfur-rich zone.

Figure 15 shows the relationship between x_{MCZ} (shown as the abscissa) and the $x_{C_{max}}$ (shown as the ordinate). Data for the tidal zone can cover half a year or two, five or ten years, whereas only ten-year data are available for the submerged zone. The diagonal dotted line, $x = y$, is included as a guide for the eye. Note that some scatter is to be expected because $x_{C_{max}}$ is the mean value of a depth interval varying in thickness between 1 and 3 mm, while x_{MCZ} is determined on a thin section taken perpendicular to the surface, but only representing 40 mm x 20 μ m at each depth. This is important with regard to both the accuracy and the representative sample volume. For the tidal exposed concrete, $x_{C_{max}}$ and x_{MCZ} appear to coincide, whereas the few data from the submerged zone indicate that in this zone $x_{C_{max}}$ precedes x_{MCZ} . This is to be expected because $x_{C_{max}}$ should coincide with the deeper end of the microstructurally changed zone, i.e., the end of the sulfur-enriched zone, as mentioned above.

To elucidate the relationship between x_{MCZ} and x_{Cmax} as a function of time, x_{Cmax} is compared with x_{MCZ} as a function of exposure time for all six concretes in Figure 16 and Appendix G. Both x_{MCZ} and x_{Cmax} gradually move inwards over time, and the microstructurally changed zone, x_{MCZ} , reaches a depth of 4–10 mm after ten years in the concretes investigated. This zone will have altered diffusion characteristics, which should be taken into account, when predicting chloride ingress. This topic is dealt with in Section 4.4.

Journal Pre-proof

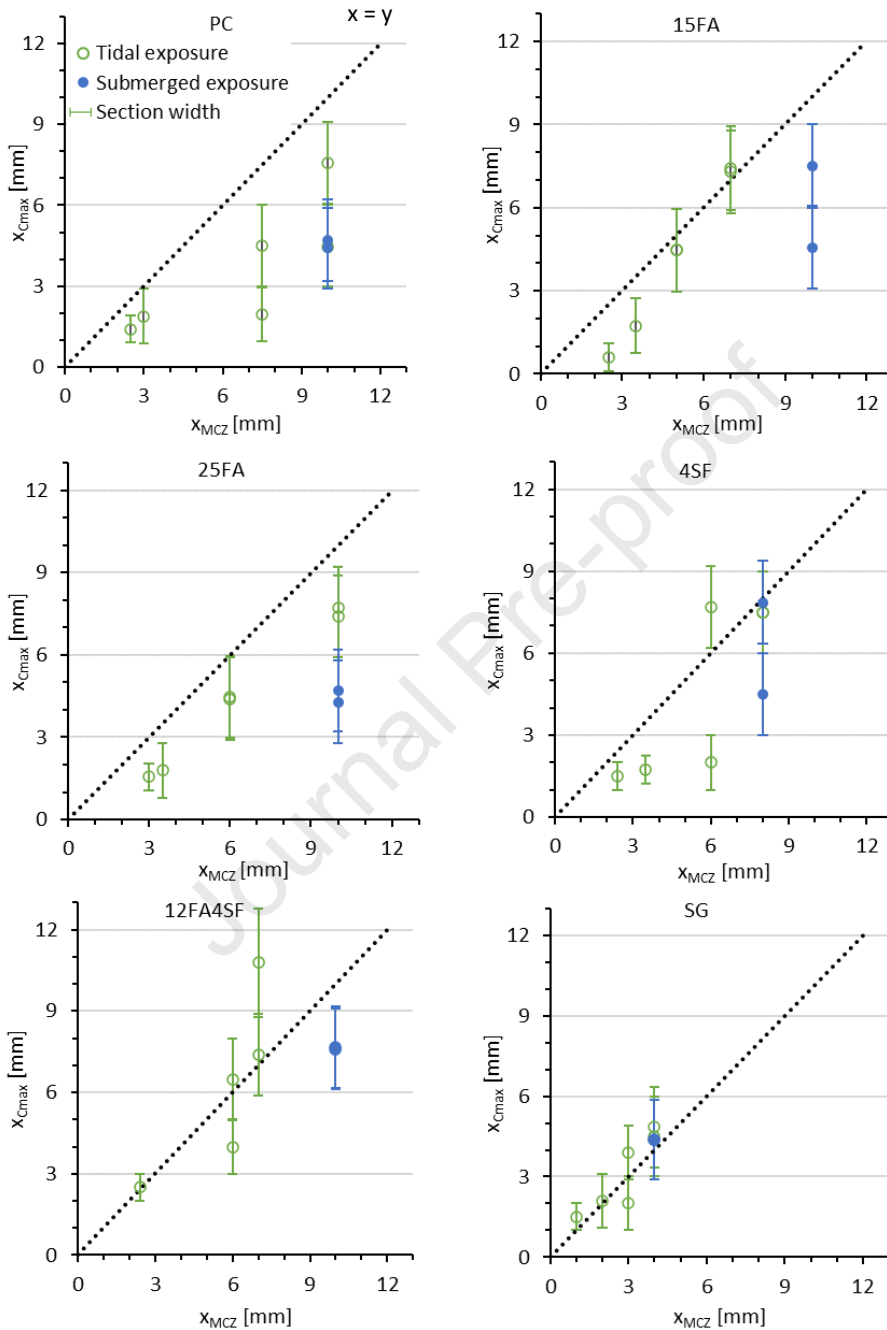


Figure 15: Comparison of the depth of the microstructurally changed zone (x_{MCZ}) with the depth of maximum chloride content (x_{Cmax}). x_{Cmax} from both the west and east-facing surfaces of the panels are included to give an impression of the uncertainties. Unfilled circles = tidal exposure (for half a year or two, five or ten years). Filled circles = submerged exposure (for ten years). The lines (error bars) indicate the width of sections. $x = y$ is indicated with a dotted line as a guide for the eye.

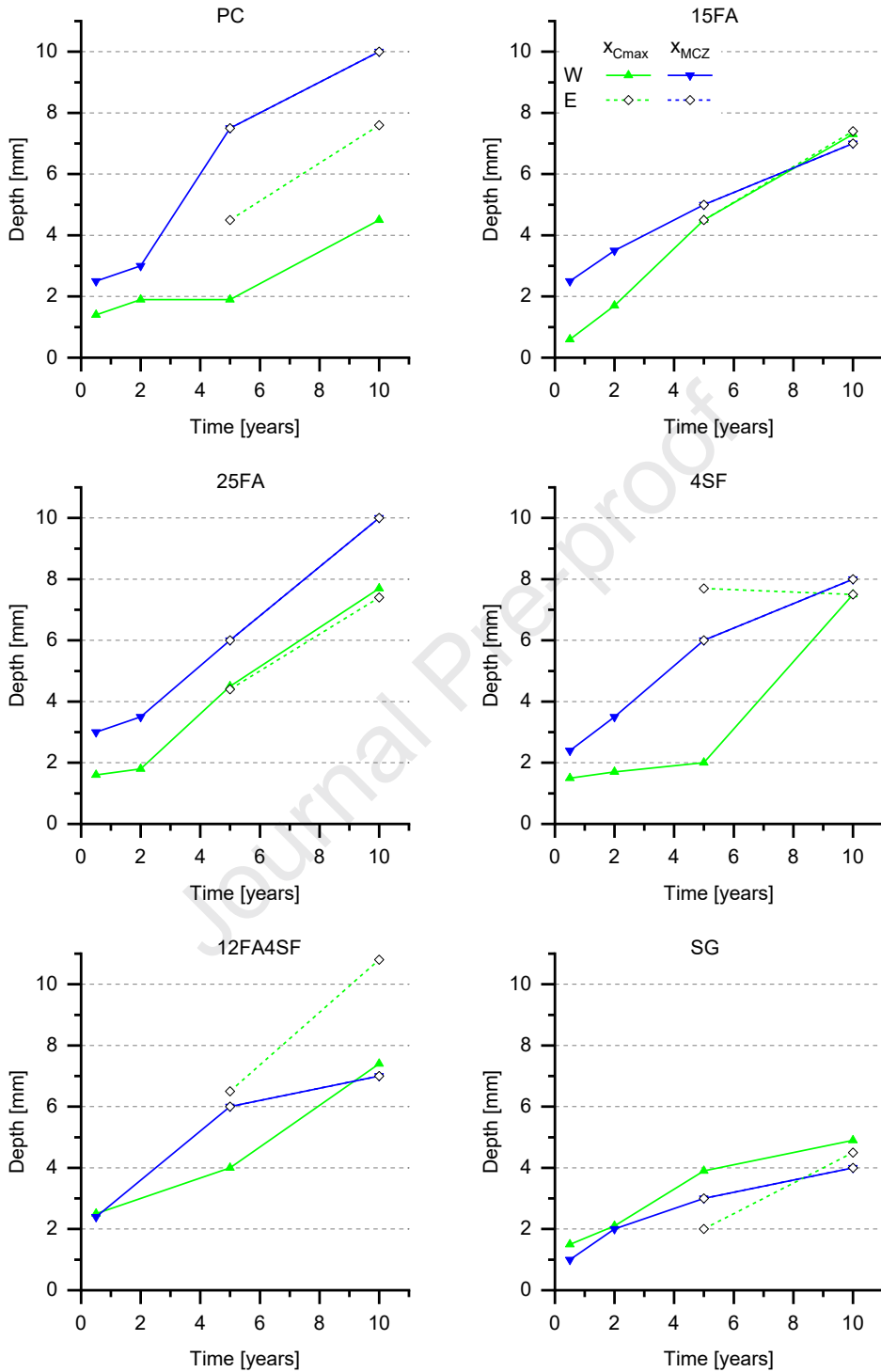


Figure 16: Development of chloride peak depth (x_{Cmax}) and the depth of microstructurally changed zone (x_{MCZ}).

4.3.3 Relationship between the portlandite profiles and chloride ingress profiles.

Figure 14 also enables us to study the relationship between the portlandite (CH) profiles and the chloride ingress and DCS profiles, as well as the depth of the microstructurally changed zone for the investigated concretes. The decrease in the CH profiles towards the exposed surface gives an indication of the extent of leaching, because CH is one of the first hydrates to dissolve upon leaching [67]. In the case of the PC, SF, and SG concretes, the leaching depth (as indicated by a clear drop in the CH content) seems to agree rather well with the depth of the microstructurally changed zone. In the case of the concretes containing fly ash (15FA, 25FA and 12FA4SF), the gradual decrease in CH continues beyond the microstructurally changed zone and tends to level out only at greater depths. This could be due to the pozzolanic reaction of the fly ash in the zone behind the microstructurally changed zone. In this zone, the pH could still be sufficiently high to activate the pozzolanic reaction and the DCS has not fallen to the background level, which indicates that there is moisture available for the reaction. A gradual decrease in CH that only levels out at greater depths was also found by De Weerd et al. [57], who suggested it might be due to pozzolanic reaction. Furthermore, Frías et al. [68] found that the CH content decreases more in pastes containing fly ash than in PC paste, when immersed in aggressive solutions containing chloride and/or sulphate. This potential pozzolanic reaction and consequent continuous refinement of the pores in the concretes containing fly ash might, in combination with increased binding [69], explain the sharper decrease in the chloride content in this zone for the concretes containing fly ash than for the others [70]. Note that the decrease in portlandite could not be explained by carbonation, as the depth of carbonation was 1-3 mm, whereas the depth of leaching was 10-15 mm. Comparable depths of carbonation were found in tidal and submerged exposure.

4.4 Recommendations on valid depth for verification of chloride ingress prediction models

In this study, a microstructurally changed zone was observed to occur both in the tidal and the submerged zones of marine-exposed concretes (Section 4.3). The depth of microstructural changes (x_{MCZ}) increased over time and correlated with the depth of the maximum chloride content (x_{Cmax}).

Based on the observed relationship between the evolution of x_{MCZ} and x_{Cmax} , it is recommended that only chloride data from sections taken deeper than the microstructurally changed zone are used from field data when assessing the remaining service life of structures and when verifying chloride ingress prediction models, unless reactive transport models are used. For the data presented here for six concrete panels exposed for ten years, this exclusion includes the chloride peak.

The observed gradual progression of x_{MCZ} and x_{Cmax} means that the approach proposed by Andrade et al. [40] for assessment of cases where neither the C_{max} nor x_{Cmax} are time-dependent is not applicable.

The square root method is an example of a reassessment method that can be applied in cases where a gradual development of C_{max} and/or x_{Cmax} occurs. The method excludes the

microstructurally changed zone by omitting the data point corresponding to C_{\max} and all data points closer to the surface [3]. However, the application of the method for design purposes requires available model parameters for the concrete and exposure in question, which necessitates either the use of well-known concretes or a relatively long period of pretesting [3].

For design purposes, reactive transport models, e.g. Stadium [71], DuCOM [72], etc., provide the possibility of predicting the entire chloride profile including the interaction between multiple species. However, to the best of the author's knowledge, their general usage is limited, perhaps due to their complexity and because not all information is disclosed.

5 Conclusion

Based on ten years of field data for 0.4 w/c concrete panels differing in binder composition (plain CEM I and blends with fly ash and/or silica fume, and slag) from the Fehmarn Belt Exposure Site combined with earlier data obtained after a half-year, two, and five years of submerged and tidal exposure, we conclude that:

- After ten years of exposure, chloride profiles from the submerged and the tidal zones were to a large extent comparable. A peaking behavior was observed, and the depth of the maximum chloride content ($x_{C_{\max}}$) progressed inwards over time in panels subjected to both tidal and submerged exposure. In general, the maximum chloride content was less than 10% higher for the tidal exposure than for the submerged exposure. Deepest ingress was found in the concretes with plain CEM I and CEM I mixed with 4% silica fume.
- A microstructurally changed zone was a generally observed feature in the outer approximately 10 mm of all six concretes after ten years of exposure, independent of the binder composition and exposure. Starting from the exposed surface, we observed: minor surface scaling, a black leached and microcracked zone rich in magnesium, a zone with bicarbonate precipitation, and a zone with a diffuse opaline shine, rich in sulfur. Comparison with earlier data showed that the depth of the microstructurally changed zone progressed inwards over time.
- A correlation was observed between chloride profiles and microstructural changes. The depth of the maximum chloride content ($x_{C_{\max}}$) was found to almost coincide with the depth of the microstructurally changed zone (x_{MCZ}). A binder-dependent increase was observed in $x_{C_{\max}}$ from 0.6–2.5 mm after six months to 4.5–10 mm after ten years, and in x_{MCZ} from 1–2.5 mm after six months to 4–10 mm after ten years; the least increase was observed for concrete containing slag.
- Limited moisture ingress combined with self-desiccation caused the degree of capillary saturation to increase towards the exposed surface from a bulk level of about 90% at a depth of 30–40 mm of the submerged concrete. This lower DCS in the bulk will limit further chloride ingress by diffusion. Due to leaching in the outer zone, all portlandite profiles decreased from a bulk level towards the exposed surface. For the concretes containing fly ash, moisture ingress and portlandite depletion progressed to a depth far beyond that of the microstructurally changed zone.

Based on the above conclusions, we recommend that data from the microstructurally changed zone should be excluded when using field data for verification of chloride ingress prediction models, unless reactive transport models are used. Because the depth of the microstructurally changed zone coincides with the depth of the maximum chloride content, for practical purposes, we recommend only using data from greater depths.

6 Acknowledgements

The authors would like to thank Femern A/S for sharing field data from the Fehmarn Belt Exposure Site. Further acknowledgements go to Kurt Kielsgaard from DTU for assistance with pressure saturation for the determination of macro porosity, and to Tone H. Nilsen and Pamela Zuschlag from NTNU for assistance with the thermogravimetric analysis.

This work was supported by the Danish Ministry of Higher Education and Science through the contract “E5 Field exposure and monitoring to extend the service life of infrastructure” (translation from Danish) granted to the Danish Technological Institute.

References

- [1] S.L. Poulsen, H.E. Sørensen, U. Jönsson, Chloride ingress in concrete blocks at the Rødbyhavn marine exposure site – Status after 5 years, 4th International Conference on Service Life Design for Infrastructures (SLD4), Delft, Netherlands, 2018, pp. 192-203.
- [2] U.H. Jakobsen, Petrographic evaluation after 5 years of exposure to seawater, 2015. http://www.expertcentre.dk/media/25643/petrographic_evaluation_5_years.pdf. (Accessed 22. Feb 2021).
- [3] S. Fjendbo, H.E. Sørensen, K. De Weerd, M.R. Geiker, The square root method for chloride ingress prediction—Applicability and limitations, *Materials and Structures* 54 2021 61. <https://doi.org/10.1617/s11527-021-01643-8>.
- [4] M.R. Geiker, H. Justnes, Prediction of Chloride Induced Corrosion for Service Life Modelling, 1st International Congress on Durability of Concrete, Trondheim, Norway, 2012.
- [5] A.V. Saetta, R.V. Scotta, R.V. Vitaliani, Analysis of chloride diffusion into partially saturated concrete, *Materials Journal* 90(5) 1993 441-451.
- [6] E.P. Nielsen, M.R. Geiker, Chloride diffusion in partially saturated cementitious material, *Cement and Concrete Research* 33(1) 2003 133-138. [https://doi.org/10.1016/S0008-8846\(02\)00939-0](https://doi.org/10.1016/S0008-8846(02)00939-0).
- [7] N. Olsson, B. Lothenbach, V. Baroghel-Bouny, L.-O. Nilsson, Unsaturated ion diffusion in cementitious materials—The effect of slag and silica fume, *Cement and Concrete Research* 108 2018 31-37. <https://doi.org/10.1016/j.cemconres.2018.03.007>.
- [8] N. Olsson, F.A. Wahid, L.-O. Nilsson, C. Thiel, H.S. Wong, V. Baroghel-Bouny, Wick action in mature mortars with binary cements containing slag or silica fume—The relation between chloride and moisture transport properties under non-saturated conditions, *Cement and Concrete Research* 111 2018 94-103. <https://doi.org/10.1016/j.cemconres.2018.06.006>.
- [9] M.A. Climent, G. De Vera, J.F. López, C. García, C. Andrade, J. Kropp, Transport of chlorides through non-saturated concrete after an initial limited chloride supply, in: C. Andrade, K. J (Eds.) *Second International RILEM Workshop on Testing and Modelling the Chloride Ingress into Concrete*, RILEM Publications SARL, 2000, pp. 173 - 187.
- [10] U.H. Jakobsen, K. De Weerd, M.R. Geiker, Elemental zonation in marine concrete, *Cement and Concrete Research* 85 2016 12-27. <https://doi.org/10.1016/j.cemconres.2016.02.006>.

- [11] J. Marchand, E. Samson, D. Burke, P. Tournay, N. Thaulow, S. Sahu, Predicting the Microstructural degradation of concrete in marine environment, Special Publication 212 2003 1127-1154.
- [12] A. Chabreli, E. Gallucci, K. Scrivener, U. Müller, Durability of field concretes made of Portland and silica fume cements under sea water exposure for 25 years, Nordic Exposure Sites – Input to revision of EN206-1, Hirtshals, Denmark, 2008, pp. 275-294.
- [13] U.H. Jakobsen, Microstructural surface deterioration of concrete exposed to seawater; results after 2 years of exposure, 14th Euroseminar on Microscopy Applied to Building Materials, Helsingør, Denmark, 2013.
- [14] P.K. Mehta, P.J. Monteiro, Concrete: microstructure, properties, and materials, McGraw-Hill Education, 2014.
- [15] P.K. Mehta, Durability of Concrete in Marine Environment – A Review, in: V.M. Malhotra (Ed.), Performance of concrete in marine environment, ACI SP-65, 1980, pp. 1-20.
- [16] Y.-J. Tang, X.-B. Zuo, G.-J. Yin, H. Davoudi, X.-N. Li, Influence of calcium leaching on chloride diffusivity in cement-based materials, Construction and Building Materials 174 2018 310-319. <https://doi.org/10.1016/j.conbuildmat.2018.04.112>.
- [17] F.P. Glasser, J. Marchand, E. Samson, Durability of concrete – Degradation phenomena involving detrimental chemical reactions, Cement and Concrete Research 38(2) 2008 226-246. <https://doi.org/10.1016/j.cemconres.2007.09.015>.
- [18] P. Hemstad, A. Machner, K. De Weerd, The effect of artificial leaching with HCl on chloride binding in ordinary Portland cement paste, Cement and Concrete Research 130 2020 105976. <https://doi.org/10.1016/j.cemconres.2020.105976>.
- [19] K. De Weerd, D. Orsáková, A.C.A. Müller, C.K. Larsen, B.M. Pedersen, M.R. Geiker, Towards the understanding of chloride profiles in marine exposed concrete, impact of leaching and moisture content, Construction and Building Materials 120 2016 418-431. <https://doi.org/10.1016/j.conbuildmat.2016.05.069>.
- [20] K. De Weerd, D. Orsáková, M.R. Geiker, The impact of sulphate and magnesium on chloride binding in Portland cement paste, Cement and Concrete Research 65 2014 30-40. <https://doi.org/10.1016/j.cemconres.2014.07.007>.
- [21] K. De Weerd, H. Justnes, The effect of sea water on the phase assemblage of hydrated cement paste, Cement and Concrete Composites 55 2015 215-222. <https://doi.org/10.1016/j.cemconcomp.2014.09.006>.
- [22] M. Geiker, Fly ash in concrete, Danish experience, Norwegian Public Roads Administration, 2015.
- [23] B.B. Jensen, R. Sørensen, T. Frølund, M. Sloth, T. Johnsen, E. Stoltzner, Farøbroerne. Betonundersøgelser 1988-2005, COWI, 2006.
- [24] K. De Weerd, Chloride binding in concrete – recent investigations and recognised knowledge gaps: RILEM Robert L’Hermite Medal Paper 2021, Materials and Structures in press.
- [25] A. Machner, M.H. Bjørndal, H. Justnes, L. Hanžič, A. Šajna, Y. Gu, B. Bary, M. Ben Haha, M.R. Geiker, K. De Weerd, Effect of leaching on the composition of hydration phases during chloride exposure of mortar, Cement and Concrete Research 153 2022 106691. <https://doi.org/10.1016/j.cemconres.2021.106691>.
- [26] W. Kunther, B. Lothenbach, K.L. Scrivener, On the relevance of volume increase for the length changes of mortar bars in sulfate solutions, Cement and Concrete Research 46 2013 23-29. <https://doi.org/10.1016/j.cemconres.2013.01.002>.
- [27] P.K. Mehta, Concrete in the marine environment, 1st ed., CRC Press, London, 2019.
- [28] N.R. Buenfeld, J.B. Newman, The development and stability of surface layers on concrete exposed to sea-water, Cement and Concrete Research 16(5) 1986 721-732. [https://doi.org/10.1016/0008-8846\(86\)90046-3](https://doi.org/10.1016/0008-8846(86)90046-3).

- [29] K. De Weerd, H. Justnes, M.R. Geiker, Changes in the phase assemblage of concrete exposed to sea water, *Cement and Concrete Composites* 47 2014 53-63. <https://doi.org/10.1016/j.cemconcomp.2013.09.015>.
- [30] H.F.W. Taylor, *Cement chemistry*, second ed., Thomas Telford Publishing, London, 1997, pp. 259-260.
- [31] K. De Weerd, B. Lothenbach, M.R. Geiker, Comparing chloride ingress from seawater and NaCl solution in Portland cement mortar, *Cement and Concrete Research* 115 2019 80-89. <https://doi.org/10.1016/j.cemconres.2018.09.014>.
- [32] M. Collepardi, A. Marcialis, R. Turriziani, The kinetics of chloride ions penetration in concrete, *Il cemento* 67 1970 157-164.
- [33] L. Mejlbro, The complete solution of Fick's second law of diffusion with time-dependent diffusion coefficient and surface concentration, in: P. Sandberg (Ed.), *Durability of concrete in saline environment*, Cementa AB, Lund, Sweden, 1996, pp. 127-158.
- [34] A.J.M. Siemes, C. Edvardsen, T.N.O. Bouw, *Duracrete: Service life design for concrete structures*, in: M.A. Lacasse, D.J. Vanier (Eds.) NRC Research Press, Ottawa, Canada, 1999.
- [35] S. Engelund, General guidelines for durability design and redesign: DuraCrete, probabilistic performance based durability design of concrete structures [Gouda]: [CUR], 2000.
- [36] *fib*, Model code for service life design - bulletin 34, *fédération internationale du béton (fib)*, Lausanne, Switzerland, 2006.
- [37] L. Tang, L.-O. Nilsson, P.A.M. Basheer, *Resistance of concrete to chloride ingress: Testing and modelling*, 1st ed., Spon Press, London, 2012.
- [38] Y. Hosokawa, K. Yamada, B.E. Johannesson, L.-O. Nilsson, Models for chloride ion bindings in hardened cement paste using thermodynamic equilibrium calculations, 2nd International RILEM symposium on advances in concrete through science and engineering, Quebec City, Canada, 2006.
- [39] M. Alexander, A. Bertron, N. De Belie, *Performance of cement-based materials in aggressive aqueous environments*, Springer, 2013.
- [40] C. Andrade, M.A. Climent, G. De Vera, Procedure for calculating the chloride diffusion coefficient and surface concentration from a profile having a maximum beyond the concrete surface, *Materials and Structures* 48(4) 2015 863-869. <https://doi.org/10.1617/s11527-015-0543-4>.
- [41] F. Toutlemonde, C. Andrade, C.V. Nielsen, S von Greve-Dierfeld, Draft of Background Document for prEN1992-1-1:2020 D7 clause 6 - Durability, CEN/TC 250/SC 2/WG 1/TG 10, 2021.
- [42] DS-EN 197-1:2011, *Cement - Part 1: Composition, specifications and conformity criteria for common cements*, Danish standard.
- [43] DS/EN 196-2:2013, *Method of testing cement - Part 2: Chemical analysis of cement*, Danish Standard.
- [44] Fehmarnbelt Exposure Site, 2015. <http://www.concreteexpertcentre.dk/30663>. (Accessed 15th of March 2021).
- [45] A. Demayo, *Elements in sea water*, in: D.R. Lide (Ed.), *CRC Handbook of Chemistry and Physics*, CRC Press, USA, 1988.
- [46] A.D. Herholdt, C.F.P. Justesen, P. Nepper-Christensen, A. Nielsen, *Beton-Bogen, Cementfabrikkernes tekniske oplysningskontor, Aalborg Portland, Aalborg, Denmark*, 1985.
- [47] DS/EN 12390-1:2000, *Testing hardened concrete - Part 1: Shape, dimensions and other requirements for specimens and molds*, Danish Standard, 2000.
- [48] U. Jakobsen, P. Laugesen, N. Thaulow, Determination of water-cement ratio in hardened concrete by optical fluorescence microscopy, *Special Publication* 191 1999 27-42.
- [49] DS/EN 12390-3 + AC:2012, *Testing hardened concrete - Part 3: Compressive Strength of Test Specimens*, Danish Standard, 2012.
- [50] DS/EN 12390-7:2012, *Testing hardened concrete - Part 7: Density of hardened concrete*, Danish Standard, 2012.
- [51] S. Fjendbo, H.E. Sørensen, K.d. Weerd, M.R. Geiker, When and How Should Chloride Profiles be Calibrated for Paste Fraction?, Manuscript submitted for publication 2021.

- [52] B. Lothenbach, P. Durdzinski, K. De Weerd, Thermogravimetric analysis, in: K. Scrivener, R. Snellings, B. Lothenbach (Eds.), *A practical guide to microstructural analysis of cementitious materials*, CRC Press, 2016, pp. 177-211.
- [53] K. Scrivener, R. Snellings, B. Lothenbach, *A practical guide to microstructural analysis of cementitious materials*, CRC Press, 2018.
- [54] E.J. Sellevold, T. Farstad, The PF-method—A simple way to estimate the w/c-ratio and air content of hardened concrete, *Third International Conference on Construction Materials: Performance, Innovations and Structural Implications and Mindess Symposium*, Vancouver, Canada, 2005.
- [55] U.H. Jakobsen, N. Thaulow, Combining Optical Fluorescent Microscopy and Scanning Electron Microscopy for the Examination of deteriorated Concrete, *Proceedings of 7th Euroseminar on microscopy applied to building materials*, Delft, Netherlands, 1999.
- [56] U. JACOBSEN, N. Thaulow, Sulphate Attack as Observed by Optical and Scanning Electron Microscopy, In: *Cement and Concrete Technology in the 2000s*, Proceedings of Second International Symposium, 2000, pp. 6-10.
- [57] K. De Weerd, M.R. Geiker, D. Orsáková, Investigation of concrete from Solsvik field station: 4 concrete cores investigated after 16 years of submerged exposure, *Norwegian Public Roads Administration*, 2015, p. 47.
- [58] T.C. Powers, T.L. Brownard, Studies of the Physical properties of hardened portland cement paste, *Portland Cement Association, Research Laboratories* 43 1948.
- [59] G.W. Washa, K.F. Wendt, Fifty year properties of concrete, *ACI Journal Proceedings* 72(1) 1975 20-28.
- [60] K. Walz, FESTIGKEITSENTWICKLUNG VON BETON BIS ZUM ALTER VON 30 UND 50 JAHREN, in: K. Walz (Ed.), *Betontechnische Berichte*, Forschungsinstitut der Zementindustrie, Düsseldorf, 1976.
- [61] M. Maage, S. Smeplass, R. Johansen, Long-term strength of high-strength silica fume concrete, *ACI Special Publication* 121 1990 399-408.
- [62] H. Al-Khaiat, N. Fattuhi, Long-term strength development of concrete in arid conditions, *Cement and Concrete Composites* 23(4-5) 2001 363-373. [https://doi.org/10.1016/S0958-9465\(01\)00004-X](https://doi.org/10.1016/S0958-9465(01)00004-X).
- [63] P.-C. Aitcin, P. Laplante, Long-term compressive strength of silica-fume concrete, *Journal of Materials in Civil Engineering* 2(3) 1990 164-170. [https://doi.org/10.1061/\(ASCE\)0899-1561\(1990\)2:3\(164\)](https://doi.org/10.1061/(ASCE)0899-1561(1990)2:3(164)).
- [64] M.D. Thomas, P.B. Bamforth, Modelling chloride diffusion in concrete: effect of fly ash and slag, *Cement and concrete research* 29(4) 1999 487-495. [https://doi.org/10.1016/S0008-8846\(98\)00192-6](https://doi.org/10.1016/S0008-8846(98)00192-6).
- [65] T. Luping, I. Löfgren, Evaluation of durability of concrete with mineral additions with regard to chloride-induced corrosion, *Department of Civil and Environmental Engineering, Chalmers University of Technology*, 2016.
- [66] T.U. Mohammed, H. Hamada, T. Yamaji, Concrete after 30 years of exposure—Part II: chloride ingress and corrosion of steel bars, *Materials Journal* 101(1) 2004 13-18.
- [67] A. Machner, M. Zajac, M.B. Haha, K.O. Kjellsen, M.R. Geiker, K. De Weerd, Stability of the hydrate phase assemblage in Portland composite cements containing dolomite and metakaolin after leaching, carbonation, and chloride exposure, *Cement and Concrete Composites* 89 2018 89-106. <https://doi.org/10.1016/j.cemconcomp.2018.02.013>.
- [68] M. Frías, S. Goñi, R. García, R.V. de La Villa, Seawater effect on durability of ternary cements. Synergy of chloride and sulphate ions, *Composites Part B: Engineering* 46 2013 173-178. <https://doi.org/10.1016/j.compositesb.2012.09.089>.
- [69] T. Cheewaket, C. Jaturapitakkul, W. Chalee, Long term performance of chloride binding capacity in fly ash concrete in a marine environment, *Construction and Building Materials* 24(8) 2010 1352-1357. <https://doi.org/10.1016/j.conbuildmat.2009.12.039>.
- [70] M. Thomas, *Supplementary cementing materials in concrete*, CRC press, 2013.

[71] J. Marchand, Modeling the behavior of unsaturated cement systems exposed to aggressive chemical environments, *Materials and Structures* 34(4) 2001 195-200.

<https://doi.org/10.1007/BF02480588>.

[72] Y. ELAKNESWARAN, T. ISHIDA, Development Of A Physical And Geochemical Model For Long-Term Performance Of Cementitious Materials, *Society for Social Management Systems Internet Journal* 2012.

Journal Pre-proof

Appendix A – Magnitude of wall effect

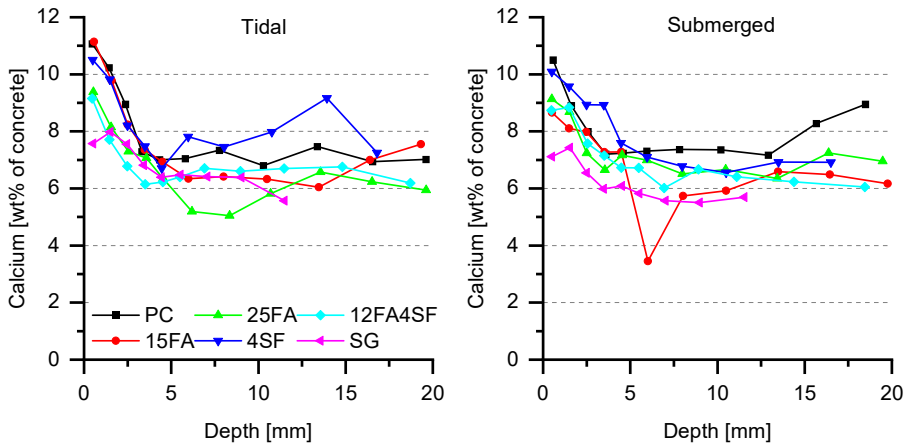
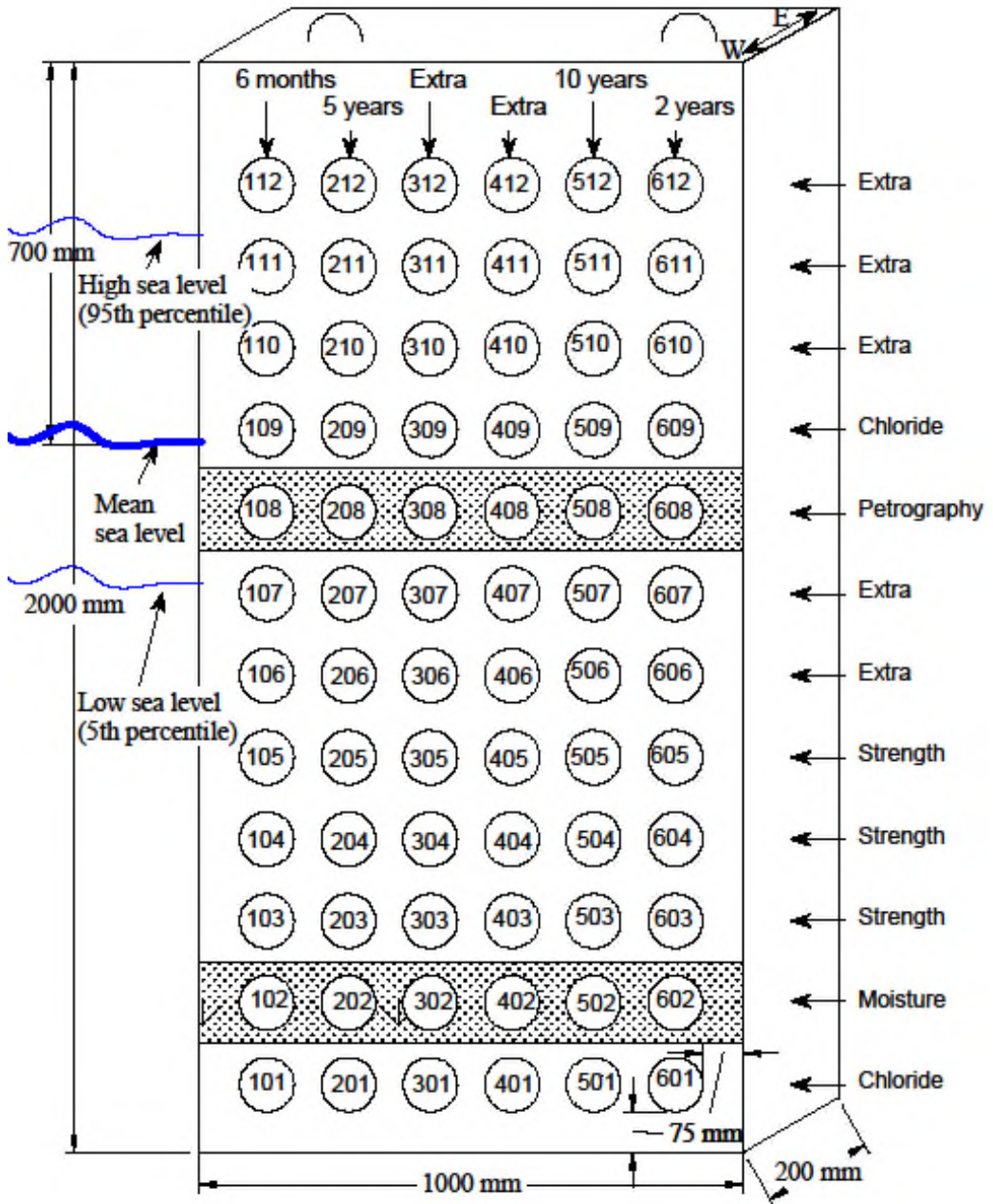


Fig. A.1: Calcium content in % by wt. of concrete as a function of depth for tidal and submerged exposure at the Fehmarn Belt Exposure Site after six months of exposure. A higher calcium content near the concrete surface indicates the presence of a wall effect.

Appendix B – Sampling plan, Fehmarn Belt Exposure Site



Location of cores extracted after a half, two, five and ten years of exposure. The pattern on the horizontal lines covering vertical positions #2 and #8 indicates that they were not cleaned prior to coring. "low" and "high" sea level are the 5th and 95th percentiles of the water level. W: west-facing, E: east-facing.

Appendix C – Calibrated chloride profiles

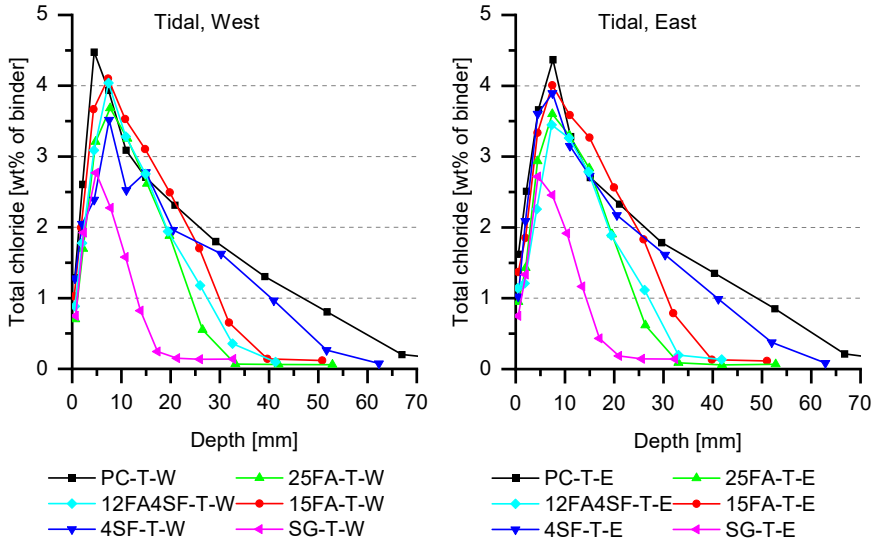


Fig. C.1: Chloride profiles after ten years of tidal exposure at Fehmarn Belt Exposure Site.

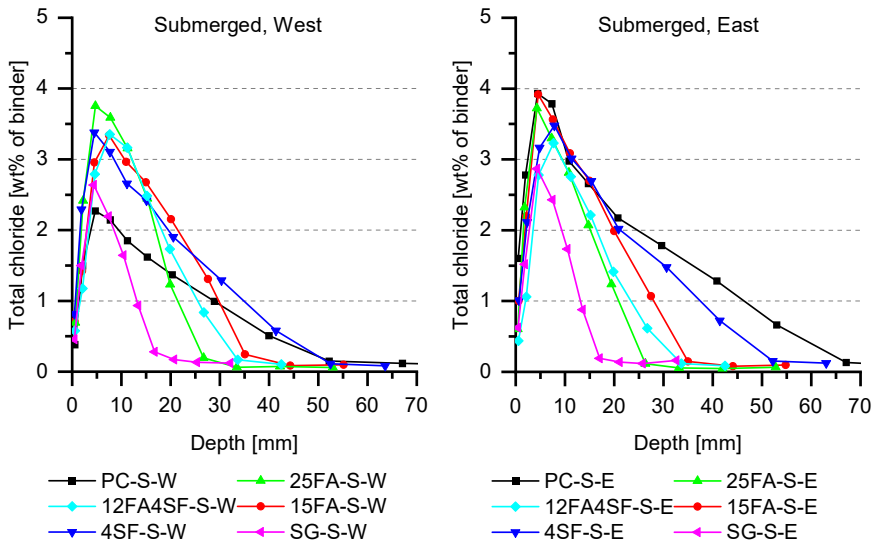


Fig. C.2: Chloride profiles after ten years of submerged exposure at Fehmarn Belt Exposure Site.

Appendix D – Surface scaling

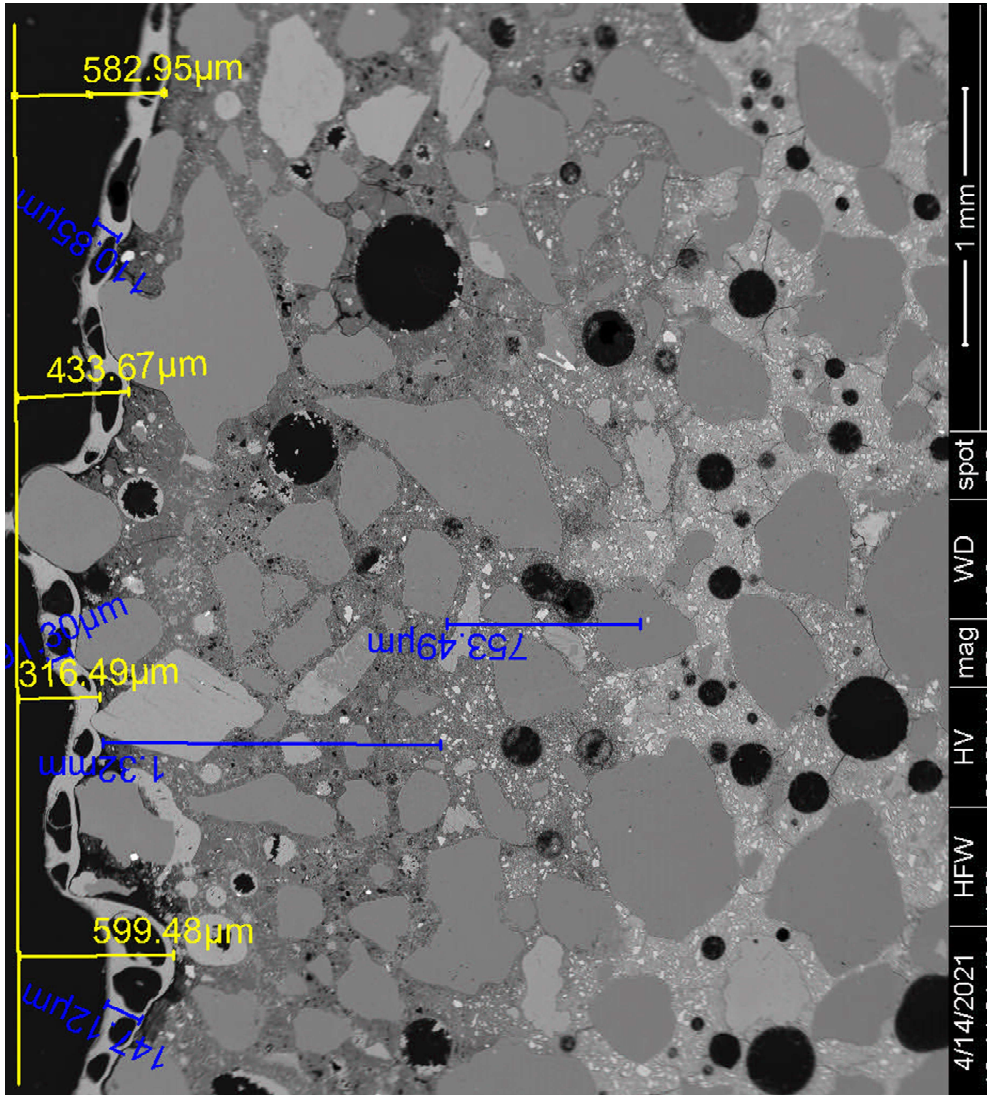


Fig. D.1: Example of observed scaling after ten years exposure at the Fehmarn Belt Exposure Site (exposed surface is to the left). The vertical yellow line indicates the assumed original concrete surface. The horizontal yellow lines indicate the assumed depth of surface scaling. The blue lines are not relevant.

Appendix E – Chloride ingress from tidal and submerged exposure

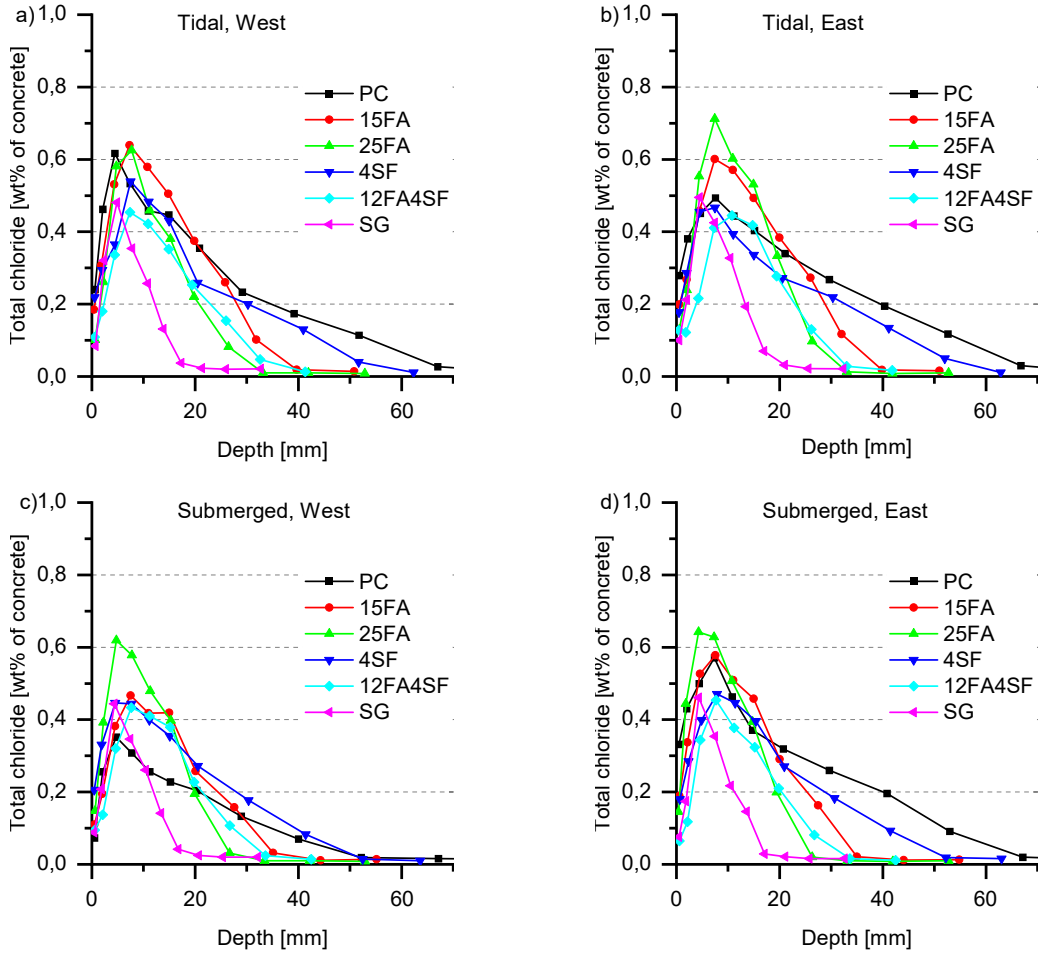


Fig. E.1: Chloride profiles measured in the six concrete panels after ten years of: a) tidal exposure (west), b) tidal exposure (east), c) submerged exposure (west), and d) submerged exposure (east).

Appendix F – Development of compressive strength over time

Compressive strength [MPa]						
Concrete ID	PC	15FA	25FA	4SF	12FA4SF	SG
28 days	57 ± 0.4	43 ± 2.5	43 ± 1.1	50 ± 1.7	50 ± 0.0	55 ± 2.4
0.5 year	58 ± 3.8	63 ± 4.2	62 ± 3.0	63 ± 3.5	62 ± 4.2	58 ± 2.2
2 years	72 ± 1.8	78 ± 0.6	73 ± 0.4	74 ± 0.8	75 ± 3.2	64 ± 0.6
5 years	70 ± 2.6	76 ± 4.2	77 ± 0.9	81 ± 1.3	79 ± 0.5	69 ± 1.2
10 years	65 ± 0.6	77 ± 1.2	75 ± 1.1	77 ± 1.5	75 ± 2.2	67 ± 0.8

Table F.1: Compressive strength ± std. dev. over time for the six concrete panels investigated.

Appendix G – Relationship between chloride ingress and the microstructurally changed zone

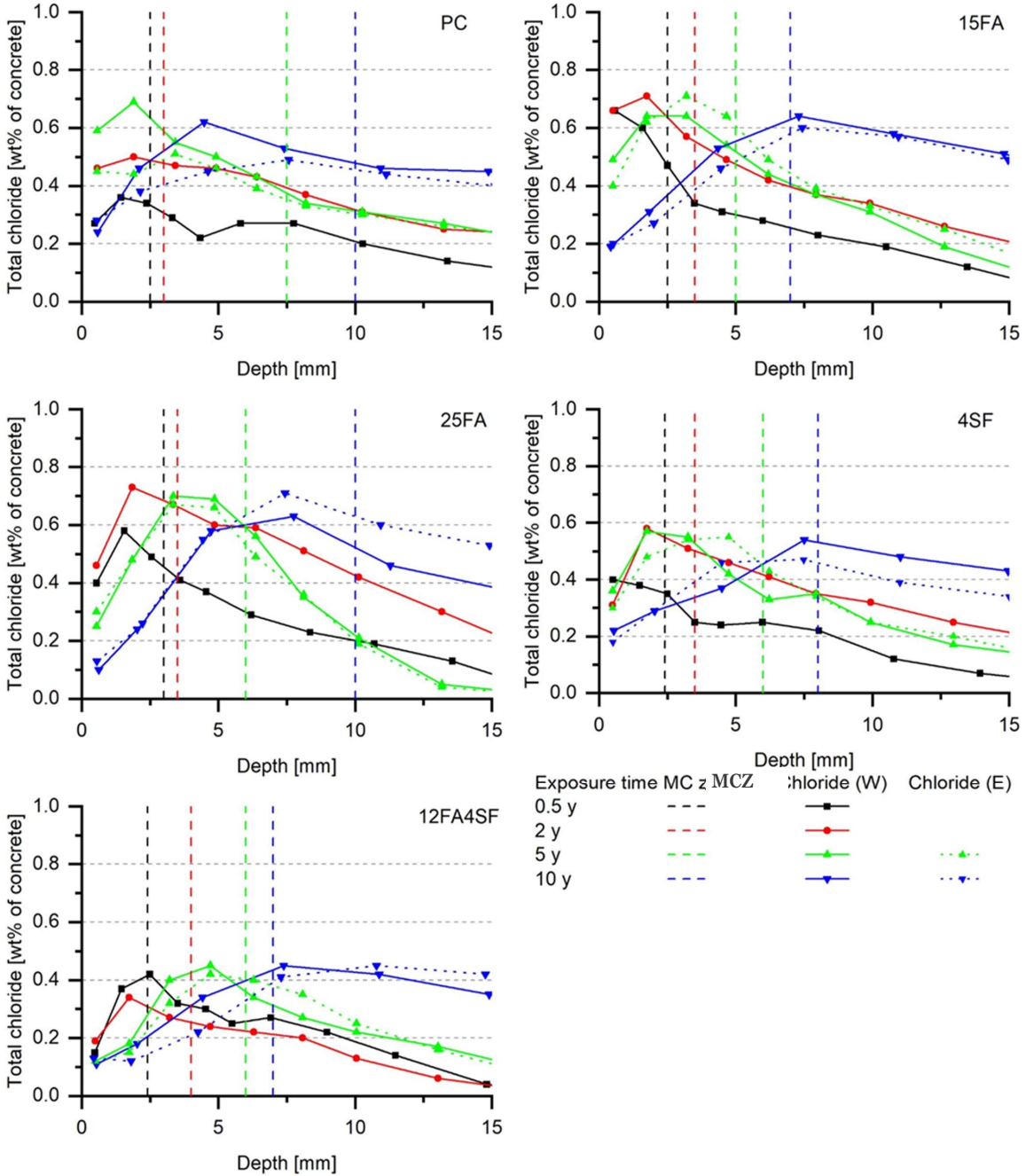


Fig. G.1: Comparison of chloride profiles with the depth of the microstructurally changed zone (MCZ) (tidal). Chloride profiles from both the west and east-facing surfaces of the panels are included to give an impression of the uncertainties.

Paper III

**Testing of chloride ingress models versus 10 years field data
from the Fehmarn Belt marine exposure site**

DRAFT

Simon Fjendbo; Henrik E. Sørensen; Klaartje De Weerd; Mette R. Geiker

This paper is awaiting publication and is not included in NTNU Open





Paper IV

When and How Should Chloride Profiles be Calibrated for Paste Fraction?

Submitted to Nordic Concrete Research (2021)

Simon Fjendbo; Henrik E. Sørensen; Klaartje De Weerd; Mette R. Geiker

When and How Should Chloride Profiles be Calibrated for Paste Fraction?

	<p>Simon Fjendbo Industrial PhD student NTNU, Department of Structural Engineering, NO-7491 Trondheim, Norway, and Danish Technological Institute, DK-2630 Taastrup, Denmark simon.fjendbo@ntnu.no and sifj@teknologisk.dk</p>
	<p>Klaartje De Weerd Professor NTNU, Department of Structural Engineering NO-7491 Trondheim, Norway klaartje.d.weerd@ntnu.no</p>
	<p>Henrik Erndahl Sørensen, Ph.D. Product manager Danish Technological Institute, DK-2630 Taastrup, Denmark hks@teknologisk.dk</p>
	<p>Mette Rica Geiker Professor NTNU, Department of Structural Engineering NO-7491 Trondheim, Norway mette.geiker@ntnu.no</p>

ABSTRACT

Due to stochastic and systematic variations in the paste fraction, data for total chloride content are occasionally calibrated using parallelly measured calcium content as a measure of the actual paste fraction – assuming non-calcareous aggregates and no calcium leaching. Data from concrete exposed at the marine Fehmarn Belt Exposure Site questions the latter assumption. In the outer zone experiencing calcium leaching (ten mm after ten years), errors will be introduced by calcium calibration. To account for the wall effect, calcium profiles from cores taken before exposure might be used to correct for the systematically higher paste fraction at cast surfaces.

Key words: Chloride profiles, Calcium calibration, Wall effect, Calcium profiles

1. INTRODUCTION

Chloride profiles are commonly determined to assess how far chloride has penetrated into the concrete. To determine these profiles, concrete powder is obtained at different depths from the exposed surface – for example by profiles grinding of an extracted concrete core. The concrete powder is then analysed for its chloride content and the results can be expressed as the chloride

content in wt.% of concrete. However, in concrete, chlorides are present in the paste fraction. The paste fraction can vary for several reasons:

- 1) Insufficient amount of concrete powder to provide a representative sample.
- 2) Systematic variations due to geometrical restrains, the so-called wall effect [1, 2] at cast surfaces. The outer surface will have a larger paste fraction than the bulk, whereas a minimum paste fraction will appear at a depth of approximately $\frac{1}{2}$ of the maximum aggregate diameter [3].
- 3) Unsystematic variations due to inhomogeneities, e.g. due to segregation.

For performance testing, specimens with cut surfaces are often used to limit the impact of the wall effect [4, 5]. However, in cores extracted from structures, the paste fraction will vary systematically in the surface near region due to the wall effect [1, 2].

To limit the impact of stochastic variation in the paste fraction of small concrete powder samples, data for total chloride content can be calibrated using the calcium content as a measure of paste fraction [3, 6, 7]. Such calibrations are based on the assumptions that (i) the aggregates do not contain calcium, and (ii) the calcium content of the paste is not altered during the exposure. However, observations in field exposed concrete question the assumption of limited leaching for some binder types [8, 9].

The objective of this present paper is to discuss when and how chloride profiles should be calibrated for paste fraction. The discussion is based on parallel chloride and calcium profiles on cores from six concrete panels differing in binder compositions determined after half a year, two, five and ten years of marine submerged and tidal exposure at the Fehmarn Belt Exposure Site. The scope is limited to discuss the influence of correction for variations in paste fraction based on measured calcium content. The impact of phase changes and leaching on chloride binding are discussed in a separate paper [10].

2. EXPERIMENTAL

2.1 Materials

Cores were extracted from concrete panels exposed at the Fehmarn Belt Exposure Site, Rødbyhavn, Denmark.

2.1.1 Concrete panels

The concrete panels had a thickness of 200 mm to delay the time until two-sided chloride ingress occurs as experienced elsewhere [11]. The width was 1000 mm to allow cores to be taken at the same level at several exposure times, and the height was 2000 mm to include both a permanently submerged zone and a tidal zone. The concrete panels were unreinforced. An overview of concrete compositions used is given in Table 1. Non-calcareous aggregates were used to prevent the aggregates from contributing to the measured calcium content by dissolving into the acidic solution used in the method for extracting chloride and calcium. The coarse aggregate consisted of 91.9-98.8 wt.% granite (gneiss) with 0-4 wt.% pegmatite and 0.6-5.8 wt.% diorite, whereas the sand consisted of quartz and feldspar. The calcium content of the binders as measured by X-ray fluorescence and the calcium content of the concrete calculated based on concrete composition are given in Table 2. Further information on the binder compositions and the production of the concrete panels can be found in [12].

Table 1 - Composition of concretes exposed at the Fehmarn Belt Exposure Site [kg/m³] [13].

ID used in this paper	PC	15FA	25FA	4SF	12FA4SF	SG
Original concrete ID	A	B	C	E	F	K
Binders	CEM I	100	85	75	96	84
[wt.%]	FA ¹⁾	15	25		12	
	SF ²⁾			4	4	
	CEM III					100
CEM I-SR5 42.5 N ³⁾	365	322	300	340	300	
CEM III/B 42.5 N ^{3,4)}						360
FA		57	100		43	
SF (added as slurry)				14	14	
Water	146	140	140	147	140	144
Sand 0-2 mm	695	671	642	695	677	689
Coarse aggregates 4-22 mm	1172	1182	1179	1172	1192	1161
w/(c + 2 SF + 0.5 FA)	0.40	0.40	0.40	0.40	0.40	0.40
w/b	0.40	0.37	0.35	0.42	0.39	0.40
Air content [vol.%]	5.8	5.4	5.5	4.8	5.2	4.8
Density [kg/m ³]	2383	2417	2373	2407	2390	2350

1) FA = Fly ash

2) SF = Silica fume (dry matter)

3) According to EN 197-1

4) SG = Ground granulated blast furnace slag cement (slag content: 67 wt.%)

Table 2 - Calcium content as wt.% of the binders and wt.% of the concretes [14].

Calcium [wt.% of binder]				Calcium [wt.% of concrete]					
CEM I	FA	SF	CEM III	PC	15FA	25FA	4SF	12FA4SF	SG
46.89	1.39	0.23	34.16	7.20	6.39	6.04	6.74	5.94	5.22

2.1.2 Exposure conditions

The concrete panels were exposed at the Fehmarn Belt Exposure Site after reaching a maturity of 43-49 days. The water temperature and salinity were measured on site. As an example, in the period May 2020 to May 2021 the monthly average temperature of the sea water varied between 1.0 and 20.1 °C with a yearly average of 10.5 °C, and the monthly average chloride content of the sea water varied between 6.0 and 8.5 g/l with an average of 7.0 g/l (assuming a distribution of ions as in the Baltic Sea [15]). The monthly average temperature in the air measured in the nearby village of Rødbyhavn varied between 2.1 and 18.2 °C with a yearly average of 11.2 °C [16].

2.1.3 Sampling

Cores (Ø 100 mm) were extracted at the mean tide level (“tidal”) and in the permanently submerged zone (“submerged”). To prevent chloride ingress from the panel sides from influencing the measured chloride profiles the cores were initially taken 75 mm from the edges after half a year and two years and then 225 mm from the edges after five and ten years. After core extraction, the core holes were repaired. The cores were divided in 10-12 surface parallel sections spanning the estimated chloride ingress depth. All sections were profile ground after half a year, two and five years of exposure. After ten years of exposure, sections of width of up to 4 mm were profile ground down to a depth of approx. 15 mm, at depths greater than 15 mm, a water-cooled diamond saw was used to saw wider sections, which were subsequently finely crushed (typical widths 19 mm including 1.6 mm of saw blade). The section widths were measured at three locations with a standard deviation of less than 0.09 mm (typically 0.02 mm).

2.2 Methods

The analyses were conducted on homogenized concrete powder samples of 4-5 g, which were weighed after drying at 105 °C overnight.

The chloride content was determined according to DS/EN 14629:2007 [17]. After drying the powder, it was dissolved in 50 ml nitric acid with an initial temperature of 75 °C made from concentrated nitric acid (68% HNO₃) diluted 1:10 and left overnight. The following day the samples were filtered and the container with filtrate was filled up to 100 ml with demineralized water. Half of the filtrate was further diluted with 50 ml demineralized water, which was then used for chloride analysis.

Calcium determination was done in parallel on 5 ml of the filtrate. A volume of 90 ml demineralized water was added to the 5 ml of filtrate, as well as 5 ml Triethylamine, 5 ml 5M NaOH and 0.15 g calcein indicator. After half a year and two years of exposure, chloride profiles were determined according to Volhard's Method described in DS/EN 14629:2007 [17] and calcium profiles were determined by titration under UV lamp as described in APM 214 [7]. A Titroline 7000 titrator from SI Analytics was used to determine chloride- and calcium content by potentiometric titration for the cores extracted after 5 and 10 years of exposure. The titrant was 0.1 M AgNO₃ for chloride and 0.1 M EDTA disodium salt for calcium analysis. The electrodes used were Ag/AgCl and Combination Electrode CA 60 respectively.

Chloride profiles were measured and expressed as calibrated or uncalibrated to the calcium content of the concrete powder sample. Calibrations for calcium content were made according to Equation 1:

$$\text{Calibrated chloride content} = \frac{\text{wt}\%Cl_{\text{measured}}}{\text{wt}\%Ca_{\text{measured}}} \times \text{wt}\%Ca_{\text{theoretical}} \quad (1)$$

Where wt%Cl_{measured} and wt%Ca_{measured} are the measured contents of chloride and calcium respectively, and wt%Ca_{theoretical} is the calcium content of the binders (by mass of concrete).

3. RESULTS AND DISCUSSION

3.1 Development of calcium leaching

Figures 1 and 2 show measured calcium profiles in cores extracted after half a year, two, five and ten years of tidal and submerged exposure. Note the x-axis is in logscale to emphasize the variation in the outer surface while showing the entire profiles. Calcium profiles with a linear x-axis are shown in Appendix A. A general trend is that the calcium content is higher in the outer surface of cores extracted at early ages, which is explained by the wall effect. After five to ten years of exposure, the calcium content in the surface near region is observed to decrease systematically. For the concretes with fly ash and slag, the calcium content measured in the outer surface of the cores extracted after five to ten years of exposure show values below the bulk values—despite initially being higher due to the wall effect. It is recognized that the method for calcium analysis was changed after two years of exposure, which may have affected the measured level. This is reflected in the measured calcium content in the bulk, but not in the outer surface of the cores. The latter is explained by a systematic decrease in calcium content over time due to calcium

leaching. For slag concrete (SG) in tidal exposure, the decrease is from approximately 8% to approximately 4% calcium by weight of concrete (of which maximum nominally 1% can be explained by the difference in baselines). The observed decrease in the calcium content at the outer surface could potentially be explained by leaching of calcium or by scaling of the surface layer (or through a combination of the two). Petrographic investigations revealed limited surface scaling of about 0.5 mm, whereas calcium hydroxide profiles indicated substantial leaching in the outer 3-9 mm [10].

When looking at the calcium profiles measured after half a year, two, five and ten years in the bulk concrete (for example at a depth of 10-20 mm, which is not affected by calcium leaching) one can observe unsystematic variations in calcium content typically ranging between nominally 1 and 2% calcium by wt. of concrete. These variations could be due to change of measurement method, poor repeatability of the calcium analysis as well as variations in the paste content of the concrete sections. The measured calcium contents in the bulk are similar to the theoretically calculated calcium contents shown in Table 2 and as dashed lines in Figure 1 and 2, although there is a tendency that the results determined by titration under UV lamp (after 0.5 and 2 years) slightly overestimate the paste content whereas the results determined by potentiometric titration (after 5 and 10 years) slightly underestimated the paste content. Nordtest Project No. 1581-02 [18] concluded, that the standard deviation of repeatability was 0.39 wt.% calcium per weight of concrete by the method used in this study, where the sample for calcium analysis is portioned out from the filtrate for chloride analysis. A variation in the calcium content of 1% calcium by weight of concrete for a concrete containing approximately 6% calcium by wt. of concrete, would correspond to a variation of approx. 60 kg of binder per m³ of concrete assuming a binder content of 360 kg per m³ of concrete, which is a considerable difference in binder content. If the variation of 1% calcium by weight of concrete is due to the limited repeatability of the calcium analysis, the correction would introduce an error of approx. (1/6 or) 17% in the corrected chloride content when calibrated to the paste content.

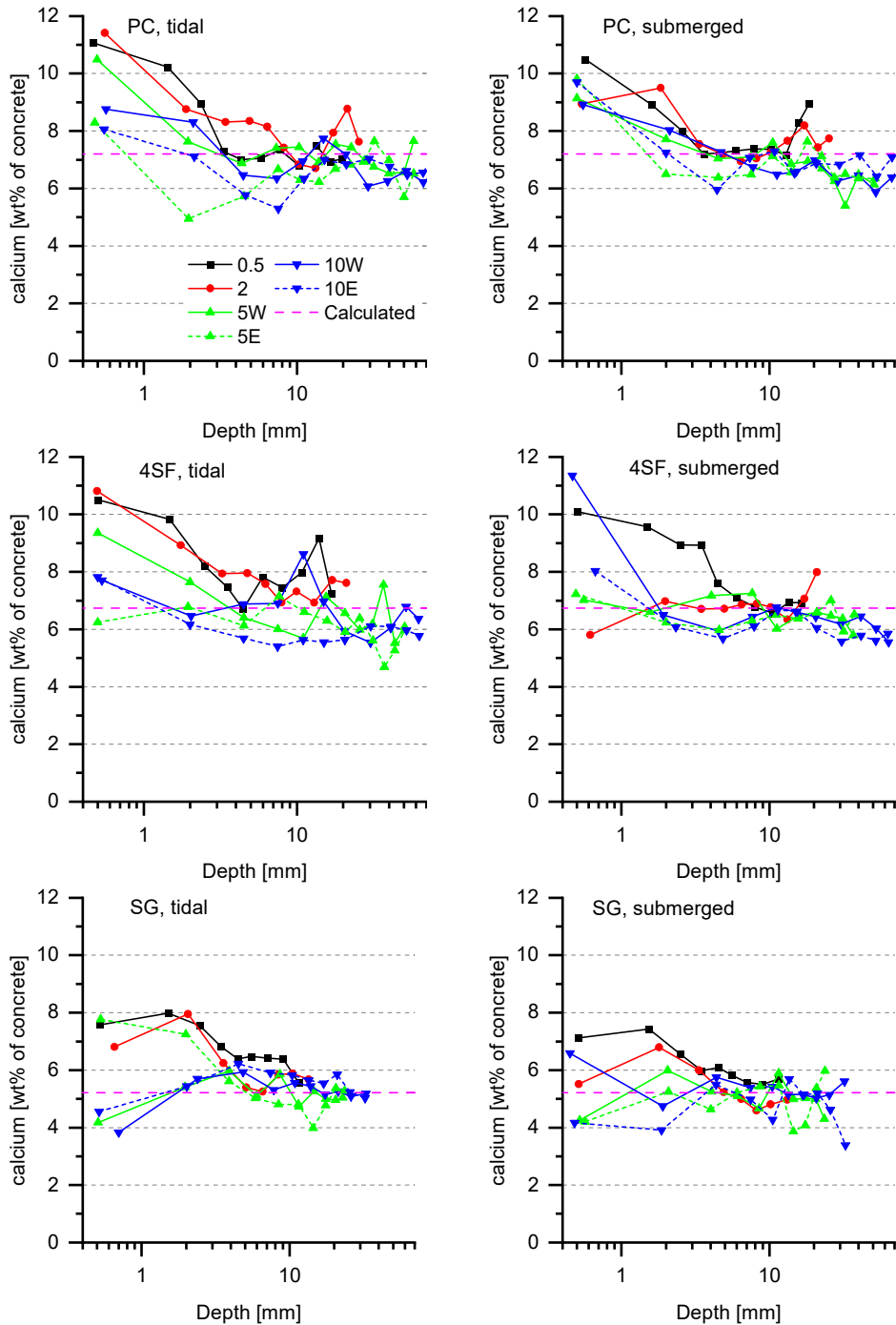


Figure 1 - Calcium profiles measured after half a year, two, five and ten years for concrete PC, SF and SG in tidal- (left) and submerged exposure (right). All profiles are from the west-facing side of the panels, unless marked “E” for the east-facing side. The dashed line corresponds to the calcium content of the concrete calculated based on concrete composition (Table 2).

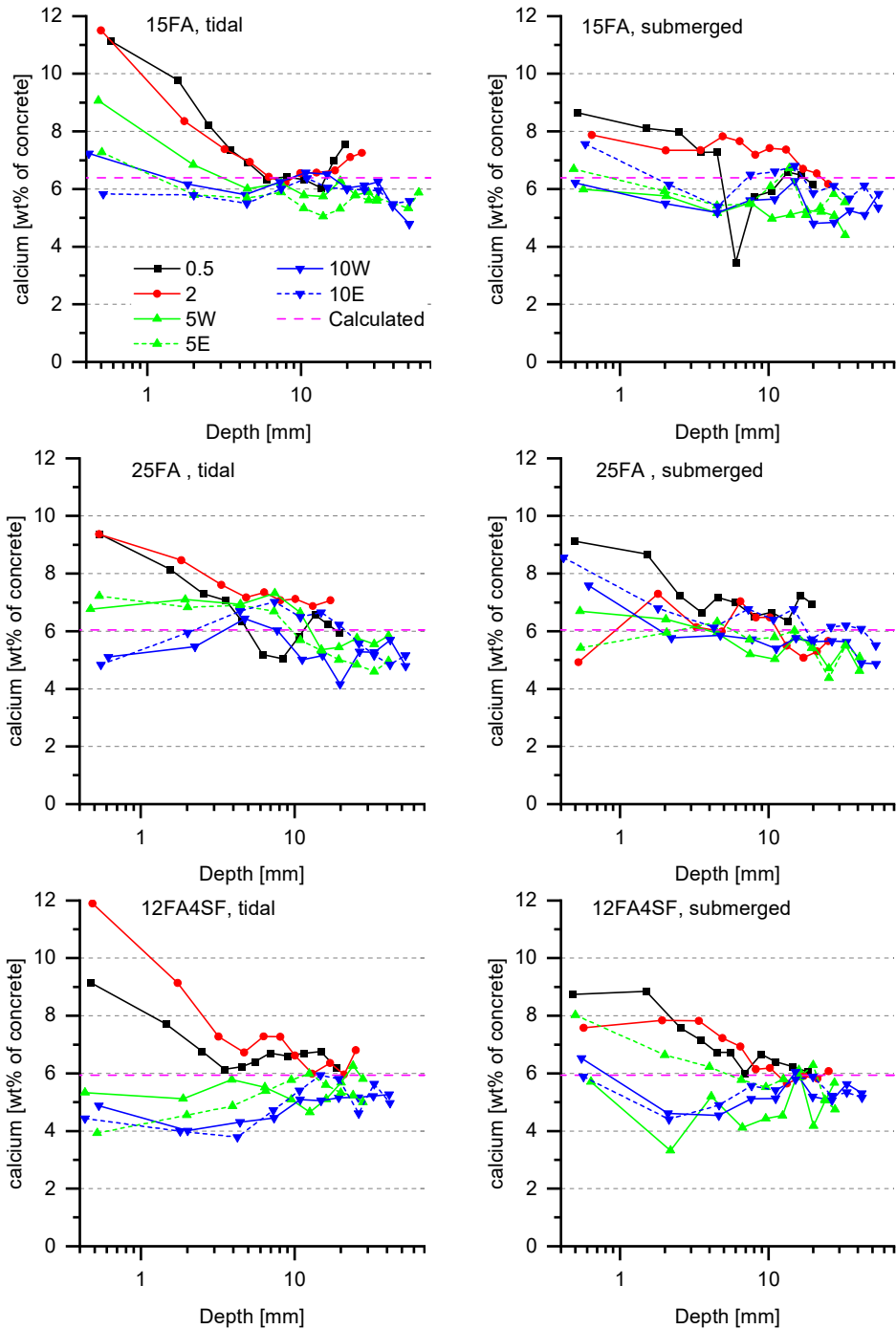


Figure 2 - Calcium profiles measured after half a year, two, five and ten years for concrete 15FA, 25FA and 12FA4SF in tidal- (left) and submerged exposure (right). All profiles are from the west-facing side of the panels, unless marked “E” for the east-facing side. The dashed line corresponds to the calcium content of the concrete calculated based on concrete composition (Table 2).

3.2 Impact of calcium leaching on chloride profiles

The impact of correcting chloride profiles for the paste fraction using the calcium content according to Equation 1 is discussed in the following. Figures 3 and 4 illustrate the difference between uncalibrated and calibrated chloride profiles over time for data from both the tidal and submerged exposure. Note the x-axis is in logscale to emphasize the effect of calibration on both the surface near zone and the bulk. Chloride profiles with a linear x-axis are shown in Appendix B. The impact of applying calibration or not on the observed maximum chloride concentration (C_{\max} ; “peak value”) and its depth ($x_{C_{\max}}$) as a function of the exposure time is shown in Figure 5.

From Figures 3 and 4 one can observe generally higher chloride contents near the surface for uncalibrated chloride profiles up to two years of exposure than when the chloride content is calibrated through Equation 1. This is explained by the wall effect, which causes a higher paste fraction in the outermost surface, and thus a relatively higher chloride content of the concrete than of the paste. However, after five years, the feature is less pronounced, and in some cases after ten years the uncalibrated chloride profiles show a lower chloride content near the surface than the calibrated ones. Within the bulk of the concrete (e.g. deeper than 10 mm), the calibration at first glance does not seem to have a large influence on the chloride profiles. However, when looking at the chloride profiles of 25 FA after ten years of tidal exposure, one can observe that the variation in the calcium content from 4-6% calcium by wt. of concrete for this specific concrete (see Figure 2) does result in a considerable difference between the uncalibrated and calibrated chloride profile e.g. at a depth of 20 mm 0.22% chloride by wt. of concrete vs 0.32% chloride by wt. of concrete respectively (see Figure 4). This illustrates that calcium calibration can have a considerable effect on the chloride profiles, also in the bulk.

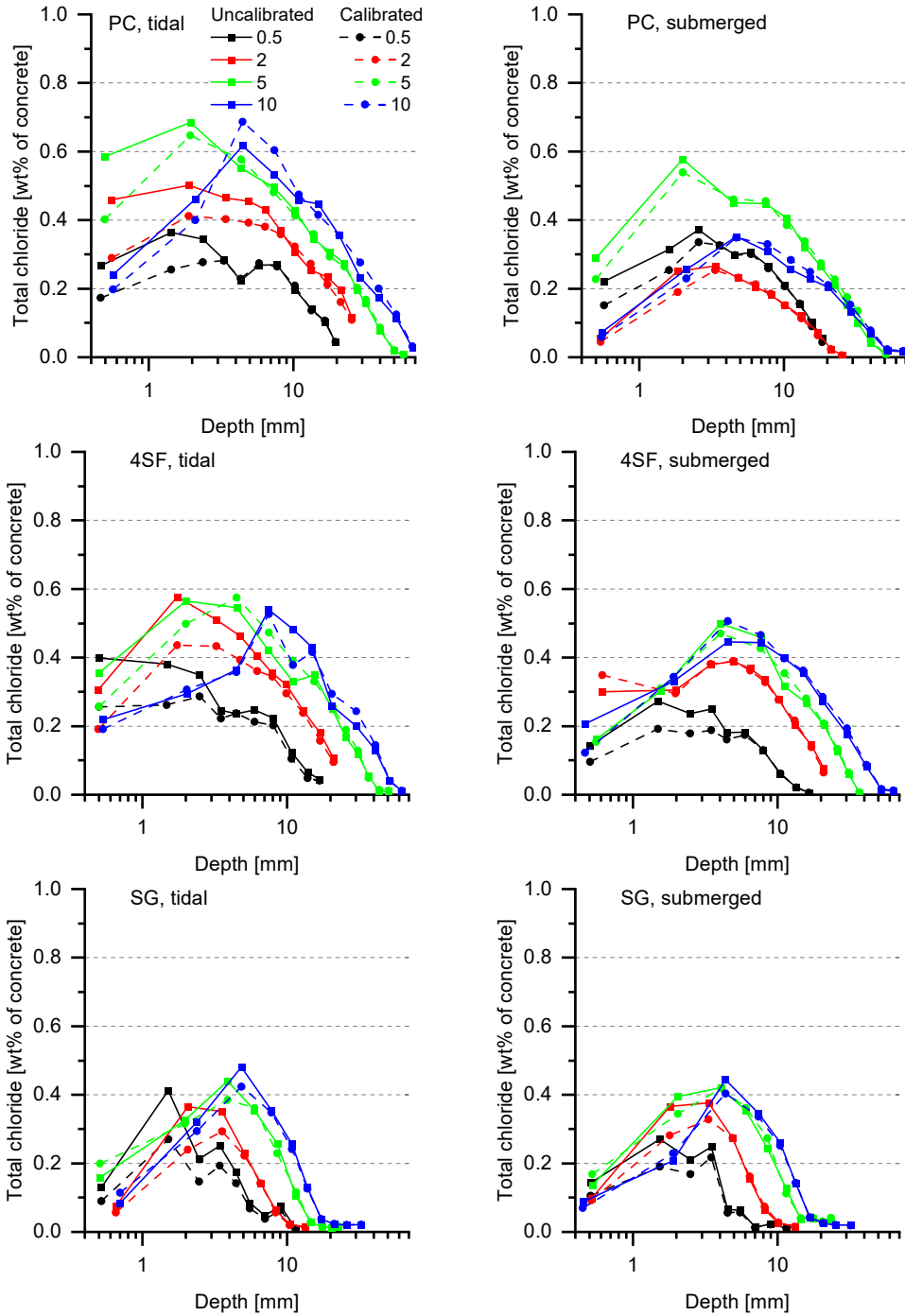


Figure 3 - Uncalibrated and calibrated chlorides profiles for concrete PC, 4SF and SG after half a year, two, five and ten years in tidal- (left) and submerged exposure (right). All profiles are from the west-facing side. Full line: uncalibrated. Dashed line: calibrated to parallelly measured calcium profiles. x-axis in logscale.

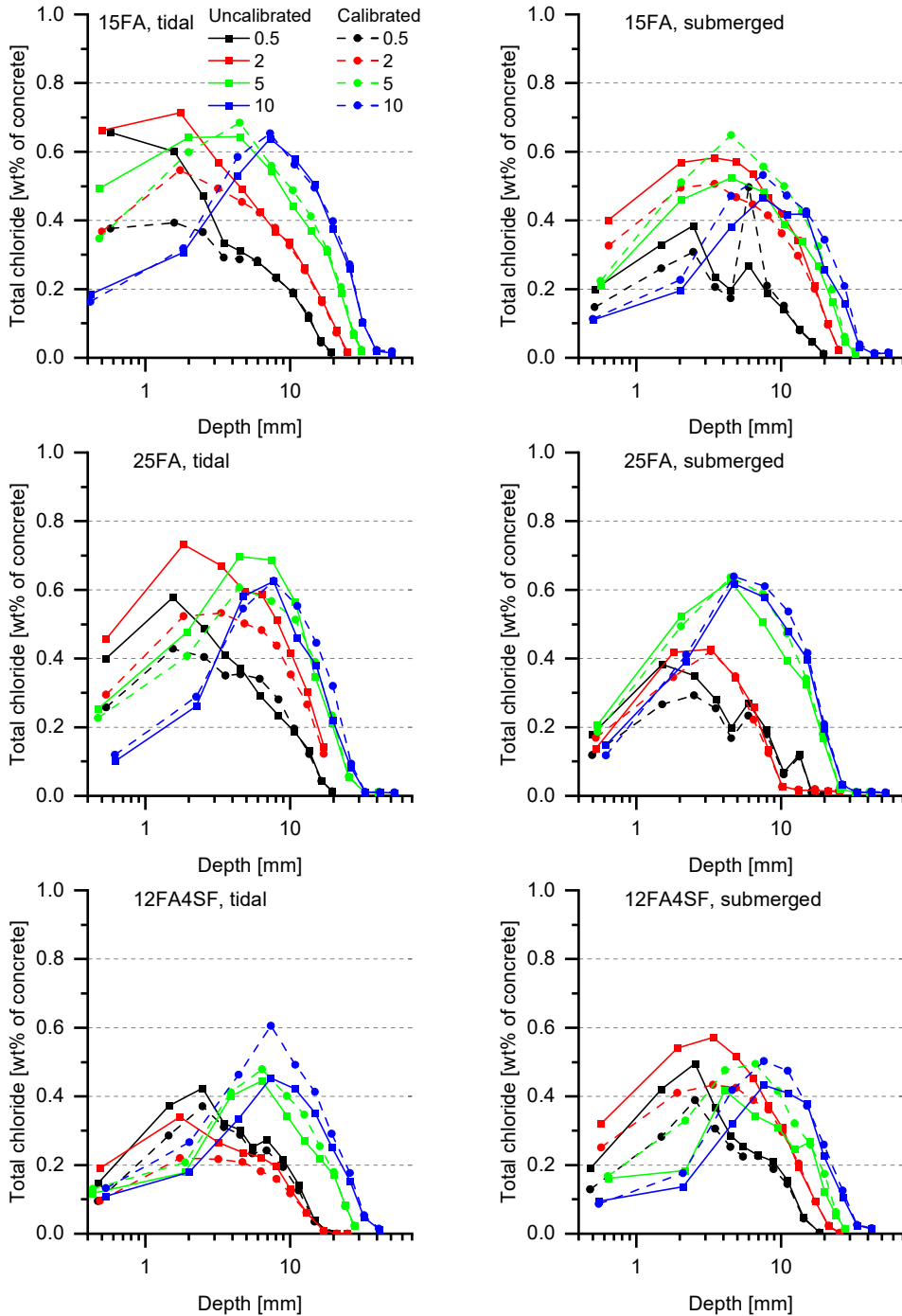


Figure 4 - Uncalibrated and calibrated chlorides profiles for concrete 15FA, 25FA and 12FA4SF after half a year, two, five and ten years in tidal- (left) and submerged exposure (right). All profiles are from the west-facing side. Full line: uncalibrated. Dashed line: calibrated to parallelly measured calcium profiles. x-axis in logscale.

Figure 5 shows that the depth of the maximum chloride content, $x_{C_{\max}}$, shifts towards greater depths with time both for calibrated and uncalibrated chloride profiles. The development of C_{\max} with time is described in further detail in [10]. It should be noted that at early exposure times (half a year and two years) calibrated profiles can show a deeper $x_{C_{\max}}$ compared to the uncalibrated ones. This is explained by the calibration of the measured chloride content when divided by a measured calcium content – which for young specimens with limited leaching – increases with proximity to the surface due to the variation of paste content (the wall effect).

For all calibrated chloride profiles, the maximum chloride content, C_{\max} , increases from two to ten years of exposure, whereas for most uncalibrated chloride profiles C_{\max} does not show an increase in this period. The increase for the calibrated C_{\max} is due to the lower C_{\max} at early ages caused by the calcium calibration taking into account the increased paste fraction at the surface. However, over time several factors influence the calibrated and uncalibrated C_{\max} differently:

- The calcium levels near the surface drop due to leaching (Figures 1 and 2). For PC, 15FA, 4SF and 12FA4SF this effect proceeds beyond C_{\max} , thus causing the calibrated C_{\max} to artificially increase with time.
- $x_{C_{\max}}$ shifts inward when time progresses, toward depths with lower paste fractions, which may conceal a potential increase in C_{\max} over time – if no calibration for the systematic variation in paste fraction is performed.
- For both calibrated and uncalibrated chloride profiles, $x_{C_{\max}}$ shifts over time towards wider profile ground sections resulting in that the maximum chloride content, C_{\max} , being averaged over a larger sample volume. This typically causes a reduction of the measured C_{\max} .

The combination of the above factors is assumed to be the explanation of why the uncalibrated in contrast to calibrated chloride profiles show a relatively constant C_{\max} from 2 to 10 years, and even a decrease in C_{\max} is observed for 15FA, 25FA and 4SF.

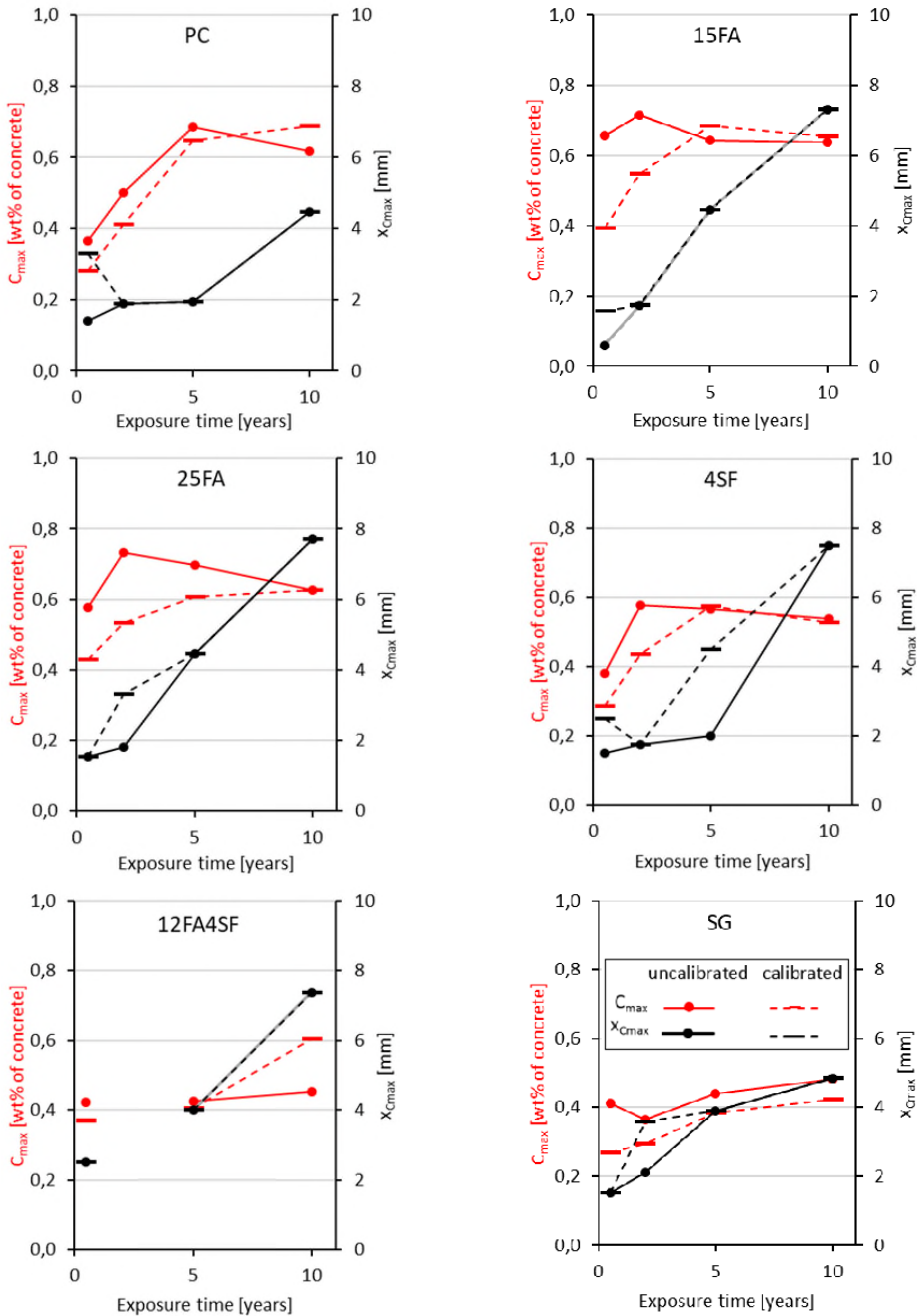


Figure 5 - Difference between calibrated and uncalibrated values of maximum chloride content (C_{max}) and the mean depth of the sampling interval containing C_{max} ($x_{C_{max}}$) at exposure times half a year, two, five and ten years for all investigated concretes (tidal exposure, west-facing surface). Full line: uncalibrated. Dashed line: calibrated to parallelly-measured calcium profiles. Data points for 12FA4SF are not connected as data points for the outlier after 2 years exposure is missing.

3.3 Assumptions, advantages and disadvantages for methods of calcium calibration

When performing no calibration of the chloride profiles for the paste fraction, it is assumed, that the paste fraction is homogeneously distributed in the concrete and is not affected by the exposure.

When performing a calibration of the chloride profiles for the paste fraction using the calcium content, e.g. according to Equation 1, it is assumed that the calcium/binder ratio as a function of time is constant and that the aggregates do not contribute to the measured calcium content, while the paste fraction may vary as a function of depth.

The data presented in Figure 1 shows that the concretes initially had a higher calcium content at the outer surface compared to the bulk and that leaching occurred over time. Figure 1 also shows an unsystematic variation between calcium measurements in the undisturbed bulk of approximately nominally 2% calcium by wt. of concrete. This unsystematic variation can be considered as a combination of variations in paste fraction and measurement error. In Section 3.2 an increasing trend of the calibrated C_{\max} was shown over time and how the corresponding $x_{C_{\max}}$ at early exposure times may be found at a greater depth than when no calibration is performed. Considering these observations, neither the assumptions for calibration nor absence of calibration provide accurate results and both approaches have advantages and disadvantages, which may vary by depth.

Calibration to parallelly measured calcium profiles has the advantage that it considers variations in paste-aggregate ratio. This is convenient:

- a) To correct for stochastic variations in the paste fraction, both within a single profile but even more importantly when comparing chloride profiles (increasingly important when the ratio of maximum aggregate size to sample volume increases).
- b) To recalculate the chloride content from wt.% of concrete to wt.% of binder considering the wall effect.

However, the approach is based on the assumption that no calcium leaching occurs, which is highly questionable considering e.g. the data in Figures 1 and 2. This unsuitable assumption causes an error in the outermost part of the chloride profile, including both the maximum chloride content (C_{\max}) and its depth $x_{C_{\max}}$ (see Figure 5). Further conducting parallel calcium measurements is time-consuming.

On the other hand, undertaking no calcium calibration neither considers the impact of the wall effect on the paste fraction nor the stochastic variation in the paste fraction. The advantages are that the data are unaffected by calcium leaching and that it takes much less time to perform the analysis. For performance testing of unexposed concretes, the potential impact of the wall effect is typically overcome by testing cut surfaces [4, 5]. Stochastic variations can be limited by increasing the sample size (most effectively by increasing the diameter of the core). In this study a core diameter was used, which exceeded five times the diameter of the largest aggregate in the concrete.

A potential third approach could be to correct the paste fraction to an initially measured calcium profile. This method assumes that the paste fraction as a function of depth in the investigated core is representative for all cores from a given concrete. The approach has the advantage that it corrects for a systematically higher paste fraction near the surface (about 25-100% higher than in

bulk), but it does not correct for the stochastic variation in the paste fraction between cores (5-30% difference between cores taken from same panel after 6 months in submerged and tidal exposure). Also, it requires that the initial calcium content is measured at depths, which corresponds to or are fractions of the depth intervals applied at later ages. This third approach is not investigated here due to the lack of suitable initial calcium profiles.

3.4 Recommendations on when and how to use calcium calibration

Caution is required when using chloride data from the leached zone of long-term exposed concrete. This is supported by a recent paper [10], in which the authors of the present paper recommended that only chloride data from sections taken deeper than an observed microstructurally changed zone should be used from field data when assessing the remaining service life of structures and when testing chloride ingress prediction models, unless reactive transport models are used [10].

A considerable impact of calcium calibration is expected when fitting chloride ingress models based on e.g. the error function solution to Fick's second law [19] to field data. For example, a different evolution in surface concentration would be calculated in the HETEK model as suggested by the evolution in Figure 5 [20] and a higher driving force for diffusion in the form of C_s could be calculated when fitting the error function solution to Fick's second law [19] to calibrated profiles, where calcium leaching is dominant in comparison to the wall-effect and has occurred to depths included in the fit (typically beyond $x_{C_{max}}$ such as for PC, 15FA, 4SF, 12FA4SF). An alternative solution could be to exclude the data points of the chloride profiles, where calcium leaching has occurred, provided sufficient data points are available.

At depths unaffected by calcium leaching – typically beyond the chloride peak – it can be an advantage to calibrate to calcium content to correct for unsystematic variations in paste fraction between samples. However, the repeatability of the calcium determination should be determined to ensure that one does not introduce a considerable error to the chloride profiles during calcium calibration. When the maximum chloride concentration and its position are of interest – which is typically near the surface affected by systematic variations from both the wall effect and leaching – it is suggested to calibrate to an initially or early measured calcium profile. Alternatively, uncalibrated data can be utilized.

4. CONCLUSIONS

Calcium calibration of chloride profiles is used to account for the higher paste fraction in the volume closest to the surface due to the wall effect and for stochastic variations in the paste content in concrete in general. However, due to calcium leaching errors can be introduced to the calibrated chloride contents in the leached part of the profile. Based on chloride and calcium profiles measured on well-cured concretes (equivalent w/c of 0.4) marine exposed at the Fehmarn Belt Exposure Site, the following conclusions can be drawn:

- The calcium content near the surface (up to 5-10 mm) was at early ages higher than in the bulk confirming the wall effect causing a higher paste fraction.
- Due to leaching, the calcium content gradually decreased during exposure and after 10 years, a decrease was observed to about 4 mm for the slag containing concrete (SG) and about 10 mm for all the remaining concretes. The calcium leaching resulted in the calcium content no longer being a suitable measure of the paste fraction up to this depth.
- The zones affected by the wall effect and leaching, extended beyond the depth of the maximum chloride content, are questioning the use of chloride data from the volume closest to the surface.
- After 10 years of exposure, the calibrated maximum chloride content (“chloride peak”) was in several cases higher than the uncalibrated one due to a decrease in the calcium content to a depth extending beyond that of the chloride peak.

Although in theory it is an advantage to calibrate for unsystematic variations in paste fraction at depths unaffected by calcium leaching, uncertainties and systematic variations in paste fraction may outweigh the benefits of such calibration. When the maximum chloride concentration and its position are of interest e.g., for modeling, it is suggested to calibrate to an initially or early measured calcium profile to account for systematic variations from both the wall effect and leaching – or alternatively to use uncalibrated data. In all cases, the repeatability of the calcium determination should be reported, and it should be confirmed that the aggregates do not contribute to the measured calcium content.

ACKNOWLEDGEMENTS

The authors would like to thank Femern A/S for sharing field data from the Fehmarn Belt Exposure Site. This work was supported by the Danish Ministry of Higher Education and Science through the contract “E5 Field exposure and monitoring to extend the service life of infrastructure (translation from Danish)” granted to the Danish Technological Institute (DTI).

REFERENCES

1. Zou R, Yu A: “The packing of spheres in a cylindrical container: the thickness effect”. *Chemical engineering science*, Vol 50, No. 9, 1995, pp. 1504-1507
2. Larrard F D: “Packing density and homogeneity of granular mixes”. Chapter 1, “Concrete mixture proportioning: a scientific approach” (Edited by F. De Larrard), CRC Press, London, UK, 1999, pp. 1-76.
3. Hansen E Ø, Iskau M R, Hasholt M T: “Chloride Ingress in Concrete with Different Age at Time of First Chloride Exposure”. *Nordic Concrete Research*, Vol 55, No. 2, 2016, pp. 9-26.
4. NORDTEST: “NT BUILD 443 Concrete, hardened: accelerated chloride penetration”. Espoo, Finland, 1995, 5 pp.
5. Danish Standard: “DS/EN 12390-11:2015, Testing hardened concrete - Part 11: Determination of the chloride resistance of concrete, unidirectional diffusion”. København, Danmark, 35 pp.
6. Poulsen S L, Sørensen H E: “Chloride ingress in old Danish bridges”. Proceedings, 2nd International Congress on Durability of Concrete (ICDC), New Delhi, India, 2014.
7. Danish Road Directorate: “HETEK Report No.94: Chloride penetration into concrete – Relevant test methods”. “APM 214 Concrete testing - Hardened concrete - Calcium content” (edited by , J.M. Frederiksen, Vedbæk, Denmark, 1995, 3 pp. (in Danish).
8. Weerdt K D, Orsáková D, Müller A C A, Larsen C K, Pedersen B M, Geiker M R: “Towards the understanding of chloride profiles in marine exposed concrete, impact of leaching and moisture content”. *Construction and Building Materials*, Vol. 120, No. 1, 2016, pp. 418-431.
9. Glasser F P, Marchand J, Samson E: “Durability of concrete – Degradation phenomena involving detrimental chemical reactions”. *Cement and Concrete Research*, Vol. 38, No. 2, 2008, pp. 226-246.
10. Fjendbo S, Sørensen H E, Weerdt K D, Geiker M R: “Correlating the development of chloride profiles and microstructural changes in marine concrete up to ten years”. *Manuscript submitted for publication*, 2021.
11. Boubitsas D, Tang L, Utgenannt P: “Chloride Ingress in Concrete Exposed to Marine Environment-Field data up to 20 years’ exposure”. CBI Report to SBUF Project 12684, 2014.
12. Fehmarnbelt Exposure Site: <http://www.concreteexpertcentre.dk/30663>. (Accessed 15th of March 2021), 2015.
13. Poulsen S L, Sørensen H E, Jönsson U: “Chloride ingress in concrete blocks at the Rødbyhavn marine exposure site – Status after 5 years”. *Proceedings*, 4th International Conference on Service Life Design for Infrastructures (SLD4), Delft, Netherlands, 2018, pp. 192-203.
14. Pade C: “Concrete Blocks for Exposure Site at Rødbyfærgehavn” Unpublished, 2010.
15. Herholdt A D, Justesen C F P, Nepper-Christensen P, Nielsen A: ”Beton-Bogen” (the concrete book). Cementfabrikkernes tekniske oplysningskontor, Aalborg Portland, Aalborg, Denmark, 1985. (in Danish)
16. DMI, 2020: <https://www.dmi.dk/vejarkiv/>.(Accessed 3rd of January 2020).
17. Danish Standard: “DS/EN 14629:2007, Products and systems for the protection and repair of concrete structures - Test methods - Determination of chloride content in hardened concrete”. København, Danmark, 16 pp.
18. SP Swedish National Testing and Research Institute: “Estimation of Cement/Binder Profile Parallel to the Determination of Chloride Profile in Concrete: NORDTEST Project No. 1581-02,Borås, Sweden, 2003, 34 pp.

19. Collepardi M, Marcialis A, Turriziani R: “The kinetics of chloride ions penetration in concrete”. *Il cemento*, Vol. 67, 1970 pp. 157-164.
20. Mejlbro L: “The complete solution of Fick’s second law of diffusion with time-dependent diffusion coefficient and surface concentration”, Chapter 8, “Durability of concrete in saline environment” (Edited by P. Sandberg), Cementa AB, Lund, Sweden, 1996, pp. 127-158.

APPENDIX A

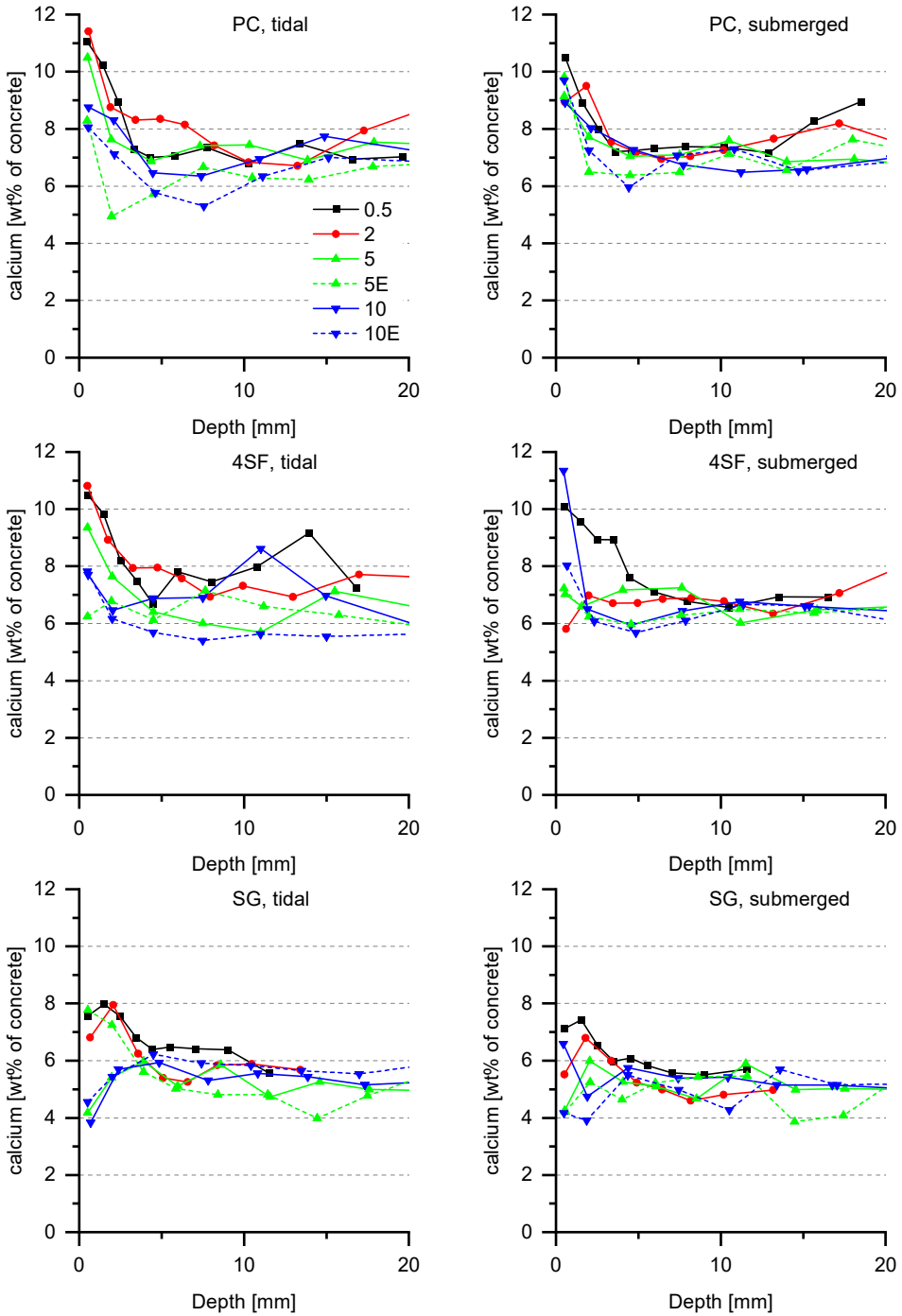


Figure A.1 - Calcium profiles measured after a half, two, five and ten years for concrete PC, SF and SG exposed at the Fehmarn Belt Exposure Site in tidal- (left) and submerged exposure (right). All profiles were from the west facing side, except those marked "E" for east.

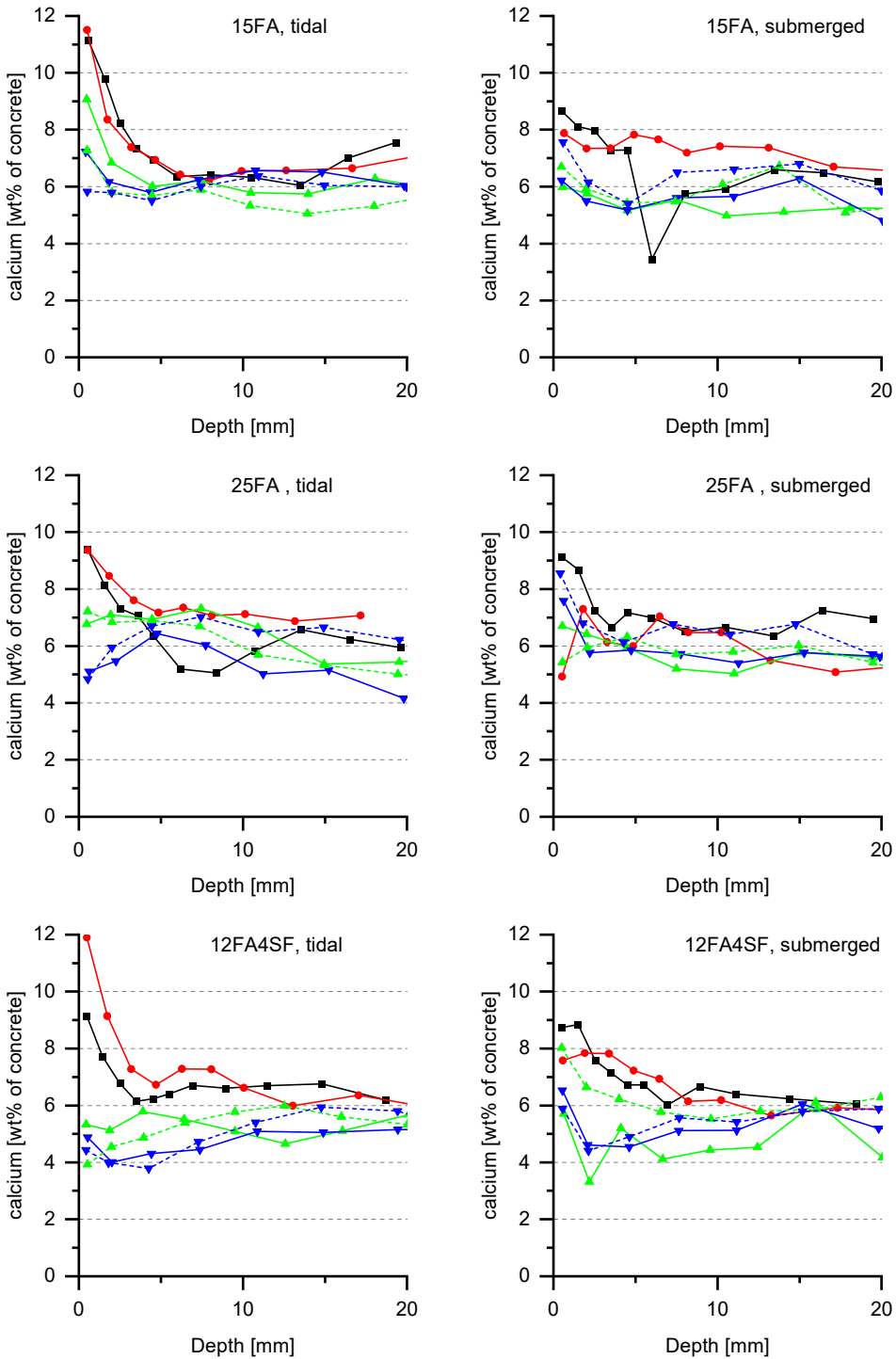


Figure A.2 - Calcium profiles measured after a half, two, five and ten years for concrete 15FA, 25FA and 12FA4SF exposed at the Fehmarn Belt Exposure Site in tidal- (left) and submerged exposure (right). All profiles were from the west facing side, except those marked “E” for east.

APPENDIX B

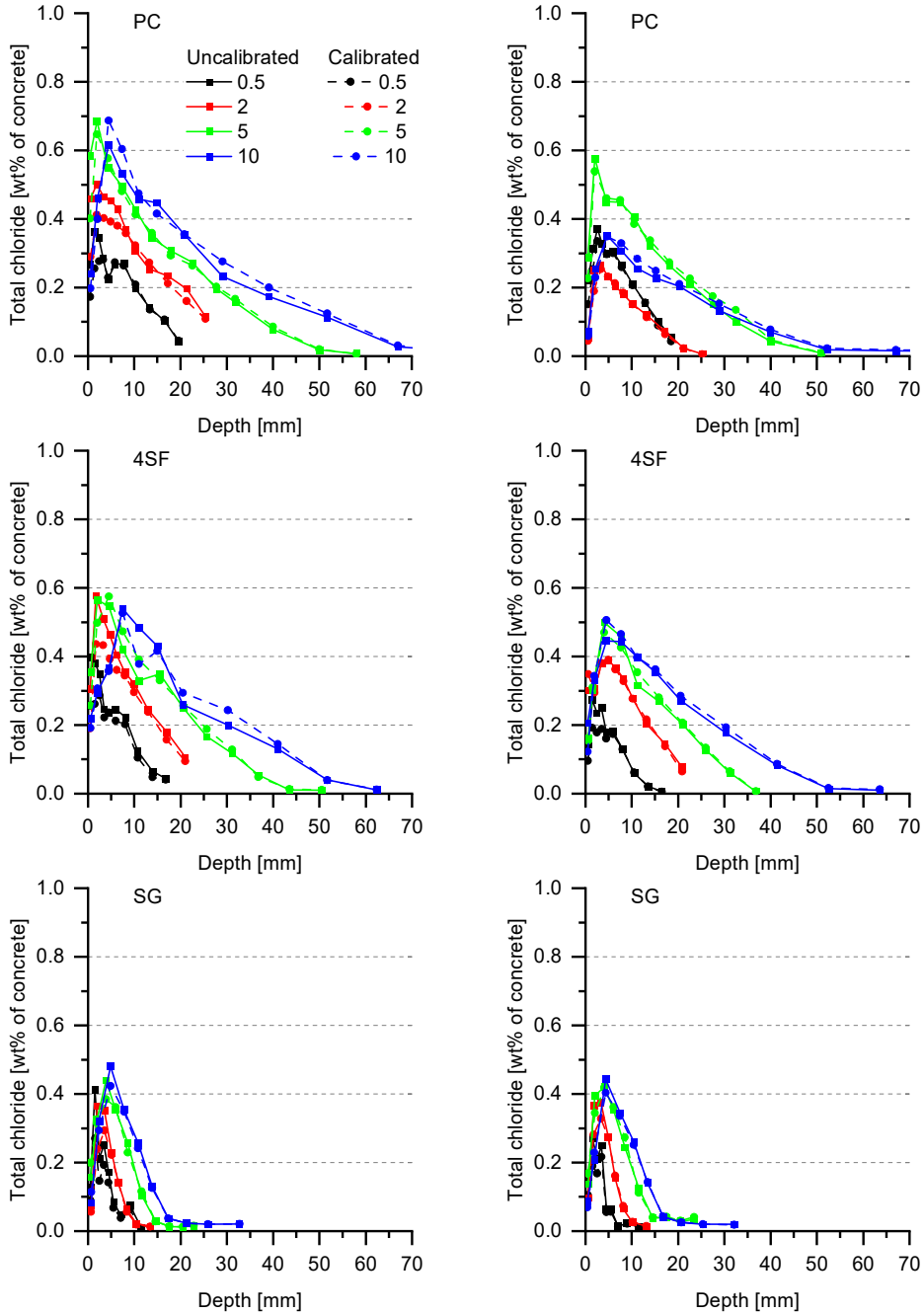


Figure B.1 - Uncalibrated and calibrated chlorides profiles for concrete PC, 4SF and SG at exposure a half, two, five and ten years in tidal- (left) and submerged exposure (right). All profiles were from the west facing side. Full line: uncalibrated. Dashed line: calibrated to parallelly measured calcium profiles. x-axis in linear scale.

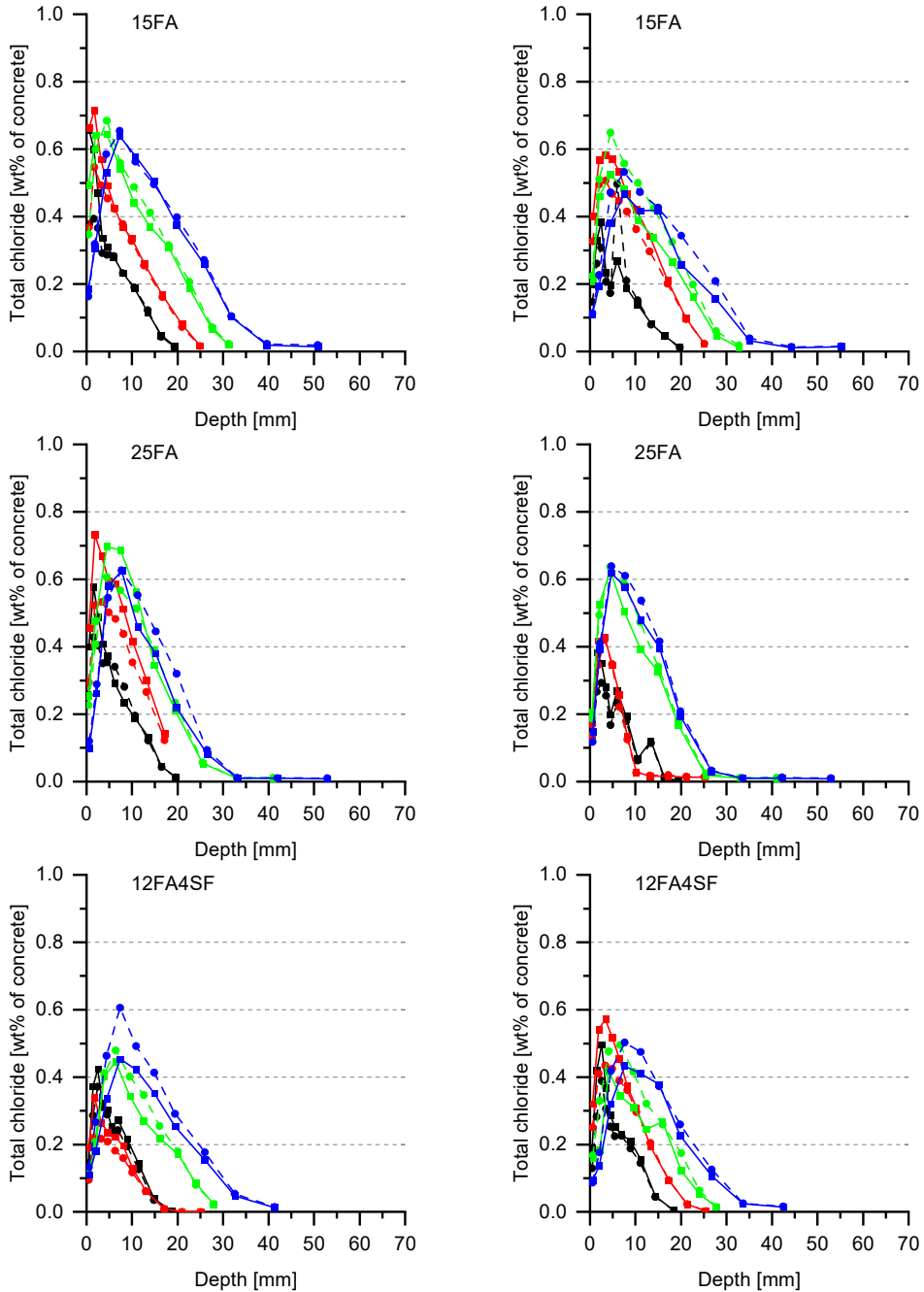


Figure B.2 - Uncalibrated and calibrated chlorides profiles for concrete 15FA, 25FA and 12FA4SF at exposure times a half, two, five and ten years in tidal- (left) and submerged exposure (right). All profiles were from the west facing side. Full line: uncalibrated. Dashed line: calibrated to parallelly measured calcium profiles. x-axis in linear scale.

Part III – Appendices

Part III – Appendix A

Appendix A Details on the Fehmarn Belt Exposure Site

An overview of the Fehmarn Belt Exposure Site is shown in Figure A1. The water temperature, salinity and water level varied as shown in Figure A2 and Table A1. Figure A3 show the location of cores extracted after a half, two, five and ten years of exposure.



Figure A1: Location and photo of the Fehmarn Belt Exposure Site [54].

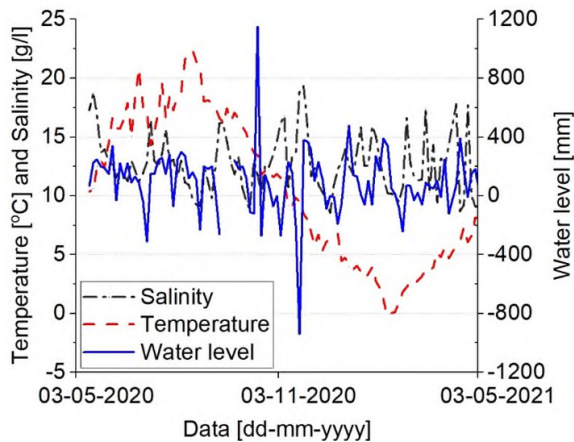


Figure A2: Water temperature, salinity, and water level at the Fehmarn Belt Exposure Site for one year.

Table A1: Exposure conditions at the Fehmarn Belt Exposure Site (average of timespan shown in Figure A1).

Average temperature (atmosphere) [°C]	11.2 (monthly min.: 2.1, monthly max.: 18.2)
Average temperature (sea water) [°C]	10.5 (min.: -0.3, max.: 22.4)
Average salinity (sea water) [g/l]	12.7 (min.: 8.6, max.: 19.3)
Average chloride content (sea water) [g/l]	7.0 ^{a)} (min.: 4.7, max.: 10.6)

a) Assuming a distribution of ions in the sea water as in the Baltic Sea [55].

Part III – Appendix A

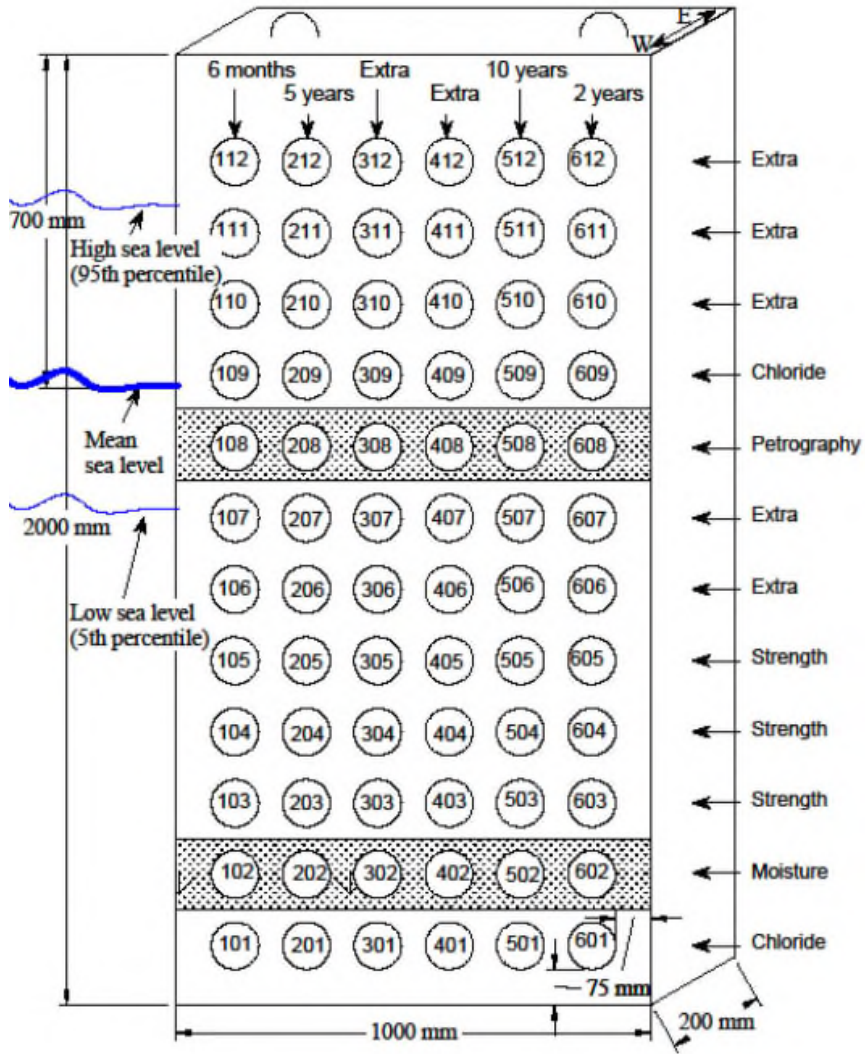


Figure A3: Location of cores extracted after a half, two, five and ten years of exposure. The pattern on the horizontal lines covering vertical positions #2 and #8 indicates that they were not cleaned prior to coring.

Part III – Appendix B

Appendix B Details on exposed concretes and constituent materials

Table B1 gives an overview of the mixture proportions of the concretes analyzed in this study. All cement notations are according to EN 197-1 [56]. Table B2 gives information on the chemical composition of binders as measured by X-ray fluorescence according to EN 196-2 [57].

Table B1: Mixture proportions of concrete exposed at the Fehmarn Belt Exposure Site [kg/m³] [15].

Field exposure site	Fehmarn Belt Exposure Site													
Concrete ID in thesis	PC	15FA	25FA	25FA_SCC	4SF	12FA4SF	12FA4SF_noAEA	12FA4SF_high_wc	12FA4SF_low_wc	12FA4SF_SCC	SG	SG_noAEA	SG_SCC	SG_rapid
Original concrete ID	A	B	C	D	E	F	G	H	I	J	K	L	M	N
Group I	x	x	x		x	x					x			
Group II				x			x	x	x	x		x	x	x
Powder composition [wt.%]	CEM I	100	85	75	75	96	84	84	84	84	84			
	FA ^{a)}		15	25	25		12	12	12	12	12			
	SF ^{b)}					4	4	4	4	4	4			
	CEM III											100	100	100
CEM I-SR5 42.5 N^{c)}	365	322	300	336	340	300	310	276	330	350				
CEM I 52.5 N^{c)}														108
CEM III/B 42.5 N^{c,d)}											360	375	410	
FA		57	100	112		43	44	39	47	50				
SF (added as slurry)					14	14	15	13	16	17				
GGBS^{e)}														252
Water	146	140	140	157	147	140	145	145	135	163	144	150	164	144
Polycarboxylate ether superplasticizer (BASF Glenium SKY 532 SU)							3.8							
Polycarboxylate ether superplasticizer (BASF Glenium SKY 532 S)		2.3	2.2											
Polycarboxylate ether superplasticizer (BASF Glenium SKY 540)	2.8			2.9	2.7	2.9		2.6	3.6	3.4	2.3	2.6	2.9	2.9
Air entraining agent	1.7	1.7	2.3	4.0	0.7	1.6	0.0	1.5	2.3	2.2	0.8	0.0	1.6	1.0
Sand	695	671	642	678	695	677	731	700	671	687	689	702	686	689
Coarse aggregates	1172	1182	1179	1053	1172	1192	1182	1182	1182	1067	1161	1185	1065	1162
w/(c + 2SF + 0.5 FA)	0.40	0.40	0.40	0.40	0.40	0.40	0.40	0.45	0.35	0.40	0.40	0.40	0.40	0.40
w/b	0.40	0.37	0.35	0.35	0.42	0.39	0.39	0.44	0.34	0.39	0.40	0.40	0.40	0.40

a) FA = Fly ash

b) SF = Silica fume (dry matter)

c) According to EN 197-1

d) GGBS content: 67 wt.%

e) GGBS = Ground Granulated Blast-furnace Slag

Part III – Appendix B

Table B2: Chemical composition of binders as measured by X-ray fluorescence according to EN 196-2.
 “-” means that the amount has not been measured.

	CEM I-SR5 42.5 N [% by wt.]	CEM I 52.5 N [% by wt.]	CEM III [% by wt.]	FA [% by wt.]	SF [% by wt.]	GGBS [% by wt.]
Al ₂ O ₃	2.91	5.34	9.44	20.5	-	13.0
SiO ₂	24.8	20.0	30.5	60.3	95.4	34.9
CaO	65.6	63.4	47.8	1.56	0.32	40.1
CO ₂	0.15	1.30	0.75	-	-	0.52
Cl ⁻	0.00	0.03	0.08	0.01	0.04	0.02
Fe ₂ O ₃	2.34	3.78	0.74	7.39	-	0.40
MgO	0.75	0.86	4.88	-	-	8.09
SO ₃	2.24	3.29	2.54	0.46	0.23	2.72
Na ₂ O _{eq}	0.40	0.61	0.78	2.76	0.72	0.78
Na ₂ O	-	-	0.33 ¹⁾	-	0.19 ¹⁾	-
K ₂ O	-	-	0.48 ¹⁾	-	0.80 ¹⁾	-
Loss on ignition	0.65	2.24	1.05	3.17	1.34	0.27

1) Value declared by producer in a technical data sheet.

Details on production and curing are found in Paper II.

Part III – Appendix C

Appendix C Additional experimental work

Table C.1: Overview of experimental work

Exposure site	Fehmarn Belt Exposure Site										DTI exposure site
	Tidal					Submerged					
Concretes	PC, 15FA, 25FA, 4SF, 12FA4SF, SG	12FA4SF_noAEA, 12FA4SF_hwc, 12FA4SF_lwc, SG_noAEA, SG_rapid	25FA_SCC, 12FA4SF_S CC, SG_SCC,	PC_NC, 12FA4S F_NC, SG_NC	PC, 15FA, 25FA, 4SF, 12FA4SF, SG	12FA4SF_noA EA, 12FA4SF_hwc, 12FA4SF_lwc, SG_noAEA, SG_rapid	25FA_SCC, 12FA4SF_S CC, SG_SCC	PC_NC, 12FA4S F_NC, SG_NC	PC, 12FA4SF, SG	15FA, 25FA, 25FA_SCC, 4SF, 12FA4SF_noAEA, 12FA4SF_hwc, 12FA4SF_lwc, 12FA4SF_SCC, SG_noAEA, SG_SCC, SG_rapid	
Initial testing											
Compressive strength 28d										x	x
Chloride migration coefficient 28 days										x	x
Chloride migration coefficient 180 days (NT Build 492)										x	x
Chloride diffusion coefficient NT build 443										x	
Long term testing	Core ¹										
Cl & Ca profiles (6 mth)	1, 9	x	x	x		x	x	x			
Cl & Ca profiles (2 years)	1, 9	x	x	x	x	x	x	x	x		
Cl & Ca profiles (5 years)	1, 9	x (W & E)	x (W & E)	x (W & E)	x	x (W & E)	x (W & E)	x (W & E)	x		
Chloride migration coefficient (2, 5 & 8 years)	-									x	x
SEM-EDX (½ & 2 years)	8					PC, 15FA, 4SF, SG		12FA4SF_S CC, 25FA_SCC			
Petrography (28 days)										x	x
Petrography (½, 2 & 5 years)	8	x	x	x							
Carbonation depth (9 years)	-									x	x
Compressive strength (½, 2, 5 years)	3, 4, 5					x	x	x			
Manual potential measurements (on-going)	-	x	x	x		x	x	x			
Automated potential measurements (real-time)	-				x				x		

Concrete compositions and details on constituent materials are given in Appendix B.

Cores are taken at the following depth below mean tide level (mm): 1: 1175 2: 1025 3: 875 4: 725 5: 575 8: 125 9: -25

Appendix D Investigation of carbonation of selected concretes in urban environment

- Comparison of the techniques pH indicator and optical microscopy for determination of carbonation depths on Portland cement, fly ash, slag and combined fly ash and silica fume concretes.

Comparison of the techniques pH indicator and optical microscopy for determination of carbonation depths on Portland cement, fly ash, slag and combined fly ash and silica fume concretes.

Abstract

The aim of this paper is to compare the information gained from determination of carbonation depths measured by pH indicator and optical microscopy for four samples naturally exposed in urban environment outside the Danish Technological Institute for 8 years. Thymolphthalein was used as the pH indicator and the optical microscopy was performed on thin sections. The terminology proposed in (Revert, De Weerd et al. 2016) was used to characterize the carbonation depth and front. The carbonation depths determined by pH indicator and optical microscopy are in good agreement when considering the impact of sampling.

Introduction

Carbonation induced corrosion is one degradation mechanism, which can cause premature deterioration of reinforced concrete structures. Carbonation is the process where hydration products containing calcium react with CO₂ to form calcium carbonate thereby lowering the pH of the pore solution and rendering steel depassivated. The rate of carbonation is influenced by the porosity, composition and humidity of concrete (Jacobsen, Sellevold et al. 2009). In addition to the hydration products, unhydrated phases such as alite and belite may carbonate (Papadakis, Vayenas et al. 1991).

Bier (1986) found that the carbonation depths in well-cured samples containing fly ash or blast furnace slag can be a factor of 2 greater than when ordinary Portland cement is used (Bier 1986).

Several methods are available for determination of carbonation in concrete as described by (Revert, De Weerd et al. 2016). Methods include pH indicator, thermogravimetric analysis, Fourier-transformed infrared spectroscopy, X-ray diffraction, optical microscopy, scanning electron microscopy, mercury intrusion porosimetry, magic-angle spinning nuclear magnetic resonance spectroscopy, gammadensimetry and chemical analysis (Revert, De Weerd et al. 2016). In the present paper the techniques pH indicator and optical microscopy is utilized and compared.

The most common way to study carbonatization depth in concrete is to spray a solution containing a pH indicator. Traditionally phenolphthalein has been used, but due to the carcinogenic classification of phenolphthalein, thymolphthalein is increasingly used instead. thymolphthalein has the property to be blue above pH 9.3-10.5 and colorless below. The carbonation depth is thus detected by the depth in which the color change from blue to colorless.

By optical microscopy carbonation can be identified by cross-polarized light as opaline and bright colors due to presence of calcite crystals (and absence of calcium hydroxide). This is a

sharp contrast to the darker colors of the non-carbonated areas. By polarized light carbonation may be identified by absence of un-hydrated cement grains. Finally, fluorescent mode can reveal changes in porosity due to carbonation if an un-carbonated reference is available and the w/c is sufficiently low (Jakobsen, Laugesen et al. 1999).

The aim of this paper is to compare the information gained from determination of carbonation depths measured by pH indicator and optical microscopy for four samples exposed at urban exposure outside of the Danish Technological Institute for 8 years and to predict the carbonation depth after 120 years of exposure.

Experimental

Material

Four concrete elements differing in binder compositions (Table 1) were investigated for microstructural changes due to carbonation. After homogenization in pan mixer, the elements were cast in plywood molds lubricated with mold oil. The elements were demolded at an age corresponding to minimum 24 maturity hours. Immediately after demolding, the blocks were wrapped in plastic secured firmly with tape. Each panel remained indoors until the block had reached minimum 14 maturity days, where after the blocks could be moved outside if required to control maturity gain. The exact maturity of the blocks was monitored closely using cast-in temperature sensors. The plastic was removed when the blocks reached a maturity of 28-42 days. The exposure environment was in average 8.8 °C with 412 ppm CO₂, 674 mm precipitation and 1447 hours of sunshine (Buis 2019, DMI 2020).

Table 1: Composition of concretes selected for optical microscopy (Poulsen, Sørensen et al. 2018)

Concrete ID:		PC	25FA	12FA4SF	SG	
Powder composition wt%	Low alkali SR cement CEM I 42.5 N	CEM I 42.5 N	100	75	84	
	Slag cement ¹	CEM III/B 42.5 N				100
	Fly ash	EN 450-1 N		25	12	
	Silica fume	50 %-wt slurry			4	
Concrete composition	Cement	kg/m ³	365	300	300	360
	Fly ash	kg/m ³		100	43	
	Silica fume, solid matter	kg/m ³			14	
	Water content	l/m ³	146	140	140	144
	Aggregate 0/2	kg/m ³	695	642	677	689
	Aggregate 4/8	kg/m ³	377	367	377	373
	Aggregate 8/16	kg/m ³	266	271	272	263
	Aggregate 16/22	kg/m ³	529	541	543	525
	Air entraining agent	kg/m ³	1.7	2.3	1.6	0.8
	Superplasticizer	kg/m ³	2.8	2.2	2.9	2.3
Eqv. w/c ratio	-	0.4	0.4	0.4	0.4	

¹⁾ 67 wt% ground granulated blast furnace slag content

Methods

At an age of 8 years cores were drilled using a 100 mm drill. The cores were cut through lengthwise and any surface water was blown away by pressurized air. For each core, one cut

surface was immediately analyzed by pH indicator, whereas the other was impregnated with fluorescent epoxy within one hour after cutting to stop further carbonation and to prepare thin sections for optical microscopy.

pH indicator

A thymolphthalein solution was prepared by dissolving 0.1 g thymolphthalein in 20 g deionized water and 80 g of ethanol. The solution was sprayed on freshly cut surfaces and the depth of carbonation was measured as the depth of color change in seven equally distributed points. Whenever this resulted in a measurement point in an aggregate particle, the average carbonation depth between the two sides of the aggregate particles was used. From these 7 points $x_{c,avg}$ (average of seven measurement points), $x_{c,max}$ (maximum measured carbonation depth excluding cracks) and $x_{c,crack}$ (carbonation depth along crack) was determined.

Optical microscopy

Microstructural changes were investigated using optical microscopy of thin sections. Thin sections were studied by an optical microscope Nikon Eclipse LV 100 POL. CH and CC crystals were observed using crossed polarized light. Carbonation depth was measured in 10 equally distributed lines across the width of the sample. Porosity changes due to carbonation were studied by comparing the intensity of the fluorescent light transmitted through the sample.

Terminology

The terminology proposed in (Revert, De Weerd et al. 2016) was used to characterize the carbonation depth and front. i.e. the carbonation depth $x_{c,i}$ is the distance at location i from the outer surface inwards to which a color change is observed on a freshly split sample sprayed with a pH indicator. The carbonation depth is described by the spatial variation:

- Average (\bar{x}_c)
- Median (\tilde{x}_c)
- Range (δ_x)

The carbonation front is the area/volume in which the measured property (e.g. pH) changes due to carbonation. See Figure 1 (Revert, De Weerd et al. 2016).

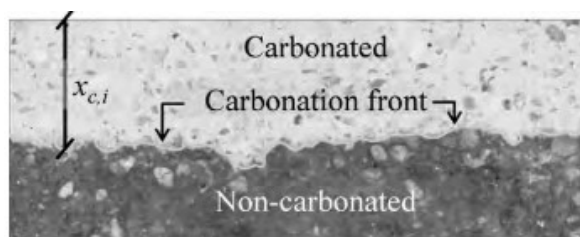


Figure 1: Used terminology to describe extent of carbonation (Revert, De Weerd et al. 2016).

Results

pH indicator

Carbonation was solely detected from the originally exposed surface and thus no carbonation occurred subsequent to drilling and extracting cores. Figure 2 shows sample PC, 25FA, 12FA4SF and SG sprayed with thymolphthalein (exposed surface facing downwards).

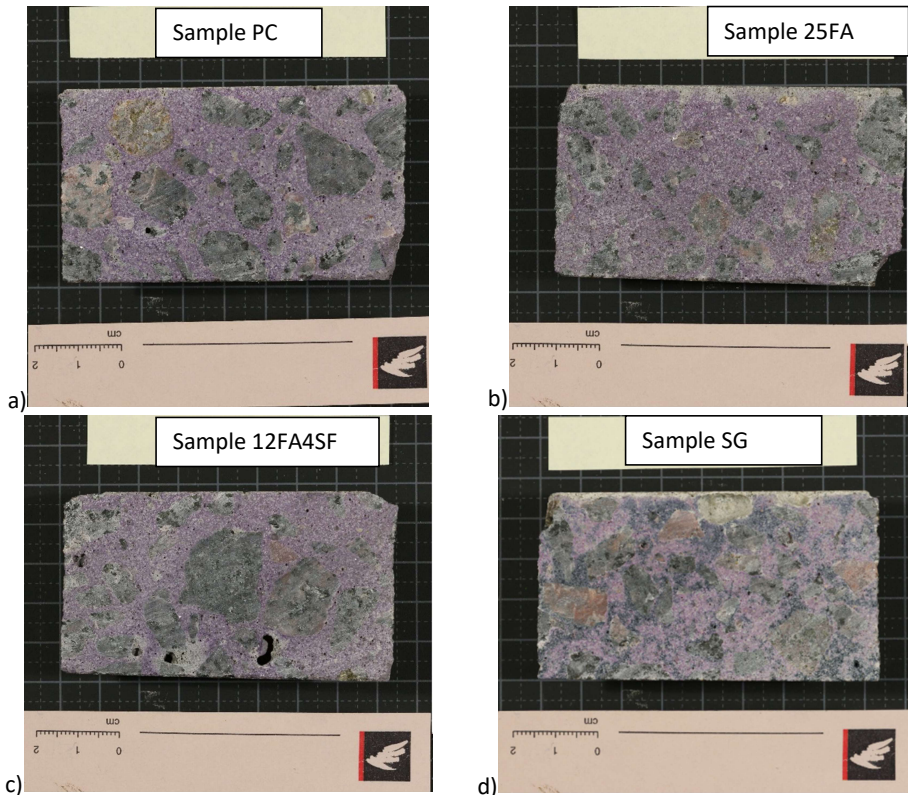


Figure 2: a) Sample PC, b) Sample 25FA, c) Sample 12FA4SF and d) Sample SG sprayed with Thymolphthalein. Exposed surface pointing upwards.

Significantly larger carbonation depths are observed for concrete 25FA and SG than for PC and 12FA4SF. SG has an almost uniform carbonation front, whereas the carbonation front in concrete 25FA varies across the width of the specimen. Figure 3 illustrates the spatial variation of carbonation depth in the four concretes determined by Thymolphthalein indicator.

Part III – Appendix D

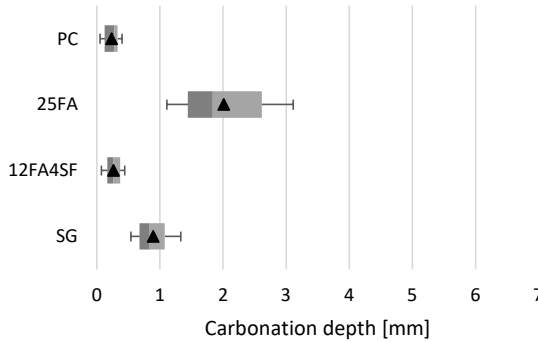


Figure 3: Spatial variation of carbonation depths determined using thymolphthalein. Boxes: values from 2nd and 3rd quartile and \bar{x}_c , whiskers: δ_x , black triangles: \bar{x}_c .

Optical microscopy

Concrete PC

Figure 4C reveals a higher porosity in the surface region gradually increasing over about 500 μm . It is therefore not surprising carbonation is registered at the surface of concrete PC after 8 years of exposure to an urban environment (Figure 4B). The air void structure is fair.

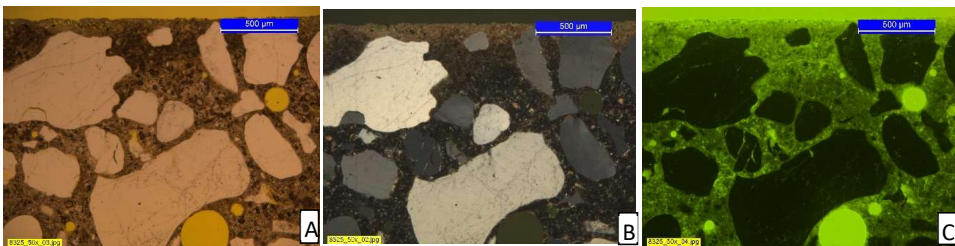


Figure 4: Picture of area in concrete PC with representative carbonation in the three modes polarized light (A), X-polarized light (B) and Fluorescence (C). Concrete exposed for 8 years in urban environment. Exposed surface pointing upwards.

No cracks were observed in the surface and only few inside the thin section. However, Figure 5 shows a carbonated spot inside concrete PC possibly originating from a crack extending from the surface out of the plane of the thin section. The diameter of the carbonated spot within the concrete is approximately twice that of the penetration depth from the surface, suggesting the carbonation could have occurred from an initial crack resulting from drying shrinkage.

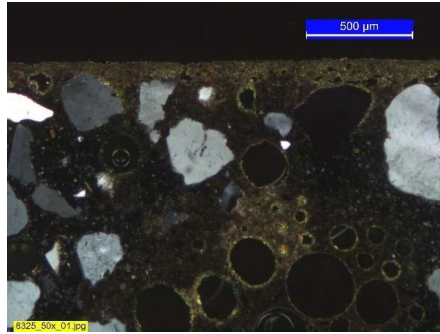


Figure 5: Carbonated area along crack inside of concrete PC, which does not extend from the surface in the plane of the thin section. Exposed surface pointing upwards.

Concrete C

Figure 6B shows carbonation exceeding 1 mm in depth. Figure 6C reveals a uniform paste porosity, but an air void structure with air voids slightly agglomerating near aggregate particles. Contrary, a thin section prepared after 28 maturity days showed a weakly increasing porosity towards the surface thereby suggesting that carbonation following 8 years of urban exposure may have decreased the porosity of concrete 25FA.



Figure 6: Picture of area in concrete 25FA with representative carbonation in the three modes polarized light (A), X-polarized light (B) and Fluorescence (C). Concrete exposed for 8 years in urban environment. Exposed surface pointing upwards.

Concrete 25FA studied after eight years of urban exposure has two fine cracks. Figure 7 shows carbonation along a 11 mm long crack. The carbonated area along the crack is observed to be wide initially and end in a reservoir suggesting that the crack extends out of the plane of the thin section prior to returning. No cracks were detected on a thin section prepared after 28 maturity days, but the carbonation depth along the crack on Figure 7 suggests that this crack might have been there from an early stage.

The carbonation depth of concrete 25FA has a relatively wide spatial distribution, which might be influenced by surface cracks either inside or outside the plane of this thin section.

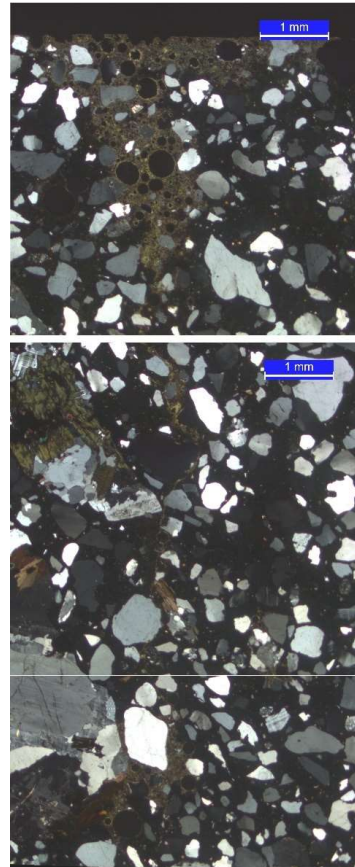


Figure 7: Large crack in concrete C. Exposed surface pointing upwards.

Concrete F

Figure 8C shows a uniform paste porosity increasing slightly towards the surface. The air void structure is poor with large clusters. Further cracks along aggregate and in the paste is observed. Despite the mentioned flaws, only a small carbonation depth is observed in concrete 12FA4SF (Figure 8B).

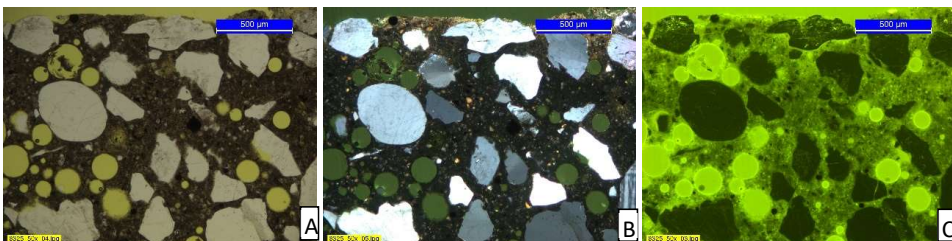


Figure 8: Picture of area in concrete 12FA4SF with representative carbonation in the three modes polarized light (A), X-polarized light (B) and Fluorescence (C). Concrete exposed for 8 years in urban environment. Exposed surface pointing upwards.

No cracks were observed in the surface. Very few paste and adhesion cracks were observed. Figure 9A and -B show additional examples of the poor air void structure in concrete 12FA4SF. The air is highly clustered around large aggregate particles. Figure 9C show carbonation in a large air void cluster near the surface of concrete F.

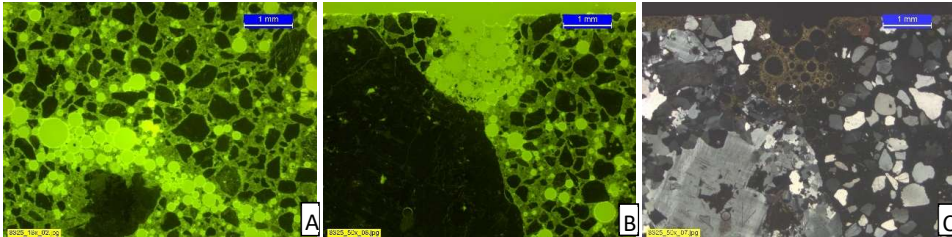


Figure 9: A) Poor air void structure in the interior of concrete 12FA4SF. B) Large air void cluster near the surface of concrete F. C) Carbonation in the large air void cluster shown on Figure 9B. Exposed surface pointing upwards.

Concrete K

Figure 10C shows a markedly higher porosity in the outer 1 mm of concrete SG. The area of increased porosity observed on Figure 10C corresponds well with the carbonated area observed on Figure 10B. Judging from the area of concrete K shown on Figure 10 it might seem like the porosity is lower in the outer 0.5 mm than between 0.5-1mm. This feature is however not representative for the entire thin section and could be caused by a crack or air voids located in the third dimension in the depth 0.5-1mm. Generally, the air voids appear well-distributed.

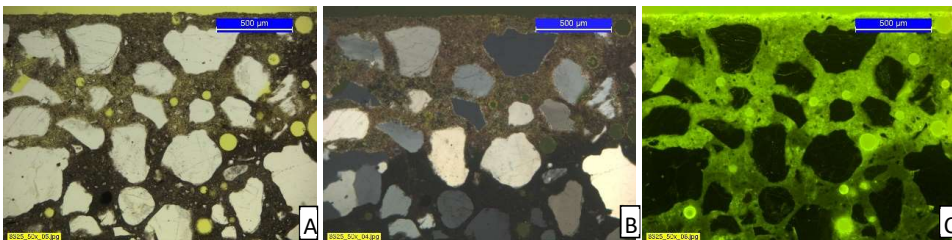


Figure 10: Picture of area in concrete SG with representative carbonation in the three modes polarized light (A), X-polarized light (B) and Fluorescence (C). Concrete exposed for 8 years in urban environment. Exposed surface pointing upwards.

Figure 11A shows high porosity for concrete SG after 28 maturity days extending through the entire thin section. By comparing Figure 11A and Figure 10C it is clear, that a significant densification of concrete SG in the region behind the outer one mm has occurred within 8 years of exposure in urban environment. This densification occurred behind the carbonation front shown in Figure 10B.

Figure 11B shows adhesion cracks along aggregate particles of concrete SG exposed in urban environment for 8 years.

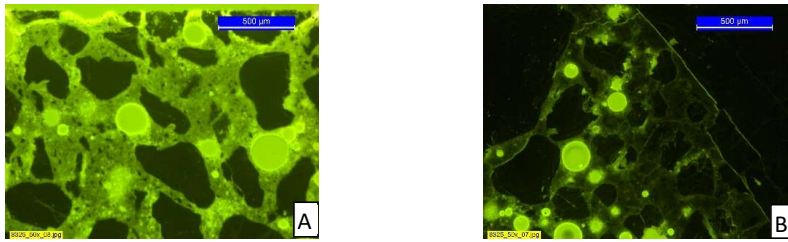


Figure 11: Porous surface of concrete K prior to exposure (28 maturity days) (A), adhesion cracks near aggregate particles of concrete exposed for 8 years in urban environment (B). Exposed surface pointing upwards.

Figure 12A shows partly unhydrated cement grains in the interior of concrete SG at 100x magnification. Figure 12B shows the outer ~0.5 mm of concrete SG, where probably due to carbonation much less unhydrated cement grains are present.

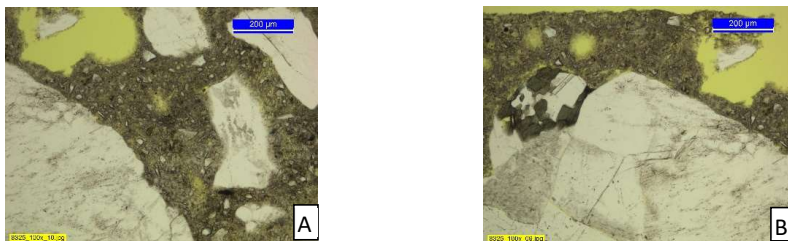


Figure 12: Partly unhydrated cement grains in the interior of concrete K detected in polarized light at 100x magnification (A), Absence of unhydrated cement grains due to carbonation detected in polarized light at 100x magnification (B). Exposed surface pointing upwards.

Summary of carbonation depths as measured by optical microscopy

Figure 13 illustrates the spatial variation of carbonation depths in the 4 concretes determined by Optical microscopy.

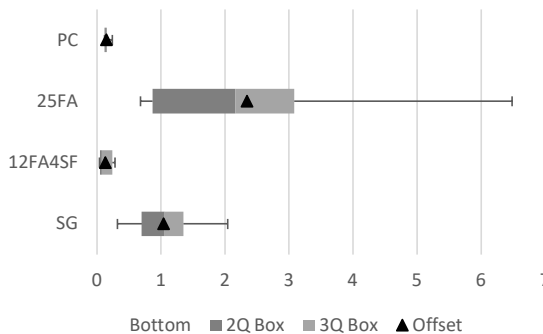


Figure 13: Spatial variation of carbonation depths determined using optical microscopy. Boxes: values from 2nd and 3rd quartile and \bar{x}_c , whiskers: δ_x , black triangles: \bar{x}_c .

Discussion

When comparing carbonations depths measured with different techniques, the influence of sampling must be considered. The method pH indicator has a clear transition in color,

whereas the method optical microscopy can be more subjective due to a possible wider transition from completely carbonated through partly carbonated to non-carbonated. The method pH indicator is convenient to apply, whereas optical microscopy provides additional information on e.g. porosity changes and cracks.

Figure 14 show a comparison between the spatial distribution of carbonation depth as determined by the pH indicator thymolphthalein (THY) and optical microscopy (OM). It is seen, that considering the large range of determined carbonation depths, the average carbonation depths determined by THY and OM agree well. It is observed, that for the low carbonation depths of concrete PC and 12FA4SF the carbonation depth is determined as lower by OM than by THY, while it is opposite for the larger carbonation depths.

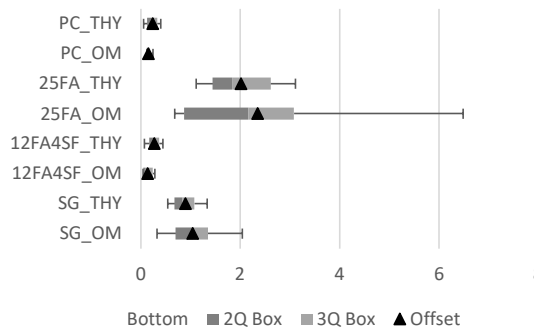


Figure 14: Comparison of spatial variation of carbonation depths determined using Thymolphthalein indicator (THY) and optical microscopy (OM). Boxes: values from 2nd and 3rd quartile and \bar{x}_c , whiskers: δ_x , black triangles: \bar{x}_c .

By optical microscopy carbonation along two fine cracks in concrete 25FA was observed. This information is not available by simply spraying pH indicator, but it might be a contributing factor to the non-uniform carbonation front observed at Figure 2B.

Carbonation depths after 120 years predicted based on an assumption of the carbonation depth being linear with square root time can be found in Table 2.

Table 2: Carbonation depths after 120 years predicted based on an assumption of the carbonation depth being linear with square root time. Both mean value and value based on the measured maximum value are given. THY = as determined by thymolphthalein indicator and OM = as determined by optical microscopy.

Concrete	PC		25FA		12FA4SF		SG	
	Mean	Max	Mean	Max	Mean	Max	Mean	Max
THY	0.9	1.6	7.8	12.0	1.0	1.7	3.5	5.1
OM	0.6	0.9	9.1	25.1	0.5	1.1	4.0	7.9

Conclusion

The following conclusions were drawn:

- The carbonation depths determined by pH indicator and optical microscopy are in relatively good agreement when considering the impact of sampling.
- A pH indicator is easy to apply, while optical microscopy provides additional information
- 5-11 times larger carbonation depths were found for concretes containing fly ash and slag compared to plain Portland cement concrete after eight years of urban exposure.
- Carbonation depths after 120 years based on an assumption of the carbonation depth being linear with square root time are predicted to less than 2 mm for PC and 12FA4SF, whereas SG reach 4.0 mm (mean), 7.9 mm (max) and 25FA reach 9.1 mm (mean), 25.1 mm (max).

Acknowledgements

This research is part of a Ph.D. project financed by the Danish Ministry of Higher Education and Science as a part of the contract “E5 Field exposure and monitoring to extend the service life of infrastructure (translation)” owned by the Danish Technological Institute (DTI); we acknowledge the financial support.

References

- Bier, T. A. (1986). "Influence of type of cement and curing on carbonation progress and pore structure of hydrated cement pastes." MRS Online Proceedings Library Archive **85**.
- Buis, A. (2019). "The Atmosphere: Getting a Handle on Carbon Dioxide." Retrieved 03-01-2020, 2020, from <https://climate.nasa.gov/news/2915/the-atmosphere-getting-a-handle-on-carbon-dioxide/>.
- DMI (2020). "Danish meteorological institute." Retrieved 03-01-2020, 2020, from <https://www.dmi.dk/vejarkiv/>.
- Jacobsen, S., et al. (2009). TKT 4215 Concrete Technology 1, Department of Structural Engineering NTNU.
- Jakobsen, U., et al. (1999). "Determination of water-cement ratio in hardened concrete by optical fluorescence microscopy." Special Publication **191**: 27-42.
- Papadakis, V. G., et al. (1991). "Fundamental modeling and experimental investigation of concrete carbonation." Materials Journal **88**(4): 363-373.
- Poulsen, S. L., et al. (2018). Chloride ingress in concrete blocks at the Rødbyhavn marine exposure site – Status after 5 years. 4th International Conference on Service Life Design for Infrastructures (SLD4). Delft, Netherlands: 192-203.
- Revert, A. B., et al. (2016). "Carbonation Characterization of Mortar with Portland Cement and Fly Ash, Comparison of Techniques." Nordic Concrete: 60.

Part III – Appendix E

Appendix E Overview of chloride ingress models

Overview of chloride ingress prediction models.

Model Type	Duracrete [6]	fib Model Code [4]	HETEK [58]	ClinConc engineering expression [21]	Stadium [36]
Time- dependent D_a	x	x	x	x	Not applicable
Time- dependent C_s			x	x (through time dependent chloride binding)	Not applicable
Empirical (E) or Physical (Phy)	E	E	E	Phy	Phy
Multi species				(x) (including OH ⁻)	x
Analytical (A) or Numerical (N)	A	A	A	A	N
Primary function(s)	erf	erf	ψ_p -function	erf	Nernst- Planck & Poisson
Driving force	Total chloride	Total chloride	Total chloride	Free chloride	Multi species
Comment	Includes a curing factor.	Based on Duracrete.	Includes the ψ_p -function to cope with a time- dependent surface concentration.	Exclusively for submerged exposure. Also exists as a more comprehensive numerical model.	

